Novel engineered Metal nanodevices and their potential use in therapeutic and biomedical application

Mohammed, Wanisa Ibrahim

Swansea University
Prifysgol Abertawe

Novel engineered metal nanodevices and their potential use in therapeutic and biomedical application

Wanisa Ibrahim Abdussalam Mohammed

Thesis submitted to Swansea University in fulfilment of the requirements for the Degree of Doctor of Philosophy

October 2017

SUMMARY

Gold nanoparticles (AuNPs) are considered to have significant potential as in photothermal therapy, drug delivery and antibiotic activities due to their optical properties, chemical stability and biocompatibility. AuNP surface functionalisation plays an important role in cellular uptake and producing cellular responses. For this reason, novel AuNPs (5-26 nm) functionalised by a new family of a phosphonioalkylthiosulfate/thioacetate in this thesis, and have been shown to be stable for a period up to 6 months with no obvious evidence for any aggregation.

Production of novel cationic phosphonium AuNPs (8-11 nm) by borohydride reduction of a gold (III) salt, dispersed in water or dimethylsulfoxide (DMSO) for their potential use in biomedical applications is outlined in Chapter **2**.

The environment around cancer cells is known to be mildly acidic with pH of 6.0 to 7.2, which is lower than in healthy cells. Based on the pH factor, AuNPs have shown abilities to induce cancer cell death *via* a photothermal therapy after aggregation. For this reason, our cationic phosphonium AuNPs were subjected to investigate their stability over time and at a pH range of 3-11. This work is described in Chapter **3**. The synthesised AuNPs were primarily characterised using both UV-visible spectra and Dynamic light scattering (DLS). The pH study suggested that the optimum pH range for the AuNP colloidal samples to remain stable (without aggregation) is between pH 9.2 and pH 5.1. Within this range, the diameters recorded by the DLS were 9.6 ± 0.9 nm, and the aggregation (instability) was noted at pH < 5 and > 9. The structural characterisations of all ligands in this thesis were confirmed by using ATR, ESI-MS and NMR, while the influence of the ligands on the formation and stability of AuNPs was investigated by DLS, TEM and UV-Vis measurements, and described in Chapter **2** to **6**.

Green methods used to synthesis AuNPs using ascorbic acid, as bio-reducing agent was important nowadays, especially within the biological cells due to its low toxicity. Well-monodispersed AuNPs were prepared by the reduction of $KAuCl_4$ using $NaBH_4$ and ascorbic acid as reducing agents. Using different reducing agent power, obtained different results for AuNPs that functionalised with same conditions in Chapter **4**. Small sizes with higher stability up to 6 months were generated when $NaBH_4$ was used as reducing agent. Where AuNPs of different sizes are known to produce contradictory results sometimes in *vivo* and in *vitro* bio-application.

AuNPs functionlised by di-phosphine oxide thiol ligand are considered to be very active against bacteria, and have broad bio-applications. The work on AuNPs functionlised by novel related phosphine oxide thiols ligands is discussed in Chapter **5**.

Due to antibiotic drug resistance to some kinds of bacterial infection, development of new antibacterial agents is necessary. This thesis describes a study of the efficiencies of different concentrations of AuNPs (8-17 nm) on non-pathogenic bacteria including, *Escherichia coli* NCIB 8277 and *Staphylococcus aureus* ATCC 6538P in (Chapter **6**). AuNPs exhibited excellent antibacterial sensitivity to both kinds of bacteria especially at high concentration (30 µL) of AuNPs.

DECLARATION AND STATEMENTS

DECLARATION

This work has not previously been accepted in substance for any degree and is not being concurrently submitted in candidature for any degree.

Signed ……. (candidate)

Date …….

STATEMENT 1

This thesis is the result of my own work and investigation, except where otherwise stated. Where correction services have been used, the extent and nature of the correction is clearly marked in a footnote(s).

Other sources have been acknowledged by giving explicit references. A bibliography is appended.

Signed ……. (candidate)

Date …….

STATEMENT 2

I hereby give consent for my thesis, if accepted, to be available for photocopying and for inter-library loan, and for the title and summary to be made available to outside organisations.

Signed ……. (candidate)

Date …….

NB: Candidates on whose behalf a bar on access has been approved by the University (see Note 7), should use the following version of Statement 2.

I hereby give consent for my thesis, if accepted, to be available for photocopying and for inter-library loans **after expiry of a bar on access approved by the Swansea University.**

Signed ……. (candidate)

Date …….

ACKNOWLEDGEMENTS

I would like to express my ultimate gratitude and special appreciation to my supervisor **Dr. Yon Ju-Nam** for her continuous inspirational guidance, motivation, encouragement and for giving suggestions and showing the right direction throughout the entire period of my study.
I would also like to thank my other supervisor **Dr Paolo Bertoncello**. My deepest appreciation also goes to **Dr Jesus J. Ojeda** for his help. I sincerely appreciate Mr **Ian Matthews** and **Dr. Peter Douglas** for their help in the chemical lab

I truly thank Sebha University and **Prof. Bashir M. Eshtewi (**Deputy Minister, Ministry of Higher Education) for their financial support and continuous help to pursuit my academic degree.

I would also like to express my appreciation to my father, who died unfortunately in the first year of my Ph.D. and he was waiting for this moment eagerly. I will also never stop appreciating my mother and my husband patience, unlimited encouragement and their endless love throughout my study. Also, a great appreciation to my sister, brothers, my mother in law. My thanks and appreciates also go my friends and lab-mates in special **Claire Barnes, Thomas Jones** and **Mona Alyobi** for their motivation and support during this work.

Table of Contents

SUMMARY i

DECLARATION AND STATEMENTS ii

ACKNOWLEDGEMENTS iii

TABLE OF FIGURES x

DEFINITION-ABBREVIATION xvi

DEFINITION-CHEMICAL STRUCTURES xvii

Chapter 1: Literature review 1

1.1 Introduction 1

1.1.1 Optical and chemical properties of gold nanoparticles (AuNPs) 2

1.1.2 Synthesis of gold nanoparticles 5

1.1.2.1 Synthesis of AuNPs using chemical methods 6

1.1.2.2 Purification of gold nanoparticles 8

1.2 Functionalisation of gold nanoparticles 10

1.2.1 Functionalisation of AuNPs using protecting organic ligands 10

1.3 Stability of colloids gold nanoparticles 11

1.4 Biocompatibility of gold nanoparticles 13

1.4.1 Principle of cationic cellular uptake of gold nanoparticles 14

1.4.2 Physicochemical properties of cationic functionalised AuNPs inside of the extracellular fluid 17

1.4.3 Toxicity of gold nanoparticles 18

1.4.4 Accumulation of gold nanoparticles in organism tissue 20

1.5 Application of gold nanoparticles in biology and medicine 21

1.5.1 Gold nanoparticles for cancer diseases 21

1.5.2 Gold nanoparticles against bacteria 24

Aims of the project 25

Outline of the thesis 25

1.6 References 27

Chapter 2: Highly stable noble metal nanoparticles dispersed in biocompatible solvents: synthesis of cationic phosphonium gold nanoparticles in water and DMSO 39
2.1 Abstract 39
2.2 Introduction 39
2.3 Materials and Methods 42
2.3.1 General Information 42
(e) Ultraviolet-Visible Absorption Spectroscopy (UV-visible): 43
(f) Transmission Electron Microscopy (TEM) 43
2.3.2 Cationic phosphonium ligand syntheses 43
2.3.2.1 Synthesis of tri(p-tolyl)phosphoniopropylthiosulfate zwitterion (4) 43
2.3.2.2 Synthesis of triphenylphosphoniopropylthiosulfate (4C) 45
2.3.2.3 Synthesis of (3-thioacetylpropyl)triphenylphosphonium bromide (5) 45
2.3.3 Synthesis of cationic phosphonium gold nanoparticles in water and DMSO 46
2.3.3.1 Cationic phosphonium gold nanoparticles dispersed in water 46
2.3.3.2 Cationic phosphonium gold nanoparticles dispersed in DMSO 46
2.4 Results and Discussion 47
2.4.1 Synthesis of tri(p-tolyl)phosphoniopropylthiosulfate zwitterion (4) 47
2.4.2 Cationic phosphonium gold nanoparticles dispersed in water and DMSO 47
2.4.3 UV-Visible and TEM studies 48
2.5 Conclusions 53
2.6 Characterisation of the cationic phosphonium ligands 54
2.7 References 56
Chapter 3: Synthesis of potential pH-sensitive cationic phosphonium AuNPs in aqueous medium 60
3.1 Abstract 60
3.2 Introduction 61
3.3 Materials and Methods 64
3.3.1 Cationic Phosphonium Ligand Synthesis 65

3.3.1.1 Synthesis of the (3-thioacetylpropyl)triphenylphosphonium bromide ligands....65
3.3.2 Synthesis of functionalised AuNPs using 4A and 4B ligands in DMSO 67
3.3.3 Dynamic Light Scattering.....67
3.4 Results and Discussion 68
3.4.1 Synthesis of 4A and 4B ligands.....68
3.4.1.1 Characterisation of the colloidal solutions of AuNPs functionalised with 4A and 4B by using UV-Visible and DLS studies 69
3.4.2 pH stability study 73
3.4.2.1 Study of the stability of 5-AuNPs in acidic conditions.....73
3.4.2.2 Study of the stability of 5-AuNPs in basic conditions.....78
3.5 Study of the stability of 4B-AuNPs in acid and basic conditions of 1M HCl and NaOH. 82
3.5.1 Acidic study UV-Vis and DLS results.....83
3.5.2 Basic study UV-Vis and DLS results of 4B-AuNPs.....85
3.6 Study of the stability of functionalised 4A-AuNPs in acid and basic conditions of 1M HCl and NaOH.....89
3.6.1 Acidic study UV-Vis and DLS results of add 4A-AuNP. 89
3.6.2 Basic study UV-Vis and DLS results.....92
3.7 Stability of 5, 4A and 4B-AuNPs with changing pH after one and half month. 95
3.8 Conclusions.....96
3.9 References.....99
Chapter 4: Green synthesis of positively charged biocompatible gold nanoparticles in water: use of ascorbic acid as reducing agent.....105
4.1 Abstract.....105
4.2 Introduction.....106
4.3 Materials and Methods.....109
4.3.1 Cationic phosphonium ligand syntheses.....109

4.3.1.1 Synthesis of tri(phenyl) (4C) and tri(p-tolyl)phosphoniopropylthiosulfate (4) zwitterion 109

4.3.1.2 Synthesis of (3-thioacetylpropyl)triphenylphosphonium bromide (5). 109

4.3.1.3 Syntheses of the (6-thioacetylhexyl)triphenylphosphonium bromide derivatives ligands 109

4.3.1.4 Synthesis of tri(phenyl)phosphoniohexylthiosulfate derivatives zwitterion 112

4.3.2 Protecting AuNPs by synthesis of phosphonium-monolayer using protecting ligands including thioacetate and thiosulfate ligands using $NaBH_4$ reduction in (H2O/DMSO) and comparison with ascorbic acid reduction in water 114

4.3.2.1 Synthesis of cationic phosphonium gold nanoparticles by NaBH4 in H2O / DMSO 114

4.3.2.2 Syntheses AuNPs using ascorbic acid as reducing agent 114

4.4 Results and Discussion 115

4.4.1 Syntheses of 4C, 5, 4, 8D, 8B, 8A, 9D, and 9A ligands 116

4.4.2 Characterisation of the colloidal solutions of AuNPs using $NaBH_4$ in comparison with ascorbic acid as reducing agent via using UV-Visible and DLS studies 118

4.4.2.1 Characterisation of AuNPs using transmission electron microscopy 127

4.5 Conclusion 131

4.6 References 133

Chapter 5: Synthesis AuNPs functionalised by phosphine oxide derivatives in DMSO 138

5.1 Abstract 138

5.2 Introduction 139

5.3 Materials and Methods 143

5.3.1 Cationic phosphonium ligand synthesis 143

5.3.1.1 Synthesis of (3-thioacetylpropyl)di-(p-tolyl)phosphine oxide(12A) and (3-thioacetylpropyl)diphenylphosphine oxide (12D) 143

5.3.1.2 Synthesis of (3-thioacetylpropyl)thio-diphenylphosphine oxide (15) 145

5.3.1.3 Synthesis of (3-thioacetylethyl-N-methylamine)diphenylphosphine oxide (18) 146

5.3.2 Synthesis of phosphine oxide gold nanoparticles derivatives in DMSO using $NaBH_4$ as reducing agent....148

5.3.3 Synthesis AuNPs using (3-thioacetylpropyl)di(p-tolyl)phosphine oxide, in aqueous solution using ascorbic acid as reducing agent....148

5.4 Results and Discussion....149

5.4.1 Synthesis of 12A and 12D....149

5.4.2 Synthesis of (3-thioacetylpropyl)thio-diphenylphosphine oxide (15)....150

5.4.3 Synthesis of (3-thioacetyl-N-ethylmethylamine)diphenylphosphine oxide (18)....151

5.4.4 Stability of gold nanoparticles using (12A), (12D), (15), and (18) in DMSO by using $NaBH_4$ and ascorbic acid as reducing agents....152

5.4.5 UV-Visible and DLS studies....153

5.5 Conclusion....158

5.6 References....160

Chapter 6: Antimicrobial activities of novel gold nanoparticles agent against Escherichia coli and Staphylococcus aureus bacteria....166

6.1 Abstract....166

6.2 Introduction....167

6.3 Experimental Section....172

6.3.1 Materials and Methods....172

6.3.2 Antibacterial activity....172

6.3.3 Antimicrobial mechanism of cationic phosphonium AuNPs....173

6.3.4 Synthesis of tris(2,4,6-trimethoxyphenyl)phosphoniopropylthio- chloride zwitterion (2C)....174

6.3.5 Synthesis of (6-thioacetylhexyl)tris(2,4,6-trimethoxyphenyl)-phosphonium bromide ligands zwitterion (8B)....174

6.3.6 Synthesis gold nanoparticles....176

6.4 Results and Discussion....177

6.4.1 Characterisation of the cationic AuNP functionalised by tris(2,4,6-trimethoxyphenyl)phosphoniopropylthiolchloride zwitterion (2C) and 8B by using UV-Visible and DLS studies....186
6.4.2 Characterisation of the cationic phosphonium ligands....189
6.4.3 Tris(2,4,6-trimethoxyphenyl)phosphoniopropylthiochloride zwitterion (2C)....189
6.4.4 (6-thioacetylhexyl)-tris(2,4,6-trimethoxyphenyl)phosphonium bromide zwitterion (8B)....189
6.5 Conclusion....190
6.6 References....192
Chapter 7: Conclusion of thesis....197
7.1 Conclusions and future work....197
Appendix....200

TABLE OF FIGURES

Figure 1.1. Different types of gold nanoparticles [3].....1
Figure 1.2. Chemical structure of AuNP functionalised by ligand contains three parts including the sulfur atom (binding directly with Au due to its strong affinity), alkyl chain and a tetraethylene glycol spacer [21].....3
Figure 1.3. AuNPs characterised via (A) UV-vis spectrum; size distribution of AuNPs by using both DLS (B) and TEM (C), the scale bar is 10 nm) [32].....5
Figure 1.4. Brust-Schiffrin method: preparation of functionalised of AuNP by using two phases solvent system [39].....7
Figure 1.5. Diagrammatic depiction of stabilisation of AuNPs [77].....13
Figure 1.6. Interactions between different surfaces charges of AuNPs with SK-BR-3 (human breast cancer) cells [39].....15
Figure 1.7. AuNPs functionalised by primary amine with their transfection ability into cultivated cells [97].....16
Figure 1.8. Triphenylphosphonium cation used as non-viral DNA delivery vectors in gene therapy [105].....17
Figure 1.9. Intracellular Au-concentration as determined by ICP-MS analysis as a function of time. Where data present the average of three experiments with standard deviation [110]. ...20
Figure 1.10. Structure of Gemcitabine (left) and Cetuximab (right) (Figure is taken from https://pubchem.ncbi.nlm.nih.gov/compound/gemcitabine#section=Top.....23

Figure 2.1. UV-visible absorption spectra of the colloidal solutions of AuNPs functionalised using 4C as protecting ligand. The different UV-visible spectra represent these NPs dispersed in water at time = 0, and DMSO at time = 0, 6 and 12 weeks. Where time = 0 is the initial time of the 4C-AuNP preparation.....49
Figure 2.2. UV-visible absorption spectra of the colloidal solutions of AuNPs functionalised using 5 as protecting ligand. The different UV-visible spectra represent these NPs dispersed in water at time = 0, and DMSO at time = 0, 6 and 12 weeks.....50
Figure 2.3. UV-visible absorption spectra of the colloidal solutions of AuNPs functionalised using 4 as protecting ligand. The different UV-visible spectra represent these NPs dispersed in DMSO at time = 0, 6 and 12 weeks.....51

Figure 2.4. Representative TEM micrographs of cationic phosphonium AuNPs synthesised using 4C (TEM1), 5 (TEM2), and 4 (TEM3) as protecting ligands in DMSO, and corresponding particle size histograms. 52

Figure 3.1. Chemical structures of (3-thioacetylpropyl)tris(2,4,6-trimethoxyphenyl)phosphonium bromide (4B) and (3-thioacetylpropyl)triphenyl-phosphonium bromide (5). 67
Figure 3.2. The colour comparison of initial (a) and after six months solutions (b) of 4B functionalised AuNPs. 71
Figure 3.3. UV-Visible absorption spectra of the colloidal solutions of AuNPs functionalised using 4A as protecting ligand. The different UV-visible spectra represent these NPs dispersed in DMSO/water at time = 0, 1, 2, 3, 4, and 5 months. Where time = 0 is the initial time of the 4A-AuNPs prepartion. 72
Figure 3.4. UV-visible absorption spectra of the colloidal solutions of AuNPs functionalised using 4B as a protecting ligand. The different UV-visible spectra represent these 4B-AuNPs dispersed in DMSO/water at time = 0, 1, 2, 3, 4, 5, and 6 months. 72
Figure 3.5. Data collected through UV-Vis across the pH range produced via adding HCl to the 5-AuNPs solution in (Run 1), pH < 7.5, where the HCl additions were from (5-30 µL). . 76
Figure 3.6. Data collected by using DLS analysis of the samples 5-AuNPs in (Run 1) to give the diameter size and standard deviations for each pH, pH < 7.5 and the HCl additions were from (5-30 µL). 77
Figure 3.7. Data collected through UV-Vis at each pH recorded in (Run 1) of 5-AuNPs. It can be observed that the shape and height of the surface plasmon bands alter as the pH is altered and that the peak of the absorption shift towards 536 nm as will describe in detail in the following sections. pH > 7.5. 79
Figure 3.8. Data of 5-AuNPs for measurements taken for DLS (Run 1) at increasing pH values, where 1M NaOH additions were from (5-30 µL). 82
Figure 3.9. Data collected through UV-Vis across the pH range produced by adding HCl to the 4B-AuNPs solution in (Run 1) of the acidic study, pH < 7.5 and the 1M HCl additions were from (0 - 35µL). 84
Figure 3.10. Data collected through DLS analysis of the samples in (Run 1) to give the diameter size and standard deviations for each pH range produced by adding HCl to the 4B- AuNPs solution, pH < 7.5. 84

Figure 3.11. Data collected through UV-Vis across the pH range produced by adding 1M NaOH (5-30 µL) to the 4B-AuNPs solution in (Run 2) of the basic study, pH > 7.5. 87
Figure 3.12. Data collected through DLS analysis of the samples in (Run 2) to give the diameter size and standard deviations for each pH range produced by adding NaOH to the 4B-AuNPs solution, pH > 7.5. 87
Figure 3.13. The transition in colour for the aliquots taken during (Run 2) at (e) 0 µL and (f) 25 µL of the acidic pH study for 4B-AuNPs. pH < 7.5. 88
Figure 3.14. The transition in colour for the aliquots taken during (Run 2) at (d) 0 µL and (c) 30 µL of the basic pH study for 4B-AuNPs. pH > 7.5. 88
Figure 3.15. Data collected through UV-Vis across the pH range produced by adding 1M HCl (5-30 µL) to the 4A-AuNPs solution in (Run 1) of the acidic study. (pH < 7.5). 91
Figure 3.16. Data collected through DLS analysis of the samples in (Run 1) to give the diameter size and standard deviations for each pH range produced by adding HCl (5-30 µL) to the 4A-AuNPs solution. (pH < 7.5). 91
Figure 3.17. Data collected through UV-Vis across the pH range produced by adding 1M NaOH (5-30 µL) to the 4A-AuNPs solution in (Run 3) of the basic study. 94
Figure 3.18. Data collected through DLS analysis of the samples in (Run 3) to give the diameter size and standard deviations for each pH range produced by adding 1 M NaOH to the 4A-AuNPs solution. 94
Figure 3.19. Data collected through UV-Vis of 5-AuNPs solution (Run 3) after one and half month when (pH <7.5) in the left and (pH > 7.5) in the right. 95
Figure 3.20. Data collected through DLS analysis of 5-AuNPs solution (Run 3) after one and half month in both acidic conditions, pH < 7.5 (in the left) and basic conditions, pH > 7.5 (in the right). 96

Figure 4.1. UV-Vis for the stability of the 8D-AuNPs dispersed in H_2O/DMSO, using $NaBH_4$ as reducing agent at time = 0, 1 and 2 months. Where time = 0 is the initial time of the frish 8D-AuNPs synthesed. 120
Figure 4.2. The size and standard deviation of each diameter range measured by DLS, and was taken at a different time value for 8D-AuNPs, where time = 0 is the first time of the fresh 8D-AuNPs synthesised using $NaBH_4$ as reducing agent. Where time = 0 is the initial time of the 8D-AuNPs preparation. 120

Figure 4.3. UV-Vis for the stability of the 8A-AuNPs dispersed in H_2O/DMSO, using $NaBH_4$ as reducing agent at time = 0, 1, 2, 3, 4, 5, and 6 months respectively. Where time = 0 is the initial time of the 8A-AuNPs preparation. 121
Figure 4.4. The size and standard deviation of each diameter range taken at a different time value for 8A-AuNPs, using $NaBH_4$ as reducing agent by using DLS. 121
Figure 4.5. UV-Vis for the stability of the 4C-AuNPs dispersed in aqueous solution at time = 0, 1, 3, 4, 5, 6, and 7 weeks respectively. Using ascorbic acid as reducing agent. 125
Figure 4.6. The size and standard deviation of each diameter range taken at a different time value for 4C-AuNPs as reported by DLS study. Using ascorbic acid as reducing agent. 125
Figure 4.7. UV-Vis study for the stability of the 5-AuNPs dispersed in aqueous solution at time = 0, 1, 3, 6, and 8 weeks respectively. Using ascorbic acid as reducing agent. 126
Figure 4.8. The size and standard deviation of each diameter range taken at a different time value for 5-AuNPs as reported by DLS study. Using ascorbic acid as reducing agent. 126
Figure 4.9. TEM micrographs of cationic phosphonium 8B-AuNPs using $NaBH_4$ as reducing agent (TEM4.1), 4-AuNP (TEM4.2), and 8B-AuNP (TEM4.3) as protecting ligands in case ascorbic acid had used, and corresponding particle size histograms. 130

Figure 5.1. UV-visible absorption spectra of the colloidal solutions of AuNPs functionalised using 12A as protecting ligand. The different UV-visible spectra represent these AuNPs dispersed in DMSO at time = 0, 1, 2, and 3 months. Solutions prepared using different dilution factors. 154
Figure 5.2. UV-visible absorption spectra of the colloidal solutions of AuNPs functionalised using 12D as protecting ligand. The different UV-visible spectra represent these nanoparticles dispersed in DMSO at time = 0, 1, 2, 3, and 5 months respectively. Solutions prepared using different dilution factors. 155
Figure 5.3. UV-visible absorption spectra of the colloidal solutions of AuNPs functionalised using 15 as protecting ligand. The different UV-visible spectra represent these AuNPs dispersed in DMSO at time = 0, 1, 3, and 5 months. Solutions prepared using different dilution factors. 155
Figure 5.4. UV-visible absorption spectra of the colloidal solutions of AuNPs functionalised using 18 as protecting ligand. The different UV-visible spectra represent these AuNPs dispersed in DMSO at time = 0, 1, 2, and 3 months respectively. Solutions prepared using different dilution factors. 156

Figure 5.5. UV-visible absorption spectra of the colloidal solutions of AuNPs functionalised using 12A as protecting ligand using ascorbic acid as reducing agent. The different UV-visible spectra represent these AuNPs dispersed in aqueous solution at time = 0, 1, 3, 5, 7 and 8 weeks respectively. Solutions prepared using different dilution factors. 156

Figure 6.1. Percentage of inhibition of S. aureus, which treated by 4C-AuNPs, 8B-AuNPs, 2C-AuNPs, and 4A-AuNPs at different, concentrations (1.36 µg-30 µL), (0.63 µg-15 µL), (0.363 µg-8 µL), and (0.181 µg-4 µL) respectively.....179
Figure 6.2. Percentage of inhibition of E. coli, which treated by 4C -AuNPs, 8B- AuNPs, 2C-AuNPs, and 4A-AuNPs at different, concentrations (1.36 µg-30 µL), (0.63 µg-15 µL), (0.363 µg-8 µL), and (0.181 µg-4 µL) respectively.....179
Figure 6.3. An antibacterial activity of four kinds of AuNPs against S. aureus. Where A = 4C-AuNPs, B = 8B-AuNPs, C = 2C-AuNPs and D = 4A-AuNPs. 1, 2, 3, 4 are represent, concentrations (1.36 µg-30 µL, 0.63 µg-15 µL, 0.363 µg-8 µL, 0.181 µg-4 µL respectively). 182
Figure 6.4. An antibacterial activity of four kinds of AuNPs against E. coli, where A = 4C-AuNPs, B = 8B-AuNPs, C = 2C-AuNPs and D = 4A-AuNPs. 1, 2, 3, 4 are represent, concentrations (1.36 µg-30 µL, 0.63 µg-15 µL, 0.363 µg-8 µL, 0.181 µg-4 µL respectively). 183
Figure 6.5. An antibacterial activity of 4C-AuNPs against E. coli and S. aureus bacteria, at different, concentrations (1.36 µg-30 µL), (0.63 µg-15 µL), (0.363 µg-8 µL), and (0.181 µg-4 µL) respectively. Where, (*** represents $p \leq 0.0001$), (** represents $p \leq 0.001$), (*represents $p \leq 0.05$). 183
Figure 6.6. An antibacterial activity of 8B-AuNPs against E. coli and S. aureus bacteria, at different, concentrations (1.36 µg-30 µL), (0.63 µg-15 µL), (0.363 µg-8 µL), and (0.181 µg-4 µL) respectively. 184
Figure 6.7. An antibacterial activity of 2C-AuNPs against E. coli and S. aureus bacteria, at different, concentrations (1.36 µg-30 µL), (0.63 µg-15 µL), (0.363 µg-8 µL), and (0.181 µg-4 µL) respectively. Where (*** represents p-value ≤ 0.0001), (** represents $p \leq 0.001$), (*represents $p \leq 0.05$). 184
Figure 6.8. An antibacterial activity of 4A-AuNPs against E. coli and S. aureus bacteria, at different, concentrations (1.36 µg-30 µL), (0.63 µg-15 µL), (0.363 µg-8 µL), and (0.181 µg-4 µL) respectively. (*** represents p-value ≤ 0.0001), (** represents $p \leq 0.001$). 184

Figure 6.9. UV-visible absorption spectra of the colloidal solutions of AuNPs functionalised using 2C as protecting ligand. The different UV-visible spectra represent these Au nanoparticles dispersed in DMSO at time = 0, 2, 4, 6, 8, 10, 12 and 14 weeks. 187
Figure 6.10. DLS for AuNP functionalised by 2C. Sizes increased as time increased 187
Figure 6.11. UV-visible absorption spectra of the colloidal solutions of AuNPs functionalised using 8B as protecting ligand. The different UV-visible spectra represent these nanoparticles dispersed in DMSO at time = 0, 1, 2, 4, 7, 9 and 11 weeks. 188
Figure 6.12. DLS of AuNPs synthesised using 8B as protecting ligand in DMSO, and corresponding particle size histograms. 188

DEFINITION-ABBREVIATION

AuNPs	Gold nanoparticles
AgNP	Silver nanoparticle
BSM	Brust−Schiffrin method
CTAB	Cetyltrimethylammonium bromide
DMSO	Dimethyl sulfoxide
DCM	Dichloromethan
DNPs	Diamond nanoparticles
MDR	Multidrug resistant
MelNP	Melanin-like nanoparticle
mp	Melting point
MPA	3-mercaptopropionic acid
NPs	Nanoparticles
NMs	Nanomaterials
NB	Nutrient broth
PAH	Poly(allylamine hydrochloride)
ROS	Reactive oxygen species
RNS	Reactive nitrite species
SPB	Surface plasmon band
SAMs	Self-Assembled Monolayers
SPR	Surface plasmon resonance spectroscopy
TPP	Triphenylphosphine
WHO	Wold Health Organisation
XDR	Extensively-drug resistant
QDs	Quantum dots

DEFINITION-CHEMICAL STRUCTURES

Number of structures	Chemical structure	Name of the structure
4A	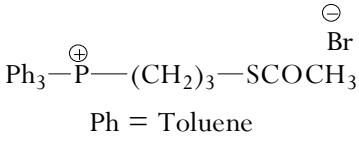	(3-Thioacetylpropyl)tri(*P*-tolyl)-phosphonium bromide
4B	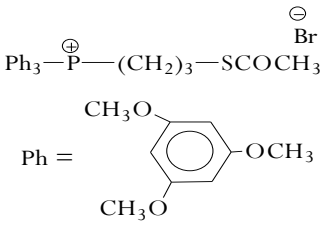	(3-Thioacetylpropyl)tris(2,4,6-trimethoxy-phenyl)phosphonium bromide
2C	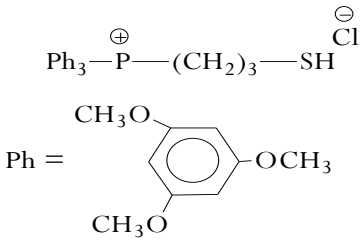	Tris(2,4,6-trimethoxyphenyl)phosphonio-propylthiochloride
4C	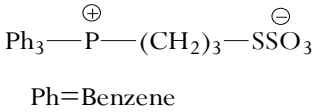	Triphenylphosphoniopropyl-thiosulfate zwitterion
4	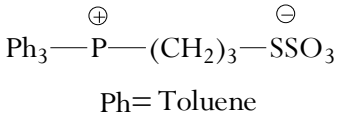	Tri(*p*-tolyl)phosphoniopropyl- thiosulfate zwitterion
5	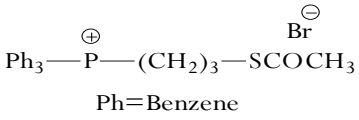	(3-Thioactylpropyl)triphenyl-phosphonium bromide
8A	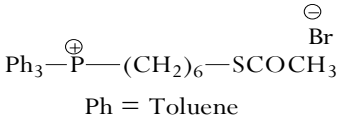	(6-Thioacetylhexyl)tri(*p*-tolyl)-phosphonium bromide

8B	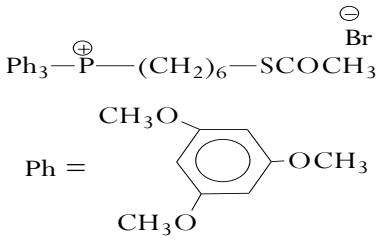	(6-Thioacetylhexyl)tris(2,4,6-trimethoxy-phenyl)phosphonium bromide
8D	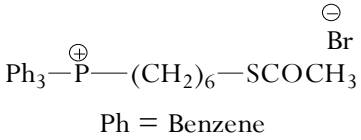	(6-Thioacetylhexyl)triphenyl-phosphonium bromide
9A	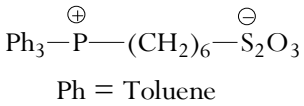	Tri(*p*-tolyl)phosphoniohexylthiosulfate zwitterion
9D	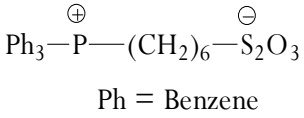	Tri(phenyl)phosphoniohexylthiosulfate zwitterion
12A	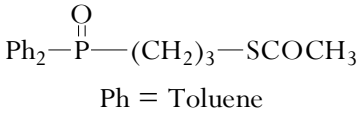	(3-Thioacetylpropyl)di-(*p*-tolyl)-phosphine oxide
12D	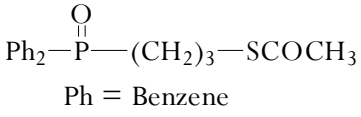	(3-Thioacetylpropyl)diphenylphosphine oxide
15	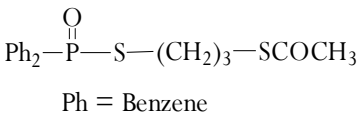	(3-Thioacetylpropyl)thiodiphenyl-phosphine oxide
18	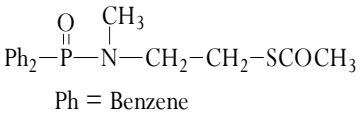	(3-Thioacetylethyl-N-methylamine)-diphenylphosphine oxide

Chapter 1: Literature review

1.1 Introduction

The development of safe and simple methods in order to detect and cure serious diseases, such as cancer, is considered to be one of the biggest challenges for researchers in the field of biotechnology and medical research [1]. Metal nanoparticles, including Au (gold), Ag (silver) and Cu (copper) nanoparticles (NPs), have been widely investigated over the past two decades as a result to their unique optical and chemical properties such as size, a high surface area [2]. For a specific critical application, the modification of NP surface using biocompatible materials is required. For instance, there are several types of gold nanoparticles (AuNPs) based on shape, size and chemical composition. These include spherical, nanorods, nanoshells, nanocages and SERS nanoparticles (AuNPs with a significant surface-enhanced Raman scattering properties) (Figure 1.1). Development of NP synthetic methods is still ongoing and most of the different types of metal NPs can be manufactured with well-controlled size distribution [3].

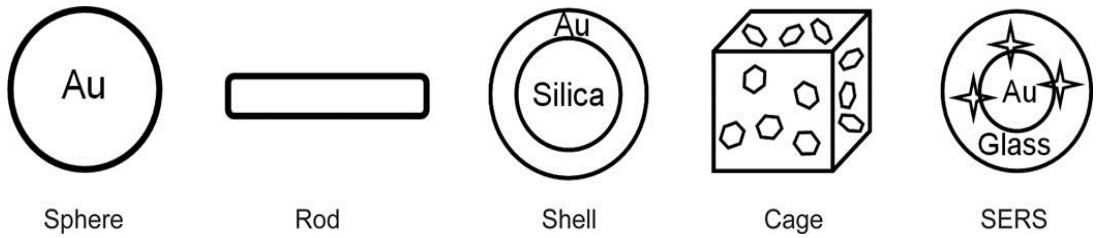

Figure 1.1. Different types of gold nanoparticles [3].

Nanotechnology has been applied in therapeutic treatment mostly in drug delivery in cancer therapy [4]. This is due to the fact that functionalised NPs have the ability to recognise and integrate with a biological matrix *via* the protecting ligands on their surface [5, 6]. For several years, NPs have been tested in the medical field in order to reduce side effects of cancer drugs by decreasing dosage of cancer drugs [4]. Some of the metal NPs reported in the literature have comparable sizes when compared to some biomolecules. Examples of these are proteins (1–20 nm), viruses (~20 nm), DNA (~diameter 2 nm), cell surface receptors (~10 nm), cell membrane (~6–10 nm), and haemoglobin (~5 nm) [7- 9].

NPs of 50 nm or less in size have shown ability to interact with DNA, proteins, enzymes and cell receptors extracellularly and intracellularly in human cells, which are hundred to thousand times bigger than these NPs [10]. For instance, smaller NPs of ≤ 20 nm in size have shown the ability to exit blood vessels and circulate throughout the body [10]. During the last decade, AuNPs were heavily tested for biomedical applications, (such as imaging, gene and photothermal therapies, and drug delivery) due to their unique or novel optical and chemical properties, as well as their stability [11-13].

The main focus of this literature review will be on the chemical and physical properties of biocompatible functionalised AuNPs, their synthesis, and stabilisation. Furthermore, their application in biomedicine will be discussed.

1.1.1 Optical and chemical properties of gold nanoparticles (AuNPs)

As previously mentioned, due to the unique optical, physical, chemical properties, stability and biocompatibility of AuNPs, they have been used in drug delivery, medical diagnosis and in cancer therapy [14]. AuNPs can be easily functionalised with several drugs or organic moieties *via* surface modification, which helps the uptake of such NPs by cell membranes [15, 16]. AuNPs are able to form stable bonds with sulfur containing molecules such as sulfides and thiols [17, 18].

These molecules have a strong affinity for noble metals and tend to protect AuNPs *via* forming well-ordered, self-assembled monolayers (SAMs), which leads to good dispersion, easy characterisation, and extraordinary stability. With no protecting ligands and no electrostatic repulsion, bare AuNPs tend to aggregate in solution as result to their high surface energy [17, 19]. Thiol containing ligands protect the AuNP surface against oxygen adsorption, which leads to increase their stability. In addition, the binding of functional molecules to the surface of AuNPs is facilitated through thiol groups, leading to a relatively stable Au-sulfur bond [20].

Moreover, 23-mercapto-3,6,9,12-tetraoxatricosan-1-ol (Figure 1.2) has been considered to be an excellent ligand base for biological applications and this structure can be easily adjusted to provide selective binding which makes AuNPs a promising platform for methodical biological studies [21]. Thiol and amine functionalised ligands can be used in order to synthesise stable AuNPs in both aqueous and organic media [22-25].

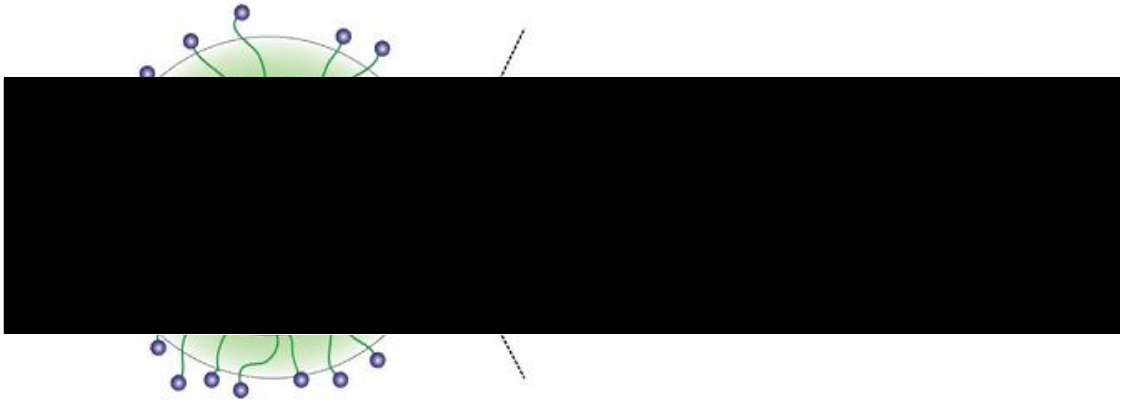

Figure 1.2. Chemical structure of AuNP functionalised by ligand contains three parts including the sulfur atom (binding directly with Au due to its strong affinity), alkyl chain and a tetraethylene glycol spacer [21].

Amine functionalised ligands have been used to stabilise the AuNPs, and produced NP sizes (from 2.5 to 7 nm), depending on the conditions of the synthesis. However, it is worth mentioning that the covalent bonds between Au atoms in the NP surface and amine are weaker compared with thiol groups [26, 27]

Amines, such as alkyl amines and the amino acid lysine are also used as protective ligands but their stability for AuNPs are moderate compared to both thiol and phosphine ligands. In order to get high AuNPs stability, aryl phosphines such as triphenylphosphine (TPP) and its' derivatives are used due to their phenyl rings which provide stability to AuNPs as a result to oxidation resistance of the phosphine itself [26]. Furthermore, thiols have higher affinity than phosphines towards AuNP surfaces. Phosphines showed lower binding energy compared to thiols [20, 28, 29].

The ligand ($Au_{55}[PPh_3]_{12}Cl_6$) was used to protect gold nanoclusters which have good properties such as uniform size and high chemical stability [17]. In contrast, small phosphine stabilised AuNPs with chemical formula $Au_{55}[(C_6H_5)_2P(C_6H_4SO_3Na)]_{12}Cl_6$ have been found to be highly cytotoxic in several cell lines, due to the interaction of these AuNPs with the DNA [20, 26]. Diphosphines can be also used as AuNPs protecting ligands. For example, 2,2'-bis(diphenylphosphino)-1,1'-binaphthyl was used to stabilise 1.7 nm AuNPs [26, 30].

AuNPs have different properties when they vary in size. For instance, colloidal solutions of spherical AuNPs are red with the SPR (surface plasmon resonance spectroscopy) band centred at approximately 520 nm and this band is often weakly dependent on the size of

the particle. However, strong changes have been noted with different shapes [31]. UV-Vis spectroscopy was used for real-time monitoring of AuNP size as shown in Figure 1.3 [32].

DLS and TEM have used measure the size and monodispersity of AuNPs [32]. Shape and size of the AuNPs can be controlled by varying experimental conditions such as reaction time, pH, capping agent and temperature, as well as the concentration ratio of reactants [2, 31].

As mentioned earlier, colloidal AuNPs, have different applications, based on their size and shape. With decreasing size, a lot of changes in physical and chemical reactivity were observed, such as an increase in the surface/volume ratio and a decrease in the melting temperature of AuNPs with size increased. AuNPs with size smaller than 5 nm were excellent for applications in catalysis. AuNPs can be formed by the deposition of a gold precursor, most often gold in the oxidation state Au (III) reduced to Au (0) and following its reduction into AuNPs due to a thermal treatment. This process is called deposition-reduction, as result of the instability of Au (III) compounds, a thermal treatment even under an oxidising atmosphere, oxygen or air, generally leads to producing AuNPs [33-35].

Particles with sizes of 10–300 nm offer strong light scattering, mostly in the visible range, and surface atoms are generally more active compared to closed-packed atoms inside the particle, as a result of their outwardly exposed dangling bonds [36].

The goal from controlling of growth of shaped AuNPs is to avoid any aggregation or instability, which makes NPs less hazardous for biomedical applications by avoiding degradation processes such as partial oxidation or undesired sintering of particles [37, 38].

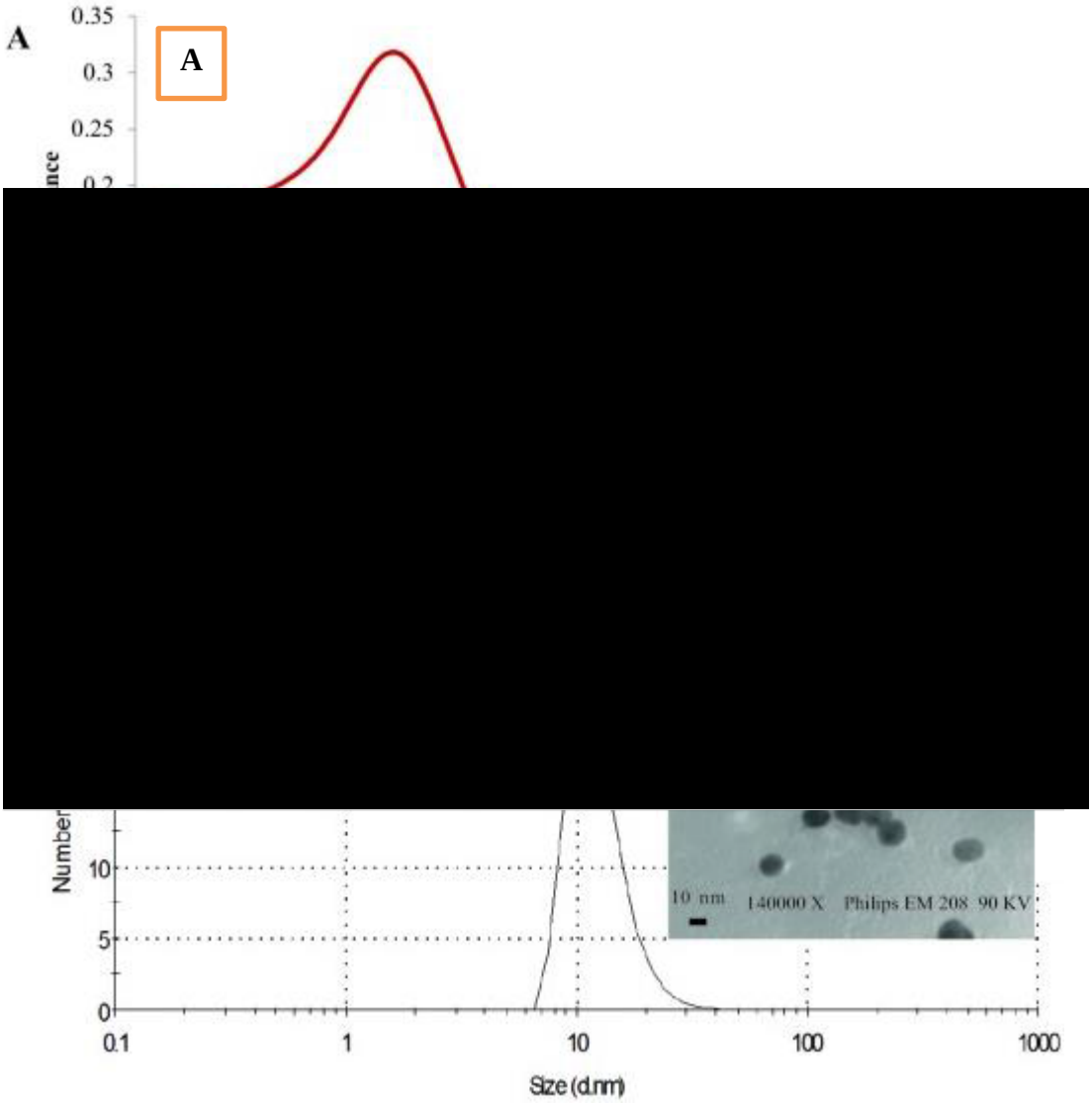

Figure 1.3. AuNPs characterised via (A) UV-vis spectrum; size distribution of AuNPs by using both DLS (B) and TEM (C), the scale bar is 10 nm) [32].

AuNPs are chemically stable and resistant to oxidation compared to other NPs such as silver nanoparticles [15]. It is worth mentioning that other similar materials such as silver and platinum exhibit similar properties in NP form. AuNPs, however, are much less expensive than platinum, and much less reactive than silver, making them a much better candidate for use in biomedical treatments [15].

1.1.2 Synthesis of gold nanoparticles

AuNPs were discovered by Faraday in 1857 [21, 39] who demonstrated the mechanism of formation of pure gold colloids and this synthesis was considered the bases a lot of the chemical routes for obtaining AuNPs with controlled shape, size and surface chemistry.

The first structural studies of AuNPs have been produced since 1951 by Turkevich., et al., [39-41], *via* electron microscopy. This was furthered significantly by Frens [39] who showed the possibility to control the size of spherical AuNPs from about 16 to 150 nm. These studies became starting point for many of the colloidal AuNP synthetic methods developed and reported in the literature [39-41]. The size of AuNPs can be controlled *via* varying the ratio of gold salt, reducing agent and stabiliser as mentioned early [2, 31, 39, 42].

1.1.2.1 Synthesis of AuNPs using chemical methods

AuNPs are produced due to a reduction of $HAuCl_4$ by a large number of reducing agents such as sodium citrate, borohydrides, formaldehyde, ascorbic acid, hydrazine, and hydroxylamine [43]. Sodium citrate has used as a reducing reagent and a protection ligand at the same time and AuNPs produced with variety of size / shape based on different concentration of citrate / $HAuCl_4$ ratios used [43, 44].

Small size of AuNPs are produced as a result of a faster reduction causing a high nucleation rate and a supersaturated solution. Small sized AuNPs were resulting of using a strong reducing agent such as sodium borohydride compared to a weakly reducing agent such as sodium citrate [45-47].

The aqueous reduction of $AuCl_4^-$ can be performed with an alternative reducing agent such as ascorbic acid (as a weak reducer). This is mentioned in Chapter 4 in the current study. The same protecting ligands were used in the case of $NaBH_4$ (used as a strong reducing agent), resulting in creating different shapes, sizes and stability of AuNPs. Poor stability, with big sizes of AuNPs was noted when ascorbic acid was used as reducing agent [45-47].

According to Goia, D and Matijević, E., [48] iso-ascorbic acid was used as reducing agent for $AuCl_4^-$ in aqueous solutions to generate monodispersed spherical AuNPs with sizes ranging from 5 nm to 80 nm. Sizes and shapes of AuNPs strongly depend on the concentration of protecting ligand used as well as on concentration of the ascorbic acid [43, 48].

1.1.2.1.1 Synthesis of gold nanoparticle in two phase solvent system and stabilisation by thiols

AuNPs of small sizes (2−2.5 nm) have been synthesised by Brust−Schiffrin method (BSM). Different functionalised metal NPs have been synthesised for the past 20 years by using this method. The stability of the synthesised particles was as a result of using alkane thiols, which offer strong Au-S bonds to the particle surface and good passivation. Instead of adding different amounts of reducing agent, the produced size can be in BSM by using different amounts of alkane thiol in the solution [49]. Despite BSM being widely studied, the synthesis process is not completely understood [50].

Another strategy used to produce cationic functionalised AuNPs is ligands exchange of monolayer protected AuNPs in the organic solvent as shown in Figure 1.4 [39, 51].

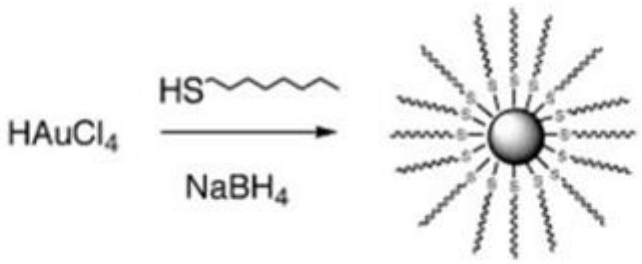

Figure 1.4. Brust-Schiffrin method: preparation of functionalised of AuNP by using two phases solvent system [39].

Using capping agents with strong affinity for gold is a common approach, which leads to the synthesis of AuNPs with good size dispersion in water. In some case, an additional step is required to transfer the NPs into water [31,52]. However, the phase transfer from aqueous to organic phase is often not easy, as result to the poor water solubility of the protecting ligands, which are used to stabilise the NPs. Various strategies have been used in order to facilitate this transfer, such as decrease the surface tension by an addition of acetone or a strong acid in order to neutralise charged AuNPs [39, 53].

Syntheses of AuNPs in aqueous solution have some advantages as AuNPs can be functionalised with different biocompatible ligands and bio-molecules, such as, DNA, enzymes, peptide. However, there is no possibility of coating AuNPs with bio-molecules in organic solvents [39, 53, 54].

In addition, AuNPs have prepared in aqueous solution with SPR bands in the near infrared and this kind of AuNPs is quite useful in biological applications, allowing for AuNPs in biological fluids without any interference from absorption of other biological molecules [31]. For example, bio-molecules with both negative and positive charged end groups such as peptides were functionalised an AuNPs in the size range 6, 8, and 16 nm, in aqueous solution. Some advantages were noted when protected ligands possessed different end charges. This will help to overcome aggregation, and generate NPs with high quality and narrow dispersions. These charged NPs can be used in biomedical applications [39, 55]. It is well known that the cationic NPs undergo different mechanisms in order to entry cells, and this will be based on NPs size, charge density, shape, purity and stability; and also based on cellular environment [56-58].

1.1.2.2 Purification of gold nanoparticles

Purification is required to obtain high-purity NPs samples; the results of NPs can be skewed due to small amounts of impurities. Purification methods are also important to develop reliable, rapid and convenient with NP produced high purity. Purification of NP samples can often be more challenging than the preparation itself. Filtration and solvent rinsing are the most used purification steps. These purification methods are normally sufficient to remove any impurities including residual Au salts and extra free ligands [28, 59]. In addition, filtration was used to remove small-molecule impurities from water-soluble NPs and for the isolation of small NPs from larger NPs in a single process. For example, 3-nm AuNPs functionalised by thiol-ligands was purified and separation of a poly-disperse sample into fractions of different core diameters. It is confirmed that, diafiltration generated higher degrees of purity of NPs compared with NPs purified by dialysis or a combination of solvent washes, ultracentrifugation, and chromatography [59].

In addition, there are many purification methods have been used in order to remove non-AuNPs components and decreasing the polydispersity, such as centrifugation, solvent extraction, ion-exchange, dialysis and diafiltration. Centrifugation is commonly used to remove non-AuNP components [59]. However, it has been informed that about 1.3% of the citrate that used in the synthesised AuNPs solution stayed in the treated solution after the purification process finished and could result in unneeded effects as changing in size of AuNPs and aggregation [59, 60].

Purification still has significant challenges to produce NPs without any affection on their structures and properties. For instance, purification has been found to have a significant impact on the optical properties of CdSe-NPs [61, 62]. Also, AuNPs were rapidly decomposed in the presence of excess thiol ligand [28, 59]. Furthermore, AuNPs in aqueous solution are not easy to purify, as result of the similar solubility of both the AuNPs and the impurities [60, 63, 64].

According to Sweeney, SF., et al., [59] colloidal NPs dispersed in non-hydroxylic solvents were separated using ultracentrifugation in an organic solvents which grant quick separation and high purification. By using this method colloidal NPs, synthesised and dispersed in an organic solution can be directly separated after production without transfer to an aqueous solution. This can avoid any possible aggregation of NPs [59].

Biomedical application of NPs functionalised by biomolecules to form bio-conjugated systems is receiving much attention. However, purification of these NP bio-conjugates from unbound free bio-ligands such as peptides is still a significant challenge due to similar solubility. The purification of the NP bio-conjugate such as polypeptide linkers is important in biological applications [60].

Alele, N., et al., [65] demonstrated that, removal of excess of unbound peptides after the bio-conjugation stage through AuNPs synthesis was achieved *via* exploiting the sieving properties of commercial regenerated cellulose (RC) ultrafiltration (UF) membranes. The polymeric membranes were used in order to remove unbound peptides from mixtures with bio-conjugated AuNPs-peptide. The purification function is depended on separating components of various sizes; selection is narrowed down by porous polymeric membranes which control the separation mechanism based on pore size and solute size variation [65].
Where traditional purification methods for bio-conjugated NP are considered to have some disadvantages such as being highly time consuming, tendency of aggregation and precipitation, and waste of required solvents [65, 66].

Furthermore, the stabilisation agents that are used for the preparation of the nanoparticles are considered as toxic additives; such as Cetyltrimethylammonium bromide (CTAB), for this reason, the impurities of NPs must be removed before any biomedical applications [60, 65].

1.2 Functionalisation of gold nanoparticles

Functionalisation of the NP surface is essential and can be achieved *via* the addition of a suitable protected ligands to the reaction solution. This will enhance stability of NPs and size control [67]. AuNP are usually coating with organic ligands. These ligands have to bind to the AuNPs surface and contain functional groups including carboxylate, phosphine, amine, or thiol groups [68].

1.2.1 Functionalisation of AuNPs using protecting organic ligands

In 1981 [26], AuNPs were synthesised in a non-polar organic solvent with phosphine as stabilising ligand for 1.4 nm AuNPs diameter. As well, AuNPs were stabilised with alkanethiols in 1993 by Mulvaney and Giersig, who illustrated the possibility of using thiols with a variety of chain lengths [26, 55]. Synthesis of highly stable AuNPs has been reported in the literature, using a mixture of citrate and thiol-containing ligands as coating agents [68, 69].

The chemical stability of mono-, di- and tri-thiol-stabilised AuNPs (2 nm diameter) was also investigated by Srisombat and co-workers [70]. They found excellent results when they stabilised AuNPs with di-thiols [28, 71].

It is found that the reaction time strongly depends on the type of thiol ligand (aromatic thiol or alkyl thiol) and this time generally increased with increasing chain length. Reactions times are usually longer in case aromatic thiols, and normally require more than 12 h to complete the reaction and that producing AuNPs with different sizes [28, 72].

Additionally, carboxylates such as trisodium citrate can also act as AuNP protecting ligands, due to electrostatic interaction with the NP surface [26, 73].

In addition, some protecting ligands used to functionalised AuNPs contain more than one function group such as mercaptosuccinic acid, 3-mercaptopropanoic acid, *p*-mercaptophenol, p-mercaptobenzoic acid, ω-bromoalkanethiols, and ω-carboxylic acid-alkanethiols, which contains carboxylate and thiol functional groups [74]. For example, Sihai Chen and Keisaku Kimura [75], prepared different sizes of highly stabilised AuNPs in a single-phase system based on the reduction of gold (III) by $NaBH_4$ in methanol using mercaptosuccinic acid (MSA) as the stabilising thiol ligand [75].

1.3 Stability of colloids gold nanoparticles

The stability of nanoparticles in solution is mostly dependent on the surface properties of NPs such as surface charge and protecting ligand structure [6]. Stable novel AuNPs have been synthesised and characterised with different ligands at different pH in this thesis. The pH-sensitive metal NP according to the present invention can be prepared by attaching a compound varying in charge with pH to the surface of the metal NP [6].

A new synthetic route has been used for the synthesis of monodisperse AuNPs *via* varying the solution pH with controlled concentrations of $HAuCl_4$ and reducing agent [44]. In addition, pH value was considered the important parameter, to control the size and shape of AuNPs. For example, the results showed that spherical AuNPs in the range of 10–20 nm were observed at pH 7, where the results indicated the stability of AuNPs for exacts three months with only a little aggregation. It is noted that strong relationship between pH increasing and both of the reducing power and reaction rate increasing correspondingly and that could contribute to the formation of thermodynamic-favoured spherical particles [76].

In this thesis, AuNPs functionalised with different ligands were subjected to a study of stability over time at a variety of pH. A systematic analysis of the synthesis of the ligands, AuNPs and stability studies were carried out to determine the suitability of the AuNPs for both bio-recognition and drug delivery purposes. We used some different thiol-containing ligands as modification ligands of AuNPs and evaluated the abilities of these thiol ligands for stabilising colloidal AuNPs with different pH values and gold salt concentrations. Different effects of various thiol ligands on the stability of AuNPs and that confirmed using UV / Vis spectroscopy and DLS (Dynamic light scattering). It was found that ligands containing (methoxy-benzene groups)-modified AuNPs were most stable compared to other thiol compounds containing (benzene or toluene). From the literature, it found the spherical AuNPs at pH values < 7 were not conserved and aggregation occurs quickly. However, partial stabilisation was observed for pH < 7, the situation improved drastically for pH values above 7. While for pH 8.0, a plasmon resonance peak was observed at about 530 nm for up to 3 h. and at pH 10.0, the peak position was remained at 524 nm and remained stable for up to 2 months [77].

Due to the importance of pH which is considered a key parameter for several biological processes and also a significant indicator for disease progression, such as endocytosis, (a process in which substances have been engulfed by cells, is involved with changing pH values from neutral to acidic (pH 6.2-4.5) [78, 79]). Tumour cells have an acidic microenvironment which is different from other normal cells, as result to the high metabolic rate and inadequate oxygen supply of tumour cells [80, 81]. This plays a significant role in cancer treatment nowadays, using AuNPs which are aggregated at low pH. The aggregates absorb far-red and near infrared (NIR), which can be used for photothermal therapies guaranteeing maximal tissue penetrations [82-84]. The NIR light irradiation is used as photothermal therapy of cancer cells without making any damaging for normal cells, which have pH at 7.4 [82].

AuNPs have been fabricated with pH-aggregation behaviours of modifying their surface with mixed-charge self-assembly monolayers compromising negatively and positively charged thiol ligands. AuNPs can respond to pH change and form aggregates [83, 85]. For example, some of the negative charges would be shielded at lower pH due to the protonation of the carboxyl group in MUA (11-mercaptoundecanoic acid) which leads to rapid aggregations between AuNPs [83].

For instance, the AuNPs coated by primary amines were dispersed under mildly acidic conditions such as pH 6. While, were not stable at pH 9, for the reason, the primary amines are no longer protonated at pH 9. It can be stressed that AuNPs can efficiently accumulate and form aggregates inside of cells. The accumulated AuNPs aggregates can destroy cancerous cells in response to the external illumination system. Furthermore, the AuNPs with proper surface ligand composition exhibited aggregation in a tumour of acidic pH. Investigations of pH-induced aggregation behaviours of spherical mixed charge-AuNPs, is mainly founded on small sizes (≤ 16 nm) nanoparticles [82].

pH-induced aggregations were obtained at pH 7.0, 7.8, and 9.2 at different size 15, 21, and 33 nm of mixed charge-AuNPs, respectively [82]. At significantly differing pH**,** the size of AuNPs is dependent on the initial pH of the aqueous solution. Thus, the stabilisation of AuNPs in pH > 7 can be due to the conversion of $[AuCl_4]^-$ to a less reactive $[AuCl_{(4-n)}\ (OH)_n]^-$ anion, where (n) increases with pH increased (Figure 1.5) [77, 86,87].

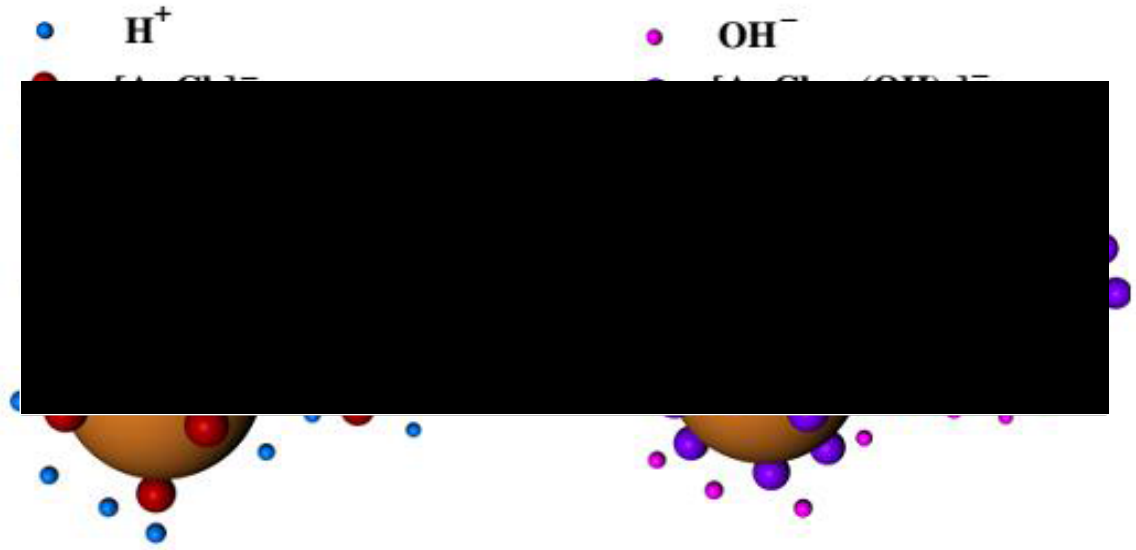

Figure 1.5. Diagrammatic depiction of stabilisation of AuNPs [77].

At pH larger than 6.5, spherical AuNPs are obtained with diameter 15 nm [88]. In addition, it is noted that AuNPs were more broadly distributed at lower pH conditions. For example, at pH lower than approximately 3.8, AuNPs can no longer dispersed after completed preparation which is similar to the results collected from this thesis [88].

According to Nam, J., et al., [89] conjugated Doxorubicin AuNPs, 10 nm in size, were designed to aggregate in a mildly acidic environment within tumour cells to treat WHAT CANCER. Furthermore, they effectively accumulate in cancer cells up to 17 times more than the control due to enhanced permeation and retention [89]. The high tumour accumulation of AuNPs is thought to result from the efficient permeation into cancer cells through their small size and their aggregation capability, which can diffuse and penetrate deeply into the extracellular matrix of tumour cells [89].

1.4 Biocompatibility of gold nanoparticles

Researchers illustrated AuNPs are non-toxic and have minimal toxicity over a large range of concentration, encouraging researchers to use AuNPs in medical applications [15, 58, 90]. Furthermore, AuNPs at higher concentrations inhibit both the production of reactive oxygen species (ROS) and reactive nitrite species (RNS). Also, AuNPs have confirmed biocompatible properties such as nontoxicity, non-immunogenic, and high tissue permeability without impeding cell functionality [58]. Recent advances of AuNPs,

conjugated with biomolecules have encouraged scientists to tailor AuNPs for purposes, such as, chemical reactions inside cells. The reason for the successful development of these challenging tasks depends on both surface structure design and their ability to synthesis AuNPs bio-conjugates with the desired sizes based on bio application [15].

There is a current interest in modifying the surface chemistry of AuNPs, due to excellent advantages of AuNPs in cancer treatment when compared with other metal NPs. These advantages are based on their enhanced scattering, absorption properties and efficient bio-conjugation [91]. AuNPs also have shown to possess good ability in cancer cell imaging due to the strong scattering properties. Their strong absorption characteristics can offer the possibility to use them in photo-thermal therapy [22, 92]. It has been shown that apoptosis of cancer cells can be induced with less than half of the energy this is needed when HaCaT benign cells are incubated with anti-EGFR antibody conjugated AuNPs. According to the literature, it is found that the cancer cells require less than half the laser energy to be killed than the healthy cells [92].

1.4.1 Principle of cationic cellular uptake of gold nanoparticles

There are several studies about the cationic AuNPs [39, 93, 94]. These positively charged AuNPs have been used as scaffolds for DNA binding by Rotello, VM and co-workers [98]. This finding resulted from their interaction with negatively charged DNA, showing their transfection ability into a cultivated cell line. As well as, it is found that AuNPs with cationic average 68% were better and viable transfections vector in comparison with highly charged cationic AuNPs [39, 95].

Cationic AuNPs have been used as DNA transfection agents. For example, aminoethanethiol capped AuNPs of roughly 33 nm in diameter showed high transfection efficiency. Another example for transfection used cationic lipid coated AuNPs of 14 nm in size [39, 96, 97].

It is important to note that similar NPs have exhibited different mechanisms of entry into different cells. For example, the cationic AuNPs have the ability to target the nucleus after cross cell membranes. However, negative AuNPs and neutral AuNPs that have the same size and shape of cationic AuNPs cannot penetrate cell membranes [39, 98-101]. In addition, cationic AuNPs can bind to negatively charged groups of the cell membrane, and across the plasma membrane *via* generation of transient holes. Moreover, the positive

charge encourages AuNPs to interact with anionic phospholipids within the cell membrane and causing endocytosis [39, 102].

According to Cho, EC., et al, [39, 101] the neutral and negatively charged AuNPs such as (citrate- and poly vinyl alcohol (PVA)-coated AuNPs have a low affinity to interact with the cell membrane (Figure 1.6). However, positively charged AuNPs have a high-affinity binding with cell membrane [39, 98].

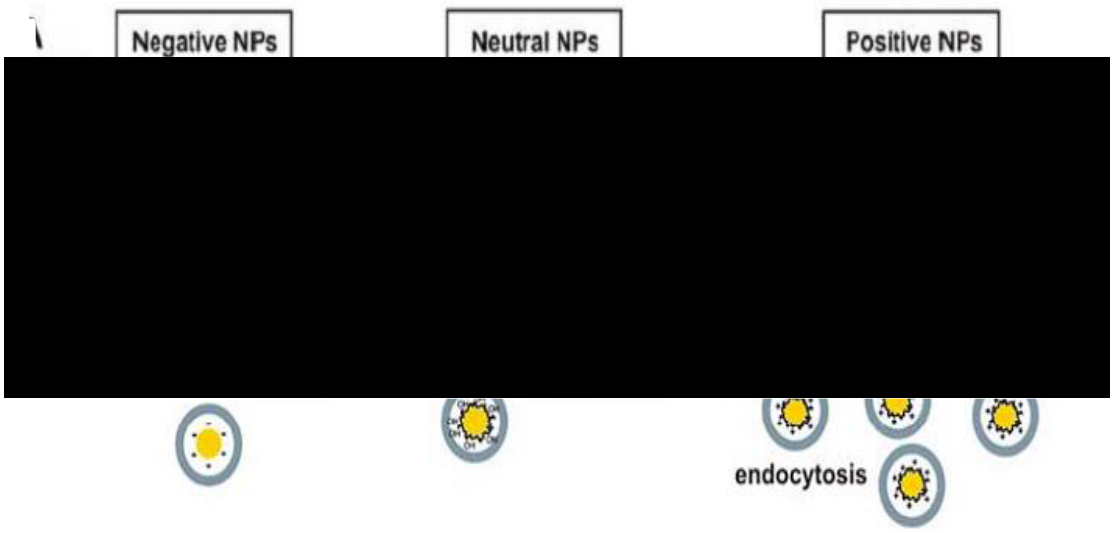

Figure 1.6. Interactions between different surfaces charges of AuNPs with SK-BR-3 (human breast cancer) cells [39].

Cationic AuNPs modified with 2-aminoethanethiol, have a short alkyl chain, formed a complex with plasmid DNA, and could be transfected into cultivated cells as shown Figure 1.7 [100].

Cationic AuNPs and the DNA complexes have been used functional gene delivery, in a strong controlled release manner of DNA at a desired site triggered *via* exogenous stimulation, such as light irradiation [97]. Also, attachment of DNA vaccine to AuNPs *via* protamine appears to stabilise the DNA. These Au–protamine–DNA conjugates supply the DNA resistance to physicochemical and temperature-accelerated degradation and prolong the DNA vaccine activity [103, 104].

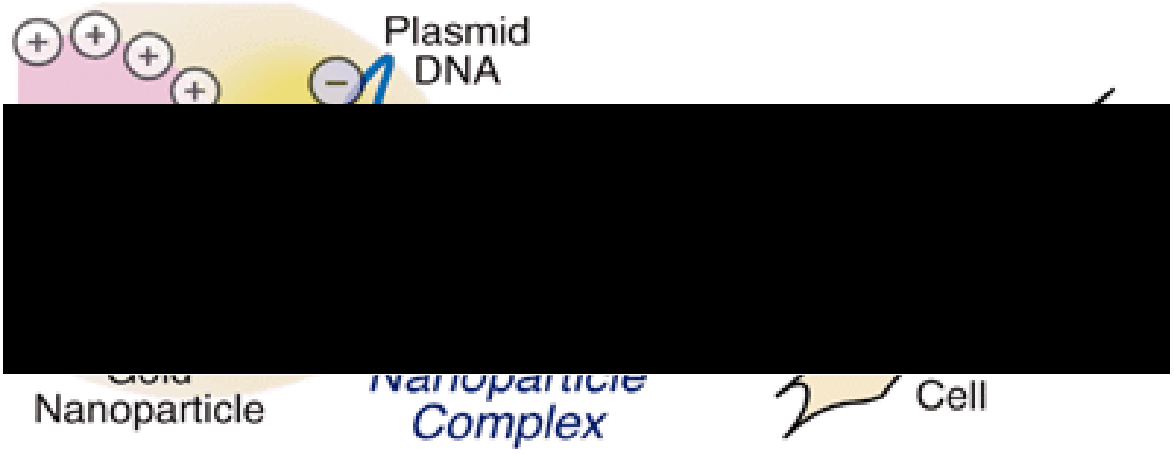

Figure 1.7. AuNPs functionalised by primary amine with their transfection ability into cultivated cells [97].

The phosphonioalkanethiol functionalised AuNPs was be suitable for therapy mitochondrial gene. It has been shown, when an antioxidant was attached to phosphonioalkanethiol, the resulting conjugate accumulated several hundred-fold within mitochondria in cells, blocked mitochondrial oxidative damage, and influenced mitochondrial redox signalling (Figure 1.8) [105]. Also, this conjugate has been found to block oxidative damage in isolated mitochondria and cells far more effectively in comparison with untargeted antioxidant counterparts due to their concentration within mitochondria [106-108].

Moreover, it is showed that cationic lipophilic compounds which contained a triphenylphosphium group selectively have been accumulated in the mitochondria of carcinoma cells in comparison with healthy cells as consequence of the characteristically elevated plasma membrane potentials of neoplastic cells [105].

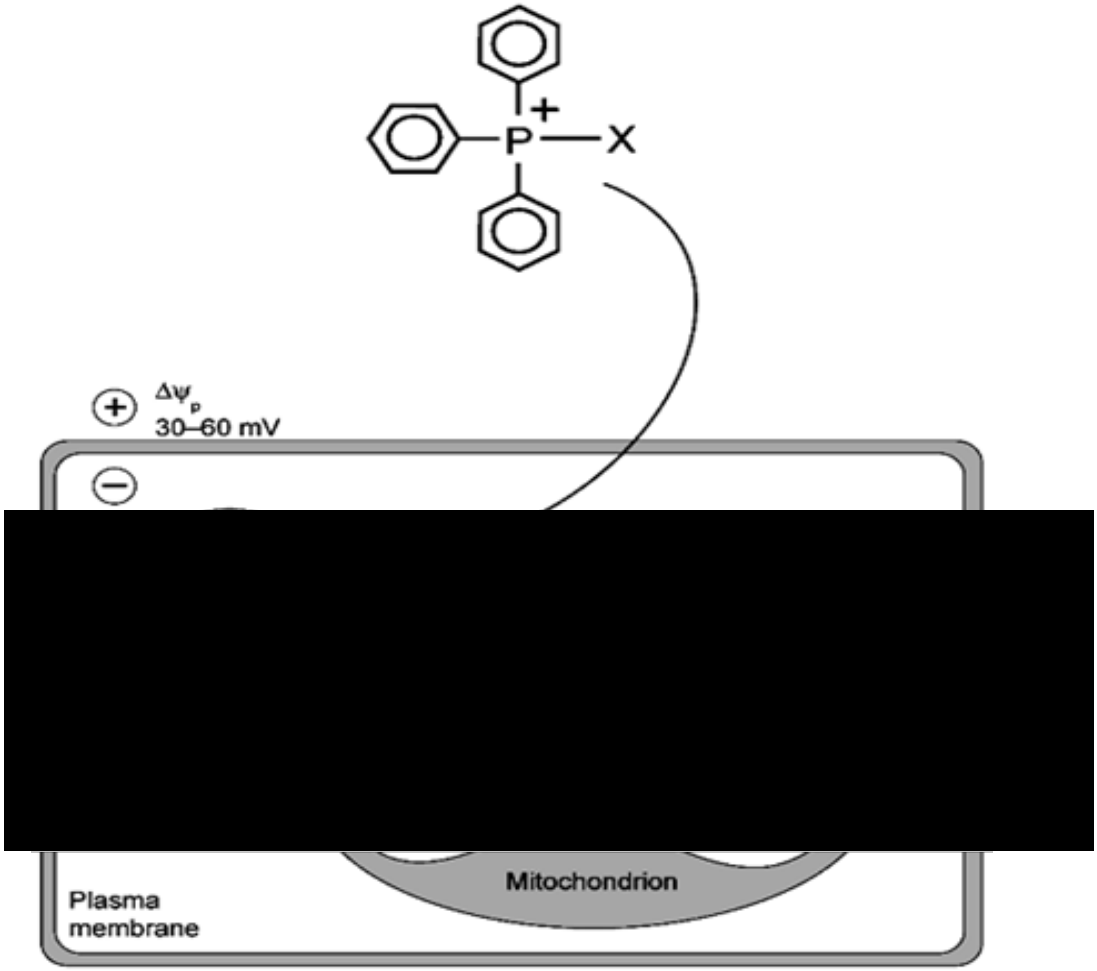

Figure 1.8. Triphenylphosphonium cation used as non-viral DNA delivery vectors in gene therapy [105].

1.4.2 Physicochemical properties of cationic functionalised AuNPs inside of the extracellular fluid

AuNPs enter the body by different ways such as dermal exposure, oral administration and intravenous injection, and then contact with bio-molecules such as lipids, proteins, and nucleic acids. Proteins and other biomolecules can be easily adsorbed onto AuNPs surface to form a protein corona around AuNPs when AuNPs enter biological fluids. This leads to decrease the free energy of surface AuNPs. Creation of a corona may change structures of adsorbed proteins and eliminate the proteins physiological function, causing the loss of original targeting capabilities *via* the high ionic strength and protein layer density around surface of AuNPs, that can induce several cellular responses such as, increased lysosomal permeability, activated cell apoptosis in different organs or tissues [109].

Moreover, the composition NPs and surface charge are key determinants of protein adsorption, particularly with cationic AuNPs which interact with the protein's negatives

charge. Also, interactions of NPs with proteins can affect the biocompatibility of NPs and their internalisation in cells [39, 57, 110]. The formation of a corona of AuNPs protein is the main factor was for the nano-bio mediator to interact with the cells. From the literature, it is found that the S–S bonds were broken in order to form Au–S bonds, causing changes in the conformation of lysozyme on the surface of AuNPs, inducing protein unfolding and protein–AuNPs assembly formation, and resulting in protein aggregation [109].

1.4.3 Toxicity of gold nanoparticles

AuNPs toxicity studies have been contradictory, with interactions between AuNPs and tissues at the cellular level, intracellular and molecular level still misunderstood [111]. Although some studies have shown no cell toxicity after AuNPs interaction, other in *vitro* and in *vivo* studies have demonstrated the production of reactive oxygen species cell, mitochondrial toxicity, release of cytokines, necrosis and apoptosis [101, 111]. In order to be useful for cancer treatment, the AuNPs must be non-cytotoxicity for normal cells. This cytotoxicity has been much studied, and several parameters have involved the concentration, the nature of the ligands bonded to the AuNPs core and the targeted cells [54]. Furthermore, improvement of in *vitro* cytotoxicity was suggested that the delivery according to the AuNPs of anticancer drug could improve their power especially, perhaps *via* improved cellular uptake. AuNPs use near-infrared radiation to induce cytotoxicity effect, where toxicity of AuNPs depend on their concentration [112]. It also can significantly be seen that after 24 hours of incubation with bio-conjugates, AuNPs positive and negative, no particles showed significant toxicity at concentrations of 0.5 nM and 5 nM of AuNP [110].

According to results reported in 2008 some AuNPs are toxic for cancer cells at a concentration of 100 µM [54, 113], however not for immune cells. The precursors $HAuCl_4$ and (CTAB) which are used for their synthesis are toxic at a concentration of 100 µM. AuNPs functionalised by ligands positive charged are generally toxic at concentrations below those at which negatively charged ligands are cytotoxic. For example, AuNPs functionalised tri(methyl)ammonium-ended alkylthiolate ligands completed are more toxic compared with those ended with carboxylates [54, 114].

In addition, in previous study, 15 nm citrate capped AuNPs were toxic in cancer cells, but less toxicity from 1.4 nm AuNPs capped with triphenyl phosphine mono-sulfonate [101,

115]. It was noted that toxicity was slightly higher for cationic NPs compare with the anionic ones, maybe due to a different interaction of NPs with cellular membranes [101].

Additionally, 1.4 nm diameter of AuNPs causing cell death produced rapid necrosis *via* oxidative stress and mitochondrial damage, in a matter of hours [101, 115, 116]. AuNPs are synthesised with a variety of coatings, which also seems to influence the toxicity, for instance, triphenylyphosphine, a commonly used ligand functionalised AuNPs 1.4 nm appears to be more toxic particles comparing with similar size coated with glutathione. Toxicity appears to depend on the size and ligand type and as such can potentially be controlled [101, 117]. Additionally, increasing the hydrophobicity of the particles leads to increasing their cytotoxicity and also ROS production [26]. On the contrary, some researchers confirmed the AuNPs, even if not toxic, but are not totally bio-compatible. This confuse can be due to different factors influencing the potential toxicity of AuNPs which include surface chemistry, coating materials, shape, size, and biological target tested [118].

It is important to distinguish between cytotoxicity and cell damage. AuNPs that show little or no cytotoxicity by several standard tests, may still be able to cause serious damage to the cells. For instance, 13 nm AuNPs functionalised citrate are not toxic, according to an assay in a dosage in the skin cells, while the particles, are used the formation of abnormal actin filaments, leading to a decline of the proliferation of cell, motility and adhesion [39].

There was no indication of any AuNPs effect could have on the cell metabolism or proliferation. This result is significant, given the increased absorption in the case cationic AuNPs bio-conjugates [110]. Furthermore, Colloidal AuNPs are well-known and safety in human cells have been characterised [92]. Substantially all cases showed a higher uptake of bio-conjugates for cationic surfactants compared with their anionic counterparts (Figure 1.9) [110].

Maximum uptake (44.5%) was observed for 5 nm bio-conjugates cationic AuNPs after 3 hours, and a dilution of 10 times of the particles leads to 31.5% of uptake in the same incubation period. This contrasts with the maximum of 5% of uptake was obtained in the best case internalisation with bio-conjugates anionic AuNPs (incubation of 5 nM concentration AuNPs at 3 hours) (see Figure1.9) [110]. Bio-conjugated AuNPs positive

surface charge can be responsible for more interaction with the cell membrane; can be attracted as result to of the inherent negative charge of phospholipid bilayers. From there, it seems that the AuNPs did not penetrate and passes through the membrane, but accumulated until the membrane is recycled and AuNPs internalised in endosomes, as revealed by TEM [110, 119]. Also, tumour tissues are more permeable and more heterogeneous in size larger in comparison with normal tissues [54, 120].

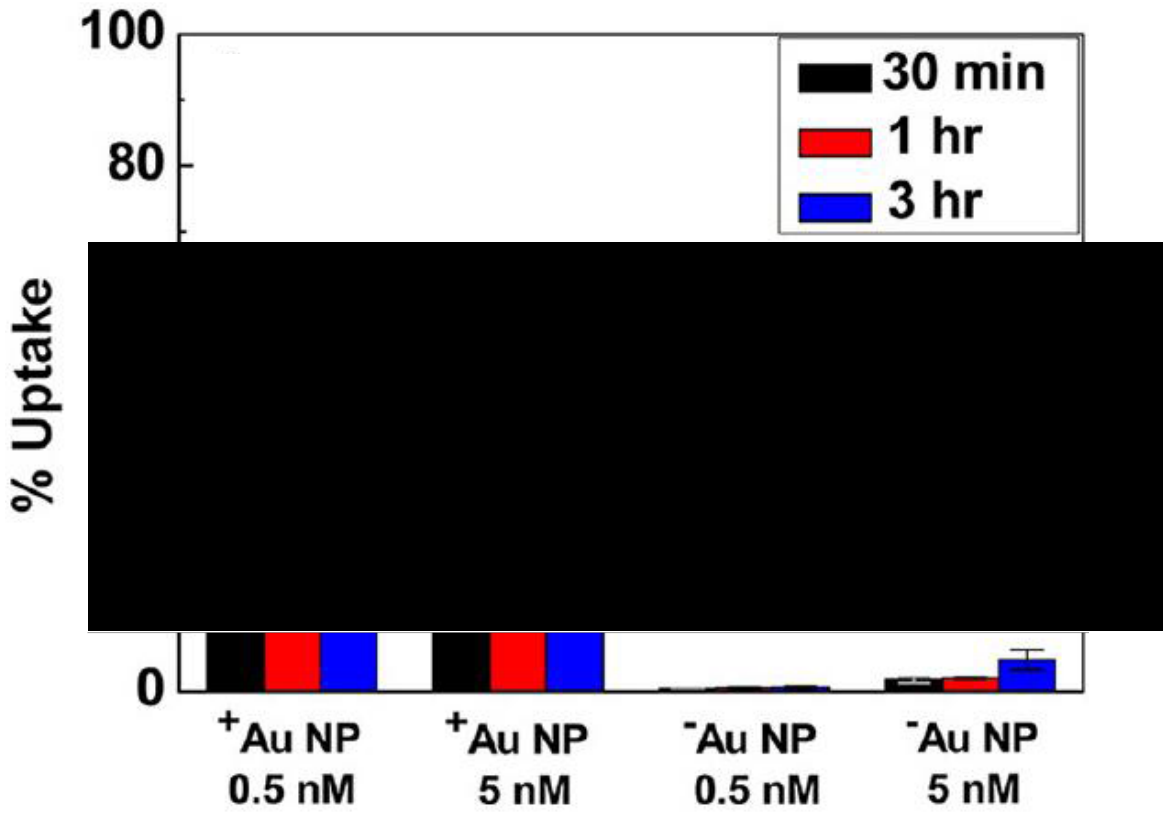

Figure 1.9. Intracellular Au-concentration as determined by ICP-MS analysis as a function of time. Where data present the average of three experiments with standard deviation [110].

1.4.4 Accumulation of gold nanoparticles in organism tissue

AuNPs with the small size should be rapidly cleared from the interstitial space of cancer cells; compared with a large AuNPs size which has slow clearance from the tumour cells, due to the effective accumulation and high retention of the large AuNPs in the cancer region [89, 121].

The effects of using AuNPs and distribution depend on the way in which they are administered (subcutaneously, intramuscularly, or surface) and their size. The AuNPs

reach the lymph nodes more easily when their administration is subcutaneous. The administrations have been found to accumulate predominantly in the bladder, liver, and lungs regardless of size. In fact, 10 nm AuNPs accumulate in many tissues, while 200 nm AuNPs were detected mainly in the liver, bladder, and blood, brain, and pancreas [54, 117, 122].

According to Hirn and o-workers [123] the percentage of accumulation of the AuNPs in various organs and tissues was different based on their sizes and surface charge. The accumulation is increased with size decrease. Also, AuNPs 2.8 nm negatively or positively charged, were found in the spleen. Positively charged AuNPs have shown a significantly higher accumulation percentage (11.4%) than the negative AuNPs (8.6%) [123].

1.5 Application of gold nanoparticles in biology and medicine

Multifunctional NPs have been developed *via* new experiments which aim to encapsulate both therapeutic and imaging agents in one nano-carrier and including more than one ligand on the surface. Thus, they have the capacity of targeted tumour imaging and the delivery of therapeutic agents [16].

1.5.1 Gold nanoparticles for cancer diseases

There are several treatments for cancer including chemotherapy, radiotherapy, gene therapy, but all therapies have disadvantages such as effective on healthy cells. So, one of the significant challenges is to confine the treatment only to the tumour cell without causing damage to healthy cells [15, 111].

AuNPs have been used as carriers for delivery drug to target genes in desired cancer cells. Likewise, AuNPs used as multifunctional NP *via* combining diagnosis, imaging with a treatment of cancer diseases at the same time [15, 111, 124]. AuNPs have a high accumulation and more ability to penetrate in cancer cells than in healthy cells. This may be due to rich permeable vasculature around the tissues of cancer cells. However, the conventional therapy of cancer disease does not effectively differentiate between cancerous and normal cells [15, 93, 125].

One of the important challenges in cancer therapy includes the low bioavailability and toxicity of cancer drugs. NPs can play a crucial role by delivering drugs in a targeted fashion to the cancer cells which will decrease the systemic toxicity of the anticancer drugs [126], also, NPs have the ability to improve on drug tolerability, circulation half-life and efficacy [127].

In addition, the AuNPs functionalised to be sensitive to pH were also used in order to stimulate the drug release triggered at a specific site of disease using the low pH condition of the tumour cells. The AuNP was stable at pH 7.4 and does not undergo hydrolysis for a long time. In contrast, at pH 5.0 the AuNP was rapidly and completely hydrolysed in 2 h and the release of drugs from AuNP was remarkably faster at pH 5.0 compared at neutral pH [80]. Furthermore, about 9% to 15% of patients benefited from surgery by removed cancer tissue. For example, for all stages of pancreatic cancer, they found the median survival is 3-5 months from diagnosis [126]. It is predicted that, if NP carrying anticancer drugs can be supplied in a targeted manner, inhibition of tumour growth with a reduced toxicity can be achieved [10].

In addition, there is a strong interest to modify existing drugs in order to improve pharmacokinetics, reducing the side effects and allowing the delivery of higher doses to the target tissues. An important manifestation of potential AuNPs multifunctional drug delivery has been the use of 5 nm AuNPs as a delivery vehicle, covalently bound to the active agent such as Cetuximab and Gemcitabine (see Figure 1.10). The payload of therapeutic pancreatic cancer drug can be achieved with minimal accumulation in the in the liver or kidney. Low gemcitabine doses (2 mg kg^{-1}) resulting in 80% inhibition of tumour growth in an orthotopic model of pancreatic cancer in comparison with 30% inhibition with conjugated agents in combination [111, 128, 129].

Patra, CR., et al., [126] illustrated that, only 30% to 40% AuNPs that bound gemcitabine was released after an incubation period of 6 hours, and about 45% was released from the nanocomposites over 24 hours. These results indicate stability of the nano-conjugates in a physiologic salt concentration [126].
It has been reported that, a dose of 250 mg/kg of gemcitabine in pancreatic tumour caused 58% inhibition of tumour growth. However, a dose of 7.5 mg/kg did not inhibit tumour growth significantly [126].

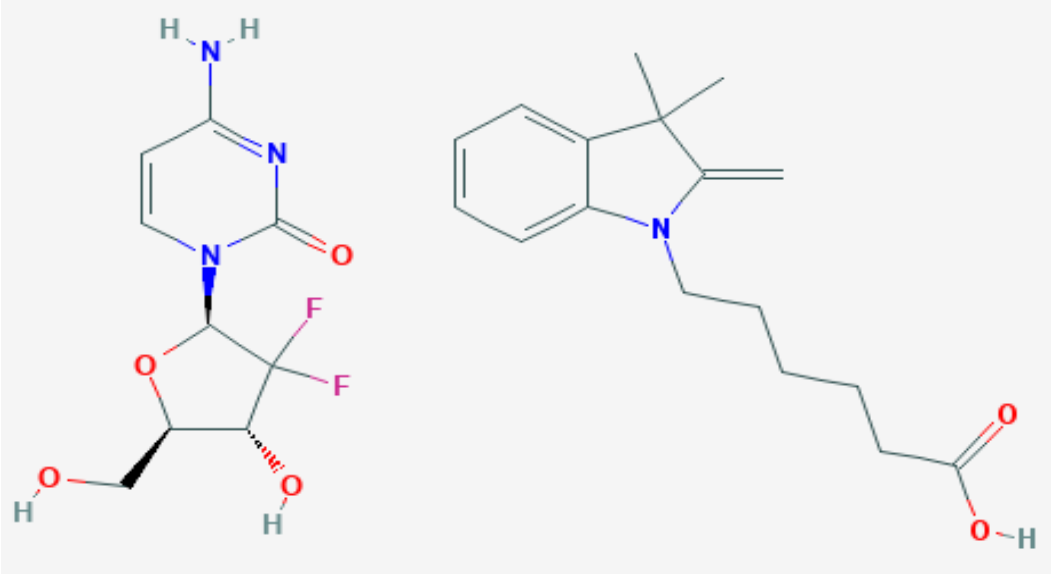

Figure 1.10. Structure of Gemcitabine (left) and Cetuximab (right) (Figure is taken from https://pubchem.ncbi.nlm.nih.gov/compound/gemcitabine#section=Top

It is obvious that, there was not any increased gemcitabine retention upon Nano-conjugation compared with free gemcitabine alone. These results demonstrate that the observed effectiveness at a lower dose is due to the targeted delivery and not due to a greater retention of Nano-conjugation [126, 130]. In addition, in order to increase NP retention in tumour cells, NPs have been designed to reverse their surface charge from neutral / negative to positive at the tumour site as shown in the literature [127].

According to Patra, CR., et al., [10] combination NPs with drugs in chemotherapy has been demonstrated to be better than drugs alone for many solid tumours [10]. Recent reports have shown no effect of toxicity in mice up to 1 year after injection of AuNPs 1.9 nm [126].

Hyperthermia has been used to induce apoptotic cell death in many cancer tissues. However, due to difficulties in heating deep tumours to therapeutic temperatures after initial treatment have limited the use of hyperthermia in the treatment of cancer. All recently nanomedical research offer the potential to specifically target metal NPs to tumour cells. [111, 131].

1.5.2 Gold nanoparticles against bacteria

Bio-applications of nanoparticles have increased markedly in recent years. It was detected that bacterial count in the liver was decreased about 20-fold after AuNPs conjugated ciprafloxicin were used as antibiotics compared to the free drug. The AuNPs are less toxic to biological system. The dose of antibiotics for the treatment purpose is often much higher than the dose required in order to kill the pathogens. This could produce toxic effects in the dose. Dose should be reduced by successful AuNPs antibiotic therapy and for this reason AuNPs have been used to address the problem associated with traditional antibiotics [132]. AuNPs functionalised by specific ligands offer significant effect in this field. For instance, the synthesis of thiol-stabilised AuNPs with core diameters between 5-26 nm in this thesis, have an effect on some kinds of bacteria, (Chapter 6). Successful application of some of the AuNPs exhibited high antibacterial activity. Different concentrations of AuNPs were tested as anti-bacteria. High concentrations had a high effect on both kinds of bacteria including *Escherichia coli* and *Staphylococcus aureus*. This demonstrated that, the inhibition of a bacterium by AuNPs is dose-dependent [133, 134].

Aims of the project

The aim of this thesis is to synthesise and characterise novel cationic alkane thiolate derivatives, which are used to functionalise AuNPs for potential uses as alternative biorecognition and drug delivery systems. Within this research area, laboratory work was focused on the synthesis and stability of these AuNPs. Comparison between phosphonium-thiolates ligands (Ph_3-P-$(CH_2)_n$-S_2O_3) with different aromatic groups such as benzene, toluene or trimethoxy-benzene has been carried out, in order to see potential effects on the stability of the functionalised AuNPs. The AuNPs synthesis conduct in one of two ways with reduction by a biphasic solvent system of DCM/water, and monophasic medium DMSO. The cationic phosphonium AuNPs investigate with their stability over time at a pH range of 3-11. AuNPs prepare by the reduction of $KAuCl_4$ using different reducing agent power including sodium borohydride and ascorbic acid as biocompatible reducing agents, and that can be used to assess the hydrophobic, cationic properties of the AuNPs for use in biorecognition such as antibiotic.

Outline of the thesis

In Chapter 2, a brief description of the analytical methods employed to characterise all the novel compounds obtained in this thesis is outlined. The analytical devices used to include FTIR, NMR, ESMS, TEM, DLS and UV-Vis. Synthesis phosphonium cationic AuNPs in a two-phase liquid-liquid (DCM/H_2O) and one phase (DMSO), described in Chapters 3 to 5.

Chapter 3 contains the description of the synthesis of cationic AuNPs reduced by sodium borohydride as reducing agent in aqueous medium and the stability of AuNPs have been measured at different pH (3-11). The influence of the different ligands on the stability of AuNPs is investigated by TEM and UV-Vis measurements.

Chapter 4 synthesis AuNPs by different reducing power including ascorbic acid as biocompatible reducing agent (weak) and $NaBH_4$ (strong) are presented. Big sizes with less stability have been generated in the case of the ascorbic acid was used compared in the case of $NaBH_4$.

Chapter 5 AuNPs have been stabilised through using protecting ligands such as phosphine oxide derivative ligands.

Chapter 6 demonstrates the bio applications of cationic phosphonium AuNPs with average size from 8.0-11 nm, where AuNPs in this thesis offered ability to effect on some kinds of bacteria including, Gram- Negative Bacteria such as *E. coli* and the Gram-Positive Bacteria like *Staphylococcus aureus*.

Chapter 7 contains a summary of the conclusion and some suggestions for future work.

1.6 References

1. Yao, J., Yang, M and Duan, Y, *Chemistry, biology, and medicine of fluorescent nanomaterials and related systems: new insights into biosensing, bioimaging, genomics, diagnostics, and therapy.* Chemical reviews, 2014. **114**(12): p. 6130-6178.

2. Shan, J and Tenhu, H, *Recent advances in polymer protected gold nanoparticles: synthesis, properties and applications.* Chemical Communications, 2007(44): p. 4580-4598.

3. Cai, W., Gao, T., Hong, H and Sun, J, *Applications of gold nanoparticles in cancer nanotechnology.* Nanotechnology, science and applications, 2008. p.17-32.

4. De Jong, WH and Borm, PJ, *Drug delivery and nanoparticles: applications and hazards.* International journal of nanomedicine, 2008. **3**(2): p. 133-194.

5. Sapsford, KE., Algar, WR., Berti, L., Gemmill, KB., Casey, BJ., Oh, E., Stewart, MH and Medintz, IL, *Functionalizing nanoparticles with biological molecules: developing chemistries that facilitate nanotechnology.* Chemical reviews, 2013. **113**(3): p. 1904-2074.

6. Gao, J., Huang, X., Liu, H., Zan, F and Ren, J, *Colloidal stability of gold nanoparticles modified with thiol compounds: bioconjugation and application in cancer cell imaging.* Langmuir, 2012. **28**(9): p. 4464-4471.

7. Alexis, F., Rhee, J-W., Richie, JP., Radovic-Moreno, AF., Langer, R and Farokhzad, OC. *New frontiers in nanotechnology for cancer treatment*. in *Urologic Oncology: Seminars and Original Investigations*. Elsevier. 2008.26(1): p.74-85.

8. Loos, M, *Carbon Nanotube Reinforced Composites: CNT Polymer Science and Technology*. Elsevier. 2014.p. 1-33.

9. Ju-Nam, Y and Lead, J, *Properties, Sources, Pathways, and Fate of Nanoparticles in the Environment.* Engineered Nanoparticles and the Environment: Biophysicochemical Processes and Toxicity, 2016. P. 39-117.

10. Patra, CR., Bhattacharya, R., Mukhopadhyay, D and Mukherjee, P, *Fabrication of gold nanoparticles for targeted therapy in pancreatic cancer.* Advanced drug delivery reviews, 2010. **62**(3): p. 346-361.

11. Zhao, Y., Gu, X., Ma, H., He, X., Liu, M and Ding, Y, *Association of glutathione level and cytotoxicity of gold nanoparticles in lung cancer cells.* The Journal of Physical Chemistry C, 2011. **115**(26): p. 12797-12802.

12. Medley, CD., Smith, JE., Tang, Z., Wu, Y., Bamrungsap, S and Tan, W, *Gold nanoparticle-based colorimetric assay for the direct detection of cancerous cells.* Analytical chemistry, 2008. **80**(4): p. 1067-1072.

13. Cheng, Y., Samia, AC., Meyers, JD., Panagopoulos, I., Fei, B and Burda, C, *Highly efficient drug delivery with gold nanoparticle vectors for in vivo photodynamic therapy of cancer.* Journal of the American Chemical Society, 2008. **130**(32): p. 10643.

14. Wang, P., Lin, Z., Su, X and Tang, Z, *Application of Au based nanomaterials in analytical science.* Nano Today, 2017. **12**: p. 64-97.

15. Sitharaman, B, *Nanobiomaterials handbook.* CRC Press. 2011. P. 1-7.

16. Misra, R., Acharya, S and Sahoo, SK, *Cancer nanotechnology: application of nanotechnology in cancer therapy.* Drug Discovery Today, 2010. **15**(19): p. 842-850.

17. Lifeng, J., Tao, H., Zhipeng, L and Xue-Mei, L, *Monolayer-protected gold nanoparticle surface-bound catalysts: preparation and application.* Chinese Journal of Catalysis, 2010. **31**(11): p. 1307-1315.

18. Devi, JM, *Simulation studies on structural and thermal properties of alkane thiol capped gold nanoparticles.* Journal of Molecular Graphics and Modelling, 2017. **74**: p.359-365.

19. Park, J-W and Shumaker-Parry, JS, *Strong resistance of citrate anions on metal nanoparticles to desorption under thiol functionalization.* ACS nano, 2015. **9**(2): p. 1665-1682.

20. Leifert, A., Pan-Bartnek, Y., Simon, U and Jahnen-Dechent, W, *Molecularly stabilised ultrasmall gold nanoparticles: synthesis, characterization and bioactivity.* Nanoscale, 2013. **5**(14): p. 6224-6242.

21. Moyano, DF., Duncan, B and Rotello, VM, *Preparation of 2 nm gold nanoparticles for in vitro and in vivo applications.* Nanomaterial Interfaces in Biology: Methods and Protocols, 2013: p. 3-8.

22. Kalimuthu, P and John, SA, *Studies on ligand exchange reaction of functionalized mercaptothiadiazole compounds onto citrate capped gold nanoparticles.* Materials Chemistry and Physics, 2010. **122**(2): p. 380-385.

23. Verma, HN., Singh, P and Chavan, R, *Gold nanoparticle: synthesis and characterization.* Veterinary world, 2014. **7**(2): p. 72-77.

24. Volkert, AA., Subramaniam, V and Haes, AJ, *Implications of citrate concentration during the seeded growth synthesis of gold nanoparticles.* Chemical Communications, 2011. **47**(1): p. 478-480.

25. Martin, MN., Basham, JI., Chando, P and Eah, S-K, *Charged gold nanoparticles in non-polar solvents: 10-min synthesis and 2D self-assembly.* Langmuir, 2010. **26**(10): p. 7410-7417.

26. Leifert, A and Simon, U, *Syntheses and characterization of biologically active gold nanoparticles*. Doctoral dissertation, RWTH Aachen University, Fachgruppe Chemie. 2013.

27. Leff, DV., Ohara, PC., Heath, JR and Gelbart, WM, *Thermodynamic control of gold nanocrystal size: experiment and theory.* The Journal of Physical Chemistry, 1995. **99**(18): p. 7036-7041.

28. Woehrle, GH., Brown, LO and Hutchison, JE, *Thiol-functionalized, 1.5-nm gold nanoparticles through ligand exchange reactions: Scope and mechanism of ligand exchange.* Journal of the American Chemical Society, 2005. **127**(7): p. 2172-2183.

29. Oliveira, MM., Ugarte, D., Zanchet, D and Zarbin, AJ, *Influence of synthetic parameters on the size, structure, and stability of dodecanethiol-stabilized silver nanoparticles.* Journal of colloid and interface science, 2005. **292**(2): p. 429-435.

30. Tamura, M and Fujihara, H, *Chiral bisphosphine BINAP-stabilized gold and palladium nanoparticles with small size and their palladium nanoparticle-catalyzed asymmetric reaction.* Journal of the American Chemical Society, 2003. **125**(51): p. 15742-15743.

31. Baptista, P., Pereira, E., Eaton, P., Doria, G., Miranda, A., Gomes, I., Quaresma, P and Franco, R, *Gold nanoparticles for the development of clinical diagnosis methods.* Analytical and bioanalytical chemistry, 2008. **391**(3): p. 943-950.

32. Ahmadpour-Yazdi, H., Hormozi-Nezhad, M., Abadi, A., Sanati, MH and Kazemi, B, *Colorimetric assay for exon 7 SMN1/SMN2 single nucleotide polymorphism using gold nanoprobes.* BioImpacts: BI, 2013. **3**(4): p. 185-194.

33. Bond, GC, *Introduction to the physical and chemical properties of gold.* Gold Nanoparticles for Physics, Chemistry and Biology, Imperial College Press, London, 2012: p. 29-42.

34. Louis, C, *Chemical Preparation of Gold Nanoparticles on Surfaces.* Gold Nanoparticles for Physics, Chemistry and Biology, 2012: p. 139-171.

35. Miller, J., Kropf, A., Zha, Y., Regalbuto, J., Delannoy, L., Louis, C., Bus, E and Van Bokhoven, JA, *The effect of gold particle size on Au-Au bond length and*

reactivity toward oxygen in supported catalysts. Journal of Catalysis, 2006. **240**(2): p. 222-234.

36. Seo, D and Song, H, *Synthesis of gold nanoparticles in liquid phase.* Gold Nanoparticles for Physics, Chemistry and Biology, 2012: p. 103-139.

37. Brust, M and Kiely, CJ, *Some recent advances in nanostructure preparation from gold and silver particles: a short topical review.* Colloids and Surfaces A: Physicochemical and Engineering Aspects, 2002. **202**(2): p. 175-186.

38. Kumar, A., Boruah, BM and Liang, X-J, *Gold nanoparticles: promising nanomaterials for the diagnosis of cancer and HIV/AIDS.* Journal of Nanomaterials, 2011. **2011**(22).

39. García Fernández, L., Puntes, F and Boix Borràs, E, *Introducing gold nanoparticle bioconjugates within the biological machinery.* Doctoral dissertation, Autonomous University of Barcelona, 2013.

40. Kimling, J., Maier, M., Okenve, B., Kotaidis, V., Ballot, H and Plech, A, *Turkevich method for gold nanoparticle synthesis revisited.* The Journal of Physical Chemistry B, 2006. **110**(32): p. 15700-15707.

41. Tyagi, H., Kushwaha, A., Kumar, A and Aslam, M, *A Facile pH Controlled Citrate-Based Reduction Method for Gold Nanoparticle Synthesis at Room Temperature.* Nanoscale research letters, 2016. **11**(1):362.

42. Jazayeri, MH., Amani, H., Pourfatollah, AA., Pazoki-Toroudi, H and Sedighimoghaddam, B, *Various methods of gold nanoparticles (GNPs) conjugation to antibodies.* Sensing and Bio-Sensing Research, 2016. **9**: p. 17-22.

43. Khan, Z., Singh, T., Hussain, JI and Hashmi, AA, *Au (III)–CTAB reduction by ascorbic acid: Preparation and characterization of gold nanoparticles.* Colloids and Surfaces B: Biointerfaces, 2013. **104**: p. 11-17.

44. Ji, X., Song, X., Li, J., Bai, Y., Yang, W and Peng, X, *Size control of gold nanocrystals in citrate reduction: the third role of citrate.* Journal of the American Chemical Society, 2007. **129**(45): p. 13939-13948.

45. Ojea-Jiménez, I., Romero, FM., Bastús, NG and Puntes, V, *Small gold nanoparticles synthesized with sodium citrate and heavy water: insights into the reaction mechanism.* The Journal of Physical Chemistry C, 2010. **114**(4): p. 1800-1804.

46. Wang, Y., Aili, D., Selegård, R., Tay, Y., Baltzer, L., Zhang, H and Liedberg, B, *Specific functionalization of CTAB stabilized anisotropic gold nanoparticles with polypeptides for folding-mediated self-assembly.* Journal of Materials Chemistry, 2012. **22**(38): p. 20368-20373.

47. Bastús, NG., Comenge, J and Puntes, V, *Kinetically controlled seeded growth synthesis of citrate-stabilized gold nanoparticles of up to 200 nm: size focusing versus Ostwald ripening.* Langmuir, 2011. **27**(17): p. 11098-11105.

48. Goia, D and Matijević, E, *Tailoring the particle size of monodispersed colloidal gold.* Colloids and Surfaces A: Physicochemical and Engineering Aspects, 1999. **146**(1): p. 139-152.

49. Perala, SRK and Kumar, S, *On the mechanism of metal nanoparticle synthesis in the Brust–Schiffrin method.* Langmuir, 2013. **29**(31): p. 9863-9873.

50. Uehara, A., Booth, SG., Chang, SY., Schroeder, SL., Imai, T., Hashimoto, T., Mosselmans, JFW and Dryfe, RA, *Electrochemical insight into the Brust–Schiffrin synthesis of Au nanoparticles.* Journal of the American Chemical Society, 2015. **137**(48): p. 15135-15144.

51. Schmid, G and Lehnert, A, *The complexation of gold colloids.* Angewandte Chemie International Edition, 1989. **28**(6): p. 780-781.

52. Chen, G., Takezawa, M., Kawazoe, N and Tateishi, T, *Preparation of cationic gold nanoparticles for gene delivery.* Open Biotechnology Journal, 2008. **2**(1): p. 152-156.

53. Wei, G-T., Yang, Z., Lee, C-Y., Yang, H-Y and Wang, CC, *Aqueous− organic phase transfer of gold nanoparticles and gold nanorods using an ionic liquid.* Journal of the American Chemical Society, 2004. **126**(16): p. 5036-5037.

54. Llevot, A and Astruc, D, *Applications of vectorized gold nanoparticles to the diagnosis and therapy of cancer.* Chemical Society Reviews, 2012. **41**(1): p. 242-257.

55. Gittins, DI and Caruso, F, *Spontaneous phase transfer of nanoparticulate metals from organic to aqueous media.* Angewandte Chemie International Edition, 2001. **40**(16): p. 3001-3004.

56. Ojea-Jimenez, I and Puntes, V, *Instability of cationic gold nanoparticle bioconjugates: the role of citrate ions.* Journal of the American Chemical Society, 2010. **132**(14): p. 5322-5322.

57. Chithrani, BD., Ghazani, AA and Chan, WC, *Determining the size and shape dependence of gold nanoparticle uptake into mammalian cells.* Nano letters, 2006. **6**(4): p. 662-668.

58. Shukla, R., Bansal, V., Chaudhary, M., Basu, A., Bhonde, RR and Sastry, M, *Biocompatibility of gold nanoparticles and their endocytotic fate inside the cellular compartment: a microscopic overview.* Langmuir, 2005. **21**(23): p. 10644-10654.

59. Sweeney, SF., Woehrle, GH and Hutchison, JE, *Rapid purification and size separation of gold nanoparticles via diafiltration.* Journal of the American Chemical Society, 2006. **128**(10): p. 3190-3197.

60. Balasubramanian, SK., Yang, L., Yung, L-YL., Ong, C-N., Ong, W-Y and Liya, EY, *Characterization, purification, and stability of gold nanoparticles.* Biomaterials, 2010. **31**(34): p. 9023-9030.

61. Krpetic, Z., Nativo, P., Sée, V., Prior, IA., Brust, M and Volk, M, *Inflicting controlled nonthermal damage to subcellular structures by laser-activated gold nanoparticles.* Nano letters, 2010. **10**(11): p. 4549-4554.

62. Schneider, G and Decher, G, *From functional core/shell nanoparticles prepared via layer-by-layer deposition to empty nanospheres.* Nano letters, 2004. **4**(10): p. 1833-1839.

63. Kanaras, AG., Kamounah, FS., Schaumburg, K., Kiely, CJ and Brust, M, *Thioalkylated tetraethylene glycol: a new ligand for water soluble monolayer protected gold clusters.* Chemical Communications, 2002(20): p. 2294-2295.

64. Weare, WW., Reed, SM., Warner, MG and Hutchison, JE, *Improved synthesis of small (d core≈ 1.5 nm) phosphine-stabilized gold nanoparticles.* Journal of the American Chemical Society, 2000. **122**(51): p. 12890-12891.

65. Alele, N., Streubel, R., Gamrad, L., Barcikowski, S and Ulbricht, M, *Ultrafiltration membrane-based purification of bioconjugated gold nanoparticle dispersions.* Separation and Purification Technology, 2016. **157**: p. 120-130.

66. Sapsford, KE., Tyner, KM., Dair, BJ., Deschamps, JR and Medintz, IL, *Analyzing nanomaterial bioconjugates: a review of current and emerging purification and characterization techniques.* Anal. Chem, 2011. **83**(12): p. 4453-4488.

67. Zhou, J., Ralston, J., Sedev, R and Beattie, DA, *Functionalized gold nanoparticles: synthesis, structure and colloid stability.* Journal of colloid and interface science, 2009. **331**(2): p. 251-262.

68. Valkenier, H., Malytskyi, V., Blond, P., Retout, M., Mattiuzzi, A., Goole, J., Raussens, V., Jabin, I and Bruylants, G, *Controlled Functionalization of Gold Nanoparticles with Mixtures of Calix [4] arenes Revealed by Infrared Spectroscopy.* Langmuir, 2017. **33**(33): p. 8253-8259.

69. Biju, V, *Chemical modifications and bioconjugate reactions of nanomaterials for sensing, imaging, drug delivery and therapy.* Chemical Society Reviews, 2014. **43**(3): p. 744-764.

70. Srisombat, L-O., Park, J-S., Zhang, S and Lee, TR, *Preparation, characterization, and chemical stability of gold nanoparticles coated with mono-, bis-, and tris-chelating alkanethiols.* Langmuir, 2008. **24**(15): p. 7750-7754.

71. Botequim, D., Maia, J., Lino, M., Lopes, L., Simoes, P., Ilharco, L and Ferreira, L, *Nanoparticles and surfaces presenting antifungal, antibacterial and antiviral properties.* Langmuir, 2012. **28**(20): p. 7646-7656.

72. Johnson, S., Evans, S., Mahon, S and Ulman, A, *Alkanethiol molecules containing an aromatic moiety self-assembled onto gold clusters.* Langmuir, 1997. **13**(1): p. 51-57.

73. Daniel, M-C and Astruc, D, *Gold nanoparticles: assembly, supramolecular chemistry, quantum-size-related properties, and applications toward biology, catalysis, and nanotechnology.* Chemical reviews, 2004. **104**(1): p. 293-346.

74. Pérez-Mirabet, L., Surinyach, S., Ros, J., Suades, J and Yáñez, R, *Gold and silver nanoparticles surface functionalized with rhenium carbonyl complexes.* Materials Chemistry and Physics, 2012. **137**(2): p. 439-447.

75. Chen, S and Kimura, K, *Synthesis and characterization of carboxylate-modified gold nanoparticle powders dispersible in water.* Langmuir, 1999. **15**(4): p. 1075-1082.

76. He, S., Guo, Z., Zhang, Y., Zhang, S., Wang, J and Gu, N, *Biosynthesis of gold nanoparticles using the bacteria Rhodopseudomonas capsulata.* Materials Letters, 2007. **61**(18): p. 3984-3987.

77. Tyagi, H., Kushwaha, A., Kumar, A and Aslam, M, *pH-dependent synthesis of stabilized gold nanoparticles using ascorbic acid.* International Journal of Nanoscience, 2011. **10**(04n05): p. 857-860.

78. Yu, M., Zhou, C., Liu, J., Hankins, JD and Zheng, J, *Luminescent gold nanoparticles with pH-dependent membrane adsorption.* Journal of the American Chemical Society, 2011. **133**(29): p. 11014-11017.

79. Song, J., Kim, J., Hwang, S., Jeon, M., Jeong, S., Kim, C and Kim, S, *"Smart" gold nanoparticles for photoacoustic imaging: an imaging contrast agent responsive to the cancer microenvironment and signal amplification via pH-induced aggregation.* Chemical Communications, 2016. **52**(53): p. 8287-8290.

80. Lv, Y., Hao, L., Hu, W., Ran, Y., Bai, Y and Zhang, L, *Novel multifunctional pH-sensitive nanoparticles loaded into microbubbles as drug delivery vehicles for enhanced tumor targeting.* Scientific reports, 2016. **6**(29321).

81. Tan, S., Wu, T., Zhang, D and Zhang, Z, *Cell or cell membrane-based drug delivery systems.* Theranostics, 2015. **5**(8): p. 863–881.

82. Li, H., Liu, X., Huang, N., Ren, K., Jin, Q and Ji, J, *"Mixed-charge self-assembled monolayers" as a facile method to design pH-induced aggregation of large gold nanoparticles for near-infrared photothermal cancer therapy.* ACS applied materials & interfaces, 2014. **6**(21): p. 18930-18937.

83. Nam, J., Won, N., Jin, H., Chung, H and Kim, S, *pH-induced aggregation of gold nanoparticles for photothermal cancer therapy.* Journal of the American Chemical Society, 2009. **131**(38): p. 13639-13645.

84. Mura, S., Nicolas, J and Couvreur, P, *Stimuli-responsive nanocarriers for drug delivery.* Nature materials, 2013. **12**(11): p. 991-1003.

85. Jung, S., Nam, J., Hwang, S., Park, J., Hur, J., Im, K., Park, N and Kim, S, *Theragnostic pH-sensitive gold nanoparticles for the selective surface enhanced Raman scattering and photothermal cancer therapy.* Analytical chemistry, 2013. **85**(16): p. 7674-7681.

86. Yagi, S., Oeda, N and Kojima, C, *Electroless Growth of Size-Controlled Gold Nanoparticles Using Hydroquinone.* Journal of the Electrochemical Society, 2012. **159**(7): p. H668-H673.

87. Yang, H., Heng, X and Hu, J, *Salt-and pH-resistant gold nanoparticles decorated with mixed-charge zwitterionic ligands, and their pH-induced concentration behavior.* RSC Advances, 2012. **2**(33): p. 12648-12651.

88. Patungwasa, W and Hodak, JH, *pH tunable morphology of the gold nanoparticles produced by citrate reduction.* Materials Chemistry and Physics, 2008. **108**(1): p. 45-54.

89. Nam, J., La, W-G., Hwang, S., Ha, YS., Park, N., Won, N., Jung, S., Bhang, SH., Ma, Y-J and Cho, Y-M, *pH-responsive assembly of gold nanoparticles and "spatiotemporally concerted" drug release for synergistic cancer therapy.* ACS nano, 2013. **7**(4): p. 3388-3402.

90. Chen, H., Dorrigan, A., Saad, S., Hare, DJ., Cortie, MB and Valenzuela, SM, *In vivo study of spherical gold nanoparticles: inflammatory effects and distribution in mice.* PLoS One, 2013. **8**(2): p. e58208.

91. Dykman, L and Khlebtsov, N, *Gold nanoparticles in biomedical applications: recent advances and perspectives.* Chemical Society Reviews, 2012. **41**(6): p. 2256-2282.

92. Huang, X, *Gold nanoparticles used in cancer cell diagnostics, selective photothermal therapy and catalysis of NADH oxidation reaction*. Doctoral dissertation, Georgia Institute of Technology, 2006.

93. Railsback, JG., Singh, A., Pearce, RC., Mcknight, TE., Collazo, R., Sitar, Z., Yingling, YG and Melechko, AV, *Weakly charged cationic nanoparticles induce DNA bending and strand separation.* Advanced materials, 2012. **24**(31): p. 4261-4265.

94. Tkachenko, AG., Xie, H., Liu, Y., Coleman, D., Ryan, J., Glomm, WR., Shipton, MK., Franzen, S and Feldheim, DL, *Cellular trajectories of peptide-modified gold particle complexes: comparison of nuclear localization signals and peptide transduction domains.* Bioconjugate chemistry, 2004. **15**(3): p. 482-490.

95. Goodman, CM., Mccusker, CD., Yilmaz, T and Rotello, VM, *Toxicity of gold nanoparticles functionalized with cationic and anionic side chains.* Bioconjugate chemistry, 2004. **15**(4): p. 897-900.

96. Li, P., Li, D., Zhang, L., Li, G and Wang, E, *Cationic lipid bilayer coated gold nanoparticles-mediated transfection of mammalian cells.* Biomaterials, 2008. **29**(26): p. 3617-3624.

97. Niidome, T., Nakashima, K., Takahashi, H and Niidome, Y, *Preparation of primary amine-modified gold nanoparticles and their transfection ability into cultivated cells.* Chemical Communications, 2004(17): p. 1978-1979.

98. Cho, EC., Xie, J., Wurm, PA and Xia, Y, *Understanding the role of surface charges in cellular adsorption versus internalization by selectively removing gold nanoparticles on the cell surface with a I2/KI etchant.* Nano letters, 2009. **9**(3): p. 1080-1084.

99. Ghosh, SK and Pal, T, *Interparticle coupling effect on the surface plasmon resonance of gold nanoparticles: from theory to applications.* Chemical reviews, 2007. **107**(11): p. 4797-4862.

100. Arvizo, RR., Miranda, OR., Thompson, MA., Pabelick, CM., Bhattacharya, R., Robertson, JD., Rotello, VM., Prakash, Y and Mukherjee, P, *Effect of nanoparticle surface charge at the plasma membrane and beyond.* Nano letters, 2010. **10**(7): p. 2543-2548.

101. Sabella, S., Galeone, A., Vecchio, G., Cingolani, R and Pompa, P, *AuNPs are toxic in vitro and in vivo: a review.* Journal of Nanoscience Letters, 2011. **1**(3) : p. 145-165.

102. Harush-Frenkel, O., Debotton, N., Benita, S and Altschuler, Y, *Targeting of nanoparticles to the clathrin-mediated endocytic pathway.* Biochemical and biophysical research communications, 2007. **353**(1): p. 26-32.

103. Almeida, JPM., Figueroa, ER and Drezek, RA, *Gold nanoparticle mediated cancer immunotherapy.* Nanomedicine: Nanotechnology, Biology and Medicine, 2014. **10**(3): p. 503-514.

104. Delong, RK., Akhtar, U., Sallee, M., Parker, B., Barber, S., Zhang, J., Craig, M., Garrad, R., Hickey, AJ and Engstrom, E, *Characterization and performance of nucleic acid nanoparticles combined with protamine and gold.* Biomaterials, 2009. **30**(32): p. 6451-6459.

105. Ross, M., Kelso, G., Blaikie, F., James, A., Cocheme, H., Filipovska, A., Da Ros, T., Hurd, T., Smith, R and Murphy, M, *Lipophilic triphenylphosphonium cations as tools in mitochondrial bioenergetics and free radical biology.* Biochemistry (Moscow), 2005. **70**(2): p. 222-230.

106. Ross, MF., Da Ros, T., Blaikie, FH., Prime, TA., Porteous, CM., Severina, II., Skulachev, VP., Kjaergaard, HG., Smith, RA and Murphy, MP, *Accumulation of lipophilic dications by mitochondria and cells.* Biochemical journal, 2006. **400**(1): p. 199-208.

107. Pompe, W., Rödel, G., Weiss, H-J and Mertig, M, *Bio-nanomaterials: designing materials inspired by nature*. John Wiley & Sons, 2013.

108. Han, M., Vakili, MR., Soleymani Abyaneh, H., Molavi, O., Lai, R and Lavasanifar, A, *Mitochondrial delivery of doxorubicin via triphenylphosphine modification for overcoming drug resistance in MDA-MB-435/DOX cells.* Molecular pharmaceutics, 2014. **11**(8): p. 2640-2649.

109. Wang, P., Wang, X., Wang, L., Hou, X., Liu, W and Chen, C, *Interaction of gold nanoparticles with proteins and cells.* Science and Technology of Advanced Materials, 2015. **16**(3): p. 1-15.

110. Ojea-Jiménez, I., García-Fernández, L., Lorenzo, J and Puntes, VF, *Facile preparation of cationic gold nanoparticle-bioconjugates for cell penetration and nuclear targeting.* ACS nano, 2012. **6**(9): p. 7692-7702.

111. Jain, S., Hirst, D and O'sullivan, J, *Gold nanoparticles as novel agents for cancer therapy.* The British journal of radiology, 2012. **85**(1010): p. 101-113.

112. Brown, SD., Nativo, P., Smith, J-A., Stirling, D., Edwards, PR., Venugopal, B., Flint, DJ., Plumb, JA., Graham, D and Wheate, NJ, *Gold nanoparticles for the improved anticancer drug delivery of the active component of oxaliplatin.* Journal of the American Chemical Society, 2010. **132**(13): p. 4678-4684.

113. Murphy, CJ., Gole, AM., Stone, JW., Sisco, PN., Alkilany, AM., Goldsmith, EC and Baxter, SC, *Gold nanoparticles in biology: beyond toxicity to cellular imaging.* Accounts of chemical research, 2008. **41**(12): p. 1721-1730.

114. Khan, JA., Pillai, B., Das, TK., Singh, Y and Maiti, S, *Molecular effects of uptake of gold nanoparticles in HeLa cells.* ChemBioChem, 2007. **8**(11): p. 1237-1240.

115. Pan, Y., Leifert, A., Ruau, D., Neuss, S., Bornemann, J., Schmid, G., Brandau, W., Simon, U and Jahnen‐Dechent, W, *Gold nanoparticles of diameter 1.4 nm trigger necrosis by oxidative stress and mitochondrial damage.* Small, 2009. **5**(18): p. 2067-2076.

116. Heddle, JG, *Gold nanoparticle-biological molecule interactions and catalysis.* Catalysts, 2013. **3**(3): p. 683-708.

117. Sonavane, G., Tomoda, K and Makino, K, *Biodistribution of colloidal gold nanoparticles after intravenous administration: effect of particle size.* Colloids and Surfaces B: Biointerfaces, 2008. **66**(2): p. 274-280.

118. Fratoddi, I., Venditti, I., Cametti, C and Russo, MV, *How toxic are gold nanoparticles? The state-of-the-art.* Nano Research, 2015. **8**(6): p. 1771-1799.

119. Hong, R., Han, G., Fernández, JM., Kim, B-J., Forbes, NS and Rotello, VM, *Glutathione-mediated delivery and release using monolayer protected nanoparticle carriers.* Journal of the American Chemical Society, 2006. **128**(4): p. 1078-1079.

120. Barchanski, A, *Laser-Generated Functional Nanoparticle Bioconjugates: Design for Application in Biomedical Science and Reproductive Biology*. Springer, 2016.

121. Wong, C., Stylianopoulos, T., Cui, J., Martin, J., Chauhan, VP., Jiang, W., Popović, Z., Jain, RK., Bawendi, MG and Fukumura, D, *Multistage nanoparticle delivery system for deep penetration into tumor tissue.* Proceedings of the National Academy of Sciences, 2011. **108**(6): p. 2426-2431.

122. De Jong, WH., Hagens, WI., Krystek, P., Burger, MC., Sips, AJ and Geertsma, RE, *Particle size-dependent organ distribution of gold nanoparticles after intravenous administration.* Biomaterials, 2008. **29**(12): p. 1912-1919.

123. Hirn, S., Semmler-Behnke, M., Schleh, C., Wenk, A., Lipka, J., Schäffler, M., Takenaka, S., Möller, W., Schmid, G and Simon, U, *Particle size-dependent and surface charge-dependent biodistribution of gold nanoparticles after intravenous administration.* European journal of pharmaceutics and biopharmaceutics, 2011. **77**(3): p. 407-416.

124. Maeda, H, *The enhanced permeability and retention (EPR) effect in tumor vasculature: the key role of tumor-selective macromolecular drug targeting.* Advances in enzyme regulation, 2001. **41**(1): p. 189-207.

125. Conde, J., Doria, G and Baptista, P, *Noble metal nanoparticles applications in cancer.* Journal of drug delivery, 2012. **2012**. 751075: p.1-12.

126. Patra, CR., Bhattacharya, R., Wang, E., Katarya, A., Lau, JS., Dutta, S., Muders, M., Wang, S., Buhrow, SA and Safgren, SL, *Targeted delivery of gemcitabine to*

pancreatic adenocarcinoma using cetuximab as a targeting agent. Cancer research, 2008. **68**(6): p. 1970-1978.

127. Gao, W., Chan, JM and Farokhzad, OC, *pH-responsive nanoparticles for drug delivery.* Molecular pharmaceutics, 2010. **7**(6): p. 1913-1920.

128. Ghosh, P., Han, G., De, M., Kim, CK and Rotello, VM, *Gold nanoparticles in delivery applications.* Advanced drug delivery reviews, 2008. **60**(11): p. 1307-1315.

129. Han, G., Ghosh, P and Rotello, VM, *Functionalized gold nanoparticles for drug delivery.* Nanomedicine, 2007. **2**(1): p. 113-123.

130. Glazer, ES., Zhu, C., Massey, KL., Thompson, CS., Kaluarachchi, WD., Hamir, AN and Curley, SA, *Noninvasive radiofrequency field destruction of pancreatic adenocarcinoma xenografts treated with targeted gold nanoparticles.* Clinical Cancer Research, 2010. **16**(23): p. 5712-5721.

131. Cherukuri, P and Curley, SA, *Use of nanoparticles for targeted, noninvasive thermal destruction of malignant cells.* Cancer Nanotechnology: Methods and Protocols, 2010: p. 359-373.

132. Bhattacharya, D., Saha, B., Mukherjee, A., Santra, CR and Karmakar, P, *Gold nanoparticles conjugated antibiotics: stability and functional evaluation.* Nanoscience and nanotechnology, 2012. **2**(2): p. 14-21.

133. Shamaila, S., Zafar, N., Riaz, S., Sharif, R., Nazir, J and Naseem, S, *Gold nanoparticles: an efficient antimicrobial agent against enteric bacterial human pathogen.* Nanomaterials, 2016. **6**(4): p. 1-10.

134. Wang, P., Zhao, Y., Tian, Y and Jiang, X, *Multiple strategies to activate gold nanoparticles as potent antibacterial agents.* Nanomedicine: Nanotechnology, Biology and Medicine, 2016. **12**(2): p. 527-528.

Chapter 2: Highly stable noble metal nanoparticles dispersed in biocompatible solvents: synthesis of cationic phosphonium gold nanoparticles in water and DMSO

Ju-Nam, Y., Abdussalam-Mohammed, W., & Ojeda, J. J. (**2016**). Highly stable noble metal nanoparticles dispersible in biocompatible solvents: synthesis of cationic phosphonium gold nanoparticles in water and DMSO. *Faraday discussions*, *186*, 77-93.

2.1 Abstract

Synthesis of novel cationic phosphonium AuNPs dispersible in water and dimethylsulfoxide (DMSO) for their potential use in biomedical applications is outlined in this chapter. All the cationic-functionalising ligands currently reported in the literature are ammonium-based species. Here, the synthesis and characterisation of an alternative system, based on phosphonioalkylthiosulfate zwitterions and phosphonioalkylthioacetate were carried out. Phosphonioalkylthiosulfate zwitterions are readily disproportionated into phosphonioalkylthiolates *in situ* during the synthesis of AuNPs, produced by the borohydride reduction of gold (III) salt. Syntheses of cationic AuNPs using these phosphonium ligands were carried out in water and DMSO.

UV-Visible spectroscopic and TEM studies have shown that the phosphonioalkylthiolates bind to the surface of AuNPs, which are typically around 10 nm in diameter. The resulting cationic-functionalised AuNPs are dispersible in aqueous media and in DMSO, which is the only organic solvent approved by the U.S. Food and Drug Administration (FDA) for drug carrier tests. This indicates their potential future use in biological applications. In this chapter, the synthesis of a new family of phosphonium-based ligands, which behave as cationic masked thiolate ligands in the functionalisation of AuNPs is discussed. These highly stable colloidal cationic phosphonium AuNPs dispersed in water and DMSO can offer a great opportunity for the design of novel biorecognition and drug delivery systems.

2.2 Introduction

The ability of modifying noble metal NPs, such as AuNPs with various organic thiolate ligands makes them versatile systems and opens a range of possibilities for their use as

drug delivery systems [1-3], bio-sensing [4-6] and diagnostic applications. Ligands are introduced to the surface of the NP either to stabilise the particle and avoid uncontrolled aggregation, or to add functionality to the particle for biomolecular recognition, enhanced transport and anchoring properties [7]. Recent studies have shown that the size, shape and surface charge of NPs, in general, play crucial roles in their entry and subsequent access of NPs into living cells [6, 8-11]. For instance, cationic NPs are more effective penetrating into mammalian cells than anionic NPs due to electrostatic interaction between cationic NPs and negatively charged mammalian cells [12].

NP surface functionalisation plays an important role in cellular uptake and producing cellular responses [13, 14]. However, information published in the literature on how functionalised NP surface characteristics, such as aromaticity and hydrophobicity, affect cellular internalisation processes is still unclear. Al-Hajaj, NA., et al., have shown that the functionalised quantum dots they produced with non-specified ligands were taken up by lipid host mediated endocytosis in human kidney and liver cells [15]. Designing and tailoring the surface of inorganic NPs with suitable ligands may potentially offer long-term stability under a wide-range of conditions such as, high electrolyte concentration, a broad pH range, and biogenic or naturally occurring thiols [3].

Zhan, N., et al., have shown that quantum dots modified with multidentate lipoic ligand containing a zwitterionic head group can be highly biocompatible nanomaterials [16, 17], making them attractive nanodevices for clinical *in vitro* and *in vivo* imaging applications [18-20]. More recently, Rotello, VM., et al., have studied the behaviour of AuNPs with different hydrophobicities and the effect of surface functionality on hemolysis [21]. They observed a linear haemolytic behaviour with increasing hydrophobicity in the absence of serum media. Mcintosh, CM., et al., synthesised AuNPs capped with a mixture of octanethiol and 11-trimethylammonium-undecanethiol, and others functionalised with trimethylammonium cationic head groups on the surface can interact electrostatically and bind with the negatively charged phosphate backbone of 37 mer duplex DNA [22].

As in these studies reported in the literature, the majority of the cationic species investigates and used are ammonium-based groups. Here in this chapter, cationic phosphonium-based groups are also described as alternatives to the ammonium functional groups. The phosphonium groups can offer a range of advantages including the availability of a broad range of organic derivatives, which allows of designing and

producing a wide variety of functionalised AuNPs. Their ability of triphenylphosphonium head groups to travel across cell membranes is well-known [23-26]. There are also several studies on the use of phosphines and phosphine oxides to stabilise NPs. However, there have been far fewer studies of the use of organophosphorus ligands [27-29].

Additional to imparting specific functionalities to NPs, their dispersion in water or any other biocompatible solvent is crucial for their use in biomedical or biological applications. Therefore, water should be the primary solvent to be used to disperse functionalised NPs. However, in many cases, the ligands used to protect and provide functionality to NPs, and the corresponding NMs produced are not soluble or dispersible in water. It would be highly beneficial to have a range of other biocompatible solvents. One potential alternative to water could be DMSO. According to the FDA, DMSO is a solvent derived from wood, which has been the subject of considerable interest for its potential as a drug. At present, the only human use for which DMSO has been approved is for interstitial cystitis, a bladder condition. DMSO is also known as a "carrier" chemical, it could deliver substances into the bloodstream through the skin [30].

DMSO is a safe and successful component for encouraging the transdermal administration of both hydrophilic and lipophilic drugs to provide localised drug delivery [22, 31]. For all the reasons outlined here, DMSO was a chosen solvent to synthesise and disperse cationic phosphonium NPs described in this chapter.

A publication was generated from this work, and the syntheses cationic AuNPs by reducing gold (III) salt in the presence of our cationic phosphonium ligands in DMSO was reported for the first time. Also the synthesis of a new cationic phosphonium ligand, such as, tri(*p*-tolyl)phosphoniopropylthiosulfate zwitterion (**4**) used to functionalise the AuNP surface in DMSO was reported. Two previously reported phosphonium ligands, triphenylphosphoniopropylthiosulfate zwitterion (**4C**) [32] and (3-thioactylpropyl)-triphenylphosphonium bromide (**5**) [33], were used for this work to produce the cationic phosphonium AuNPs in DMSO and comparison purposes with the new ligand synthesised, tri(*p*-tolyl)phosphoniopropylthiosulfate (**4**).

2.3 Materials and Methods

2.3.1 General Information

All chemicals and solvents were purchased from Sigma-Aldrich and Fisher Scientific Ltd. For the characterisation of the ligands and functionalised AuNPs, several analytical techniques were used. TLC, ATR-FTIR, NMR, ESI-MS techniques were employed to characterise the phosphonium containing ligands. UV-Visible spectroscopy and TEM were used to characterise and obtain the size of the cationic phosphonium AuNPs. The stability of the colloidal AuNP solutions were monitored using UV-Visible technique.

(a) Thin Layer Chromatography (TLC): Analytical thin layer chromatography was carried out on Merck silica gel 60 F254 plates by using mixtures of methanol: dichloromethane (DCM) as eluent system.

(b) Attenuated Total Reflectance–Fourier Transform Infrared (ATR-FTIR) Spectroscopy: IR spectra acquisition was performed on solid samples using a Nicolet 5700 FT-IR spectrometer equipped with Omnic software (version 7.1) and a Smart Omni-Sampler (ATR cell with single reflectance germanium crystal). Each recorded spectrum is the average of 32 scans with a spectral resolution of 4 cm^{-1} from 400 to 4000 cm^{-1} on a dried sample, with a background spectrum recorded before each analysis. Spectra were measured and analysed and fitted using Origin software (Version 7.5) equipped with Peak-Fitting Module (PFM).

(c) Nuclear Magnetic Resonance Spectroscopy (NMR): ^{1}H NMR spectra were acquired on a JEOL 400MHz spectrometer. Data are reported as follows: *s*, singlet; *d*, doublet; *t*, triplet; *q*, quartet; *m*, multiplet. Appropriate solvents such as dimethylsulfoxide, chloroform, diethyl ether were used to dissolve the samples to a concentration of 15 to 40 mg ml^{-1} for ^{1}H experiments.

(d) Electrospray Ionisation–Mass Spectrometry (ESI-MS): ESI-MS analyses were generally performed on the Orbitrap XL using nano- electrospray in positive or negative ionisation mode. Orbitrap XL High resolution instrument gives accurate mass measurement over the full mass range in electrospray resolution: up to 100,000 (FWHM).

Mass Range: m/z 50–2000 or m/z 200–4000. Mass Accuracy: < 3 ppm RMS with external calibration; < 2 ppm RMS with internal calibration.

All samples were initially solvated in 250µl of DCM before approximately 10µl of the solutions were added to 1ml of methanol with NH_4OAc. A portion of these samples were added to a 96 well plate to be analysed by positive nano-electrospray.

(e) Ultraviolet-Visible Absorption Spectroscopy (UV-visible): UV-visible spectra were obtained on a HITACHI U-2900 spectrophotometer with double beam principle system with data recording using Vision software version on Windows XP/2000. Samples were analysed in a UV-quartz cuvette of a 1 cm optical path. Appropriate dilutions to the original samples were carried out using either water or DMSO.

(f) Transmission Electron Microscopy (TEM): A JEOL2100 field emission gun transmission electron microscope (FEG TEM) set at 100 KV was used for the analyses of the particles and obtained the TEM micrographs. Size distribution was obtained by counting and measuring over 150 AuNPs. Deposition method was used to prepare the samples for TEM analyses. A drop of a diluted colloidal solution of the functionalised AuNPs was placed and suspended on a Holey carbon coated copper grid. Then the grids were left to dry at room temperature.

2.3.2 Cationic phosphonium ligand syntheses

The syntheses of the triphenylphosphoniopropylthiosulfate zwitterion (**4C**) and ω-thioacetylpropylphosphonium salt (**5**) were synthesised following methods previously reported [32, 33]. The tri(*p*-tolyl)phosphoniopropylthiosulfate zwitterion (**4**) synthesis and characterisation are reported for the first time in this work. The synthetic protocols used to produce the three ligands are outlined in this section.

2.3.2.1 Synthesis of tri(*p*-tolyl)phosphoniopropylthiosulfate zwitterion (4)

The synthesis of the **4** was carried out following the reactions showed in Scheme 1. In a round bottom flask with a reflux condenser a mixture of tri(*p*-tolyl)phosphine (**1**) (3.8 mmol) with approximately bromo-propanol (15 mmol) were refluxed for five hours in acetonitrile (0.024 mmol) and the solid precipitate was collected and recrystallized from ethanol (Reaction 1, Scheme1). The yield was 70%. The resulting salt (**2**) was dissolved

in hydrobromic acid (0.18 mmol, 10 ml) (48%) in a round bottom under reflux five hours (Reaction 2, Scheme 1). The reaction mixture was left to cool down, the compound appeared as yellow oil (**3**). In order to prepare the tri-*p*-tolylphosphoniopropylthiosulfate zwitterion (**4**), a mixture of ω-bromopropyl-tri(*p*-tolyl)phosphonium bromide (**3**) (1 mmol) and sodium thiosulfate (1.5 mmol) were refluxed for five hours in aqueous ethanol (1:1, 10 ml) (Reaction 3, Scheme 1). TLC was used in order to follow the progress of the reaction by using 20% : 80% methanol : DCM as mobile phase. All compounds were purified further by liquid-liquid extraction of the reaction mixture using DCM and by trituration with dry diethyl ether.

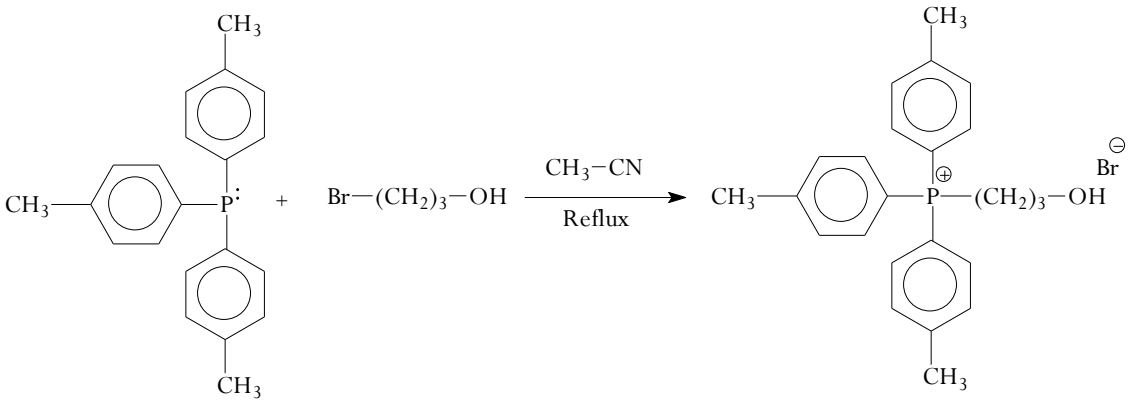

(1) Reaction 1 (2)

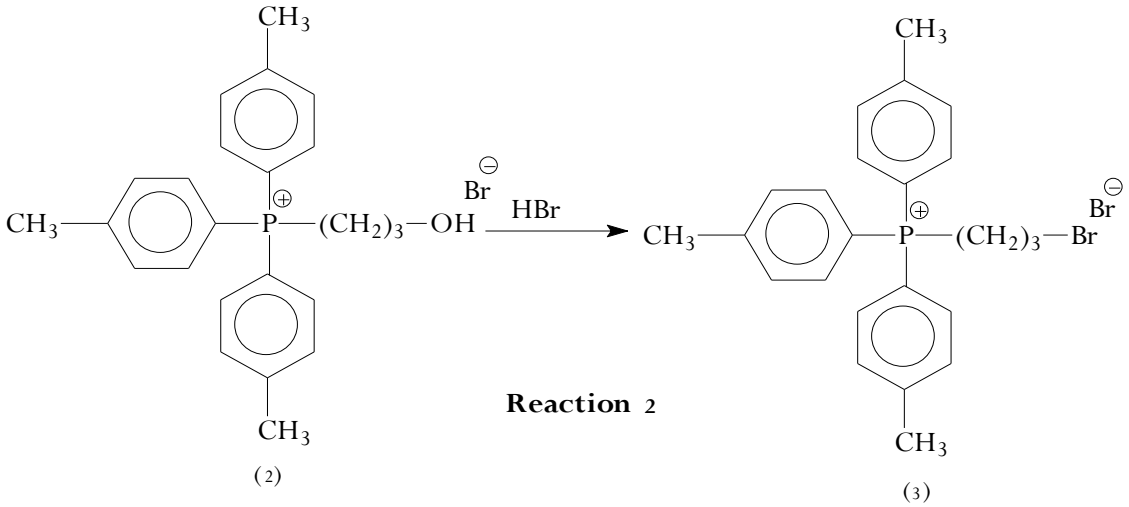

(2) **Reaction 2** (3)

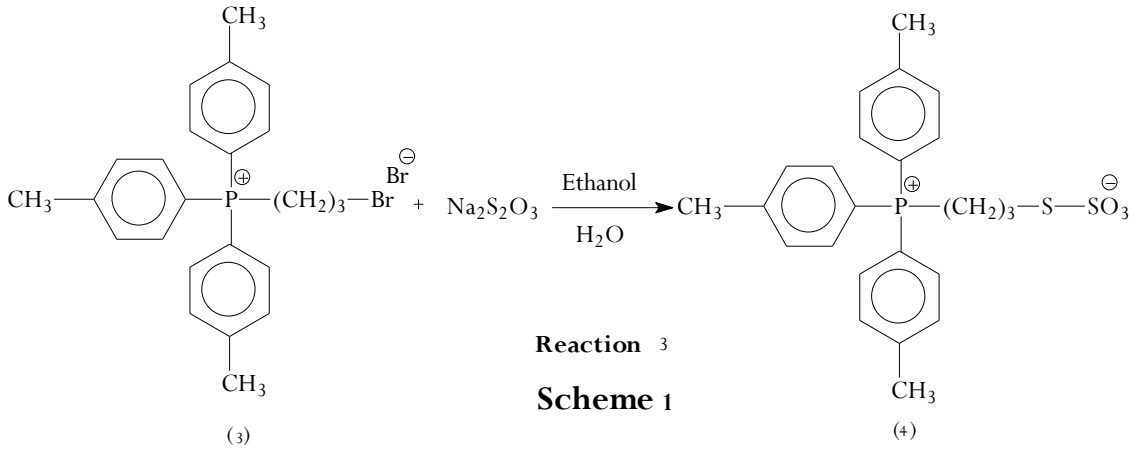

(3) (4)

Reaction 3

Scheme 1

2.3.2.2 Synthesis of triphenylphosphoniopropylthiosulfate (4C)

In order to obtain the **4C** [32], three main chemical reactions were carried out. The first stage involved the synthesis of the hydorxylpropylphosphonium salt and this was generated by a quaternation reaction of triphenylphosphine (4 mmol) and the corresponding bromo-propanol (15 mmol) in acetonitrile under reflux for four to five hours. The resulting salt was dissolved in hydrobromic acid (48%) and reaction was carried out under reflux for five hours to obtain the ω-bromopropyltriphenylphosphonium bromide salt. The latter (1 mmol) then was treated with sodium thiosulfate (1.5 mmol) in ethanol / water under reflux for five hours in order to produce the phosphoniopropylthiosulfate zwitterion. Progress of all reactions were monitored by TLC using methanol:dichloromethane 1:4 ratio as the mobile phase. All the compounds were purified by dichloromethane extraction and re-crystallisation using diethyl ether.

2.3.2.3 Synthesis of (3-thioacetylpropyl)triphenylphosphonium bromide (5)

In order to obtain the **5**, hydroxypropylphosphonium and ω-bromopropyltriphenyl-phosphonium bromide salts were also synthesised as described in the synthesis of triphenylphosphonio- propylthiosulfate zwitterion [32, 33]. Once the bromide salt (2 mmol) was produced, this was reacted with potassium thioacetate (3 mmol) in a mixture of ethanol/water. The progress of the reaction was followed by TLC using a mobile phase of methanol:dichloromethane in 1:4 ratio. The (3-thioactylpropyl)triphenylphosphonium bromide was isolated and purified by liquid-liquid extraction using DCM as the extracting solvent, and re-crystallisation of the bromide salt using diethyl ether.

2.3.3 Synthesis of cationic phosphonium gold nanoparticles in water and DMSO

The preparation of colloidal cationic phosphonium AuNP solutions in water was carried out following the principals involved in the method developed by Brust and Schifrin, a two-phase liquid-liquid system [32]. Variations were done to this method due to the solubility of the phosphonium ligands synthesised. The method for the synthesis of colloidal cationic phosphonium AuNPs in DMSO is reported for the first time and was developed in a similar fashion as the previous methods.

2.3.3.1 Cationic phosphonium gold nanoparticles dispersed in water

Solutions of the phosphonium ligands zwitterion **4C** and **5** was prepared in 20 mL of dichloromethane (DCM) (0.25 mmol and 0.30 mmol respectively) and potassium tetrachloroaurate (0.12 mmol) was also added to the DCM solution [32, 33]. This was vigorously stirred for 2 hours and until the potassium gold salt was totally dissolved. The reduction of the gold (III) to gold (0) in the presence of phosphonium ligand was carried out by adding drop by drop a freshly prepared sodium borohydride solution in water (3 ml, 400 mM) with vigorous stirring. After 20 minutes of stirring, 15 mL of deionised water was then added to the mixture. The latter is kept stirring overnight. The initial DCM was removed from the aqueous phase, as the functionalised NPs transferred to this phase. Then, three liquid-liquid extractions were carried out using DCM in order to purify the cationic phosphonium AuNPs dispersed in water.

2.3.3.2 Cationic phosphonium gold nanoparticles dispersed in DMSO

In order to prepare the colloidal AuNPs in DMSO, solutions of the phosphonium ligands, **4C**, **5**, and **4** were prepared in DMSO (0.25 mmol, 0.30 mmol, and 0.8 mmol respectively). The volume used for these solutions was 20 mL. A solution of potassium tetrachloroaurate (0.12 mmol) in DMSO (10 mL) was also prepared. Then both, ligand and gold salt solutions were mixed and stirred. The reduction was carried out by adding 5 mL of freshly prepared aqueous solution of sodium borohydride (2.0 mmol) to the DMSO mixture. In order to remove the excess of ligands in each one of the gold colloidal solutions prepared, liquid-liquid extractions were carried out using diethyl ether.

2.4 Results and Discussion

2.4.1 Synthesis of tri(*p*-tolyl)phosphoniopropylthiosulfate zwitterion (4)

The synthesis of the **4** involved the preparation of two intermediates, which were obtained and purified in order to get the zwitterion. The first compound synthesised was the hydroxylpropylphosphonium salt and this was obtained by the quaternisation of the tri(*p*-tolyl)phosphine with bromopropanol as it is showed in Scheme 1. The hydroxypropyl-tri(*p*-tolyl)phosphonium bromide was then treated with HBr in order to obtain the ω-bromopropyl-tri(*p*-tolyl)phosphonium bromide. The latter is then reacted with $Na_2S_2O_3$ in aqueous ethanol.

The resulting zwitterion was purified by trituration using diethyl ether. The final product had an oily appearance, yellow coloured. When studied by ESMS in positive ion mode, an ion corresponding to $M+H^+$ was observed (459). The ^1H NMR showed the distinctive chemical shift at 2.3 corresponding to the nine protons from the $–CH_3$ attached to the aromatic ring. This chemical shift is the main difference between the tri(*p*-tolyl)phosphoniopropylthiosulfate and the triphenylphosphoniopropylthiosulfate ^1H NMR spectra. It can be assumed that the sulfur-sulfur bond of both tri(*p*-tolyl)phosphoniopropylthiosulfate undergoes cleavage with the loss of the sulfite ion under reductive conditions as in the synthesis of gold colloidal NPs, as it was shown and reported in the case of the triphenylphosphoniopropylthiosulfate.

This cleavage will allow the sulfur of the cationic phosphonium ligand to interact with the AuNP surface. As previously mentioned, these thiosulfate and thioacetate ligands are usually known as masked thiol ligands. For **4C** and **5** similar results to the previously reported were observed when studied by IR, NMR and ESI-MS. Solubility tests were carried out to all three masked thiol ligands. They were soluble in methanol, ethanol, DMSO, chloroform and DCM.

2.4.2 Cationic phosphonium gold nanoparticles dispersed in water and DMSO

The **4C** and **5** ligands have shown their ability to functionalised and stabilised AuNPs surface in water. For this work, another biocompatible solvent, DMSO, was used in order to assist with the solubilisation of more hydrophobic ligand **4**, its interaction with AuNP surface, and then penetration into the lipophilic cell wall. These thiosulfates containing

salts are also known as Bunte salts. Shon, Y-S., et al., were the first in showing the production of alkanethiolate-AuNPs from Bunte salts [34].

They used sodium S-dodecylthiosulfate and showed that the sulfur-sulfur bond of the thiosulfate salt undergoes cleavage and acted as the free thiol [32, 34]. Functionalised AuNPs dispersed in water were obtained when **4C** and **5** ligands, and the two-phase liquid-liquid (DCM / water) method were used. However, when **4** was used as the protecting ligand with the same method, no transfer of these NPs to the water phase was observed, and, therefore, no stable gold colloidal NPs were obtained in water.
Various attempts of synthesising phosphonium cationic AuNPs were carried out using **4** as the stabilising ligand and the two phase DCM / water method. Concentration of this ligand was also increased to a double (80 mM) and same results were obtained. Therefore, in the case of **4**, even increments in the concentration of the ligand did not help to obtain the functionalised AuNPs dispersed in water.

DMSO was chosen as an alternative solvent to disperse the AuNPs functionalised with **4** ligand. Due to the properties described in the introduction, DMSO was used to synthesise AuNP functionalised with the **4**, and also be able to use more hydrophobic phosphonium ligands to fabricate carriers with potential abilities to permeate and penetrate the lipophilic cell walls.

In order to prepare the colloidal AuNPs in DMSO, a reduction of gold (III) to gold (0) was carried out in the presence of **4** in DMSO, using sodium borohydride as the reducing agent. With this reducing method using DMSO as the dispersing solvent, a ruby – coloured colloidal solution of AuNPs functionalised with **4** was obtained. Using the same method in DMSO, other colloidal solutions of AuNPs functionalised using **4C** and **5** as protecting ligands were also successfully obtained. Stability studies were also carried out in order to monitor over time the potential aggregation in the colloidal solutions prepared following this method.

2.4.3 UV-Visible and TEM studies

Using UV-Vis spectroscopy technique, formation of AuNPs in solution (either in water or DMSO) and as previously mentioned, stability of these colloidal solutions were followed. It is well-known that the dark-red colour of gold colloids dispersed in water reflects the surface plasmon band (SPB), which is a broad absorption band in the visible

region around 520 nm [35]. The SPB is due to the collective oscillations of the electrons at the surface of NPs (6s electrons of the conduction band for AuNPs) that is correlated with the electromagnetic field of the incoming light [36]. The maximum bandwidth is also influenced by the particle size [37-40]. It has been shown that for AuNPs of mean diameter of 9, 15, 22, 48, and 99 nm, the SPB maximum λ_{max} was observed at 517, 520, 521, 533, and 575 nm, respectively, in aqueous media [37, 41].

Evidence of the formation of AuNPs using the reduction method in DMSO was shown by UV-Visible spectroscopy technique. Using the DMSO as the blank, bands centred at 519 (Figure 2.1, see UV-visible spectrum at time = 0), 519 (Figure 2.2, see UV-visible spectrum at time = 0) and 529 nm (Figure 2.3, see UV-visible spectrum at time 0) were observed in the resulting UV spectra corresponding to the burgundy gold colloidal solutions prepared with triphenylphosphoniopropylthiosulfate, (3-thioactylpropyl)-triphenylphosphonium bromide and tri(*p*-tolyl)phosphoniopropylthiosulfate, respectively. Their stability was also monitored by UV-Vis spectroscopy and the DMSO solutions showed to be stable at least for 12 weeks (Figures 2.1, 2.2 and 2.3). The colloidal solutions were stored in the dark and at room temperature.

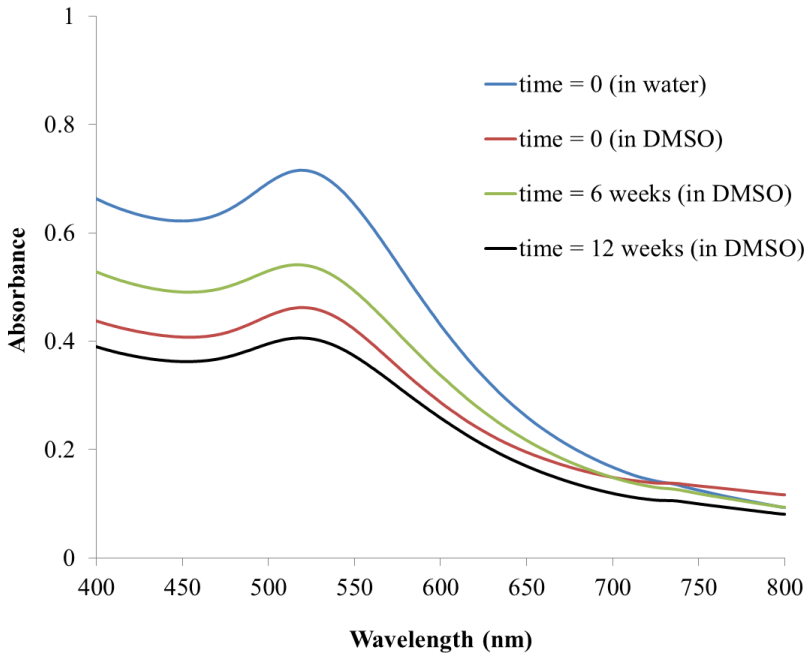

Figure 2.1. UV-visible absorption spectra of the colloidal solutions of AuNPs functionalised using **4C** as protecting ligand. The different UV-visible spectra represent these NPs dispersed in water at time = 0, and DMSO at time = 0, 6 and 12 weeks. Where time = 0 is the initial time of the **4C**-AuNP preparation.

As previously reported and repeated for this work for comparison purposes, the AuNPs synthesised using **4C** and **5** as protecting ligands, and dispersed in water showed broad bands centred at 519 nm in both cases in the UV-visible spectra (Figures 2.1 and 2.2, respectively) [32, 33, 42]. When compared the UV spectra of the colloidal solutions of AuNPs functionalised with **4C** in water and DMSO (Figures 2.1 and 2.2, see UV-visible spectra at t = 0 in water and DMSO), they did not show significant differences in the wavelengths. In our case the refractive index of the solvent DMSO has not shown to induce a shift of the SPB of our NPs as suggested in the literature [41].

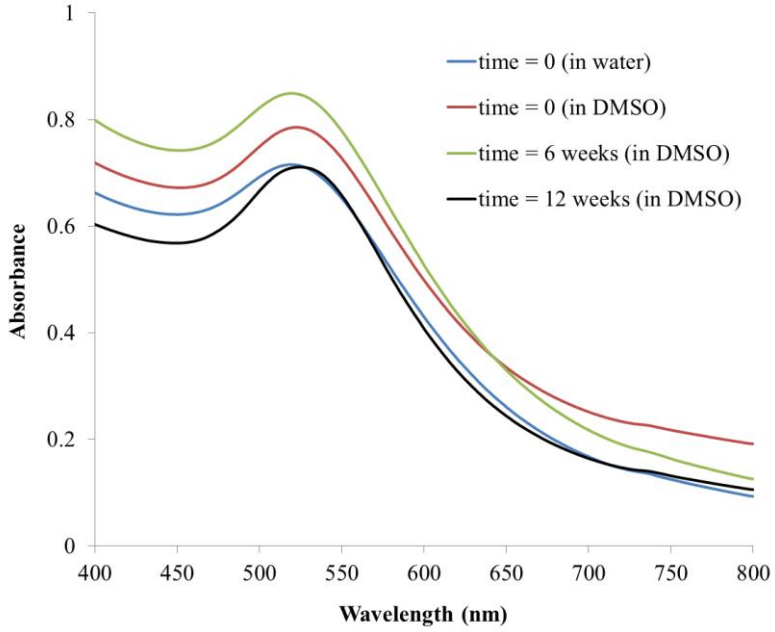

Figure 2.2. UV-visible absorption spectra of the colloidal solutions of AuNPs functionalised using **5** as protecting ligand. The different UV-visible spectra represent these NPs dispersed in water at time = 0, and DMSO at time = 0, 6 and 12 weeks.

The ligand shell also alters the refractive index and causes either a red or blue shift. This shift is especially significant with thiolate ligands, which are responsible for a strong ligand field interacting with surface electron cloud [38]. Similar evidence can be observed when compared the colloidal solutions in DMSO of AuNPs stabilised with **4C** with the one corresponding to AuNPs functionalised with **4**. Differences in wavelengths (519 and

529 nm, respectively) can be observed when ligands change in structure (see Figures 2.1 and 2.3).

The colloidal solutions of AuNPs functionalised using **4C** (Figure 2.4, **TEM1**), **5** (Figure 2.4, **TEM2**) and **4** (Figure 2.4, **TEM3**) as protecting ligands, were all analysed by TEM. Micrographs of all three AuNP samples showed spherical or semi-spherical shaped particles. Then, particle sizes for samples **TEM1**, **TEM2** and **TEM3** were obtained by analysing at least 150 particles per sample from several images taken.

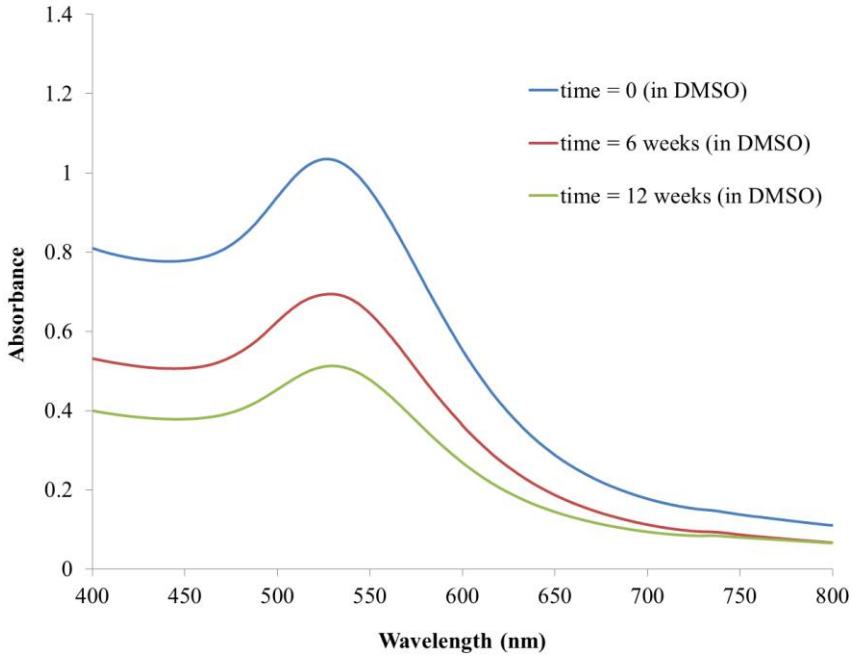

Figure 2.3. UV-visible absorption spectra of the colloidal solutions of AuNPs functionalised using **4** as protecting ligand. The different UV-visible spectra represent these NPs dispersed in DMSO at time = 0, 6 and 12 weeks.

All sample showed to be monodispersed and mean particle diameters were obtained by calculating the averages and standard deviations. For mean diameters obtained for the samples analysed were the followings: 11 ± 1 nm (**TEM1**), 8 ± 1 nm (**TEM2**) and 10 ± 1 nm (**TEM3**). Samples **TEM1** and **TEM2** showed similar particle sizes to ones reported and synthesised using the two-phase DCM/water method [32, 33].

These evidences are confirmed by the ones found in the corresponding UV-Visible spectra. Although, solvents used to disperse the NPs were different, the principle of the

reduction method used was the same and also the concentrations used for both methods, two phase DCM/water and DMSO, were similar.

In the case of the **4** functionalised AuNPs, they could only be produced using the DMSO method. The corresponding UV-Visible spectrum showed that the SPB is centred at 529 nm. With this evidence only, it could have been assumed that NPs were slightly larger in size than the ones functionalised with the **4C** ligands, which showed bands centred at 519 nm.

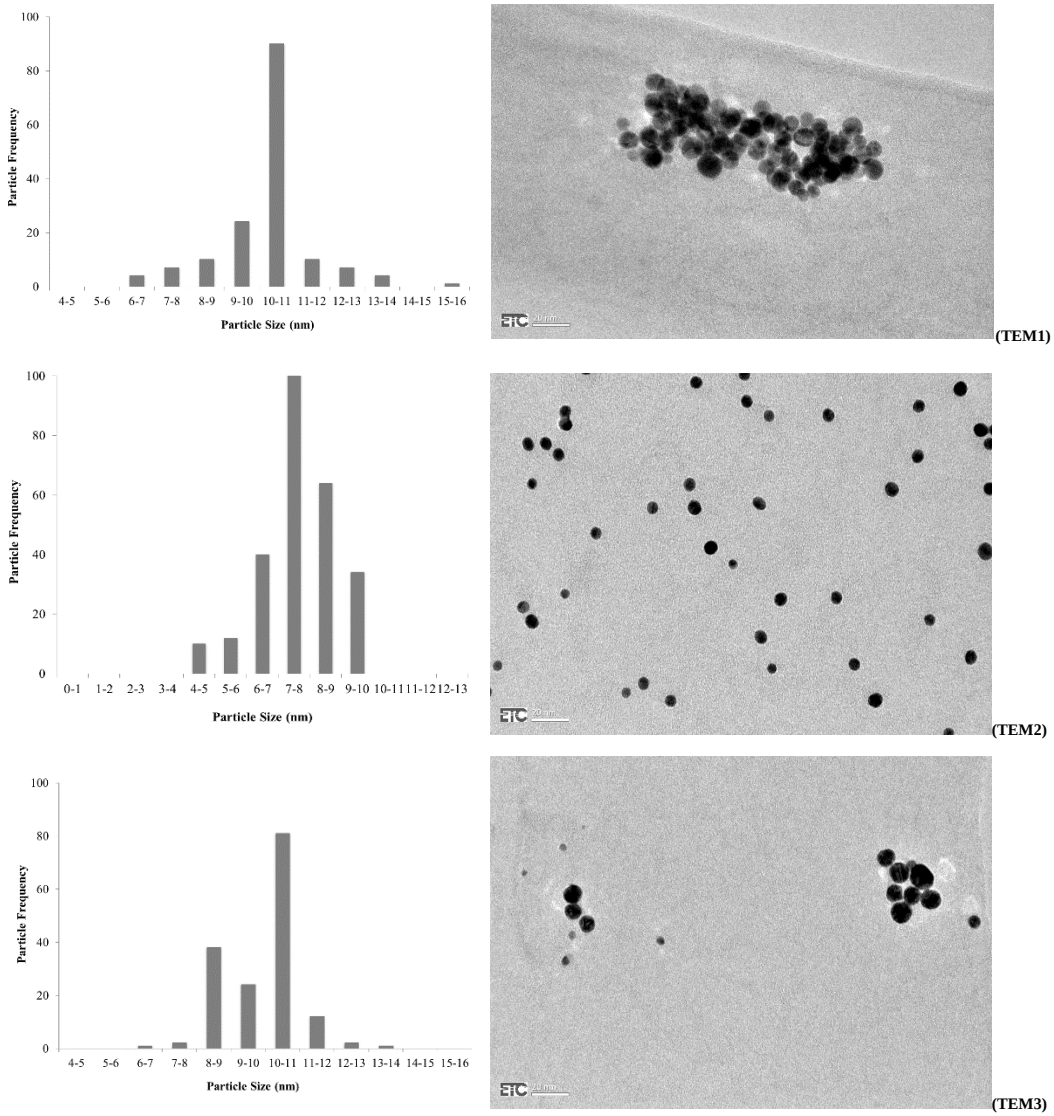

Figure 2.4. Representative TEM micrographs of cationic phosphonium AuNPs synthesised using **4C** (**TEM1**), **5** (**TEM2**), and **4** (**TEM3**) as protecting ligands in DMSO, and corresponding particle size histograms.

The slight blue shift observed in the UV-Visible spectrum of the **4** functionalised AuNPs might be due to the ligand shell altering the refractive index and interacting more strongly with the electron cloud of the NP surface, and not to the particle size. This evidence supports Su, KH., et al., experimental observations and results [38].

2.5 Conclusions

The fabrication of cationic phosphonium AuNPs using triphenylphosphoniopropylthiosulfate (**4C**) zwitterion, (3-thioactylpropyl)triphenyl-phosphonium bromide (**5**), and tri(*p*-tolyl)phosphoniopropylthiosulfate (**4**) zwitterion as protecting ligands and a reduction method in DMSO was reported for the first time; and also the synthesis of a new masked thiol, tri(*p*-tolyl)phosphoniopropylthiosulfate zwitterion (**4**). These Bunte salts and thioacetate ligands offer an advantage over the free thiol ligands as they showed better stability to air oxidation. The use of a biocompatible solvent such as DMSO to produce these NPs can represent an advantage for their potential applications as novel therapeutic agents, especially, when more hydrophobic ligands (tri(*p*-tolyl)phosphoniopropylthiosulfate zwitterion) are used to functionalised AuNPs, as they may have more affinity with the lipophilic cell walls. It was also shown that under reductive conditions in DMSO, the formation of these NPs occurred in the presence of all three cationic phosphonium ligands synthesised for this work.

The formation and the stability over time of **4C**, and **4** functionalised AuNPs in DMSO were confirmed and followed by UV-visible spectroscopy. Bands centred at 519 and 529 nm, respectively, were observed in the UV-visible spectra, and those did not change over a period of 3 months. Changes in the ligands chemical structure can probably affect the refractive index of the colloidal solution and produce a shift to the left (blue shift). As previously mentioned, **4** functionalised AuNPs were successfully produced and dispersed in DMSO, however, these NPs could not be produced using the two-phase liquid/liquid (DCM / water) method and dispersed in water. The TEM analyses of the **4C** and **4** functionalised AuNPs showed a fairly good monodispersity and particle sizes of 8 and 11 nm.

2.6 Characterisation of the cationic phosphonium ligands

Hydroxypropyl-tri(p-tolyl)phosphonium bromide (2)

IR spectrum showed absorption bands at the regions of 725–720 cm^{-1} (ν CH_2), 1600cm^{-1} (ν C-O), 3100–3000 cm^{-1}(ν CH-Aromatic), and 3344 cm^{-1} (ν C-OH). ^{1}H NMR spectrum gave signals at δ 1.8 (9H, s, 2CH_3), δ 2.0 (2H, m, -CH_2-), δ 2.6 (1H, s, OH), δ 3.4 (2H, m, P-CH_2), δ 3.6 (2H, t, OH-CH_2), and δ 7.3-7.5 (12H, m, Aromatic H) ppm. ESI-MS 363 [M - Br], 364 [M – Br] + [H^+].

ω-bromopropyl-tri(p-tolyl)phosphonium bromide (3)

IR spectrum showed absorption bands at the regions of 677cm^{-1} (ν C-Br), 748 cm^{-1} (ν CH_2), 988 cm^{-1} (ν P-CH_2), and 3100–3000 cm^{-1}(ν CH-Aromatic). ^{1}H NMR spectrum gave signals at δ 2.3 (9H, s, -CH_3), δ 2.4(2H, m, P-CH_2), δ 3.8 (2H, m, -CH_2-) and at 7.4 - 7.9 (12H, m, Aromatic H) ppm. ESI-MS 427 [M].

Tri(p-tolyl)phosphoniopropylthiosulfate zwitterion (4)

IR spectrum showed absorption bands at the regions of 725-720 cm^{-1}, (νCH_2), 1329cm^{-1} (ν S=O), 1400 cm^{-1} (ν C-S), 3100–3000 cm^{-1} (ν CH-Aromatic). ^{1}H NMR showed a signals at δ 2.3 (s, 9H, 3CH_3), δ 3.2 (t, 2H, P-$\underline{CH_2}$-CH_2-CH_2), δ 3.4 (t, 2H, P -CH_2-CH_2-$\underline{CH_2}$), δ 3.6 (m, 2H, P-CH_2-$\underline{CH_2}$-CH_2), δ 7.24 (1H, $CDCL_3$), and δ 7.3-7.6 (12H, m, Aromatic H) ppm. ESI-MS 459 [M + H^+].

Triphenylphosphoniopropylthiosulfate zwitterion (4C)

IR spectrum showed absorption bands at the regions IR spectrum showed absorption bands at the regions of 725–720 cm^{-1} (ν CH_2), 1330 cm^1 (ν S=O), 1345 cm^{-1} (C-S-), and 3100–3000 cm^{-1} (ν CH-Aromatic). ^{1}H NMR spectrum gave signals at δ 2.2 (2H, m, P-$\underline{CH_2}$-CH_2-CH_2), δ 3.3 (2H, m, P-CH_2-CH_2-$\underline{CH_2}$), δ 4.0 (2H, m, P-CH_2-$\underline{CH_2}$-CH_2) and at 7.6 - 7.8 (15H, m, Aromatic H) ppm. ESI-MS 417 [M + H^+].

(3-Thioactylpropyl)triphenylphosphonium bromide (5)

IR spectrum showed absorption bands at the regions of 735–740 cm^{-1} (ν CH_2), 1345 cm^{-1} (ν C-S), 1470–1450 cm^{-1} (ν C–H corresponding to bend-CH_2), 1678 cm^{-1} (ν C=O), and 3100–3000 cm^{-1}(ν CH-Aromatic). ^{1}H NMR showed a signals at δ 2.4 (3H, s, -CH_3), δ 2.9

(2H, m, P-$\underline{CH_2}$-CH_2-CH_2), δ 3.8 (2H, m, P-CH_2-CH_2-$\underline{CH_2}$), δ 4.1 (2H, m, P-CH_2-$\underline{CH_2}$-CH_2), and δ 7.6-7.9 (15H, m, Aromatic H) ppm. ESI-MS 380 [$M + H^+$].

2.7 References

1. Ferrari, M, *Cancer nanotechnology: opportunities and challenges.* Nature Reviews Cancer, 2005. **5**(3): p. 161-171.

2. Paciotti, GF., Kingston, DGI and Tamarkin, L, *Colloidal gold nanoparticles: a novel nanoparticle platform for developing multifunctional tumor-targeted drug delivery vectors.* Drug development research, 2006. **67**(1): p. 47-54.

3. Tonga, GY., Moyano, DF., Kim, CS and Rotello, VM, *Inorganic nanoparticles for therapeutic delivery: Trials, tribulations and promise.* Current opinion in colloid & interface science, 2014. **19**(2): p. 49-55.

4. Rosi, NL and Mirkin, CA, *Nanostructures in biodiagnostics.* Chemical reviews, 2005. **105**(4): p. 1547-1562.

5. Cheng, MM-C., Cuda, G., Bunimovich, YL., Gaspari, M., Heath, JR., Hill, HD., Mirkin, CA., Nijdam, AJ., Terracciano, R and Thundat, T, *Nanotechnologies for biomolecular detection and medical diagnostics.* Current opinion in chemical biology, 2006. **10**(1): p. 11-19.

6. Saha, K., Agasti, SS., Kim, C., Li, X and Rotello, VM, *Gold nanoparticles in chemical and biological sensing.* Chemical reviews, 2012. **112**(5): p. 2739-2779.

7. Ghosh, P., Han, G., De, M., Kim, CK and Rotello, VM, *Gold nanoparticles in delivery applications.* Advanced drug delivery reviews, 2008. **60**(11): p. 1307-1315.

8. Cho, EC., Zhang, Q and Xia, Y, *The effect of sedimentation and diffusion on cellular uptake of gold nanoparticles.* Nature nanotechnology, 2011. **6**(6): p. 385-391.

9. Kim, CS., Duncan, B., Creran, B and Rotello, VM, *Triggered nanoparticles as therapeutics.* Nano today, 2013. **8**(4): p. 439-447.

10. Cho, EC., Xie, J., Wurm, PA and Xia, Y, *Understanding the role of surface charges in cellular adsorption versus internalization by selectively removing gold nanoparticles on the cell surface with a I2/KI etchant.* Nano letters, 2009. **9**(3): p. 1080-1084.

11. Cho, EC., Au, L., Zhang, Q and Xia, Y, *The effects of size, shape, and surface functional group of gold nanostructures on their adsorption and internalization by cells.* Small, 2010. **6**(4): p. 517-522.

12. Dausend, J., Musyanovych, A., Dass, M., Walther, P., Schrezenmeier, H., Landfester, K and Mailänder, V, *Uptake mechanism of oppositely charged fluorescent nanoparticles in HeLa cells.* Macromolecular bioscience, 2008. **8**(12): p. 1135-1143.

13. Yang, H., Fung, SY and Liu, M, *Programming the Cellular Uptake of Physiologically Stable Peptide–Gold Nanoparticle Hybrids with Single Amino Acids.* Angewandte Chemie International Edition, 2011. **50**(41): p. 9643-9646.

14. Oh, E., Delehanty, JB., Sapsford, KE., Susumu, K., Goswami, R., Blanco-Canosa, JB., Dawson, PE., Granek, J., Shoff, M and Zhang, Q, *Cellular uptake and fate of PEGylated gold nanoparticles is dependent on both cell-penetration peptides and particle size.* Acs Nano, 2011. **5**(8): p. 6434-6448.

15. Al-Hajaj, NA., Moquin, A., Neibert, KD., Soliman, GM., Winnik, FOM and Maysinger, D, *Short ligands affect modes of QD uptake and elimination in human cells.* ACS nano, 2011. **5**(6): p. 4909-4918.

16. Zhan, N., Palui, G., Safi, M., Ji, X and Mattoussi, H, *Multidentate zwitterionic ligands provide compact and highly biocompatible quantum dots.* Journal of the American Chemical Society, 2013. **135**(37): p. 13786-13795.

17. Zhu, Z-J., Yeh, Y-C., Tang, R., Yan, B., Tamayo, J., Vachet, RW and Rotello, VM, *Stability of quantum dots in live cells.* Nature chemistry, 2011. **3**(12): p. 963-968.

18. Ballou, B., Lagerholm, BC., Ernst, LA., Bruchez, MP and Waggoner, AS, *Noninvasive imaging of quantum dots in mice.* Bioconjugate chemistry, 2004. **15**(1): p. 79-86.

19. He, Y., Zhong, Y., Su, Y., Lu, Y., Jiang, Z., Peng, F., Xu, T., Su, S., Huang, Q and Fan, C, *Water-Dispersed Near-Infrared-Emitting Quantum Dots of Ultrasmall Sizes for In Vitro and In Vivo Imaging.* Angewandte Chemie International Edition, 2011. **50**(25): p. 5695-5698.

20. Dubertret, B., Skourides, P., Norris, DJ., Noireaux, V., Brivanlou, AH and Libchaber, A, *In vivo imaging of quantum dots encapsulated in phospholipid micelles.* Science, 2002. **298**(5599): p. 1759-1762.

21. Saha, K., Moyano, DF and Rotello, VM, *Protein coronas suppress the hemolytic activity of hydrophilic and hydrophobic nanoparticles.* Materials horizons, 2014. **1**(1): p. 102-105.

22. Mcintosh, CM., Esposito, EA., Boal, AK., Simard, JM., Martin, CT and Rotello, VM, *Inhibition of DNA transcription using cationic mixed monolayer protected gold clusters.* Journal of the American Chemical Society, 2001. **123**(31): p. 7626-7629.

23. Murphy, MP and Smith, RaJ, *Targeting antioxidants to mitochondria by conjugation to lipophilic cations.* Annu. Rev. Pharmacol. Toxicol., 2007. **47**: p. 629-656.

24. Ross, MF., Da Ros, T., Blaikie, FH., Prime, TA., Porteous, CM., Severina, II., Skulachev, VP., Kjaergaard, HG., Smith, RaJ and Murphy, MP, *Accumulation of lipophilic dications by mitochondria and cells.* Biochemical journal, 2006. **400**(1): p. 199-208.

25. Ross, MF., Kelso, GF., Blaikie, FH., James, AM., Cocheme, HM., Filipovska, A., Da Ros, T., Hurd, TR., Smith, RaJ and Murphy, MP, *Lipophilic triphenylphosphonium cations as tools in mitochondrial bioenergetics and free radical biology.* Biochemistry (Moscow), 2005. **70**(2): p. 222-230.

26. Logan, A., Pell, VR., Shaffer, KJ., Evans, C., Stanley, NJ., Robb, EL., Prime, TA., Chouchani, ET., Cochemé, HM and Fearnley, IM, *Assessing the mitochondrial membrane potential in cells and in vivo using targeted click chemistry and mass spectrometry.* Cell metabolism, 2016. **23**(2): p. 379-385.

27. Rao, CNR., Vivekchand, SRC., Biswas, K and Govindaraj, A, *Synthesis of inorganic nanomaterials.* Dalton Transactions, 2007(34): p. 3728-3749.

28. Binder, WH., Sachsenhofer, R., Straif, CJ and Zirbs, R, *Surface-modified nanoparticles via thermal and Cu (I)-mediated "click" chemistry: generation of luminescent CdSe nanoparticles with polar ligands guiding supramolecular recognition.* Journal of Materials Chemistry, 2007. **17**(20): p. 2125-2132.

29. Pyrpassopoulos, S., Niarchos, D., Nounesis, G., Boukos, N., Zafiropoulou, I and Tzitzios, V, *Synthesis and self-organization of Au nanoparticles.* Nanotechnology, 2007. **18**(48): p. 485604.

30. http://www.accessdata.fda.gov/cms_ia/importalert_169.html .*(accessed date: 01/10/2014).* [cited accessed date: (01/10/2014).

31. Marren, K, *Dimethyl sulfoxide: an effective penetration enhancer for topical administration of NSAIDs.* The Physician and sportsmedicine, 2011. **39**(3): p. 75-82.

32. Ju-Nam, Y., Bricklebank, N., Allen, DW., Gardiner, PHE., Light, ME and Hursthouse, MB, *Phosphonioalkylthiosulfate zwitterions—new masked thiol ligands for the formation of cationic functionalised gold nanoparticles.* Organic & biomolecular chemistry, 2006. **4**(23): p. 4345-4351.

33. Ju-Nam, Y., Allen, DW., Gardiner, PHE and Bricklebank, N, *ω-Thioacetylalkylphosphonium salts: Precursors for the preparation of phosphonium-functionalised gold nanoparticles.* Journal of organometallic chemistry, 2008. **693**(23): p. 3504-3508.

34. Shon, Y-S., Gross, SM., Dawson, B., Porter, M and Murray, RW, *Alkanethiolate-protected gold clusters generated from sodium S-dodecylthiosulfate (Bunte salts).* Langmuir, 2000. **16**(16): p. 6555-6561.

35. Alivisatos, AP, *Semiconductor clusters, nanocrystals, and quantum dots.* Science, 1996. **271**(5251): p. 933.

36. D.L. Feldheim and And A.F.Colby, *Metal Nanoparticles: Synthesis, Characterization, and Applications* , . Journal of the American Chemical Society, 2002. **124**(26): p. 7874-7875.

37. Link, S and El-Sayed, MA, *Size and temperature dependence of the plasmon absorption of colloidal gold nanoparticles.* The Journal of Physical Chemistry B, 1999. **103**(21): p. 4212-4217.

38. Su, KH., Wei, QH., Zhang, X., Mock, JJ., Smith, DR and Schultz, S, *Interparticle coupling effects on plasmon resonances of nanogold particles.* Nano letters, 2003. **3**(8): p. 1087-1090.

39. Link, S., Mohamed, M and El-Sayed, M, *Simulation of the optical absorption spectra of gold nanorods as a function of their aspect ratio and the effect of the medium dielectric constant.* The Journal of Physical Chemistry B, 1999. **103**(16): p. 3073-3077.

40. Yan, B., Yang, Y and Wang, Y, *Comment on "simulation of the optical absorption spectra of gold nanorods as a function of their aspect ratio and the effect of the medium dielectric constant".* The Journal of Physical Chemistry B, 2003. **107**(34): p. 9159-9159.

41. Daniel, M-C and Astruc, D, *Gold nanoparticles: assembly, supramolecular chemistry, quantum-size-related properties, and applications toward biology, catalysis, and nanotechnology.* Chemical reviews, 2004. **104**(1): p. 293-346.

42. Ju-Nam, Y., Chen, Y-S., Ojeda, JJ., Allen, DW., Cross, NA., Gardiner, PH and Bricklebank, N, *Water-soluble gold nanoparticles stabilized with cationic phosphonium thiolate ligands.* RSC Advances, 2012. **2**(27): p. 10345-10351.

Chapter 3: Synthesis of potential pH-sensitive cationic phosphonium AuNPs in aqueous medium

3.1 Abstract

Nano-therapeutics is a rapidly progressing area of research and aims to improve therapeutic efficacy with minimal side effects by the selective augmentation of anticancer drug concentrations within tumour tissues, thus solving the problems presented by conventional chemotherapy.

The main goal of this study describes the further development of phosphonioalkyl ligands in order to use in functionalised AuNPs. The AuNPs were functionalised with ligands including (3-thioacetylpropyl)triphenylphosphonium bromide, (3-thioacetylpropyl)-tri(*P*-tolyl)phosphonium bromide and (3-thioacetylpropyl)-tris(2,4,6-trimethoxyphenyl)-phosphonium bromide. The functionalised AuNPs were investigated with their stability over time at a pH range of 3-11. The synthesised AuNPs were primarily characterised by using both UV-visible spectra and DLS.

The AuNPs synthesis were conducted in one of two ways with reduction by a biphasic solvent system of DCM/water, and monophasic medium DMSO. The synthesis of AuNPs with methoxy phosphonium head group containing ligands showed the most promising results in the pH trials. Clear evidence of the reduction of gold (III) to gold (0) and formation of colloidal AuNPs were obtained, as maximum absorbance peaks around 520 nm were observed in the UV-Visible spectra.

The stability study carried out over time. According to the DLS results, with samples of the functionalised AuNPs (3-Thioacetylpropyl)triphenylphosphonium bromide (**5**), (3-thioacetylpropyl)-tri(*P*-tolyl)phosphonium bromide, and (3-thioacetylpropyl)-tris(2,4,6-trimethoxyphenyl)phosphonium bromide, showed that, the AuNPs produced were in the range of 7.6 ± 1.4 nm to 14.30 ± 1.5 nm, 6.8 ± 1.30 nm to 12.8 ± 1.3 nm, and 5.9 ± 1.18 nm to 14.0 ± 1.3 nm, respectively. With no clear sign of aggregation. For pH 3-11, plasmon resonance band peaks were observed between 519 to 536 nm in the UV-Vis spectra.

The pH study suggested that the optimum pH range for the AuNP colloidal samples to remain fairly stable is between pH 9.2 and pH 5.1. Within this range the diameters recorded by the DLS were 10.8 ± 0.9 nm in the case of (3-Thioacetylpropyl)-triphenyl-phosphonium bromide functionalised AuNPs, 9.6 ± 1.7 nm for (3-thioacetylpropyl)-tri*(P*-tolyl)-phosphonium bromide functionalised AuNPs, and 9.6 ± 1.4 nm in the case of (3-thioacetylpropyl)-tris(2,4,6-trimethoxyphenyl)phosphonium bromide functionalised AuNPs.

In contrast, aggregation was observed in the DLS analyses for AuNP samples functionalised with (3-Thioacetylpropyl)triphenyl-phosphonium bromide at pH values higher than 8.2 ± 0.1 and lower than pH 5.5 ± 0.1, (3-thioacetylpropyl)-tris(2,4,6-trimethoxyphenyl)-phosphonium bromide at pH higher than 9.0 ± 0.15 and lower than pH 3.3 ± 0.1 and (3-thioacetylpropyl)-tri(*P*-tolyl)phosphonium bromide at pH higher than 9.1 ± 0.1 and lower than pH 5.1 ± 0.15. The aggregation of the AuNPs may be due to the electrostatic interaction between the cationic phosphonioalkyl ligands and the higher concentration of anions present in basic pH solutions. Moreover, also due to the attractive forces between these charge distributions of the different AuNPs, the repulsive forces within each particle are weakened, causing to a correspondingly lower resonance frequency. At pH lower than 4, it can be assumed that functionalised AuNP solution is fully protonated as the number of positive charges is significantly high. The increase in proton concentration results in ion exchange between protons and the thiolate groups; and therefore, in aggregation due to possible unprotected AuNPs.

According to the literature, the environment around cancer cells is known to be mildly acidic with pH of 6.0 to 7.2, which is lower than in healthy cells (pH in the range of 7.2 to 7.4). Based on this factor, pH sensitive functionalised metal NPs have shown abilities to induce cancer cell death *via* a photothermal therapy after aggregation.

3.2 Introduction

Over the past decades, cancer therapeutics has been developing as the research area that continues expanding and attracting interest. At present, cancer causes about > 8.2 million deaths annually worldwide [1, 2]. The overall field of nanotechnology was predicted by the American Foundation for Science to be worth $1 trillion in 2015. For all products and services associated [3], with Nano-medicine expected to contribute a projected $528

billion by 2019 [4], and although significant achievement has been made in the field of cancer therapy including surgery, chemotherapy, and radiation., Many patients still face unsatisfactory results due to severe drug side effects and reoccurrence of cancer [1, 2]. Consequently, the selective increase of anticancer drug concentrations inside tumour tissues remains a major challenge in improving therapeutic efficacy with minimal side effects [5].

The development of AuNPs for drug delivery offers a feasible solution for targeted and controlled delivery of anticancer drugs [6]. There are several obstacles that must be overcome in order to develop and improve existing cancer treatments to be effective, and reduce cancer drug doses and toxicity towards healthy proliferating cells. Use of AuNPs as alternatives to traditional treatments can potentially overcome multidrug resistance (MDR) against anticancer drugs [7].

Traditionally, cancer has been treated with a combination of drugs, chemotherapy, and surgery to maintain and remove the cancerous tissues present. Chemotherapy is a key part of anti-cancer therapy, but its effectiveness is often hampered by drug resistance [8-10]. Recent studies highlight that tumour microenvironment plays a predominant role in tumour cell proliferation, metastasis, and drug resistance [11]. To reduce the drug resistance and improve the specificity of the drug molecule, AuNPs can be employed depending on the type of a tumour being treated [12]. Traditional imaging techniques, such as dyes and pigments, remain crucial in diagnosis [13]. However, metallic AuNPs have gathered increasing attention in recent years as a novel tool for the diagnostic application such as imaging and diagnosis of tumour specific cells [14, 15]. Among these, metallic NPs in general, and AuNPs, in particular, have been gaining prevalence in medical application as unique drug delivery vehicles as a result to their special size, shape, and surface-dependent properties [5, 16]. In addition to this, their reported biocompatibility and non-cytotoxicity have made drug delivery the leading emerging application of AuNPs. Furthermore, the ease with which their surfaces can be functionalised also makes these NPs attractive for this application. Properly functionalised AuNPs can not only serve as a drug reservoir but also provide a long circulation time [5, 17, 18].

AuNPs can be used in conjunction with more traditional imaging methods during surgery to ensure that the efficiency of the operation is increased [19], due to the removal of all

cancerous tissues that may not have been clearly presented without increased image contrast. With certain functional groups added to the AuNPs, it has been observed that the fluorescence of AuNPs quantum dots can be seen by the unaided eye [20].

The pH sensitive metal NP based on this invention consists of a pH sensitive ligand that changes charge depending on the pH of the metal NP. For instance, according to the relevant literature, AuNPs are expected to change their surface charges from negative to positive under acidic conditions and the aggregations by electrostatic attractions, usually require two different types of particles with opposite charges. It was successfully showed that AuNPs could efficiently accumulate and form aggregates within cells, such as cancer cells that present an abnormal pH environment. The pH sensitive metal NP, based on this invention, can induce cell death through a photothermal procedure after aggregation. Therefore, this type of NPs could enable medical treatment using cell necrosis such as cancer treatment [2, 21-23].

The environment around abnormal cells like cancer cells are known to be weakly acidic within a pH of 6.0 to 7.2, in contrast, the healthy cell environment has been determined to be within a pH in the range of 7.2 to 7.4. Therapies for cancer using this property are under extensive study. For instance, poly-(3-aminoester) and hydrophilic polyethylene glycol, which can form micelle structures due to their own amphiphilicity and pH-dependent ionisation, can deliver drugs to cancer cells depending on the change in pH and kill the cells. The compounds form conjugates (liposomes, complexes, and NPs) with therapeutic molecules in order to release them in compartments or cell tissues where the pH therefrom is acidic. Because the interactions between light and AuNPs are so strong, the AuNPs display big coefficients of absorption at resonant frequencies in comparison with organic dyes [2, 24, 25]. This property can be introduced to the AuNP itself by attaching a charged compound to the surface of the metal NP [2]. When the environment of metal NPs are changed from alkaline to acidic, at least a portion of the compounds on the metal NPs'surface are hydrolysed to give them a different charge, from what they had under an alkaline environment. During the charge change, the particles aggregate due to electrostatic interaction [2, 26].

It has been shown that the photoacoustic (PA) imaging signal produced from the developed melanin-like nanoparticle (MelNP), after exposure to mildly acidic conditions (for example, pH 6), is 8.1 times stronger compare to under neutral conditions. This unique

characteristic can be used for highly sensitive *in vivo* cancer target imaging according to the response to its acidic microenvironment [27]. The wavelength of light absorbed by the pH-sensitive metal NPs becomes higher as they aggregate. One of the greatest advantages of photothermal therapy based on the pH-sensitive AuNPs is that, the absorption wavelength or surface plasmon band of aggregates corresponding to the pH-sensitive AuNPs introduced into cancer cells, shifts towards the right of the UV-Vis spectrum. Hence, this shift leads to the use of long-wavelength light, which can penetrate, deeply into the body, allowing the potential application of the pH-sensitive AuNP in photo-thermal therapy to cancer tissues located in regions deep beneath the skin [2]. Traditional photothermal therapy suffers from some drawbacks of being applicable just to cancer occurring at places a short distance from the skin, such as skin cancer due to its photosensitisers respond to short-wavelength light which could not penetrate deeply into the body. This disadvantages can be overcame via the pH-sensitive AuNPs [28, 29].

Due to the great light-harvesting effect and large surface area-to-volume of AuNPs, the thermal energy locally emitted from the AuNPs is sufficient to cause cell death. Furthermore, because cancer cells are highly vulnerable to heat compared to normal cells, the heat emitted from AuNPs, on which light is focused at a controlled intensity, can be locally insert to kill tumour cells without damaging normal cells selectively. Further, the heat released from the gold nano-shell absorbing the energy of electromagnetic pulses in the near infrared ray range can be used in order to destroy cancer cells selectively [2].

3.3 Materials and Methods

All chemicals and solvents were purchased from Sigma-Aldrich and Fisher Scientific Ltd. For the characterization of the ligands and functionalised AuNPs, several analytical techniques were used. TLC, ATR-FTIR, NMR, ESI-MS techniques were employed to characterise the phosphonium containing ligands. UV-Visible spectroscopy and Dynamic Light Scattering (DLS) were used to characterise and obtain the size of the cationic phosphonium AuNPs. Details regarding previously mentioned analytical techniques and synthesis of cationic phosphonium ligands can be found in Chapter 2. Experimental details of the synthetic procedure to obtain (3-thioacetylpropyl)-tri(*P*-tolyl)-phosphonium bromide and (3-thioacetylpropyl)-tris(2,4,6-trimethoxyphenyl)- phosphonium bromide, and their corresponding AuNPs, and DLS are outlined in this chapter. pH studies were carried out by using Jenway 3505 pH Meter / UK, that is a general purpose, laboratory

pH meter uses rotary controls for pH values. The pH meter provides better measurement accuracy than pH indicators. Moreover, pH meter requires extra calibration processes before pH can be used [30].

3.3.1 Cationic Phosphonium Ligand Synthesis

The synthese of the (3-Thioacetylpropyl)triphenyl- phosphonium bromide (**5**) zwitterion were synthesised following methods previously reported [31, 32]. The compound (**5**) is shown in experimental section / Chapter 2.

The synthesis and characterisation of (3-thioacetylpropyl)-tri(*P*-tolyl)-phosphonium bromide (**4A**), and (3-thioacetylpropyl)-tris(2,4,6-trimethoxyphenyl)-phosphonium bromide (**4B**) are outlined in the following sections.

3.3.1.1 Synthesis of the (3-thioacetylpropyl)triphenylphosphonium bromide ligands

The reactions followed to obtain (3-thioacetylpropyl)tri(*P*-tolyl)phosphonium bromide (**4A**) and (3-thioacetylpropyl)-tris(2,4,6-trimethoxyphenyl)phosphonium bromide (**4B**) are shown in Scheme 1. The compounds were synthesised *via* the reaction of tri(*p*-tolyl)phosphine (**1A**) and tri(2,4,6-trimethoxyphenyl)phosphine (**1B**) (3.8mmol) with bromo-propanol (15 mmol) in a round bottom flask under reflux for approximately five hours. Acetonitrile (0.024 mmol) was the solvent used. The oil (in the case of **2A**) and solid precipitate (for **2B**) were collected and purified using diethyl ether and ethanol respectively (Reaction 1, Scheme1). The yield was 75%, 80% respectively. The resulting salts **(2)** were dissolved in hydrobromic acid (0.18 mmol, 10 ml) (48%) in a round bottom under reflux for five hours (Reaction 2, Scheme 1). Then, ω-bromopropyl-tri(*p*-tolyl)phosphonium bromide (**3A**, 2 mmol) and ω-bromopropyl-tris(2,4,6-trimethoxyphenyl)phosphonium bromide (**3B**, 2 mmol) were reacted separately with potassium thioacetate (3 mmol), stirring overnight at room temperature in aqueous ethanol (1:1, 10ml) (Reaction 3, Scheme 1). The compounds appeared as the creamy and brown precipitates, **4A** and **4B**, respectively. TLC was used to monitor the reactions by using 10% methanol: 90% DCM as the mobile phase. Purification of ligands **4A** and **4B** were achieved by liquid-liquid extraction DCM: water, and further cleaning using diethyl ether. Melting points of purified **4A** and **4B** ligands were 90-93°C and 250-253°C, respectively.

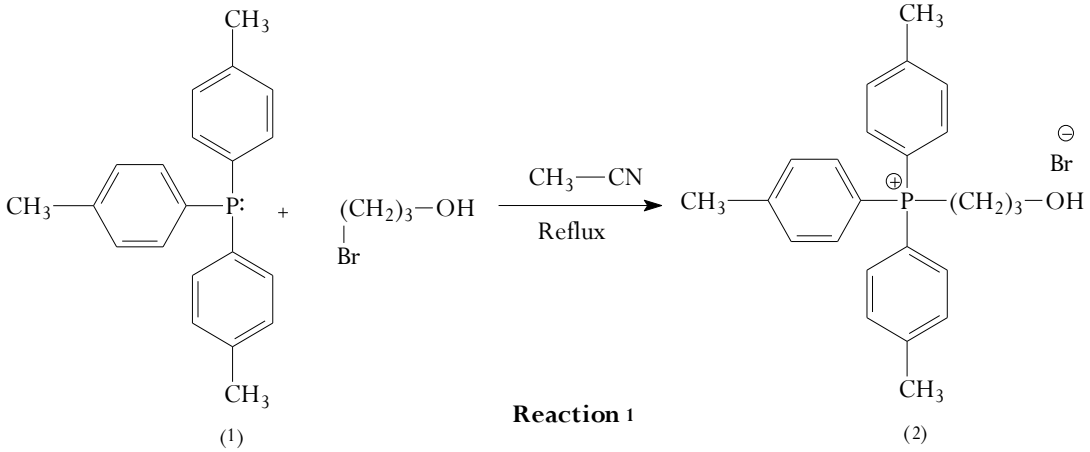

(1) **Reaction 1** (2)

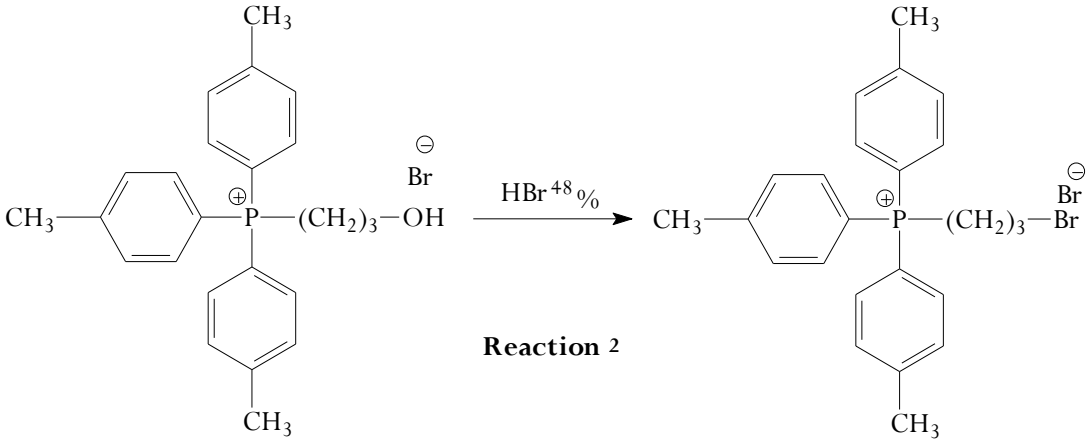

(2) **Reaction 2** (3)

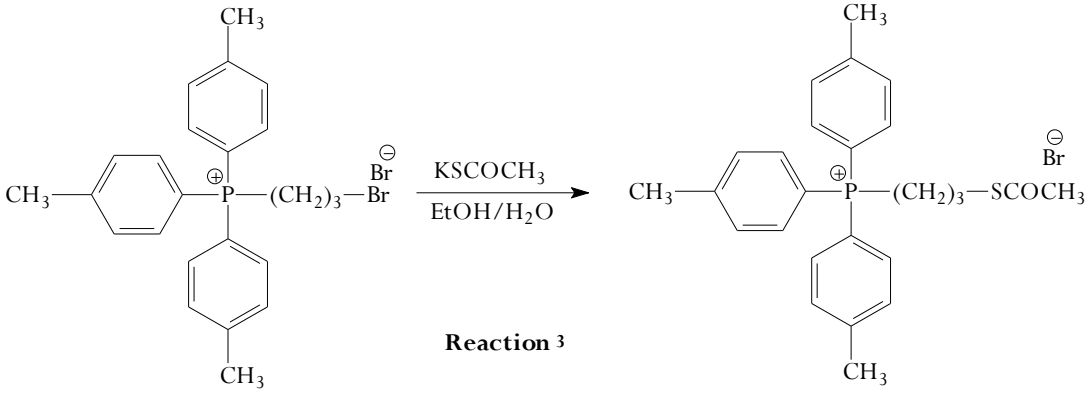

(3) **Reaction 3** (4A)

Scheme 1

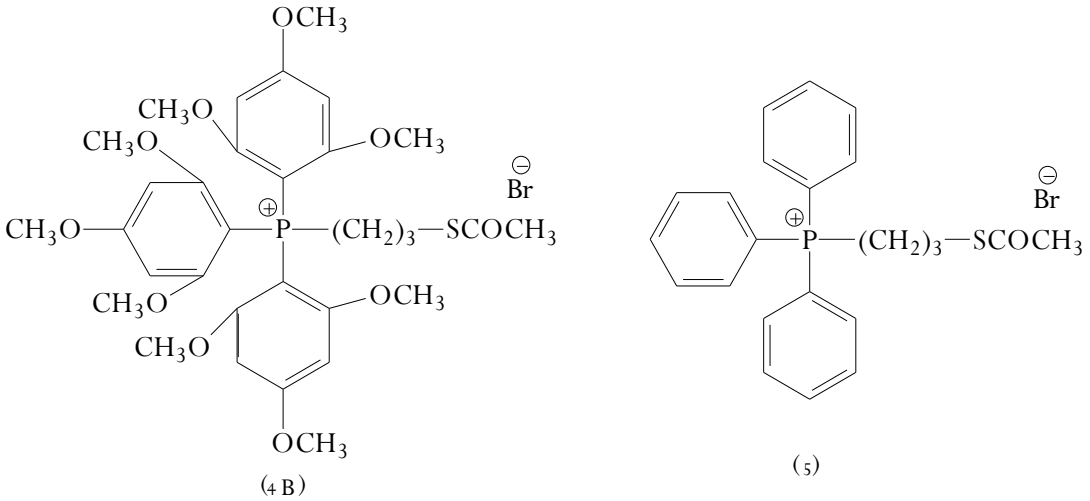

Figure 3.1. Chemical structures of (3-thioacetylpropyl)tris(2,4,6-trimethoxyphenyl)phosphonium bromide (**4B**) and (3-thioacetylpropyl)triphenyl-phosphonium bromide (**5**).

3.3.2 Synthesis of functionalised AuNPs using 4A and 4B ligands in DMSO

The synthesis of colloidal cationic phosphonium AuNPs using **4A** and **4B** ligands in DMSO were carried out in a similar fashion as the previous cationic phosphonium AuNPs. For **5**-AuNPs is shown in Chapter 2.

DMSO was used as the biocompatible solvent, instead of water due to poor solubility of these ligands in water. (3-Thioacetylpropyl)tri(*P*-tolyl)phosphonium bromide – **4A** and (3-thioacetylpropyl)-tris(2,4,6-trimethoxyphenyl)phosphonium bromide – **4B** functionalised AuNPs were successfully obtained and dispersed in DMSO by using $NaBH_4$ as reducing agent. However, AuNPs functionalised with **4A** and **4B** could not be obtained using water as the main dispersing solvent. **4A** and **4B** ligands were dissolved in DMSO (0.6 mmol, 0.30 mmol respectively). The volume of DMSO used to prepare these solutions was 30 ml. A solution of potassium tetrachloroaurate (0.12 mmol) in DMSO (10ml) was also prepared. Then both, ligands and gold salt solutions were mixed and stirred for four hours. The reduction of gold was carried out by adding 5 mL of freshly prepared $NaBH_4$ aqueous solution (0.4 M) to the DMSO mixture.

3.3.3 Dynamic Light Scattering

In order to monitor any changes in the size of cationic phosphonium AuNPs with changes in pH, Dynamic Light Scattering (DLS) technique was used. DLS work was completed using a Zetasizer Nano ZS (Malvern Instruments Ltd) which is currently top of the range and can be used for measurement of size, electrophoretic mobility and zeta potential of

the nanoparticle sample. It is possible to assess both the size and the potential aggregation of the NPs present in the solution. The technology employed is referred to as Non-Invasive Back Scatter (NIBS) technology and gives the maximum sensitivity along with the optimal size and concentration range. The sample was placed into a quartz-cuvette ensuring that it did not rise above the level specified on the equipment before being loaded into the sample compartment. Three measurements were taken from each sample after calibration of the equipment. The data collected were collated into a size distribution curve with an indication as to whether any aggregation of NPs was occurring [33].

3.4 Results and Discussion

AuNPs have prepared with different ligands as protecting ligands including as mentioned above **5**, **4A** and **4B** compounds. With changing in these ligands from benzene to toluene and methoxybenzene derivatives, the synthesis approach is described in experimental section. In order to see what different between **5**-AuNPs, **4A**-AuNPs, and **4B**-AuNPs, as well as by changing the pH values. UV−vis absorption spectroscopy showed that the maximum absorption of **4A**-NPs and **4B**-AuNPs were at 523 nm and 518 nm respectively. The DLS results illustrated that the as-prepared **4A**-AuNPs, **4B**-AuNPs had good mono-dispersion and their sizes were 6.8 ± 1.3 nm, 5.9 ± 1.2 nm respectively. All these phosphonium ligand's structure were confirmed by ATR-FTIR, ^{31}P, ^{1}H NMR and ESI-MS techniques before using them to functionalise AuNPs. Different sizes of AuNPs were generated with different stability in this Chapter. AuNPs were generally spherical shapes, and larger particles have been observed at lowest and highest pH values.

3.4.1 Synthesis of 4A and 4B ligands

(3-Thioacetypropyl)-tri(*p*-tolyl)-phosphonium bromide (**4A**) and (3-thioacetylpropyl)-tris(2,4,6-trimethoxyphenyl)phosphonium bromide (**4B**) zwitterions involved the preparation of two intermediates, as are showed in Scheme 1. The resulting zwitterions were purified by trituration using diethyl ether. When studied by ESI-MS in positive ion mode, ions corresponding to $[M\text{-}Br]^{+}$ were observed at 421.17 *m/z* for **4A** and 649.22 *m/z* for **4B**. ^{1}H NMR ($CDCL_3$) spectrum for **4A** gave signals at δ 2.3 (3H, s, Ph-$\underline{CH_3}$), 2.4 (3H, s, Ph-$\underline{CH_3}$), δ 2.5 (3H, s, Ph-$\underline{CH_3}$), δ 2.8 (2H, t, P-CH_2-), δ 1.7 (1H, s, H_2O of solvent), δ3.3 (3H, s, CO-$\underline{CH_3}$), δ 3.4 (2H, t, -$\underline{CH_2}$-SCO), δ 3.5 (2H, m, P-CH_2-$\underline{CH_2}$-CH_2), and at 7.6 - 7.8 (12H, m, Aromatic H) ppm. IR spectrum showed absorption bands at the

regions IR spectrum showed absorption bands at the regions of 710 – 731 cm^{-1} (ν CH_2), 1699 cm^{-1} (ν C=O), 1313 cm^{-1} (C-S), and 3100–3000 cm^{-1} (ν CH-Aromatic).

^{1}H NMR = ($CDCL_3$) spectrum for **4B** gave signals at δ 2.4 (2H, t, P- $\underline{CH_2}CH_2$-CH_2-), δ 1.7 (1H, s, H_2O of solvent) [34], δ3.3 (3H, s, CO-$\underline{CH_3}$), δ 3.4 (2H, t, -$\underline{CH_2}$-SCO), δ 3.7 (2H, m, -$CH_2\underline{CH_2}$-CH_2-), δ 5.6-6.3 (27H, s, Ph-$\underline{OCH_3}$), and at 8.0- 8.9 (6H, m, Aromatic H) ppm. IR spectrum showed absorption bands at the regions of 800-820 cm^{-1} (ν CH_2), 1739 cm^{-1} (ν C=O), 1591 cm^{-1} (ν C-O), 1365 cm^{-1} (C-S-), 1155 cm^{-1} (ν P=O) and 3104-3000 cm^{-1} (ν CH-Aromatic).

The structure of compound **4A** was confirmed from its correct spectral data. Thus, IR spectrum is used to detect functional groups and showed absorption band at the regions 1699 cm^{-1} which confirm entry of carbonyl group (ν C=O) to ω-bromopropyl-tri(*p*-tolyl)phosphonium bromide (**3**) [35]. In addition, there were peaks at 1739 cm^{-1} and 1591 cm^{-1}, which corresponded to a carbonyl group (ν C=O), and ether group (ν C-O) bond in **4B** respectively. Signals expected for OH group at 3455 cm^{-1} is completely disappeared in **4A** and **4B** indicating to a formation and completed the reaction [35].

^{1}H NMR spectra provided further evidence for the successful results (completed reaction) for **4A** and **4B** which confirmed the existence six protons from (-CH_2-CH_2-CH_2-) attached to the aromatic ring at chemical shifts from 2.3-3.7 ppm to produce compound **4A** and **4B**. Due to absence this group in the start material including tri(*p*-tolyl)phosphine (**1A**) in the case of **4A** and tri(2,4,6-trimethoxyphenyl)-phosphine (**1B**) in the case of **4B**. Furthermore, final products were confirmed by ESI-MS, and ions are corresponding to $[M\text{-}Br]^+$ were observed at 421.17 *m/z* for **4A**, and 649.22 *m/z* for **4B** and (expected MW **4A**, **4B** is 500.9 and 728.9 g/mol respectively [35].

3.4.1.1 Characterisation of the colloidal solutions of AuNPs functionalised with 4A and 4B by using UV-Visible and DLS studies

The reduction of Au(III) to Au(0) can be handily followed by UV-visible absorption spectroscopy [36].

The solutions of functionalised **5**-AuNPs, **4A**-AuNPs, and **4B**-AuNPs were analysed by using UV-visible and DLS. Several dilutions of the stock solution of colloidal AuNPs

were made and analysed by UV-Vis spectroscopy. This technique was used first in order to confirm AuNPs formation and then their stability. The latter was monitored every week. However, the UV-Vis spectra shown in Figures 3.3 and 3.4 are the monthly results. As previously mentioned, the stability of the colloidal solutions of **4A**-AuNPs and **4B**-AuNPs were monitored for five and six months respectively, and no clearly SPB shifts to the right of the UV-visible spectra were observed. Therefore, it can be assumed that no major aggregation within the colloidal solutions occurred during this period of time.

In particles, after storage for 5 and 6 months, suggesting high chemical and colloidal stability for these **4A**-AuNPs and **4B**-AuNPs. The shifted SBP to longer wavelength after six months can be seen *via* Figures 3.3 and 3.4 for **4A**-AuNPs and **4B**-AuNPs. Also, similar evidence can be observed when the colour of **4B**-AuNPs solution changed from red to purple colour in Figure 3.2, which also confirmed the last results but this is not substantial enough to illustrate aggregation in the sample. In addition, this change is accompanied by change the 523 nm peak shifted to 530 nm after five months in the case of **4A**-AuNPs (Figure 3.3 see UV-visible spectrum at time = 0 and time = 5 months) and from 518 nm to 529 nm after six months in the case of **4B**-AuNPs. This is in reasonable agreement with the DLS results, where the **4A**-AuNP and **4B**-AuNP changed their sizes from 6.8 ±1.3 and 5.9 ± 1.2 in initial preparation to 18.3 ± 1.5 and 9.2 ± 1.7 after 5 and 6 months respectively.

UV-Visible spectrum results are showed that, the SPB of AuNP functionalised by **4A** is centred at 523 nm which is illustrating slightly larger in size than another's ligands have functionalised AuNPs, and that confirm difference ligands that functionalised AuNPs under the same conditions, leading to different wavelengths with different stabilities of AuNPs as well. It is notable that compounds thiol-containing with specific chemical structures shown different affinities toward AuNPs, which possibly affect the colloidal stability of AuNPs and also improve its biocompatibility. The stability of nanoparticles in solution is mainly dependent on the surface properties of nanoparticles such as surface charge and ligand structure [37, 38].

According to the literature, the optical properties including the absorption maxima and absorption intensity are dependent on the size of NPs [39], and that clearly seen in our samples (Figures 3.3 and .3.4). Accordance with Mie theory, the surface plasmon resonance of the AuNPs is red shifted with an increase in particle size [40], whereas

Figures 3.3 and 3.4 illustrate shifted SPB toward right wavelength indicating to slightly increase in the size of AuNPs with the time.

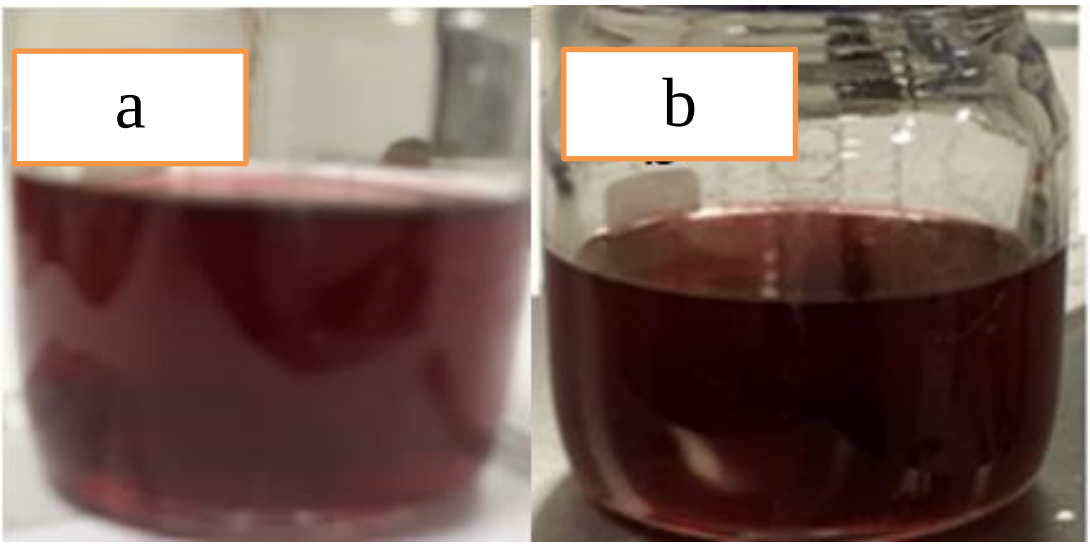

Figure 3.2. The colour comparison of initial (a) and after six months solutions (b) of **4B** functionalised AuNPs.

In addition, the colloidal solutions of **4A**-AuNPs and **4B**-AuNPs were all analysed by DLS then, particle sizes for samples were obtained by analysing at least 253 particles per sample from several results taken. All AuNPs samples have been showed spherical or semi-spherical shaped particles. It has been well established that for mean diameters obtained for the samples **4A**-AuNPs and **4B**-AuNPs analysed were the followings: 6.8 ± 1.3 nm, 5.9 ± 1.2 nm respectively. It can be seen that the DLS results of **4A**-AuNPs and **4B**-AuNPs are quite similar to the corresponding UV-Visible spectra results, which consider as evidence and confirmation each other.

The DLS data can give an idea of finer details of the actual size of AuNPs [41]. However, there are chances to obtain biased results due to the nature of the size of the AuNP samples being assessed. For instance, if any contamination is present in the solutions, it will affect the results and the accuracy of the measurement.

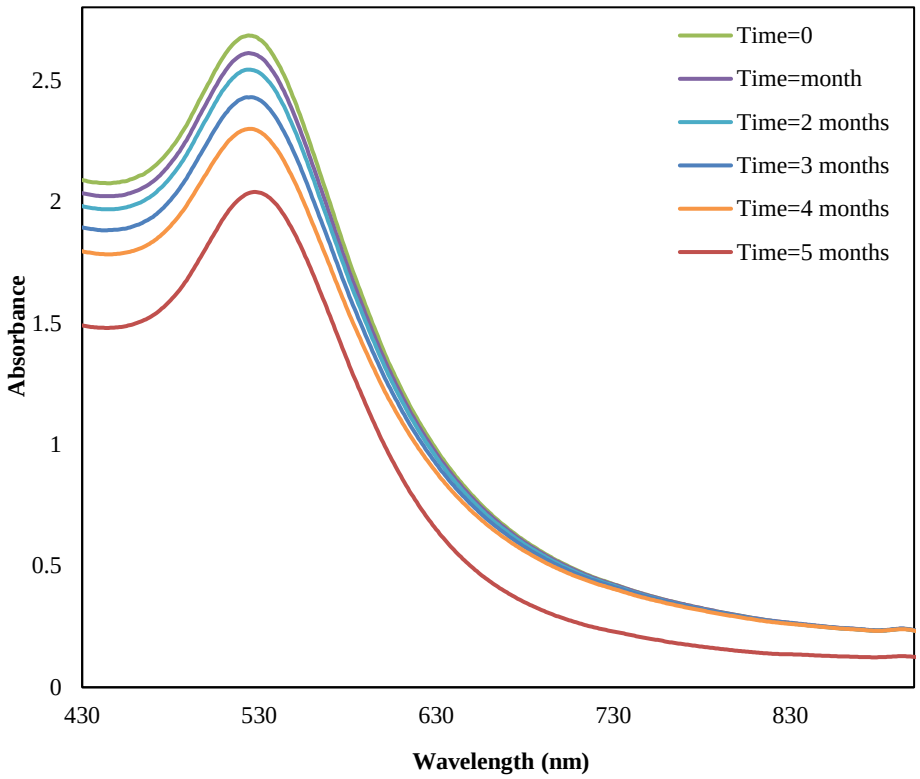

Figure 3.3. UV-Visible absorption spectra of the colloidal solutions of AuNPs functionalised using **4A** as protecting ligand. The different UV-visible spectra represent these NPs dispersed in DMSO/water at time = 0, 1, 2, 3, 4, and 5 months. Where time = 0 is the initial time of the **4A**-AuNPs prepartion.

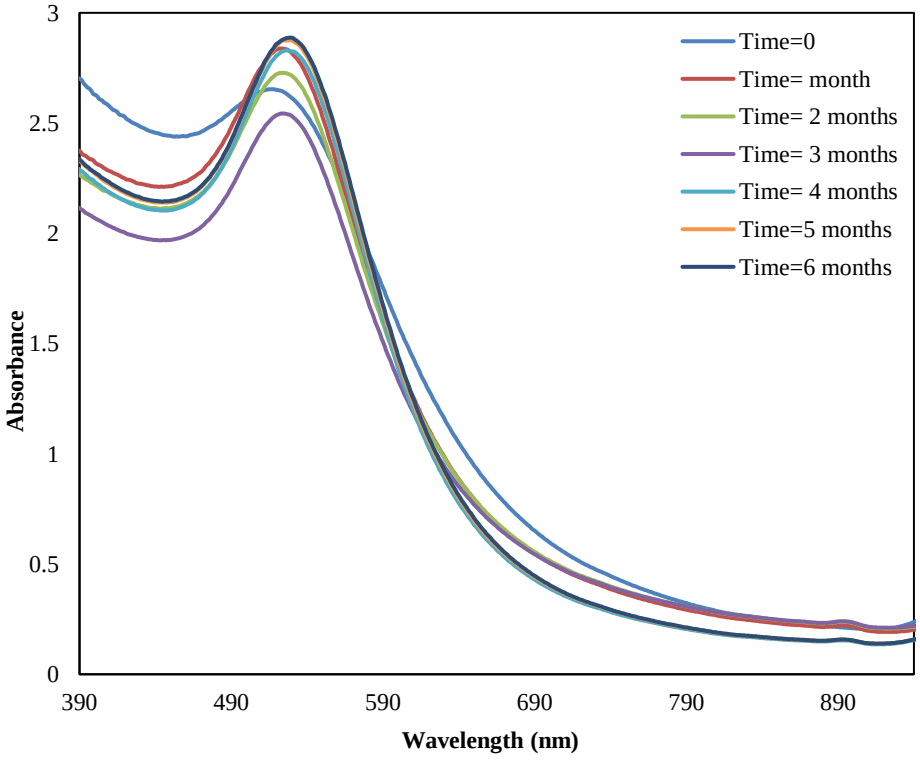

Figure 3.4. UV-visible absorption spectra of the colloidal solutions of AuNPs functionalised using **4B** as a protecting ligand. The different UV-visible spectra represent these **4B**-AuNPs dispersed in DMSO/water at time = 0, 1, 2, 3, 4, 5, and 6 months.

The bias could be overcome by carrying out a number of repetition of measurements per sample. AuNPs synthesised in this Chapter shown a small difference in size of AuNPs from 6.8 ± 1.3 nm in **4A**-AuNPs to 5.9 ± 1.2 nm in **4B**-AuNPs. Due to the change of the ligand from toluene to tris(2,4,6-trimethoxybenzene) head group, and to the nine electron donating groups (OCH_3-Ph) in the **4B** may increase the stability of AuNP [42].

3.4.2 pH stability study

According to previous literature, it was found that the addition of acid and base to the AuNPs can be changing the ionic strength of the dispersion. For instance, it is noted that AuNPs were not stable in dispersion with a high concentration (above 0.1M) of a NaCl added and instantly lead to the aggregation [43].

The pH stability study conducted required the use both **5**-AuNPs, **4A-**AuNPs and **4B-**AuNPs. Before the experiments were begun, firstly, the Jenway 3505 pH Meter was calibrated via placing the probe in a buffer solution of known pH 7 and adjusting the display. The probe was then rinsed in deionised water and placed into a pH 4 buffer solution in order to create a slope. The display was once again adjusted to show the correct pH before finally being rinsed with double-distilled water. This calibration ensures accurate results when measuring solutions of unknown pH values. When storing the probe, a buffer solution of pH 4 was used to prevent the membrane in the probe becoming slow. Set volumes of 1M HCl and 1M NaOH (5-30 µL) were added step by step to a solution of AuNPs and deionized water (ratio of 1:2) with the pH being measured after each addition. As the pH fluctuated slightly, three readings were taken in order to take an average. The first reading was taken after about two minutes after adding the HCl with the second being recorded after roughly 10 minutes. The average of the two was presented as the pH of the solution.

3.4.2.1 Study of the stability of 5-AuNPs in acidic conditions

An acidic solution of 1M HCl was prepared to add to **5**-AuNPs solution. During the experiment, the **5**-AuNPs solution was continuously stirred to avoid aggregation and ensure even distribution of the HCl.

3.4.2.1.1 Stability study at pH < 7.5 - UV-Vis results

The UV-visible absorption spectra of all the pH adjusted dispersions were recorded immediately after addition of the acid or base. The same spectra were also recorded after two months. The UV-Vis was conducted to assess the potential changes in SPBs of the gold colloidal solutions (AuNPs functionalised with **5**) at different pH values lower than 7.5. These analyses were carried out in order to determine whether aggregations occur or not.

Run 1

A 50 mL beaker was used to allow the addition of HCl solution. The **5**-AuNPs was left to stir for about 10 minutes to evenly disperse them through the water medium.
Table 3.1 tabulates appropriate amount of acid added in Run 1 of the acidic study and the corresponding pH of the solution measured. The peak of the absorbance of the pH is presented in order to assess whether the solutions were stable as the pH decreased.

Run 2, 3

Due to the need for better results, so the experiments were conducted triple times, with the ratios were kept constant. 5 mL of **5**-AuNPs was combined into a solution with 10 mL of deionized water. The solution was stirred for ten minutes before the experiment was commenced.

Table 3.1 shows the amount of HCl (5-30 µL) added to the **5**-AuNPs solution in order to lower the pH of the solution. The peak of the absorbance is also presented to assess whether any aggregation may have occurred with the change of pH.

It is clear in all experiments Table 3.1 that peaks of absorption increase slight as the pH decreases; this is due to further amounts of 1M HCl were added to the **5**-AuNPs colloidal solution. From the results illustrated, it can be suggesting that there is significant change with decreasing pH, indicated to aggregation may happen at low pH. This evidence is supported *via* the considerable shifting of the peak of the absorbance to the right of the spectra across the pH range used. The peaks of the absorbance shown in Table 3.1 give a range of wavelengths from 527 nm to 533 nm at pH values from 7.4 to 4. This result was obtained in all Run 1, Run 2 and Run 3 of the experiment furthering the reproducibility of the results presented.

Significant changes in SPBs recorded suggest that the colloidal **5**-AuNPs solutions are mono-dispersed samples at natural pH (~pH = 7.3). In addition, Tables 3.1 and Figures 3.5, 3.6 show the shape of the SPBs are changed in all experiments, which strengthen the assumption that there is obvious aggregation was occurred along just with low pH values in this chapter. According to the literature, it was described that the absorbance of AuNPs was changed with changing the pH value (pH 5.4 to 9.4), whereas at pH 6.4 noted an increase in the absorbance of AuNPs at 600 nm wavelength. Furthermore, the stability of AuNPs was decreased especially at pH 5.4 led to aggregation [37].

The aggregation of AuNPs caused to a sudden red shift in the absorption spectra of the AuNPs due to the important shortening of the distance between the NPs [37].

Table 3.1. The amount of 1M HCl (5-30 µL) added and resulting pH of the **5**-AuNPs solution along with the peak at different wavelengths and sizes diameter for (Run **1**, **2** and **3**), pH < 7.5.

Run 1				**Run 2**			**Run 3**		
Amount of 1M HCl	**pH**	**UV/Vis (nm)**	**DLS (nm)**	**pH**	**UV/Vis (nm).**	**DLS (nm)**	**pH**	**UV/Vis (nm)**	**DLS (nm)**
0 µL	7.4	527-528	7.8±1.5	7.4	528	7.9 ± 1.4	7.3	527	7.6±1.4
5 µL	6.9	529	8.6±1.7	6.8	529	8.8 ± 1.8	7.1	528	8.0±1.3
10 µL	6.6	530	9.1±1.9	6.3	530	9.4 ± 1.3	6.5	529	8.7±1.4
15 µL	6.4	530	9.6±1.4	5.6	531	10.13±1.6	6.0	531	10.3±1.2
20 µL	6.2	530	9.8±1.2	5.4	531	10.38±1.9	5.8	531	10.4± 1.8
25 µL	5.6	531	10.6±1.3	5.1	531	10.4± 1.3	5.5	531	10.5± 1.9
30 µL	4	532-533	14.7±1.5	4.3	532	13.2± 1.2	4.4	532	12.3 ±1.2

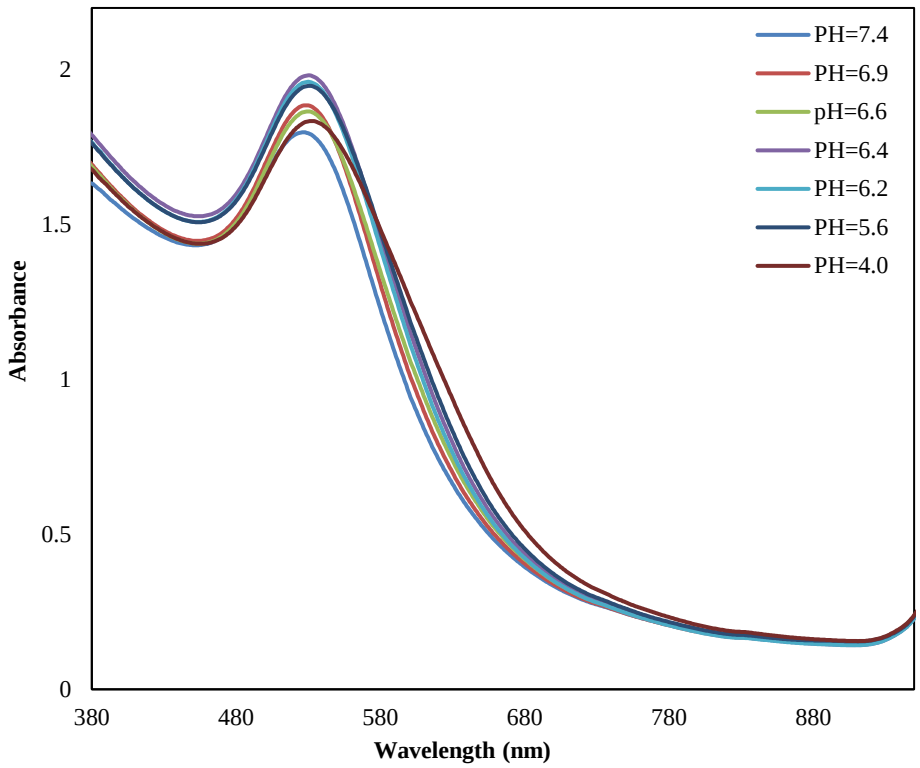

Figure 3.5. Data collected through UV-Vis across the pH range produced via adding HCl to the **5**-AuNPs solution in (**Run 1**), pH < 7.5, where the HCl additions were from (5-30 µL).

It was not expected to see aggregation with a range of pH 7.3 ± 0.1 to 5.1 ± 0.2 due to the excess of H^+ ions present in the acidic solution being added to the AuNPs solution, illustrates did not cause a change to the properties of AuNPs [44]. The AuNPs themselves are weakly positively charged meaning that with a further excess of positive cations, they are not electrostatically attracted to each other which leads to prevent any aggregation may occur. A protonation or deprotonation change as the acidity of the solution changes, and causing change of nanoparticle properties [45].

3.4.2.1.2 Stability study at pH < 7.5 - DLS results

Table 3.1 shown above the modal diameter size and corresponding standard deviation of each sample at decreasing pH. It can be observed that the sizes of the **5**-AuNPs can be easily changed by changing the pH values, and the diameters are all within the same range at pH around 7 suggesting predominantly mono-dispersion of **5**-AuNPs in the colloidal solutions. The narrowest size distribution was obtained at a pH 7.5 according to the literature [46]. The DLS data recorded is shown in Table 3.1 and Figure 3.6 for both the initial experiment and the repeats.

As before, the data for the two runs are presented comparatively for each experiment at varying pH for each analysis. DLS samples were measured at the same time UV measurements were carried out. It can be observed that the diameters of the **5**-AuNPs at the decreasing pH are significantly in the different range. The colour of the well dispersed **5**-AuNPs is wine red and changed gradually with the addition of HCl (15-30µL) amounts.

From the data collected, in Run 1, 2 and 3 (see Table 3.1), it is clear to see that, the diameters were changed from 7.6 ± 1.4 nm (pH = 7.3 ± 0.05, 0 µL HCl added) to 14.7 ± 1.5 nm (pH = 4.0 ± 0.2, 30µL HCl added) which confirmed UV results, indicated aggregation. Studies have shown that decreasing pH values of AuNPs solution leads to large polyhedrons and other irregular particles [46]. The standard deviations from the modal size for **5**-AuNPs solution around pH 7.3 are small and agglomeration of **5**-AuNPs does not occur (see Figures 3.5, 3.6). From Table 3.1, it can be seen that the **5**-AuNPs at low pH had bigger size than at pH neutral (pH = 7.3 ± 0.05), changing the colour from red to pink-purple colour.

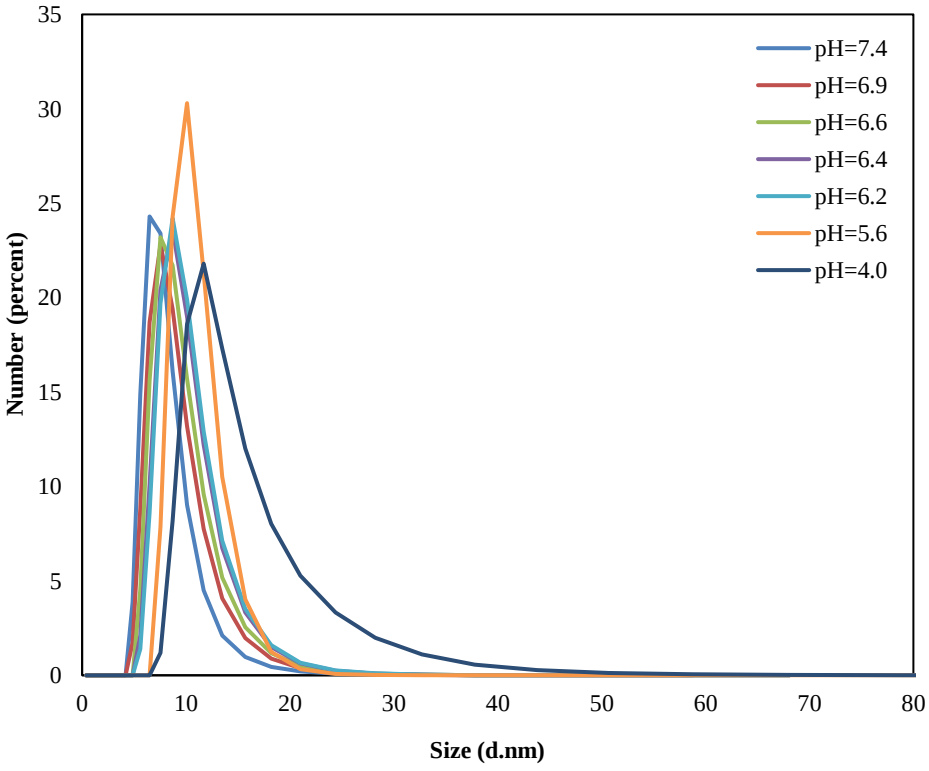

Figure 3.6. Data collected by using DLS analysis of the samples **5**-AuNPs in (**Run 1**) to give the diameter size and standard deviations for each pH, pH < 7.5 and the HCl additions were from (5-30 µL).

This indicated to aggregation, which are confirmed by DLS and UV results (data presented in Tables 3.1). In general, a colloidal AuNPs with diameters of 5-20 nm exhibit a red colour, and have an optical absorption peak around 520 nm [47].

In this Chapter, the change in the colour of the solution from deeply red colour to pink purple confirms the aggregation of the AuNPs at low pH. As mentioned earlies, the pH of cancerous cells is slightly acidic [5], so the aggregation suggests that the AuNPs would still be of use when entering the altered conditions of the tumorous tissue. AuNPs offering a strong pH-dependent adsorption cell membranes within a biological pH range (5.3-7.4) [48].

It is considering that pH plays a key role in several cellular processes and is an indicator for a pathological environment, AuNPs with pH-dependent membrane adsorption might find new applications in therapy and tumour diagnosis [48].

3.4.2.2 Study of the stability of 5-AuNPs in basic conditions

The stability of AuNPs changed by increasing the pH gradually with 1M NaOH. The starting pH was approximately 7.5 ± 0.05 for all **5**-AuNPs solutions, and the pH was increased with high NaOH concentration (30 µL) to pH = 11.3 ± 0.1 or until complete dissolution or aggregation of **5**-AuNPs. The sample solutions were stirred gently, and an appropriate amount of NaOH was added to increase the pH values, the sample solutions were stirred for about 10 minutes. The pH was measured with the pH meter, the size and size diameter of **5**-AuNPs were measured regularly with both UV and DLS, and the results were confirmed to each other.

3.4.2.2.1 AuNPs in basic conditions of 1M NaOH

5-AuNP prepared is highly stable and uniformly dispersed in the solution. It was stable for several months without any evidence for aggregation. It is known that any factor that affects the surface charge of AuNPs will result in aggregation of the AuNPs [49]. For example, pH is considering one from important factors that effect on the stability of AuNPs [50]. In this Chapter, pH of AuNPs solution has changed via added different amounts of 1M HCl as mentioned early and 1M NaOH. 1M NaOH in aliquots of between 5 and 30µL were added to solution of **5**-AuNP with continuous stirring to ensure adequate mixing.

This study shows the effect of pH in the range from pH = 7.5 ± 0.05 to pH = 11.3 ± 0.1 on the stability of AuNPs. These observations are supported by DLS and UV-Vis.

3.4.2.2.2 Stability study at pH > 7.5 - UV-Vis results

UV-Visible absorption spectroscopy was used to study the peak of the absorption at different concentration of NaOH amounts (5-30 µL) throughout the experiment and also after nearly two months to give an idea of whether aggregation occurs within the samples. 1M NaOH amounts were added to the AuNP solution to achieve the desired pH value. The pH of the solutions was increased to determine whether the **5**-AuNPs present in the solution remains stable under such conditions.

Run 1

Table 3.2 contains the pH values of the AuNPs solution after the addition of each controlled volume of the base, along with the peak of the absorbance recorded. There is a distinct shift in the peak of the absorbance or SPB of the solutions to the right of the spectra as the pH increases.

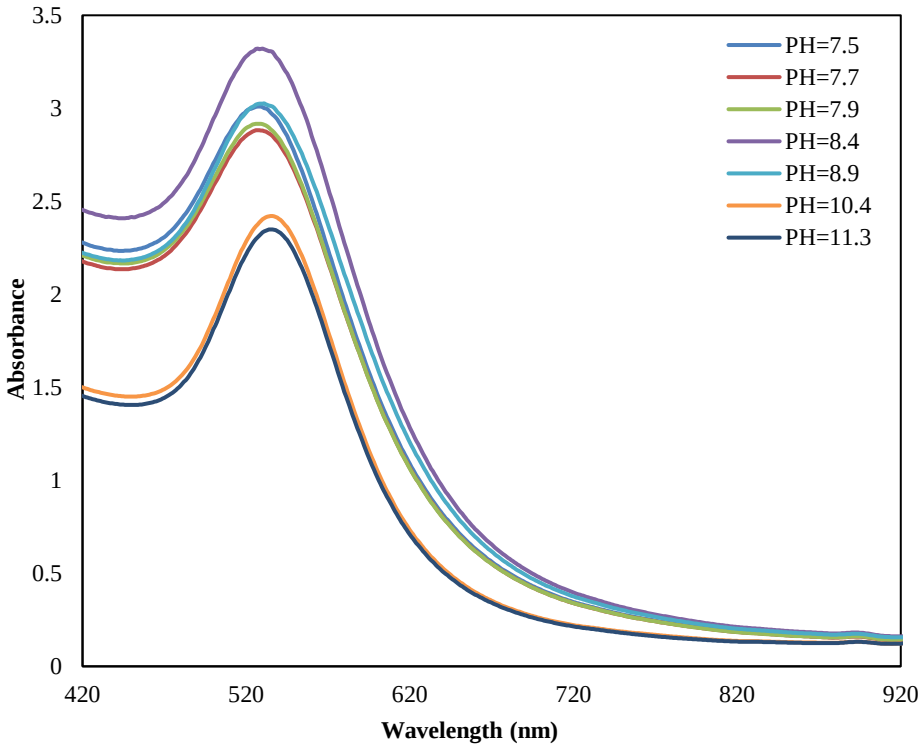

Figure 3.7. Data collected through UV-Vis at each pH recorded in (**Run 1**) of **5**-AuNPs. It can be observed that the shape and height of the surface plasmon bands alter as the pH is altered and that the peak of the absorption shift towards 536 nm as will describe in detail in the following sections. pH > 7.5.

Run 2, 3

Table 3.2 shows the data assembled through (Run 2, 3 as well) of the base pH of the **5**-AuNPs solution. From the data presented in Table 3.2, there is a clear shift in the peak of the absorption. The increase in absorbance illustrated in Tables 3.2 is associated with the dilution of the **5**-AuNPs solution by set volumes of NaOH amounts as the pH increases. Both Run 1, 2 and 3 show a similar trend with the suggestion that aggregation of **5**-AuNPs occurred due to the presence of excess OH^- anions within the colloidal solution. Tables 3.2 shows a clear shift in the peak of the absorbance and the data presented suggest a more significant shift from 527 nm to a maximum peak of the absorption of 536 nm. It can also be observed that shape of the peak broadens as the pH increases. This proposes the idea of aggregation between **5**-AuNPs as the pH increases as well as the increases in the range of diameter size of the **5**-AuNPs present in each solution [51]. This samples alteration in shape of the peaks is noted in (Run 1, 2, 3) verifying the results obtained.

Table 3.2. A mount of 1M NaOH added (**Run 1, 2, 3**) and the corresponding pH value of the **5**-AuNPs solution and maximum wavelength of the maximum absorbance peak observed, pH > 7.5.

Run 1				**Run 2**			**Run 3**		
Amount of 1M NaOH	**pH**	**UV/Vis (nm)**	**DLS (nm)**	**pH**	**UV/Vis (nm).**	**DLS (nm)**	**pH**	**UV/Vis (nm)**	**DLS (nm)**
0 µL	7.5	528	8.4 ±1.2	7.6	528	8.5±1.5	7.3	527	7.8±1.6
5 µL	7.7	528	8.6 ±1.3	7.8	529	8.7±1.4	7.6	528	8.3±1.6
10 µL	7.9	529	9.3 ±1.4	8.0	530	9.4±1.3	7.8	529	8.5±1.2
15 µL	8.4	530	9.8 ±1.5	8.2	530	9.6±1.2	8.3	530	9.8±1.5
20 µL	8.9	531	10.5±1.3	8.8	531	10.4±1.6	8.7	531	10.5±1.8
25 µL	10.4	535	12.4±1.2	9.1	530-531	10.2±1.9	9.2	531	10.8±0.9
30 µL	11.3	536	14.3±1.3	9.7	532	11.4±1.2	10.3	532	12.7±1.3

3.4.2.2.3 Stability study at pH > 7.5 - DLS results

Colloidal solutions of **5**-AuNPs were also examined at different pH > 7.5 by using DLS technique as shown in Table 3.2 and Figure 3.8. Measurements were taken at 25°C and repeated ten times. The cuvette was washed with deionised water before and in between measurements. It is notable that the diameter size dramatically increases as the pH increases in both sets of data and the standard deviations vary significantly throughout the measurements.

The DLS data measured is shown in Table 3.2 along with graphical representations of the raw data collected at each modal diameter size for each increased pH. It is noticeable that the data is varied across the pH range with an increase in diameter range from 8.4 ± 1.2 nm to 14.3 ± 1.3 nm in (Run 1 at pH from 7.5 ± 0.1 to pH 11.1 ± 0.2). A similar increase from 8.5 ± 1.5 nm to 11.4 ± 1.2 nm in (Run 2 at pH from 7.6 ± 0.1 to pH 9.7 ± 0.1), and from 7.6 ± 1.6 nm to 12.7 ± 1.3 nm in (Run 3 at pH from 7.4 ± 0.15 to pH 10.1 ± 0.15). It was expected that the DLS data would show an increase in diameter size as aggregation occurred due to an excess of OH^- anions present in the NaOH solution added [52].

The phosphonium ligands attached to the functionalised AuNPs give an overall positive charge to each particle. With an excess of OH^- dispersed throughout the colloidal AuNPs solution, the positively charged AuNPs begin to aggregate due to ion exchange and electrostatic interactions occurring in the solution [53]. The increase in size-average particle diameter relative to that obtained at pH > 9.1, again clearly indicates significant aggregation, which indicates to the ligand **5** can be stabilised AuNPs.

In this Chapter, we investigated the AuNPs show similar aggregation patterns in highly basic and lowly acidic conditions which are consistent with what is mentioned in the literature, whereas at pH, closer to neutral, the diameters recorded are within a range that could suggest a mono-dispersed solution [54].

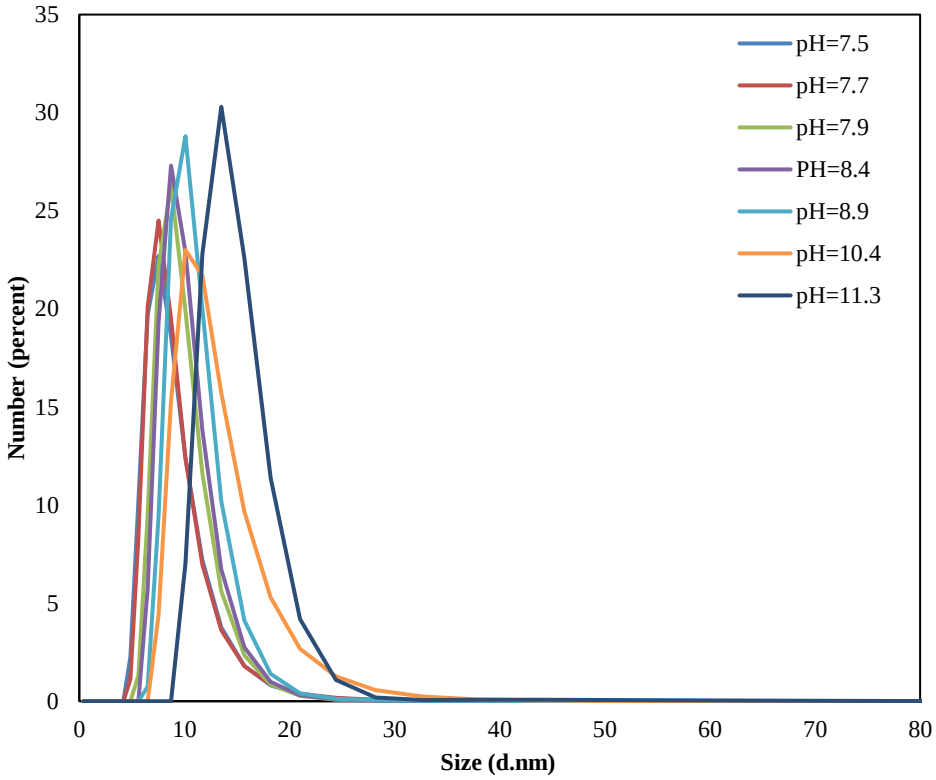

Figure 3.8. Data of **5**-AuNPs for measurements taken for DLS (**Run 1**) at increasing pH values, where 1M NaOH additions were from (5-30 µL).

In addition, it is noted that, the significant increase of λ_{max} at high pH (>12.0) and low than 4, whereas at pH < 4 redshift of λ_{max} appears at 542 nm [55]. Spherical AuNPs with size 13 nm exhibited pH-induced aggregation in mild acidic intracellular environments, which showed a possibility for photothermal cancer therapy [55].

In addition, the aggregation of spheres AuNPs can be realised in a pH-induced manner, as mentioned in the literature, was realised via the formation of mixed charged surfaces which affected by pH change due to changing the composition of the oppositely charged ligands on the surface [23, 56].

3.5 Study of the stability of 4B-AuNPs in acid and basic conditions of 1M HCl and NaOH.

The same procedure in the above sample has been used. It is important to mention that, the changing in pH value can affect the functional groups on the surface of AuNPs, accordingly, changes in the pH result in changes in AuNPs coverage. In the same hand, the pH value effects on the affinity between AuNPs and functional groups such as (3-aminopropyl)-trimethoxysilane, that used to functionalise it [57]. The pH value of the **4B-**

AuNPs changed significantly and can be easily aggregated after the HCl, NaOH amounts (5 - 30 µL) were added.

3.5.1 Acidic study UV-Vis and DLS results

From the data collected, it would be suggested that the optimum pH range for the storage and use of the functionalised **4B**-AuNPs was between pH 7.3 ± 0.1 and pH 3.0 ± 0.2 as within this range, the sizes are changed from 6.2 ± 1.6 nm to 13.8 ± 1.3 nm in 1M HCl addition (see Table 3.3, Figures 3.9 and 3.10). However, it was between pH 7.1 ± 0.1 and pH 9.0 ± 0.1 as, within this range, the size and standard deviations were changed from 6.1 ± 1.17 nm to 9.6 ± 1.4 nm in 1M NaOH amount addition.

It is noted that at higher pH, aggregation between the AuNPs occurred so storage and use of the AuNPs solution at pH above pH 8.8 or below pH 4.0 would render them unhelpful as the diameter would be too great to navigate through the tumorous cells [58]. According to Zhu, J., et al., AuNPs in the acidic solutions can be aggregated easily, and the absorption peak showed a clearly red-shift which also confirm our results in this Chapter [57].

In addition, the mean particle diameters and the width of the distributions are decreased as the pH of the solution increases. For example, at pH lesser than 5 wide size distributions of spherical particles are obtained. However, narrow size distributions are obtained at pH higher than 6 [46].

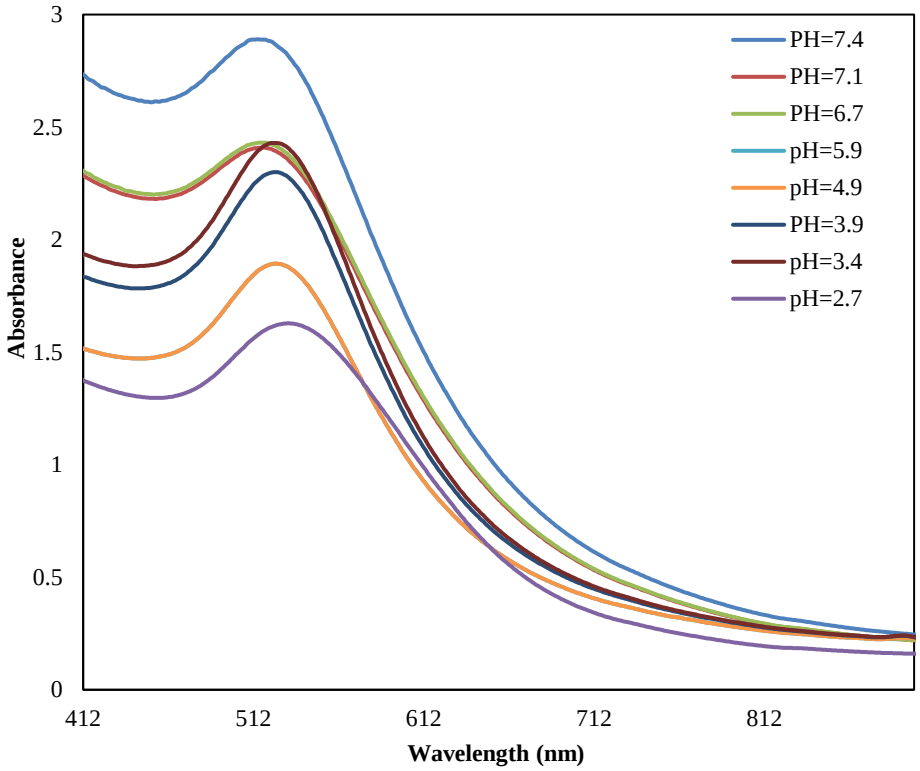

Figure 3.9. Data collected through UV-Vis across the pH range produced by adding HCl to the **4B**-AuNPs solution in (**Run 1**) of the acidic study, pH < 7.5 and the 1M HCl additions were from (0 - 35µL).

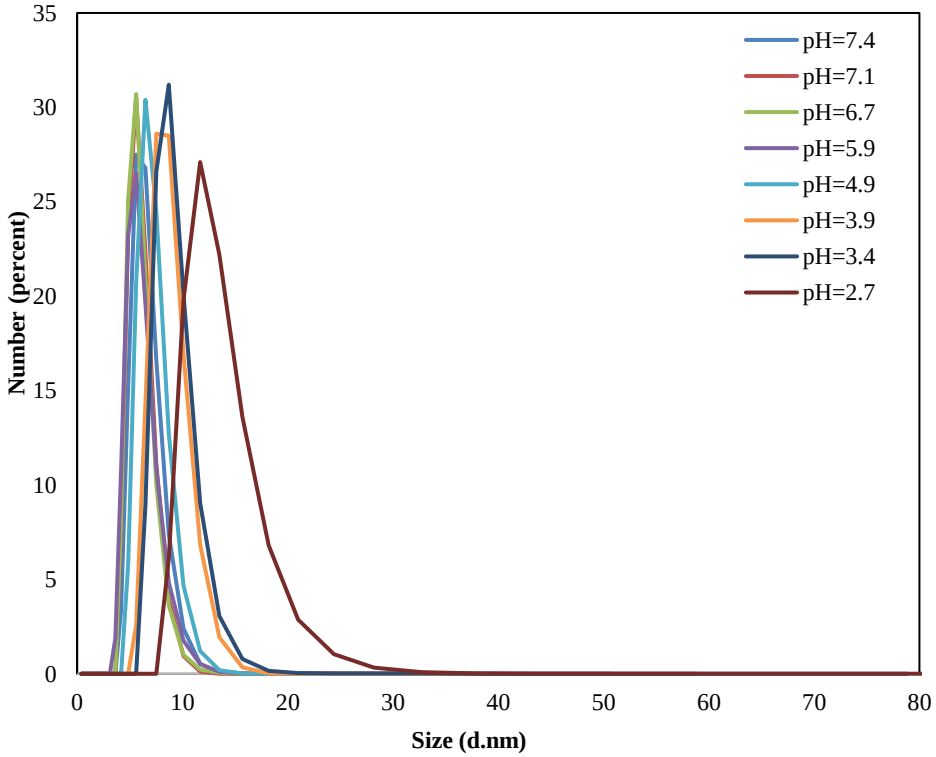

Figure 3.10. Data collected through DLS analysis of the samples in (**Run 1**) to give the diameter size and standard deviations for each pH range produced by adding HCl to the **4B**- AuNPs solution, pH < 7.5.

Table 3.3. The amount of 1M HCl added and resulting pH of the **4B**-AuNPs solution along with the peak wavelength and sizes diameter for (**Run 1**), pH < 7.5.

Run 1				**Run 2**			**Run 3**		
Amount of 1M HCl	**pH**	**UV/Vis (nm)**	**DLS (nm)**	**pH**	**UV/Vis (nm).**	**DLS (nm)**	**pH**	**UV/Vis (nm)**	**DLS (nm)**
0 µL	7.4	519	6.3±1.3	7.3	519	6.2±1.6	7.3	519	6.5±1.6
5 µL	7.1	518	5.9±1.2	6.5	518	5.7±1.2	7.1	518	5.9±1.13
10 µL	6.7	518	5.8±1.2	5.2	522	7.2±1.4	6.8	518	5.6± 1.1
15 µL	5.9	518	5.8±1.3	3.8	526	8.8±1.2	5.1	523	7.6 ± 1.2
20 µL	4.9	522	7.0±1.3	3.3	526-527	9.8±1.3	4.1	524	8.0 ± 1.6
25 µL	3.9	525	8.5±1.6	3.0	528	10.9±1.4	3.8	525	8.5 ± 1.4
30 µL	3.4	526	9.4±1.6				3.5	526	8.9 ± 1.8
35 µL	2.7	532	13.8±1.3				3.1	527	10.4± 1.2
40 µL							2.9	528	11.9± 1.3

3.5.2 Basic study UV-Vis and DLS results of 4B-AuNPs

AuNPs were aggregated at pH 10.8 and turned to blue colour as illustrated in the literature [57]. In this Chapter, **4B-**AuNPs displays a significant change in their sizes and stabilities with pH increasing as shown in Table 3.4. **4B**-AuNPs are highly stable with the change of pH except at high and low pH, which suggests of aggregation within the sample was a clear colour change from red to purple-blue. This is due to the shift in wavelengths as

seen in Figures 3.11 and 3.12 representing the UV-Vis and DLS data. The colour change observed can be seen in Figure 3.13 in acidic condition and in Figure 3.14 in basic condition.

The purple-blue colour observed is associated with larger fully protonated AuNPs as expressed in the literature [51, 59]. There was a slightly clear colour change in the solution when the HCl amounts (pH < 7.5) were dropped, refer to Figure 3.13 supporting the suggestion that a little bit aggregation occurred within the samples. However, in Figure 3.14 (pH > 7.5) the colour shift from deep red colour to purple colour due to slightly aggregation of AuNPs as well at the higher base.

Table 3.4. The amount of 1M NaOH added and resulting pH of the **4B-**AuNPs solution along with the peak wavelength and sizes diameter for (**Run 1, 2, 3**). pH > 7.5.

Run 1				**Run 2**			**Run 3**		
Amount of 1M NaOH	**pH**	**UV/Vis (nm)**	**DLS (nm)**	**pH**	**UV/Vis (nm).**	**DLS (nm)**	**pH**	**UV/Vis (nm)**	**DLS (nm)**
0 µL	7.3	519	5.9±1.2	7.1	519	6.1 ± 1.1	7.1	519	6.0±1.3
5 µL	7.6	523	6.7±1.2	7.5	523	6.6 ± 1.2	7.5	523	6.4±1.2
10 µL	8.1	524	8.08±1.1	8.0	524	8.2 ± 1.6	7.9	523	8.05±1.3
15 µL	8.6	527	8.6±1.5	8.4	526	9.2 ± 2	8.2	524	8.4±1.3
20 µL	9.1	528	9.6±1.4	9.0	528	9.5±1.8	8.8	528	9.6±1.4
25 µL	9.7	529	10.3±0.9	10.8	532	12.02±1.2	10.5	531	11.60±1.3
30 µL	10.1	530	10.56±1.2	11.2	534	14.0±1.2			

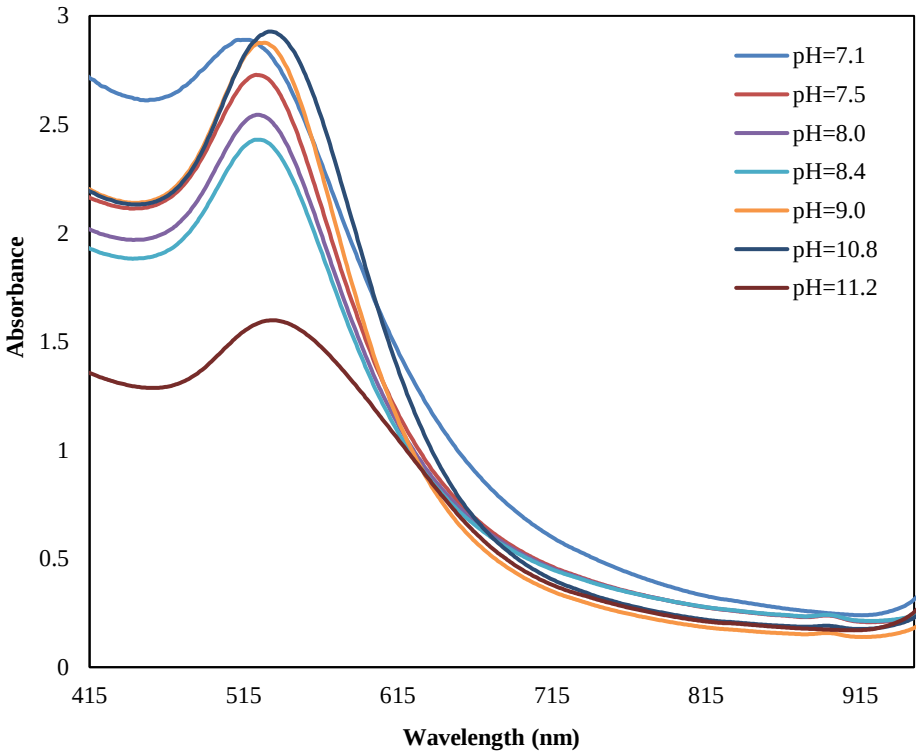

Figure 3.11. Data collected through UV-Vis across the pH range produced by adding 1M NaOH (5-30 µL) to the **4B**-AuNPs solution in (**Run 2**) of the basic study, pH > 7.5.

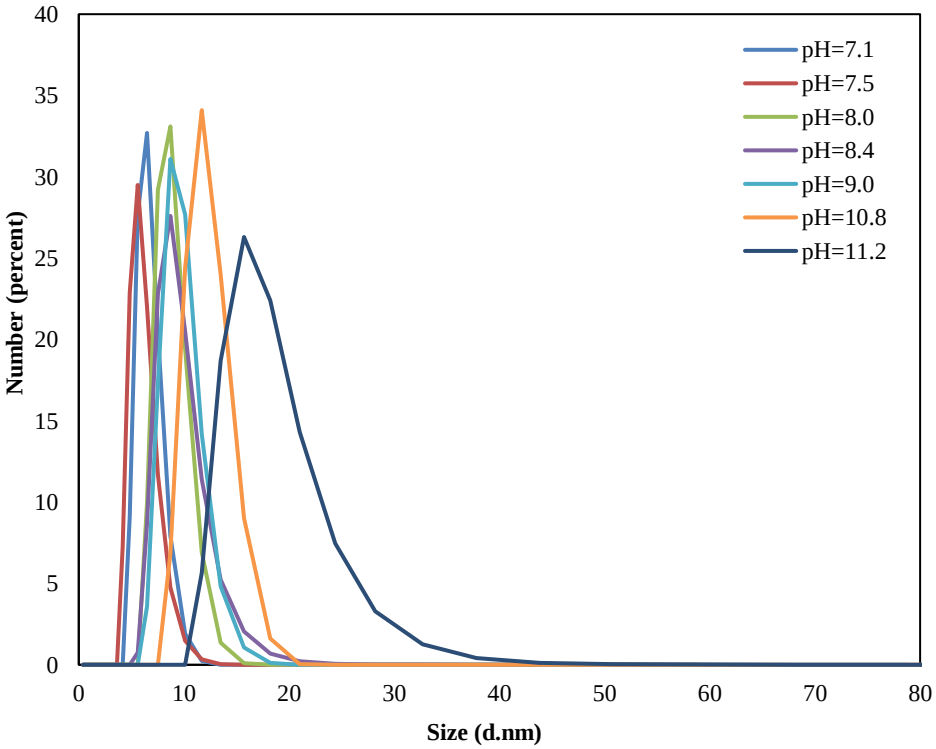

Figure 3.12. Data collected through DLS analysis of the samples in (**Run 2**) to give the diameter size and standard deviations for each pH range produced by adding NaOH to the **4B**-AuNPs solution, pH > 7.5.

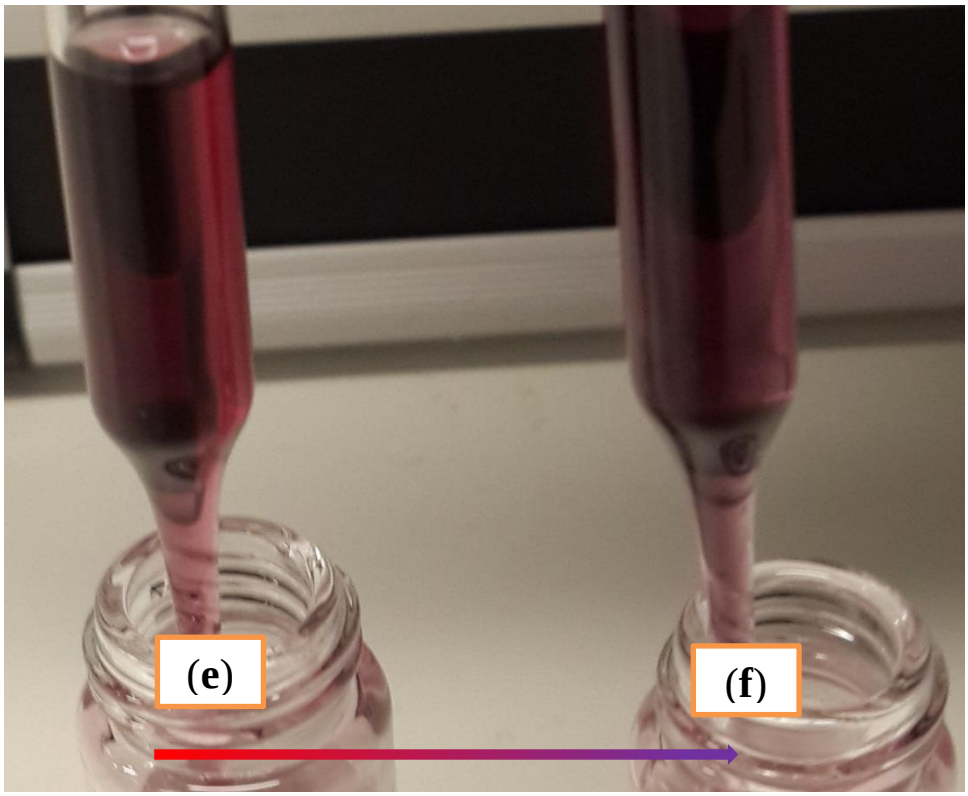

Figure 3.13. The transition in colour for the aliquots taken during (**Run 2**) at (e) 0 µL and (f) 25 µL of the acidic pH study for **4B**-AuNPs. pH < 7.5.

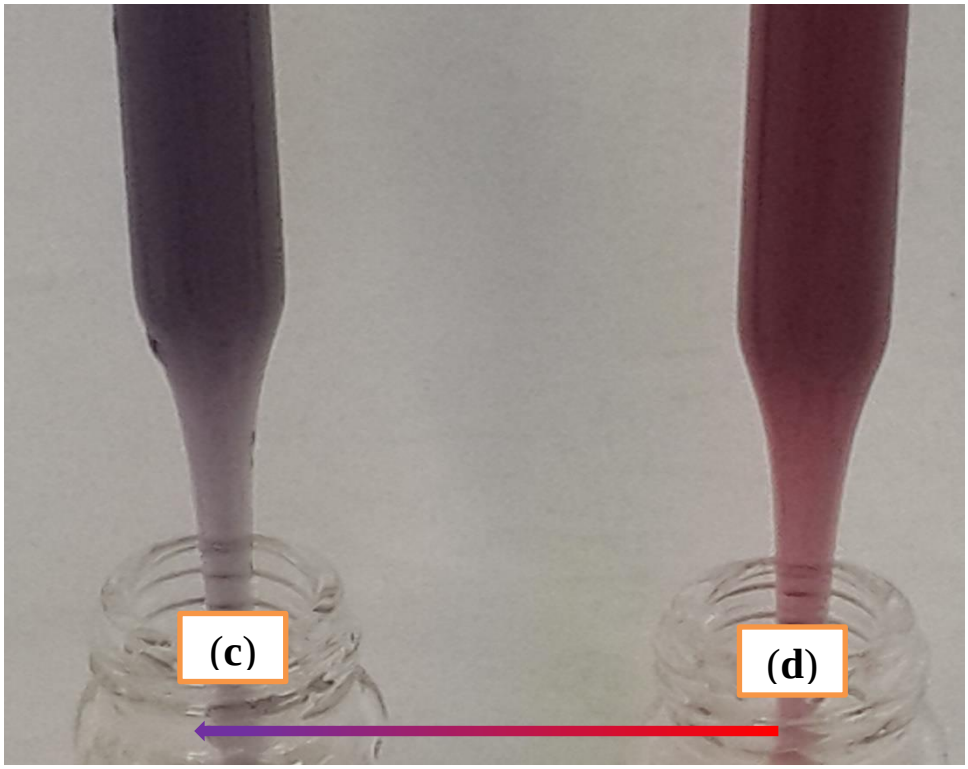

Figure 3.14. The transition in colour for the aliquots taken during (**Run 2**) at (d) 0 µL and (c) 30 µL of the basic pH study for **4B**-AuNPs. pH > 7.5.

At the arrange of pH 5.8-3.0, a red to blue colour change was observed. However, at pH 8.0-8.8, the solution still has the original red colour. Furthermore, we observed that the colour change was sensitive to pH change. For instance, it is noted that AuNPs at pH (4.5–5.5) the solutions look purple-red colour. While at pH > than 6.0 the AuNPs solutions look red colour [46]. DLS and UV-Vis measurements indicate good stability of AuNPs solutions with respect to pH changes except at low pH. In weak acidic condition (pH ~5-7), **4B**-AuNPs were stables consequently the surface of the AuNPs becomes less negatively charged.

3.6 Study of the stability of functionalised 4A-AuNPs in acid and basic conditions of 1M HCl and NaOH.

pH was adjusted with either 1M NaOH or 1M HCl. The stability of NPs depended on the pH solution. For instance, it is known that carboxymethylated chitosan nanoparticles stability's increased with increasing pH. However, the disadvantage of chitosan was its insolubility in near neutral pH. While it was soluble in acidic solutions (pH ≤ ~6). The exact pH value depends on the properties of the ligands functionalised NPs, where the solubility in acidic solutions as a result to the protonation of amino groups in chitosan. In contrast, chitosan NPs were aggregated at the neutral and alkaline solution (pH 7 ~8.5) which explained to neutralisation of an amino group in the chitosan [60, 61]. Different ligands as mentioned were functionalised AuNPs in this chapter and offered different stability with pH values changed.

3.6.1 Acidic study UV-Vis and DLS results of add 4A-AuNP.

As mentioned early with **5**-AuNPs and **4B**-AuNP, the same procedure is used. Characterisation and stability of the **4A**-AuNPs were done by using UV-vis spectroscopy and DLS. The colour of the **4A**-AuNP solution was changed from wine red to purple at both high and low pH indicating aggregation of the particles may be caused. While it was stable at natural pH (7 ~ 8) and the **4A**-AuNP maintained the red wine colour indicating no aggregation took place. In this chapter, it is achieved stable AuNPs functionalised by **4A** with size variations at pH 7.7 ± 0.1 and pH 3.7 ± 0.3 respectively between 6.8 ± 1.4 nm and 12.2 ± 1.3 nm when the concentration of 1M HCl amounts acid was varied. While the sizes were between 6.8 ± 1.30 to 11.9 ± 1.3 nm at pH 7.6 ± 0.1 and pH 10.7 ± 0.1 respectively, with variety in 1M NaOH amounts.

For pH 7.7, plasmon resonance peak was observed at 523 nm which changed to 531 nm and 532 nm at pH 3.7 ± 0.3 and 10.7 ± 0.1 respectively. Similar results of **5**-AuNPs and **4B**-AuNPs were collected for **4A**-AuNPs in pH < 7.5 where **4A**-AuNP was aggregated at pH lower than 4.7 as illustrated in Table 3.5 and Figures 3.15, 3.16.

Table 3.5. The amount of 1M HCl added and resulting pH of the **4A**-AuNPs solution along with the peak wavelength for (**Run 1, 2, 3**). (pH <7.5).

Run 1				**Run 2**			**Run 3**		
Amount of 1M HCl	**pH**	**UV/Vis (nm)**	**DLS (nm)**	**pH**	**UV/Vis (nm).**	**DLS (nm)**	**pH**	**UV/Vis (nm)**	**DLS (nm)**
0 µL	7.7	523	6.8±1.4	7.8	523	6.8±1.38	7.8	523	6.8±1.3
5 µL	7.1	524	7.1±1.2	7.2	523-524	7.0±1.5	7.3	524	7.0±1.6
10 µL	6.8	524-525	7.9±1.6	6.7	524-525	7.7±1.8	6.9	525	7.8±1.3
15 µL	6.3	525	8.1±1.9	6.1	526	8.0±1.6	6.2	526	8.2±1.8
20 µL	5.7	526	8.6±1.8	5.8	527	8.5±1.8	5.7	527	8.6±1.4
25 µL	4.9	527	9.2±1.2	5.1	526-527	8.8±1.4	5.2	526-527	8.8±1.3
30 µL	4.1	531	11.4±1.4	3.4	532	12.8±1.3	4.7	528	9.0±1.7
35 µL							3.7	531	12.2±1.3

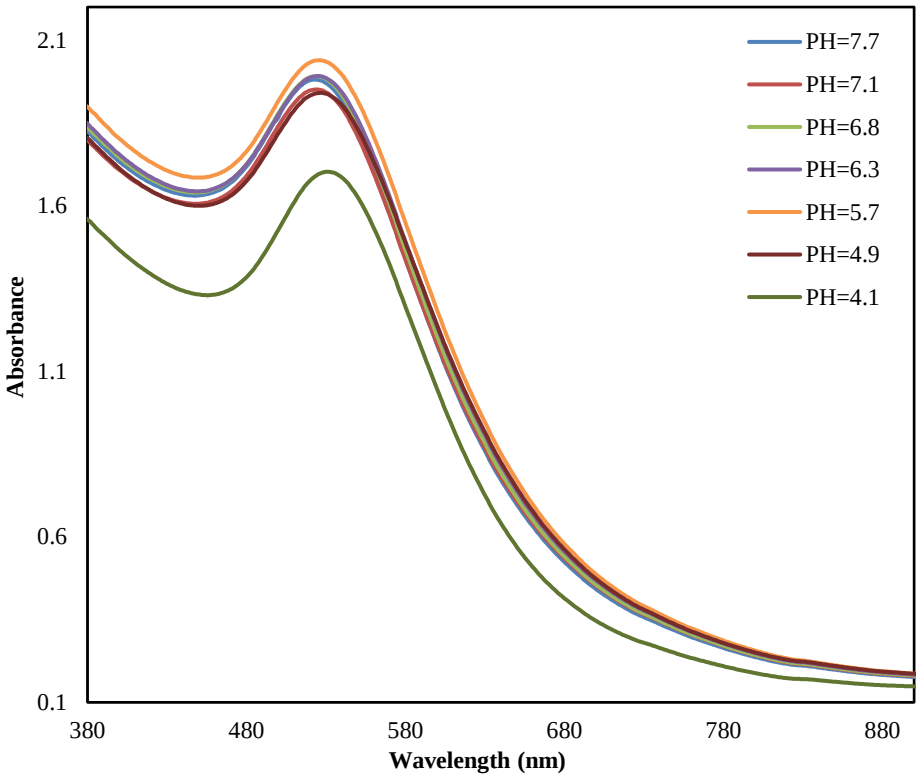

Figure 3.15. Data collected through UV-Vis across the pH range produced by adding 1M HCl (5-30 µL) to the **4A**-AuNPs solution in (**Run 1**) of the acidic study. (pH < 7.5).

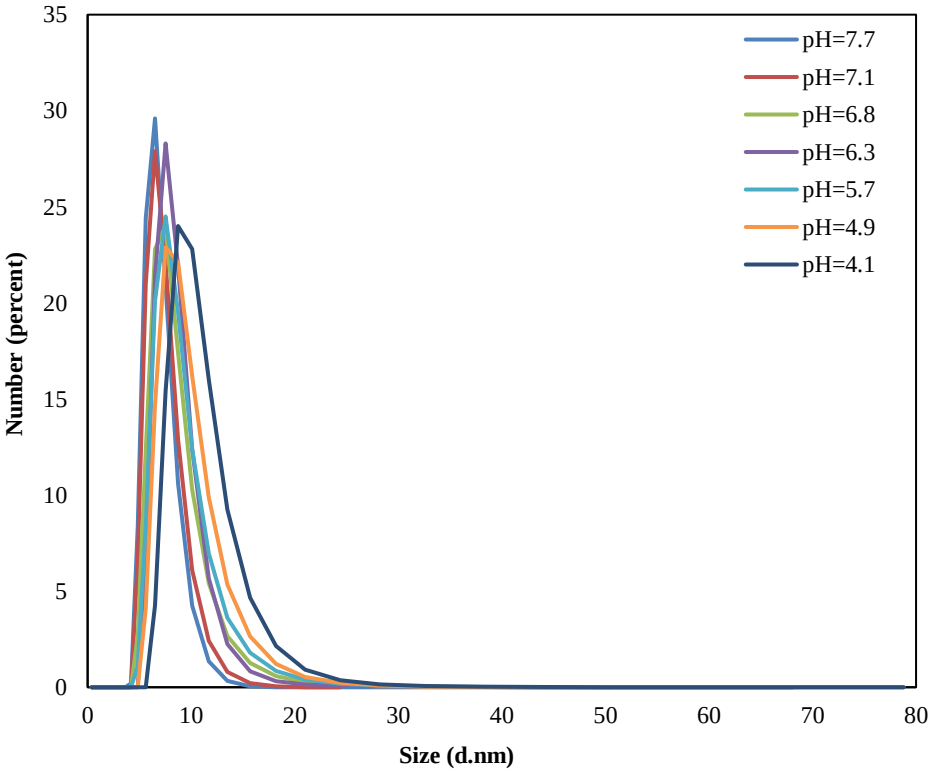

Figure 3.16. Data collected through DLS analysis of the samples in (**Run 1**) to give the diameter size and standard deviations for each pH range produced by adding HCl (5-30 µL) to the **4A**-AuNPs solution. (pH < 7.5).

Similarly, it is shown that the NPs in the pH 2.0 and pH 5.5 showed a red shift and broadening of their absorption band, where at pH 2.0 sample showed a more rapid change compare to the pH 5.5, which indicated to the aggregates. However, at pH 7.4 NPs solution showed no obvious absorption change and no noticeable aggregation occurred [21].

3.6.2 Basic study UV-Vis and DLS results

UV–Vis absorbance was measured after each pH change when 1 M NaOH (5-35 µL) amounts added, which showed a transition between 523 nm and 532 nm at pH 7.6 ± 0.1 and 10.7 ± 0.05 values respectively and sizes measured by DLS at these pH values were 6.8 ± 1.3 nm and 11.6 ±1.0 nm respectively as shows in Table 3.6, Figures 3.17 and 3.18.

Table 3.6. The amount of 1M NaOH (5-35 µL) added and resulting pH of the **4A**-AuNPs solution along with the peak wavelength and sizes diameter for (**Run 1, 2, 3**). (pH >7.5).

Run 1				**Run 2**			**Run 3**		
Amount of 1M NaOH	**pH**	**UV/Vis (nm)**	**DLS (nm)**	**pH**	**UV/Vis (nm)**	**DLS (nm)**	**pH**	**UV/Vis (nm)**	**DLS (nm)**
0 µL	7.8	523	6.9±1.1	7.7	523	6.8 ± 1.4	7.6	523	6.8±1.3
5 µL	8.1	524	7.5±1.7	7.9	524	7.2 ± 1.7	7.9	524	7.3±1.2
10 µL	8.4	525	8.2±1.4	8.2	525	7.9 ± 0.8	8.1	525	7.7±1.2
15 µL	8.8	526	9.1±0.9	8.4	526	8.3 ± 1.2	8.5	526	8.6±1.2
20 µL	9.2	527	9.6±1.7	8.8	527	9.5 ± 0.9	9.3	528	9.8±1.2
25 µL	9.8	528	10.5±1.5	9.1	528	9.7 ± 1.1	10.0	530	10.4±0.8
30 µL	10.1	531	10.8±1.3	10.8	532	11.9 ± 1.3	10.7	532	11.6 ±1.0
35 µL	10.6	532	11.3±1.3						

There are a small number of larger AuNPs within the colloidal solution that were recorded within the measuring process that caused a bias as to the actual diameter size of the AuNPs present in the solution [54]. The closeness of values of diameter for importantly differing pH values indicated the size of **4A**-AuNPs being relatively independent of adjusted initial pH of the aqueous solution, where different sizes generated at pH changing as confirmed as well in the literature [62]. For example, mean diameter of AuNPs using ascorbic acid as reducing agent at room temperature was determined by TEM and was found to be 36 ± 6, 31 ± 5, and 40 ± 5 nm for pH values of 6, 8 and 10 respectively. AuNPs stabilised just *via* adjusting the initial pH conditions of the reaction solutions, where values of diameter for differing pH indicated the size of AuNPs being approximately independent of adjusted initial pH of the aqueous solution as mentioned in the previous study [62].

The pH value affects the binding affinity between the AuNPs and functional groups. It also affects the electrostatic repulsion between the AuNPs and resulting in effects on the coverage of AuNPs. For example, AuNPs coverage decreased sharply when the pH value was increased from 4 to 8 [57]. The binding of these ligands in this chapter to the surface provides great stability to the AuNPs, which remained relatively mono-dispersed with different pH range for more than one month.

AuNPs have been agglomerated in the living cells when it used in vivo or in vitro biomedical applications, due to the presence of electrolyte which is causing to reduce the stability of AuNPs. Thus, the stability is the main concern for AuNPs in all bio-applications. In addition, there is a possibility of pH changes when the AuNPs interact with both the body fluids and blood cells which may cause a change in its stability [51]. Li, H., et al., demonstrated that the ideal photothermal therapy based on AuNPs to be well-dispersed at the normal tissue at pH 7.4. However, exhibit pH-induced aggregation properties in the cancer cells acidic at pH 6.8 − 6.5. Furthermore, illustrated the cause of the aggregation of the AuNPs returns to present of surface ligands composition. photothermal therapy did not depend on the size of the formed AuNPs aggregates but influenced by the original size of the AuNPs that tend to aggregate in slight acidic pH [56].

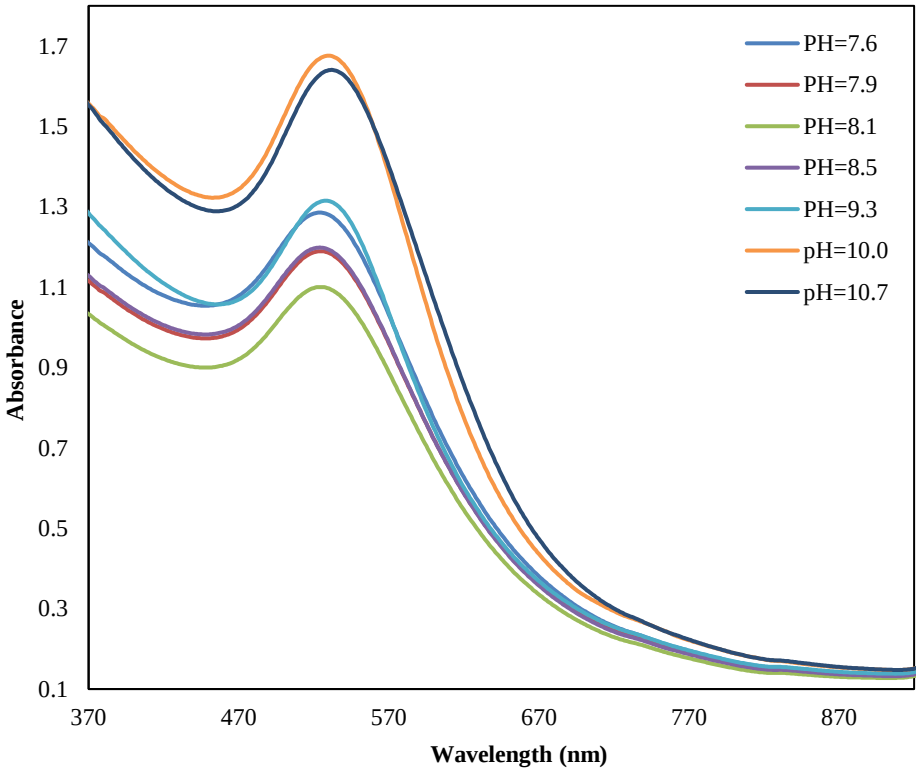

Figure 3.17. Data collected through UV-Vis across the pH range produced by adding 1M NaOH (5-30 µL) to the **4A**-AuNPs solution in (**Run 3**) of the basic study.

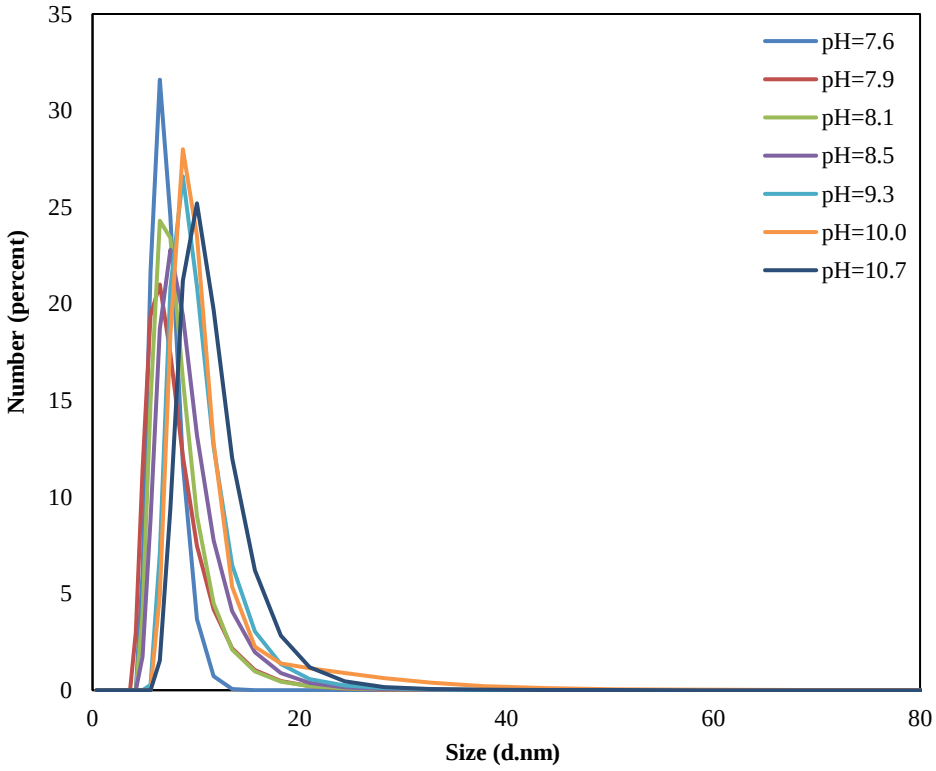

Figure 3.18. Data collected through DLS analysis of the samples in (**Run 3**) to give the diameter size and standard deviations for each pH range produced by adding 1 M NaOH to the **4A**-AuNPs solution.

3.7 Stability of 5, 4A and 4B-AuNPs with changing pH after one and half month.

It is well to note that, the AuNPs solutions functionalised with **5**, **4A** and **4B** were relatively stable with the change of pH in a particle in weak acidic and basic solutions. All samples still stable nearly two months after 1M NaOH and 1M HCl (5 - 30 µL) added, regarding UV - Vis and DLS results of **5**-AuNPs solution (Run 3) in Figures 3.19 and 3.20. The UV - Vis spectra obtained clearly indicate that the pH values were changed a little bit after about one and half month but AuNPs were stable somewhat, and there was not seen visible evidence for any clear extra aggregation, which ensure the importance of contributing our ligands in the stability of AuNPs.

In addition, the **5**-AuNPs under acidic pH additions associated to form bigger particles and the plasmon resonance band has been shifted as they grew; for example, the plasmon resonance band is shifted from 528 nm (at pH 7.0 ± 0.3) to 535 nm (at pH 3.8 ± 0.2), these results were confirmed by using DLS (see Figures 3.19, 3.20).

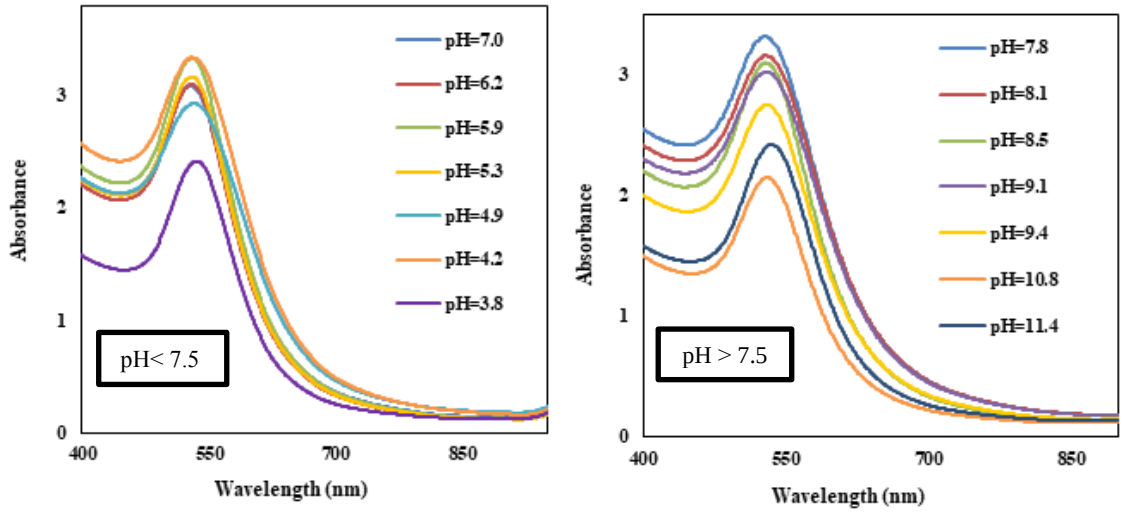

Figure 3.19. Data collected through UV-Vis of **5**-AuNPs solution (**Run 3**) after one and half month when (pH <7.5) in the left and (pH > 7.5) in the right.

The size of **5**-AuNPs was changed from 8.0 ± 1.2 at pH 7.3 to 14.9 ± 1.2 (at pH 4.4) after nearly two months when HCl added (30 µL), whereas it was 7.6 ± 1.4 to 12.24 ± 1.2 before one and half month. In the same hand, the size was changed after one and the half month from NaOH addition, where DLS measures illustrated in Figure 3.20, the size was

7.8 ± 1.6, which changed to 12.7 ± 1.3 after 30 µL NaOH added. After one and the half month, the size changed from 8.3 ± 1.4 (at pH 7.8) to 14.1 ± 1.2 (at pH 11.4) respectively. That is clearly indicative of pH-induced aggregation of AuNPs at higher amounts of HCl added. As well, the particles remained slightly stable in the presence of a different concentration of NaOH amounts in the dispersing medium, except the high concentration of NaOH amounts added.

The aggregates at different pH were comparatively stable over one month might due to the expected hydrophobic environment between aggregated AuNPs that can expel water molecules and the aggregation of AuNPs shown stabilities against hydrolysis as mentioned in the literature [22]. As stated in the previous literature, AuNPs solution at pH 2.44 have some precipitates after nearly a week, however at pH 7.09 is quite stable without any precipitate during one month, which in turn confirms our results [50]. The stability of the AuNPs studied over the course of six months suggests that the AuNPs would be beneficial over time under the conditions of the human body as once functionalised, as they are less likely to aggregate unnecessarily [63].

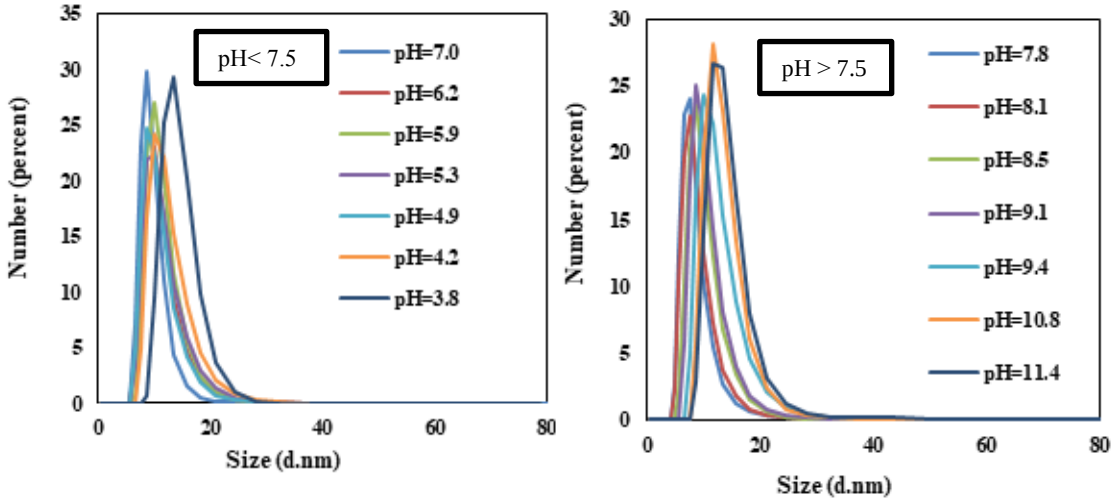

Figure 3.20. Data collected through DLS analysis of **5**-AuNPs solution (**Run 3**) after one and half month in both acidic conditions, pH < 7.5 (in the left) and basic conditions, pH > 7.5 (in the right).

3.8 Conclusions

In this part of the work, functionalised AuNPs were successfully synthesised and characterised at different pH values. The studies presented in this chapter were conducted

to assess the properties and stability of colloidal AuNPs manufactured for the potential used in alternative bio-recognition and drug delivery systems.
From previous work, it was understandable to know that, some ligands were harder to synthesise compared to others with each having unique properties. For instance, the ligands synthesised with (phenyl) groups head gave more crystalline structures than those with ligands contain a (tolyl) or (trimethoxy-benzene) that resulted in viscous waxy liquids. ATR-FTIR, NMR, ESI-MS studies confirmed the structure of the ligands in this Chapter.

From the synthesis of functionalised AuNPs, it was clear to see that the most versatile ligands were those containing methoxy groups such as **4B** or contain tolyl group such as **4A**, which produced stable AuNPs. Methoxy and tolyl groups are an ideal moiety to incorporate into a ligand, as they are donator groups and contribute electrons to the phenol group and increasing the stability of nanoparticles [64]. This changes the stability of the AuNPs within a solution as the electronegative charge is shifted. As well as, the AuNPs with shorter chain ligands synthesised produced a more crystalline structure than longer chain ligands that was easily soluble in solvents making these ligands ideal for use in biological media [65].

The data collected with regards to the stability of AuNPs over time supported the results proposed in published literature [65]. It was obvious that over the 6 months period, the stability of the AuNPs remained constant with no important shifting in the peak of the absorbance observed using UV-Vis. Previous work has illustrated that the AuNPs manufactured can remain stable over long periods of time [32, 65]. However, it is also imperative that the AuNPs remain stable within the body over shorter periods of time for therapeutic reasons [63].

All the experimentations were performed thrice, as a result of the pH stability study, it was proposed that the optimum pH of the **5**-AuNP solution was between pH 7.3 ± 0.05 and pH 4.0 ± 0.2 as this gave a diameter size range of 7.6 ± 1.4 nm.to 14.7 ± 1.5 nm. Whilst aggregation occurred clearly during the acid pH study in low acidic pH. However, in base pH study, it was pH 7.5 ± 0.05 and pH 11.3 ± 0.1 as this gave a diameter size range of 7.6 ± 1.6 nm.to 14.3 ± 1.3 nm. The stability of the solution at these pH was measured using UV-Vis data which showed that the peak absorbance wavelength

observed did not shift, except high pH, suggesting a consistent size of AuNP monodispersed within the solution [59].

In addition, AuNPs functionalised by **4B** was between pH 7.3 ± 0.1 and pH 3.0 ± 0.2 as, within this range, the size and standard deviations are within the range between 6.2 ± 1.6 nm to 13.8 ± 1.3 nm in HCl addition, which showed clearly aggregation at high addition. While, in NaOH addition, it was between pH 7.1 ± 0.1 and pH 9.0 ± 0.1 have an average diameter of 6.1 ± 1.17 nm to 9.6 ± 1.4 nm respectively with a narrow size distribution. Whereas stable **4A**-AuNPs with size variations at pH 7.7 ± 0.1 and pH 3.7 ± 0.3 respectively between 6.8 ± 1.4 nm and 12.2 ± 1.3 nm when the concentration of HCl acid was varied, While the sizes were between 6.8 ± 1.30 to 11.9 ± 1.3 nm at pH 7.6 ± 0.1 and pH 10.7 ± 0.1 respectively with variety in 1M NaOH amounts added. AuNPs are found to show similar transition pH ranges, regardless of the different protecting ligands used, and this expectation is experimentally confirmed.

The stability of the AuNPs experienced in the acidic pH study suggests that despite the weakly acidic nature of tumorous tissue [66], it would be possible for the manufactured AuNPs to selectively enter the cells required and remain stable for a suitable time period for treatment to be completed. This is because of the hydrophobic nature of the synthesised ligands introducing an affinity with the lipophilic cell walls. Not only do the hydrophobic and cationic properties of the surface coating of the AuNPs aid cell penetration, it also provides a pathway for ion exchange within the biological media of the cell [67].

The evidence presented for the stability of functionalised AuNPs at slightly lower pH (Ex 5 - 6.5) is significant as it is well documented that the pH of cancer cells is weakly acidic [66]. Whilst the work presented was conducted in vitro; future work should include in vivo biological test by cellular internalisation of the phosphonium ligand coated AuNPs. This analysis could be achieved using a biophysical technique, such as flow cytometry where the cells are suspended in a stream of fluid and passed by an electronic detection apparatus. Finally, because pH plays an important role in many cellular processes, so from this chapter, it is found that the size and shape of the AuNPs could be easily controlled via varying pH additions under acidic and basic conditions. AuNPs with pH-dependent membrane adsorption might use in soon future in tumour therapy and diagnosis.

3.9 References

1. Jang, B., Kwon, H., Katila, P., Lee, SJ and Lee, H, *Dual delivery of biological therapeutics for multimodal and synergistic cancer therapies.* Advanced drug delivery reviews, 2016. **98**: p. 113-133.

2. Kim, SJ., Jeong, SH., Chung, HK., Nam, JT and Won, NY, *pH Sensitive Metal Nanoparticle and Preparation Method*. US PatentsApplication, 2009.

3. Ratner, MA and Ratner, D, *Nanotechnology: A gentle introduction to the next big idea*. Prentice Hall Professional, 2003.

4. Wood, L, *Nanotechnology in Medical Applications.* The Global Market, 2015.

5. Madhusudhan, A., Reddy, GB., Venkatesham, M., Veerabhadram, G., Kumar, DA., Natarajan, S., Yang, M-Y., Hu, A and Singh, SS, *Efficient pH dependent drug delivery to target cancer cells by gold nanoparticles capped with carboxymethyl chitosan.* International journal of molecular sciences, 2014. **15**(5): p. 8216-8234.

6. Peer, D., Karp, JM., Hong, S., Farokhzad, OC., Margalit, R and Langer, R, *Nanocarriers as an emerging platform for cancer therapy.* Nature nanotechnology, 2007. **2**(12): p. 751-760.

7. Gottesman, MM., Fojo, T and Bates, SE, *Multidrug resistance in cancer: role of ATP–dependent transporters.* Nature Reviews Cancer, 2002. **2**(1): p. 48-58.

8. Assaraf, YG, *Molecular basis of antifolate resistance.* Cancer and Metastasis Reviews, 2007. **26**(1): p. 153-181.

9. Oishi, M., Hayashi, H., Iijima, M and Nagasaki, Y, *Endosomal release and intracellular delivery of anticancer drugs using pH-sensitive PEGylated nanogels.* Journal of Materials Chemistry, 2007. **17**(35): p. 3720-3725.

10. Torchilin, VP, *Targeted pharmaceutical nanocarriers for cancer therapy and imaging.* The AAPS journal, 2007. **9**(2): p. E128-E147.

11. Chen, S., Yang, K., Tuguntaev, RG., Mozhi, A., Zhang, J., Wang, PC and Liang, X-J, *Targeting tumor microenvironment with PEG-based amphiphilic nanoparticles to overcome chemoresistance.* Nanomedicine: Nanotechnology, Biology and Medicine, 2016. **12**(2): p. 269-286.

12. Melancon, MP., Lu, W., Zhong, M., Zhou, M., Liang, G., Elliott, AM., Hazle, JD., Myers, JN., Li, C and Stafford, RJ, *Targeted multifunctional gold-based nanoshells for magnetic resonance-guided laser ablation of head and neck cancer.* Biomaterials, 2011. **32**(30): p. 7600-7608.

13. Boisselier, E and Astruc, D, *Gold nanoparticles in nanomedicine: preparations, imaging, diagnostics, therapies and toxicity.* Chemical society reviews, 2009. **38**(6): p. 1759-1782.

14. Akhter, S., Zaki Ahmad, M., Singh, A., Ahmad, I., Rahman, M., Anwar, M., Kumar Jain, G., Jalees Ahmad, F and Krishen Khar, R, *Cancer targeted metallic nanoparticle: targeting overview, recent advancement and toxicity concern.* Current pharmaceutical design, 2011. **17**(18): p. 1834-1850.

15. Fiorito, S, *Nanotechnologies for future applications in the biomedical field.* La Clinica terapeutica, 2011. **163**(2): p. 155-158.

16. Alexiou, C, *Biomedical nanotechnologies.* Nanotechnol Rev, 2013. **2(4)**(379).

17. Kelsall, RW., Hamley, IW and Geoghegan, M, *Nanoscale science and technology*. Wiley Online Library, 2005.

18. Yang, H., Fung, S-Y., Xu, S., Sutherland, DP., Kollmann, TR., Liu, M and Turvey, SE, *Amino Acid-Dependent Attenuation of Toll-like Receptor Signaling by Peptide-Gold Nanoparticle Hybrids.* ACS nano, 2015. **9**(7): p. 6774-6784.

19. Will, O., Purkayastha, S., Chan, C., Athanasiou, T., Darzi, AW., Gedroyc, W and Tekkis, PP, *Diagnostic precision of nanoparticle-enhanced MRI for lymph-node metastases: a meta-analysis.* The lancet oncology, 2006. **7**(1): p. 52-60.

20. Sailor, MJ and Park, JH, *Hybrid nanoparticles for detection and treatment of cancer.* Advanced materials, 2012. **24**(28): p. 3779-3802.

21. Nam, J., La, W-G., Hwang, S., Ha, YS., Park, N., Won, N., Jung, S., Bhang, SH., Ma, Y-J and Cho, Y-M, *pH-responsive assembly of gold nanoparticles and "spatiotemporally concerted" drug release for synergistic cancer therapy.* ACS nano, 2013. **7**(4): p. 3388-3402.

22. Nam, J., Won, N., Jin, H., Chung, H and Kim, S, *pH-induced aggregation of gold nanoparticles for photothermal cancer therapy.* Journal of the American Chemical Society, 2009. **131**(38): p. 13639-13645.

23. Jung, S., Nam, J., Hwang, S., Park, J., Hur, J., Im, K., Park, N and Kim, S, *Theragnostic pH-sensitive gold nanoparticles for the selective surface enhanced Raman scattering and photothermal cancer therapy.* Analytical chemistry, 2013. **85**(16): p. 7674-7681.

24. Antosh, MP., Wijesinghe, DD., Shrestha, S., Lanou, R., Huang, YH., Hasselbacher, T., Fox, D., Neretti, N., Sun, S and Katenka, N, *Enhancement of radiation effect on cancer cells by gold-pHLIP.* Proceedings of the National Academy of Sciences, 2015. **112**(17): p. 5372-5376.

25. Li, C., Xia, J., Wei, X., Yan, H., Si, Z and Ju, S, *pH‐Activated Near‐Infrared Fluorescence Nanoprobe Imaging Tumors by Sensing the Acidic Microenvironment.* Advanced Functional Materials, 2010. **20**(14): p. 2222-2230.

26. Ding, H-M and Ma, Y-Q, *Controlling cellular uptake of nanoparticles with pH-sensitive polymers.* Scientific reports, 2013.

27. Ju, K-Y., Kang, J., Pyo, J., Lim, J., Chang, JH and Lee, J-K, *pH-Induced aggregated melanin nanoparticles for photoacoustic signal amplification.* Nanoscale, 2016. **8**(30): p. 14448-14456.

28. Sperling, RA and Parak, W, *Surface modification, functionalization and bioconjugation of colloidal inorganic nanoparticles.* Philosophical Transactions of the Royal Society of London A: Mathematical, Physical and Engineering Sciences, 2010. **368**(1915): p. 1333-1383.

29. Rechberger, W., Hohenau, A., Leitner, A., Krenn, J., Lamprecht, B and Aussenegg, F, *Optical properties of two interacting gold nanoparticles.* Optics communications, 2003. **220**(1): p. 137-141.

30. Jung, BG., Jo, J., Yu, JW and Lim, JK, *Investigation of Gold and Silver Nanoparticles as Acid-base pH Indicators and Their Transition pH Ranges.* Bulletin of the Korean Chemical Society, 2014. **35**(12): p. 3595-3600.

31. Ju-Nam, Y., Allen, DW., Gardiner, PH and Bricklebank, N, *ω-Thioacetylalkylphosphonium salts: Precursors for the preparation of phosphonium-functionalised gold nanoparticles.* Journal of organometallic chemistry, 2008. **693**(23): p. 3504-3508.

32. Ju-Nam, Y., Bricklebank, N., Allen, DW., Gardiner, PH., Light, ME and Hursthouse, MB, *Phosphonioalkylthiosulfate zwitterions—new masked thiol ligands for the formation of cationic functionalised gold nanoparticles.* Organic & biomolecular chemistry, 2006. **4**(23): p. 4345-4351.

33. Kaszuba, M., Mcknight, D., Connah, MT., Mcneil-Watson, FK and Nobbmann, U, *Measuring sub nanometre sizes using dynamic light scattering.* Journal of Nanoparticle Research, 2008. **10**(5): p. 823-829.

34. Gottlieb, HE., Kotlyar, V and Nudelman, A, *NMR chemical shifts of common laboratory solvents as trace impurities.* The Journal of organic chemistry, 1997. **62**(21): p. 7512-7515.

35. Zhang, T, *The grignard synthesis of triphenylmethanol.* Organic Chemistry: An Indian Journal, 2015. **11**(8): p. 288-292.

36. Liu, S., Weaver, JV., Save, M and Armes, SP, *Synthesis of pH-responsive shell cross-linked micelles and their use as nanoreactors for the preparation of gold nanoparticles.* Langmuir, 2002. **18**(22): p. 8350-8357.

37. Gao, J., Huang, X., Liu, H., Zan, F and Ren, J, *Colloidal stability of gold nanoparticles modified with thiol compounds: bioconjugation and application in cancer cell imaging.* Langmuir, 2012. **28**(9): p. 4464-4471.

38. Kobayashi, K., Wei, J., Iida, R., Ijiro, K and Niikura, K, *Surface engineering of nanoparticles for therapeutic applications.* Polymer journal, 2014. **46**(8): p. 460-468.

39. Abdelhalim, MaK., Mady, MM and Ghannam, MM, *Physical properties of different gold nanoparticles: ultraviolet-visible and fluorescence measurements.* J Nanomed Nanotechol, 2012. **3**(3): p. 178-194.

40. Mie, G, *Articles on the optical characteristics of turbid tubes, especially colloidal metal solutions.* Ann. Phys, 1908. **25**(3): p. 377-445.

41. Kanjanawarut, R., Yuan, B and Xiaodi, S, *UV-Vis spectroscopy and dynamic light scattering study of gold nanorods aggregation.* Nucleic acid therapeutics, 2013. **23**(4): p. 273-280.

42. Tonga, GY., Mizuhara, T., Saha, K., Jiang, Z., Hou, S., Das, R and Rotello, VM, *Binding studies of cucurbit [7] uril with gold nanoparticles bearing different surface functionalities.* Tetrahedron letters, 2015. **56**(23): p. 3653-3657.

43. Diegoli, S., Manciulea, AL., Begum, S., Jones, IP., Lead, JR and Preece, JA, *Interaction between manufactured gold nanoparticles and naturally occurring organic macromolecules.* Science of the Total Environment, 2008. **402**(1): p. 51-61.

44. Shen, SF., Zhao, HW., Xu, D., Wu, LP and Huang, CZ, *Colorimetric assay of melamine based on the aggregation of gold nanoparticles.* Journal of biomedical nanotechnology, 2011. **7**(5): p. 691-695.

45. Rac, O., Suchorska-Woźniak, P., Fiedot, M and Teterycz, H, *Influence of stabilising agents and pH on the size of SnO2 nanoparticles.* Beilstein journal of nanotechnology, 2014. **5**: p. 2192-2201.

46. Patungwasa, W and Hodak, JH, *pH tunable morphology of the gold nanoparticles produced by citrate reduction.* Materials Chemistry and Physics, 2008. **108**(1): p. 45-54.

47. Sato, K., Hosokawa, K and Maeda, M, *Rapid aggregation of gold nanoparticles induced by non-cross-linking DNA hybridization.* Journal of the American Chemical Society, 2003. **125**(27): p. 8102-8103.

48. Yu, M., Zhou, C., Liu, J., Hankins, JD and Zheng, J, *Luminescent gold nanoparticles with pH-dependent membrane adsorption.* Journal of the American Chemical Society, 2011. **133**(29): p. 11014-11017.

49. Wager, K., Chui, T and Adem, S, *Effect of pH on the stability of gold nanoparticles and their application for melamine detection in infant formula.* J. Appl. Chem, 2014. **7**(8): p. 15-20.

50. Shou, Q., Guo, C., Yang, L., Jia, L., Liu, C and Liu, H, *Effect of pH on the single-step synthesis of gold nanoparticles using PEO–PPO–PEO triblock copolymers in aqueous media.* Journal of colloid and interface science, 2011. **363**(2): p. 481-489.

51. Vijayakumar, S, *In vitro stability studies on gold nanoparticles with different stabilizing agents.* Int. J. Curr. Sci, 2014. **11**: p. 84-93.

52. Shipway, AN., Katz, E and Willner, I, *Nanoparticle arrays on surfaces for electronic, optical, and sensor applications.* ChemPhysChem, 2000. **1**(1): p. 18-52.

53. Weitz, D., Lin, M and Sandroff, C, *Colloidal aggregation revisited: new insights based on fractal structure and surface-enhanced Raman scattering.* Surface Science, 1985. **158**(1-3): p. 147-164.

54. Wang, Z., Zhang, Q., Kuehner, D., Ivaska, A and Niu, L, *Green synthesis of 1–2 nm gold nanoparticles stabilized by amine-terminated ionic liquid and their electrocatalytic activity in oxygen reduction.* Green Chemistry, 2008. **10**(9): p. 907-909.

55. Sun, L., Zhang, Z., Wang, S., Zhang, J., Li, H., Ren, L., Weng, J and Zhang, Q, *Effect of pH on the interaction of gold nanoparticles with DNA and application in the detection of human p53 gene mutation.* Nanoscale research letters, 2008. **4**(3): p. 216-220.

56. Li, H., Liu, X., Huang, N., Ren, K., Jin, Q and Ji, J, *"Mixed-charge self-assembled monolayers" as a facile method to design pH-induced aggregation of large gold nanoparticles for near-infrared photothermal cancer therapy.* ACS applied materials & interfaces, 2014. **6**(21): p. 18930-18937.

57. Zhu, J., Li, W., Zhu, M., Zhang, W., Niu, W and Liu, G, *Influence of the pH value of a colloidal gold solution on the absorption spectra of an LSPR-assisted sensor*. AIP Advances, 2014. **4**(3): p. 031338.

58. Döllefeld, H., Hoppe, K., Kolny, J., Schilling, K., Weller, H and Eychmüller, A, *Investigations on the stability of thiol stabilized semiconductor nanoparticles.* Physical Chemistry Chemical Physics, 2002. **4**(19): p. 4747-4753.

59. Wagers K, CT, Adem S, *Effect of pH on the Stability of Gold Nanoparticles and Their Application for Melamine Detection in Infant Formula.* J Appl Chem. , 2014. **;7(8)**: p.15-20.

60. Kalliola, S., Repo, E., Sillanpää, M., Arora, JS., He, J and John, VT, *The stability of green nanoparticles in increased pH and salinity for applications in oil spill-treatment.* Colloids and Surfaces A: Physicochemical and Engineering Aspects, 2016. **493**: p. 99-107.

61. Gan, Q., Wang, T., Cochrane, C and Mccarron, P, *Modulation of surface charge, particle size and morphological properties of chitosan–TPP nanoparticles intended for gene delivery.* Colloids and Surfaces B: Biointerfaces, 2005. **44**(2): p. 65-73.

62. Tyagi, H., Kushwaha, A., Kumar, A and Aslam, M, *pH-dependent synthesis of stabilized gold nanoparticles using ascorbic acid.* International Journal of Nanoscience, 2011. **10**(04n05): p. 857-860.

63. Salcedo, ARM and Sevilla Iii, FB, *Citrate-capped gold nanoparticles as colorimetric reagent for copper (II) ions.* Philipp. Sci. Lett, 2013. **6**: p. 90-96.

64. Wade.Lg, *Organic Chemistry.* . 8th Edition. Pearson; ed. 2012.

65. Nam, J and Kyeong, Y, *Functionalised Metal Nanoparticles as Novel Reagents for Biomedical Analysis*. 2007, Sheffield Hallam University.

66. Tavakol, S, *Acidic pH derived from cancer cells may induce failed reprogramming of normal differentiated cells adjacent tumor cells and turn them into cancer cells.* Medical hypotheses, 2014. **83**(6): p. 668-672.

67. Arvizo, R., Bhattacharya, R and Mukherjee, P, *Gold nanoparticles: opportunities and challenges in nanomedicine.* Expert opinion on drug delivery, 2010. **7**(6): p. 753-763.

Chapter 4: Green synthesis of positively charged biocompatible gold nanoparticles in water: use of ascorbic acid as reducing agent.

4.1 Abstract

Well-monodispersed AuNPs were prepared by the reduction of $KAuCl_4$ using sodium borohydride and ascorbic acid as reducing agents. Due to using different reducing agent power, we obtained different results for AuNPs that were functionalised with same ligands. The effect of two different reducing agents on size and stability of the colloidal cationic phosphonium AuNPs was investigated. Their formation and stability was monitored by using UV−Vis absorption spectroscopy, transmission electron microscopy (TEM) and dynamic light scattering (DLS). Small sizes with higher stability during a period of time were generated when $NaBH_4$ was used as reducing agent.

AuNPs functionalised by tri(phenyl)phosphoniopropylthiosulfate (**4C**) (3-thioactylpropyl)-triphenylphosphonium bromide (**5**) and tri(*p*-tolyl)phosphoniopropyl-thiosulfate (**4**) zwitterion *via* using $NaBH_4$ as reducing agent in H_2O / DMSO as solvent, the maximum absorption bands centred at 519, 519 and 529 nm respectively. While, when the ascorbic acid is used as reducing agent, the maximum absorption of AuNPs functionalised by these ligands were centred at 542, 575 and 557 nm respectively. For (6-thioacetylhexyl)tris(2,4,6-trimethoxyphenyl)-phosphonium bromide (**8B**) showed little difference between two methods, whereas the absorbance centred at 522 nm in the case of $NaBH_4$ and at 528 nm in the case using ascorbic acid as a reducing agent.

ATR-FTIR, NMR, ESI-MS techniques can be employed to identify the kinds of functionality of ligands attached to the AuNPs.

In this research, we proposed the bio-reducing agent, ascorbic acid, to synthesise the AuNPs, when compared to AuNPs fabricated by using $NaBH_4$ as reducing agent. We studied the relationship between the reducing agents and the stability / sizes of AuNPs. It was found that, various sizes with different stabilities occurred based on various reducing

agent used in this Chapter, where AuNPs of different sizes are known to produce contradictory results sometimes in *vivo* and in *vitro* bio application 00.

All these results in this Chapter, confirmed that $KAuCl_4$ could be reduced during the green synthesis of AuNPs through ascorbic acid, and the same protect ligands used in the case of $NaBH_4$. $KAuCl_4$ – $NaBH_4$ system produced small sizes with small mean deviation and indicated spherical shape. However, they were nearly poly-dispersed and poly-shaped for most process conditions when $KAuCl_4$ – ascorbic acid system was used as reducing agent. Different sizes of AuNPs usually have different bio-applications. Development of more environmentally friendly and biocompatible synthetic ways is one of the main aims to allow their use in biomedical applications. Ascorbic acid has been used as a benign naturally available reducing agent to synthesise AuNPs, due to its high water solubility, low toxicity, and biodegradability. In this chapter, a green synthesis methodology used in order to produce positively charged biocompatible AuNPs for possibility biomedical applications is outlined.

4.2 Introduction

A considerable amount of gold nanoparticle (AuNP) synthetic methods have been reported in the literature in recent years. AuNP surface has shown to interact with various organic thiolate ligands, making them versatile nanodevices for their potential use in drug delivery, imaging and biosensing applications. Therefore, the development of more environmentally friendly and biocompatible synthetic routes is one of the main aims to allow their use in biomedical applications. One of the most used reducing agents for noble metal salt reduction is sodium borohydride, a strong and excellent hydrides source. However, other reducing agents such as sodium citrate, ascorbic acid, and tannic acid are reported to be green alternatives to sodium borohydride [1-4]. Their use represents significant progress in the development of methodologies for the green synthesis of biocompatible AuNPs in their colloidal form.

Malassis, L., et al., [1] recently developed a one-step, green synthesis using biocompatible ascorbic acid. The authors used this compound as reducing and stabilising agent and carried out the synthesis at room temperature. They successfully synthesised different size gold (8 – 80 nm) and silver (20 – 175 nm) NPs by controlling the pH of either the metal salt solution or the ascorbic acid solution. Another example of the synthesis of NPs

using ascorbic acid is the one reported by Lin, SM., et al., [4]. They developed another green synthetic method to produce D-penicillamine-template copper NPs *via* ascorbic acid reduction. The authors aimed to use these NPs as mercury ion sensors. Cao, Y., et al., [5] reported a methodology to synthesise silver NPs by using tannic acid, another green alternative to sodium borohydride. The authors used the tannic acid as reducing and stabilising agent, carrying out the synthesis in a water bath at a controlled temperature of 30°C. The size of NP in a range of 7 – 66 nm were observed and the samples were monodispersed, and that silver NPs coated with tannic acid showed better colloidal stability when compared to citrate stabilised silver NPs [5].

The chemical reduction of gold salts in the presence of a variety of stabilisers, such as e.g. donor ligands, to produce zerovalent metal colloids in aqueous or organic media is considered one of the most powerful and well known synthetic methods in this field [6]. Ascorbic acid is a vitamin C, which participates in several biochemical reactions. As an influential part of the organism biochemistry, it has an antioxidant effect which is considered one of its best known biological functions [7]. Ascorbic acid has been used as a benign naturally available reducing agent to synthesise AuNPs, because of its high water solubility, low toxicity, and biodegradability [8].

In addition, metal NPs exhibited good uniform size when using ascorbic acid [9]. On the other hand, it is observed that the absorption peak of the nano-composite without ascorbic acid was quite narrow and symmetrical, indicating a narrow size distribution of NPs. However, after the ascorbic acid is added, a wider size distribution is considered by the broadening of the absorption peak of the blue mixture which confirms the induced growth of the nanoparticles [10]. The ascorbic acid diffuses to the surface of the NPs where electron transfer takes place causing the formation of the atoms and following growth of the clusters to NPs, the colour changed from colourless to blue [10, 11].

According to Luty-Błocho, M., et al., it is noted that AuNPs processing with the $HAuCl_4$ – $NaBH_4$ system produced small sizes with small mean deviation and indicated spherical shape. However, they were poly-dispersed and poly-shaped for most process conditions when $HAuCl_4$ – ascorbic acid system was used as reducing agent [12]. Furthermore, the amount of ascorbic acid plays a significant role in determining the size and shape of the AuNPs [13, 14]. AuNPs have peak wavelength between 530 and 540 nm. Sizes changes

between 10 and 23 nm were measured when varied quantities of the ascorbic acid were added [13].

Some researchers have used sodium hydroxide with ascorbic acid to reduce gold salt, because it's addition to a concentrated aqueous solution of $HAuCl_4$, causing neutralisation of its acidity and that as result to the rapid formation of hydroxyl-Au complexes such as ($AuCl_3(OH)^-$, $AuCl_2(OH)_2^-$, $AuCl(OH)_3^-$ and $Au(OH)_4^-$ with (pK1 = 8.3, pK2 = 7.5, pK3 = 6.4, and pK4 = 5.4) respectively as result of the progressive substitution of Cl^-. The concentration of these species highly depends on the pH of the reaction mixture [14, 15]. In addition, it is notable that, the $HAuCl_4$ in aqueous solution consists of $[AuCl_x(OH)_{4-x}]$ when ($x > 2$) at low pH but $[AuCl_x(OH)_{4-x}]$ when ($x < 2$) at high pH. These influences on the synthesis, structure, and property of AuNPs colloids [16].

In addition, according to Ziegler, C and EychmüLler, A, the spherical particles were generated by using of the mixture of ascorbic acid as reducing agent and sodium citrate as stabiliser ligands. Where this method proceeded, nontoxic and easy to remove stabilisers, low poly-dispersity and the large size range, which can be offered an excellent new method that can be applied in many fields of nano science [17].

Jana, NR, et al., shown that, AuNPs can be produced by controlling their sizes by using of either strong or weak reducing agent mixture. The nucleation rate was controlled via varying the ratio of strong ($NaBH_4$) reducing agents and weak reducing agent (ascorbic acid), where noted $NaBH_4$ predominantly induced nucleation, while ascorbic acid induced growth. For instance, small size (< 5 nm) produced as result to high ratios of $NaBH_4$ which induced rapid nucleation. In contrast, when lower ratios of $NaBH_4$ were used, AuNPs with broad size and shape distributions were produced because the nucleation rate was very slow and the may also causing NPs aggregates. The $NaBH_4$ – ascorbic acid method gives 4-10 nm AuNPs with varying concentration of the gold salt [18].

In this Chapter, a green synthesis methodology to produce positively charged biocompatible AuNPs for potential biomedical applications is outlined. As previously reported, the use of functionalised AuNPs in therapeutic purposes is promising. A synthesis of cationic phosphonium AuNPs was developed, by reducing gold (III) salt using ascorbic acid, a greener alternative to sodium borohydride. We also describe the

synthesis of new cationic phosphonium ligand (6-thioacetylhexyl)-tris(2,4,6-trimethoxy-phenyl)phosphonium bromide (**8B**) and tri(*p*-tolyl)phosphoniohexylthiosulfate (**9A**) zwitterion used to functionalise the AuNPs surface in mixture H_2O / DMSO. Two previously reported phosphonium ligands, triphenylphosphoniopropylthiosulfate (**4C**) zwitterion [19], (3-thioactylpropyl)triphenylphosphonium bromide (**5**) [20], tri(*p*-tolyl)-phosphoniopropylthiosulfate (**4**) and (6-thioacetylhexyl)tris(2,4,6-trimethoxyphenyl)-phosphonium (**8B**) were used for this work to produce the cationic phosphonium AuNPs in H_2O / DMSO with $NaBH_4$. Same NPs were also produced using ascorbic acid as reducing agent in aqueous solution.

4.3 Materials and Methods

All chemicals used were purchased from Sigma-Aldrich and Fisher Scientific Ltd. All reagents were used as received without further purification. All solutions were prepared with redistilled water. All the glassware was washed using aqua regia solution (HCl / HNO_3, 3:1), followed rinsing thoroughly with distilled water before use.

4.3.1 Cationic phosphonium ligand syntheses

Different techniques have been approved for synthesis various dimensions of nanoparticles and in order to functionalise their surface for improving their applications [21-23]. The main challenges in developing different strategies are their low poly-dispersity with high purity [23].

4.3.1.1 Synthesis of tri(phenyl) (4C) and tri(*p*-tolyl)phosphoniopropylthiosulfate (4) zwitterion

Synthetic method outlined in Chapter 2.

4.3.1.2 Synthesis of (3-thioacetylpropyl)triphenylphosphonium bromide (5).

Synthetic method outlined in Chapter 2.

4.3.1.3 Syntheses of the (6-thioacetylhexyl)triphenylphosphonium bromide derivatives ligands

The syntheses of (6-thioacetylhexyl)triphenylphosphonium bromide (**8D**), (6-thioacetylhexyl)tri(*p*-tolyl)-phosphonium bromide (**8A**) and (6-thioacetylhexyl)-tris(2,4,6-trimethoxyphenyl-phosphonium bromide (**8B**) are shown in Scheme 1. The

compounds were synthesised *via* reaction of tri(phenyl)phosphine (**1D**), tri(*p*-tolyl)phosphine (**1A**) and tris(2,4,6-trimethoxyphenyl)-phosphine (**1B**) (3.8mmol) with approximately bromo-hexanol (15 mmol). In a round bottom flask with a reflux condenser were refluxed for five hours in acetonitrile (0.024 mmol). A Pale yellow, brown oil and brown solid were collected, and recrystallized from diethyl ether (Reaction 1, Scheme1). The yield was 70%, 65%, and 75% respectively.

The resulting salts (**6D**), (**6A**), (**6B**) were dissolved in hydrobromic acid (0.18 mmol, 10 ml) (48%) in a round bottom under reflux five hours (Reaction 2, Scheme 1). Then a mixture of ω-bromohexyl-tri(phenylphosphonium bromide (**7D**), ω-bromohexyl-tri(*p*-tolyl)phosphonium bromide **(7A)** and ω-bromohexyl-tri(1,3,5-trimethoxy-phenyphosphonium bromide (**7B**) (2 mmol) and potassium thioacetate (3 mmol) were stirring overnight at room temperature in aqueous ethanol (1:1, 10ml) (Reaction 3, Scheme 1). The compounds looked like a yellow oil, brown oil and brown precipitate respectively (**8D**), (**8A**), (**8B**). TLC has used to monitor the reactions by using 20% methanol: 80% DCM (dichloromethane) as a mobile phase. The (6-thioacetylalkyl)-triphenylphosphonium bromide ligands (**8D**), (**8A**), (**8B**) were achieved by DCM extraction of the mixture of reaction and purified by diethyl ether. The yield was 65%, 70%, and 75% respectively. The compounds (**8D**), (**8A**) and (**8B**) looked like a yellow oil, brown oil and white precipitate respectively, with a melting point of **8B** at 206 - 208 °C.

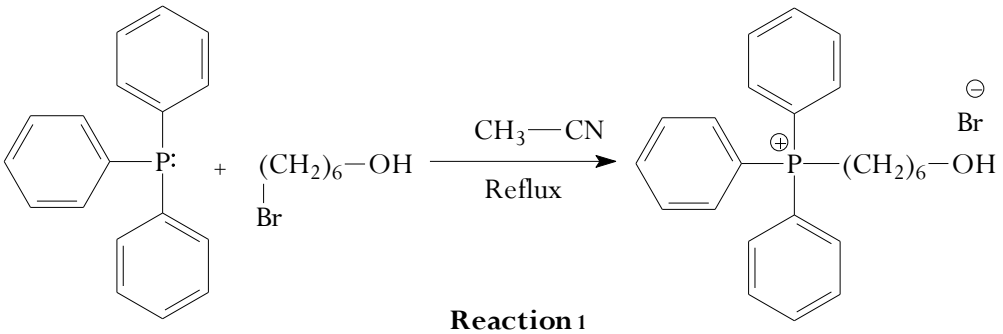

Reaction 1

(1) (6)

A) Ph = 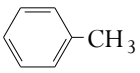

B) Ph = 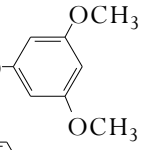

D) Ph = 

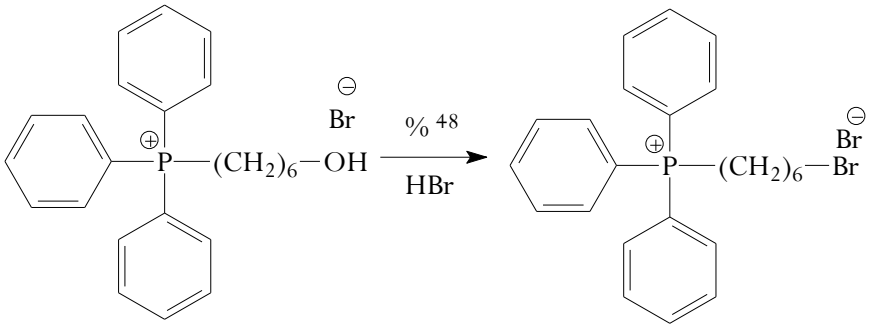

(6) **Reaction 2** (7)

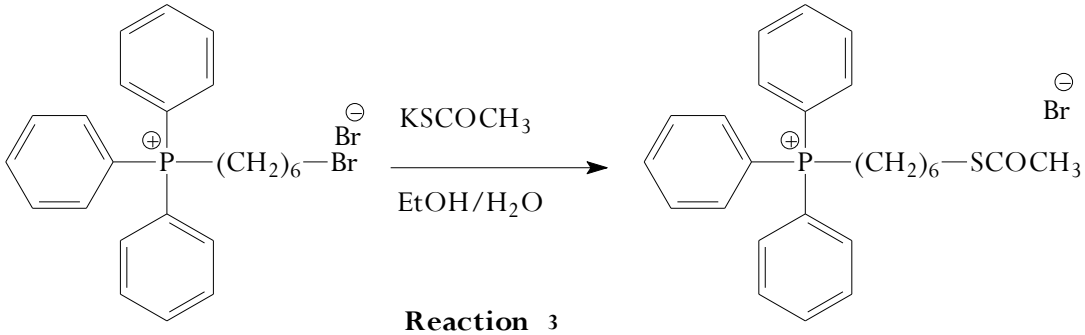

(7) **Reaction 3** (8)

Scheme 1

4.3.1.4 Synthesis of tri(phenyl)phosphoniohexylthiosulfate derivatives zwitterion

The synthesis of the tri(phenyl)phosphoniohexylthiosulfate zwitterion was carried out following the reactions showed in Scheme 2. In a round bottom flask with a reflux condenser a mixture of ω-bromohexyl-tri(phenyl)phosphonium bromide, ω-bromohexyl-tri(*P*-tolyl)-phosphonium bromide (**7D**), (**7A**) (1 mmol) and sodium thiosulfate (1.5 mmol) were refluxed for five hours in aqueous ethanol (1:1, 10 ml) (Reaction 1, Scheme 2). TLC was used in order to follow the progress of the reaction by using 10 %: 90 % methanol: DCM as a mobile phase. The compounds (**9D**) and (**9A**) looked like a white precipitate with a melting point at 64-66°C and a brown oil respectively and were purified diethyl ether. The yield was 62 %, 74 % respectively.

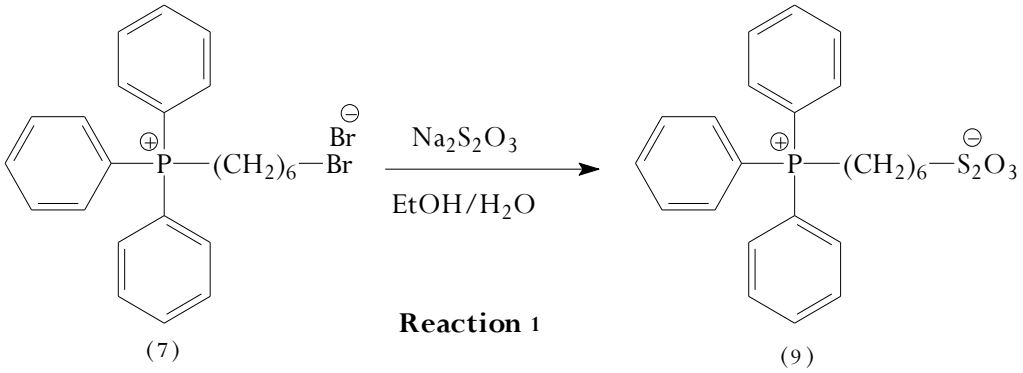

(7) (9)

Reaction 1

Scheme 2

A) Ph= CH_3

D) Ph=

Reaction Mechanism

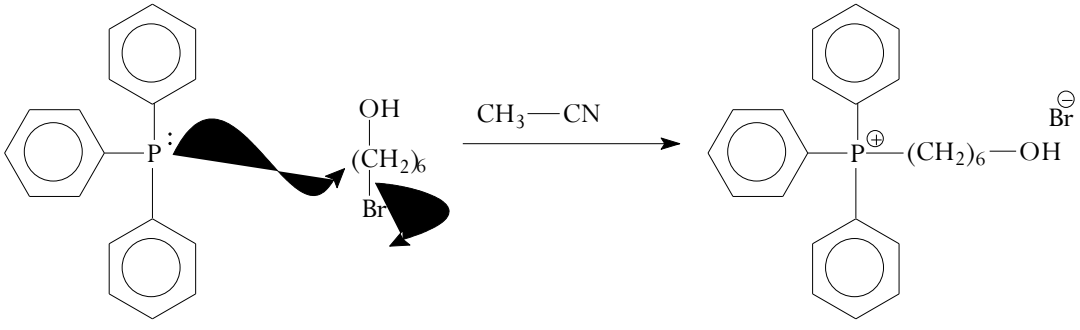

(1) (6)

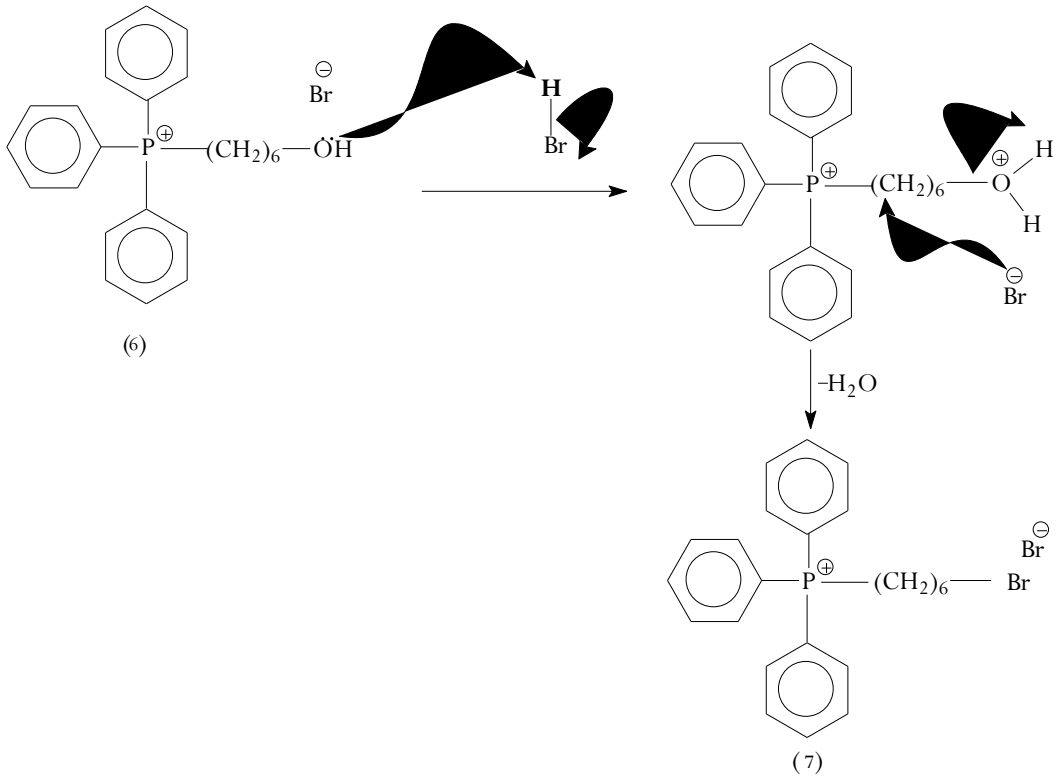

(6)

(7)

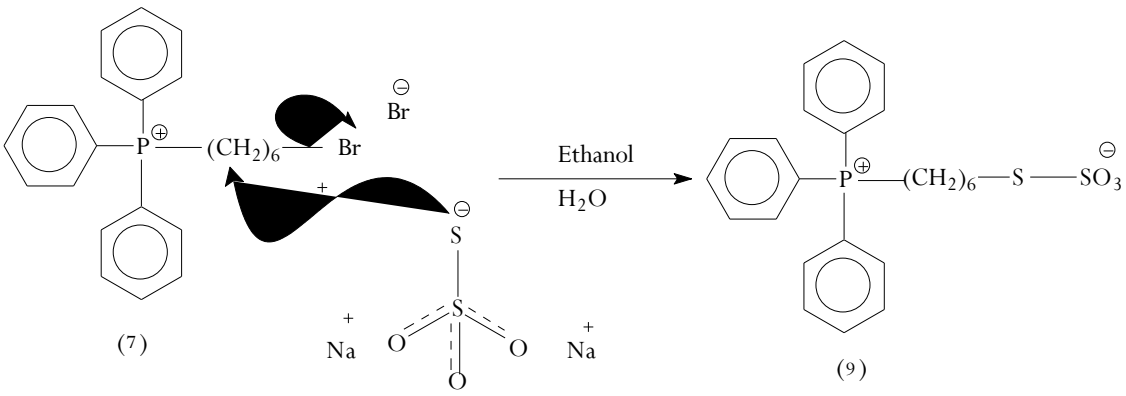

(7)

(9)

4.3.2 Protecting AuNPs by synthesis of phosphonium-monolayer using protecting ligands including thioacetate and thiosulfate ligands using $NaBH_4$ reduction in (H2O/DMSO) and comparison with ascorbic acid reduction in water

AuNPs are generally synthesised *via* the reduction of gold salts, nucleation and growth of metallic particles in solution. An aqueous synthesis is commonly nowadays carried out by the citrate-reduction route, which produces AuNPs with a narrow and mono-modal size distribution. By varying the reaction conditions, the average particle diameter can be controlled between about 2 – 200 nm [24, 25].

The synthesis of functionalised AuNPs was carried out using either $NaBH_4$ or ascorbic acid as the reducing agent to promote the formation of Au^0 and colloidal AuNPs.

4.3.2.1 Synthesis of cationic phosphonium gold nanoparticles by NaBH4 in H2O / DMSO

AuNPs functionalised by (**4C**), (**5**), and (**4**) zwitterion using $NaBH_4$ in DMSO are shown in experimental section / Chapter 2.

The triphenyl (**8D**), tri(*p*-tolyl) (**8A**), (6-thioacetylhexyl)tris(2,4,6-trimethoxyphenyl)-phosphonium (**8B**), (**9D**), and (**9A**) zwitterions were used to protect AuNPs. All these ligands have the same preparation technique, which is described below.

8D, **8A**, **8B**, **9D**, and **9A**-AuNPs were prepared in DMSO 0.8 mmol, 0.25mmol, 0.3 mmol, 0.4 mmol and 0.21 mmol respectively. The volume of DMSO used for these was 30 mL. A solution of potassium tetrachloroaurate (0.12 mmol) in H_2O (10 mL) was also prepared. Then the ligands and gold salt solutions were mixed, and stirred for five hours. The reduction was carried out by adding 5 mL of a freshly prepared aqueous solution of $NaBH_4$ (2.0 mmol) to the H_2O / DMSO mixture. In order to remove the excess of ligands in each one of the gold colloidal solutions prepared, liquid-liquid extractions were carried out using diethyl ether.

4.3.2.2 Syntheses AuNPs using ascorbic acid as reducing agent

The reduction of gold (III) salts using ascorbic acid ($C_6H_8O_6$) was a one-pot reaction using water as a solvent. The reaction equation of this reaction is as follow:

$2\ [AuCl_4]^- + 3C_6H_8O_6 = 2Au + 8\ Cl^- + 3C_6H_6O_6 + 6\ [H]^+$ [8].

4.3.2.2.1 Synthesis of AuNPs functionalised by triphenylphosphonio-propylthiosulfate (4C) zwitterion, (3-thioactylpropyl)triphenylphosphonium bromide (5), tri(*p*-tolyl) phosphoniopropylthiosulfate (4) and (6-thioacetylhexyl)-tris(2,4,6-trimethoxy- phenyl)phosphonium bromide (8B) ligands zwitterion using ascorbic acid as reducing agent.

Functionalised AuNPs were synthesised via the following procedure. The phosphonium ligands, **4C**, **5**, **4** and **8B (**0.03, 0.022, 0.026, and 0.024 mmol, respectively) were dissolved in 25 ml deionised water under a stirring speed of 800 rpm in a 60°C water bath for two hours. After the ligands were dissolved, 0.027, 0.020, 0.021, and 0.012 mmol of $KAuCl_4$ salt dissolved in 10 ml of deionised water was added to each respective ligand solution. The reaction solutions were observed to change from colourless to yellow, and the solutions were left to stir for a further four hours until the yellow colour changed to colourless. Solutions of 0.013, 0.0089, 0.0099 and 0.0054 mmol ascorbic acid in 3 ml of deionised water were freshly prepared and added to each of the colourless gold ligand solutions. Stirring was continued over moderate heat (40 °C water bath).

Once the gold-ligand solution had stirred for approximately half an hour, 0.1M NaOH solution (1mL) was added dropwise until a permanent colour change occurred. The final solutions were left to stir overnight to encourage functionalisation of the AuNPs and no extra change in colour took place, indicating the reactions were completed.

Samples were taken and analysed using UV-Vis, TEM, and DLS techniques to measure the size of AuNPs and to assess whether agglomeration had occurred between the particles [26, 27].

4.4 Results and Discussion

AuNPs were synthesised by varying experimental conditions in this chapter. It verified their sizes combining two different methods. Both $NaBH_4$ and ascorbic acid were used as reducing agents, and different sizes were noted by using three complementary techniques including DLS, UV-Vis, and TEM. This tended to give comparable results in the case of mono-dispersed particle distributions.

4.4.1 Syntheses of 4C, 5, 4, 8D, 8B, 8A, 9D, and 9A ligands

Syntheses of **4**, **5** and **4C** have shown in Chapter 2. Synthesis of **8D**, **8B**, and **8A** are shown in Scheme 1. Compounds **9D** and **9A** are shown in experimental section / in Scheme 2 as well. ATR-FTIR, NMR, ESI-MS have used for confirming these ligands are discussion below.

The resulting zwitterions were purified by trituration using diethyl ether. When studied by ESI-MS in positive ion mode. Ions corresponding to $[M\text{-}Br]^+$ was observed at 421.174 *m/z* for **8D**. IR spectrum showed absorption bands in the regions of 719 – 727 cm^{-1} (ν CH_2), 1738 cm^{-1} (ν C=O), 1372 cm^{-1} (C-S-), and 3093–3000 cm^{-1} (ν CH-Aromatic). NMR: (DMSO), ^1H NMR spectrum gave signals at δ 3.4 (2H, t, Ph_3-P-$\underline{CH_2}$-), δ 3.3 (3H, s, CO-$\underline{CH_3}$-), δ 2.7 (2H, t, -$\underline{CH_2}$-$SCOCH_3$), δ 2.5 (1H, s, DMSO (solvent)) [28], δ 2.3 (2H, m, -$\underline{CH_2}$-), δ 1.5 (2H, m, -$\underline{CH_2}$-), δ 1.3 (2H, m, -$\underline{CH_2}$-), δ 1.2 (2H, m, -$\underline{CH_2}$-) and at 7.7 – 7.9 (15H, m, Aromatic H) ppm.

Compound **8B** is going to characterising in Chapter **6**. Compound **8A** showed absorption bands in the regions IR at 723 – 720 cm^{-1} (ν CH_2), 1700 cm^{-1} (ν C=O), 1345 cm^{-1} (C-S-), 1120 cm^{-1} (ν P=O) and 3100 – 3000 cm^{-1} (ν CH-Aromatic). NMR: $\delta^{31}P$ (CD_2CL_2) = 24.5 ppm, ^1H NMR spectrum gave signals at δ 3.7 (9H, s, Ph-3$\underline{CH_3}$), δ 3.4 (2H, t, Ph_3-P-$\underline{CH_2}$-), δ 3.3 (3H, s, CO-$\underline{CH_3}$), δ 2.4 (2H, t, $\underline{CH_2}$- $SCOCH_3$), δ 1.7 (2H, m,-$\underline{CH_2}$-), δ 1.4 (2H, m, -$\underline{CH_2}$-), δ1.3 (2H, t, -$\underline{CH_2}$-), δ1.2 (2H, t, -$\underline{CH_2}$-), 5.6 (1H, s, CD_2CL_2 (solvent) [29], and at 7.4 – 7.7 (12H, m , Aromatic H) ppm. ESI-MS 467.14 $[M\text{-}SCOCH_3]^+$.

In addition, Compounds **9D** and **9A** were confirmed by ESI-MS in positive ion mode. Whereas, ions corresponding to $[M\text{-}S_2O_3H]^+$ and $[M + H]^+$ were observed at 345.17 *m/z* and 501.16 respectively.

IR and NMR were extra evidence for **9D**, whereas IR spectrum showed absorption bands at the regions of 722–720 cm^{-1} (ν CH_2), 1338 cm^{-1} (ν S=O), 1411 cm^{-1} (C-S-), and 3100–3057 cm^{-1} (ν CH-Aromatic). NMR: $\delta^{31}P$ ($CDCL_3$) = 24.7 ppm, ^1H NMR spectrum gave signals at δ 3.6 (2H, t, -$\underline{CH_2}$-SSO_3), δ 3.2 (2H, t, -$\underline{CH_2}$-P), δ 1.6 (2H, m, -$\underline{CH_2}$-), δ 1.5 (2H, m, -$\underline{CH_2}$-), δ 1.4 (2H, t, -$\underline{CH_2}$-),δ 1.3 (2H, t, -$\underline{CH_2}$-P-), and at 7.6 – 7.7 (15H, m, Aromatic H) ppm.

More information was collected for **9A** by using IR and NMR. IR spectrum showed absorption bands in the regions of 723 – 720 cm^{-1} (νCH_2), 1315 cm^{-1} ($\nu S=O$), 1379 cm^{-1} (C-S-), and 3100 – 3024 cm^{-1} (ν CH-Aromatic). NMR: $\delta^{31}P$ (CD_2CL_2) = 24.8 ppm, ^1H NMR spectrum gave signals at δ 3.4 (9H, s, Ph-$\underline{CH_3}$), δ 2.7 (2H, t, $\underline{CH_2}$-S), δ 2.4 (8H, t, -CH_2-), δ 1.5 (2H, t, -$\underline{CH_2}$-P), 5.6 (1H, s, CD_2CL_2 (solvent) and at 7.5 – 7.7 (12H, m, Aromatic H) ppm.

The clear evidence for produced **8D** and **8A** are the existence of the $SCOCH_3$ group in these compounds, which is not present in ω-bromohexyl-triphenylphosphonium bromide derivatives (**7D**, **7A**). IR spectra confirmed the absorbance at 1738 cm^{-1} and 1700 cm^{-1} for ketone group (ν C=O) group in **8D** and **8A** respectively. Further evidence for **8D** and **8A** was the absence of the OH group in IR region at 3200-3400 cm^{-1}, which has existed in intermediate **6D** and **6A** [30].

8D and **8A** were also confirmed by ^1H NMR spectroscopy which showed the ($COCH_3$) group present at δ 3.3 (3H, s, CO-$\underline{CH_3}$) for both **8D** and **8A** as shown in the previous studies [31, 32]. In addition, present twelve protons -$(CH_2)_6$ attached to the aromatic ring at chemical shifts from 1.2-3.4 ppm to produce compounds **8D** and **8A**, this group is not presented in start materials ω-bromohexyl-tri(phenyl)phosphonium bromide (**7D**) and ω-bromohexyl-tri(*P*-tolyl)-phosphonium bromide (**7A**).

When **8D** and **8A** studied by ESI-MS in positive ion mode. Ions corresponding to $[M-Br]^+$ and [M-S-$COCH_3$] were observed at 421.174 *m/z* and 467.14 *m/z* respectively. While, expected MW **8D** is 500.9 g/mol, and expected MW **8A** is 542.9 g/mol.

Furthermore, **9D** and **9A** have thiosulfate group (S_2O_3) and this is indicated from IR spectroscopy which absorbanced at 1338 cm^{-1}, also occurred absorbance's at 1131 cm^{-1} and 1207 cm^{-1} for vibrations of asymmetric and symmetric S=O and S=S bonds respectively. The literature showed that, peaks emerge in the regions 1150–1050 cm^{-1} and 1400–1200 cm^{-1}, which are characteristic of the vibrations of symmetric S=O and S=S bonds respectively within the thiosulfate ion. However, the asymmetric stretch of S=O bond was at 1420 – 1300 cm^{-1} [33, 34], and this group was absented in start material **1D** and **1A**.

^{1}H NMR spectroscopy confirmed **9D and 9A** which showed signals of $(CH_2)_6$ group at δ 1.3-3.6 ppm for, only this group in ^{1}H NMR can be considered as evidence for producing **9D** and **9A**, which as mentioned in result section above, was absent in start materials. In addition, NMR: δ ^{31}P ($CDCL_3$) spectrum gave signals at = 24.7 ppm for **9D**, and δ ^{31}P (CD_2CL_2) of **9A** was 24.8 ppm.

ESI-MS was also confirmed producing compounds **9D** and **9A.** Whereas, ions corresponding to $[M- S_2O_3H]^+$ and $[M + H]^+$ were observed at 345.17 *m/z* and 501.16 *m/z* respectively. However, expected MW **9D** is 458 g/mol and expected MW **9A** is 500 g/mol.

4.4.2 Characterisation of the colloidal solutions of AuNPs using $NaBH_4$ in comparison with ascorbic acid as reducing agent *via* using UV-Visible and DLS studies

It is known that shape of the UV–visible spectra give different information about the size of the AuNPs [14].

By using different reducing agents, AuNPs with different diameter were prepared. UV-Vis and DLS were regularly used to measure the size and size diameter, and to see the stability of AuNPs solutions through periods of time. Comparison between two methods is discussed in this chapter and clearly explains the effect of reducing agents on the size of AuNPs prepared, and also on their stabilities [35]. When a reducing agent such as sodium borohydride was used, smaller AuNPs with a diameter from 3-5 nm have been prepared [36]. AuNPs of different sizes are known to produce different results which might find application *in vivo* and *in vitro* bio application [35].

From the previous study, metal NPs can be soluble in many solvents such as (ethanol, DCM, toluene) depending on the polarity of the capping agent such as thiol ligands, which have a great affinity for noble metal surfaces, whereas the highly stable NPs were generated. Capped NPs which can be repeatedly isolated and re-dissolved in common organic solvents without showing any signs of decomposition, such as particle growth or loss of stability [37].

Syntheses of AuNPs were carried out using all these ligands in this Chapter with varying results. Synthesis **4C**-AuNPs, **4**-AuNPs and **5**-AuNPs in H_2O/DMSO by using $NaBH_4$ as

reducing agent are explained in detail in Chapter 2, while, **8B**-AuNPs is explained in Chapter 6. The synthesis of AuNPs using **4C**, **4**, **5** and **8B** ligands were successful with both directions, in the case of $NaBH_4$ and ascorbic acid as reducing agents. The rest of ligands were unable to dissolve in an aqueous solvent and there are unsuitable for the synthesis route using an ascorbic acid as reducing agent in order to functionalised AuNPs.

The unsuccessful syntheses formed a black bulk material solution that was unchanged by continuous stirring to the red colour. Multiple repeat syntheses were carried out for each ligand with changing condition of the experiment. Including the concentration of reactants, temperature and time of reaction. In order to eliminate the possibility of experimental error. Each synthesis was unsuccessful and resulted in the same black bulk material. This could be due to poor the solubility of the ligands in the water. AuNPs solutions were stored in the dark under ambient atmosphere and temperature and were reducingly taken for analysis using UV-Vis and DLS to determine the formation and stability of the AuNPs manufactured.

AuNPs functionalised by **8D** (see Figures 4.1,4.2), **8A** (see Figures 4.3,4.4), **9D** (see appendix G, Figure G4.1, G4.2)**,** and **9A**-AuNPs (see appendix G, Figures G4.3, G4.4) were produced *via* using $NaBH_4$ as reducing agent. Similar results were obtained and the peaks of absorbance were centred at 532, 523, 516 and 535 nm respectively.

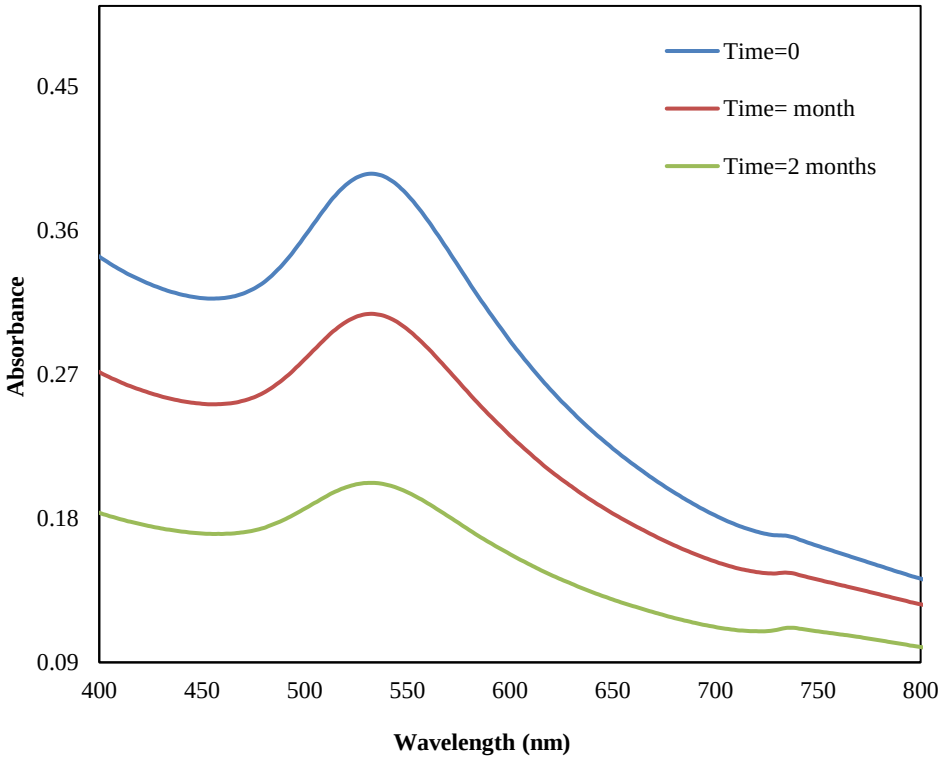

Figure 4.1. UV-Vis for the stability of the **8D**-AuNPs dispersed in H_2O/DMSO, using $NaBH_4$ as reducing agent at time = 0, 1 and 2 months. Where time = 0 is the initial time of the frish **8D**-AuNPs synthesed.

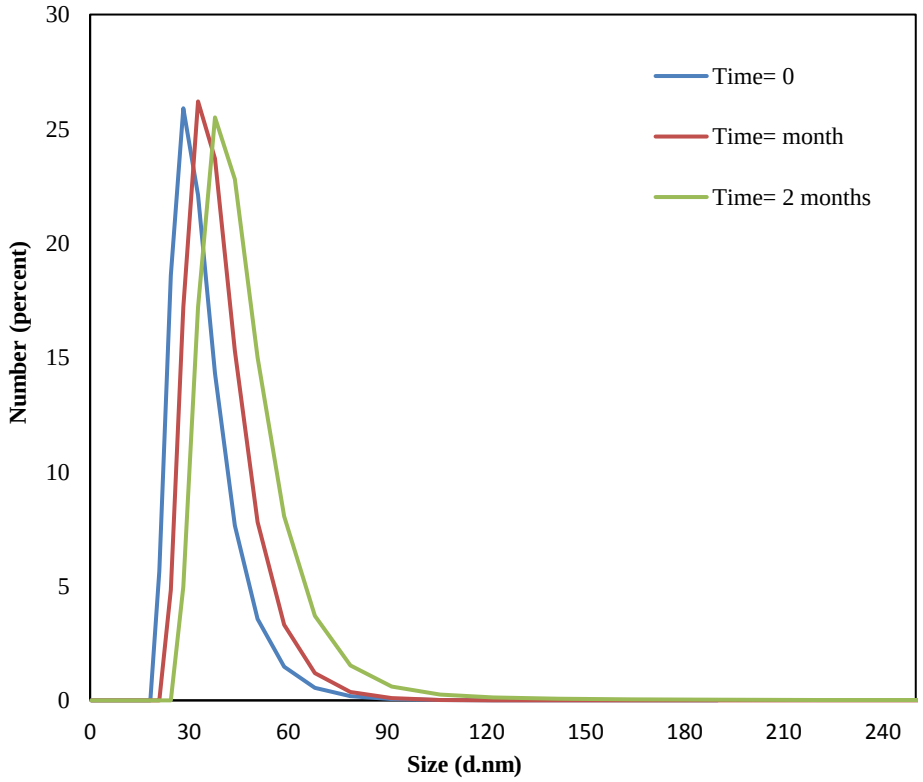

Figure 4.2. The size and standard deviation of each diameter range measured by DLS, and was taken at a different time value for **8D**-AuNPs, where time = 0 is the first time of the fresh **8D**-AuNPs synthesised using $NaBH_4$ as reducing agent. Where time = 0 is the initial time of the **8D**-AuNPs preparation.

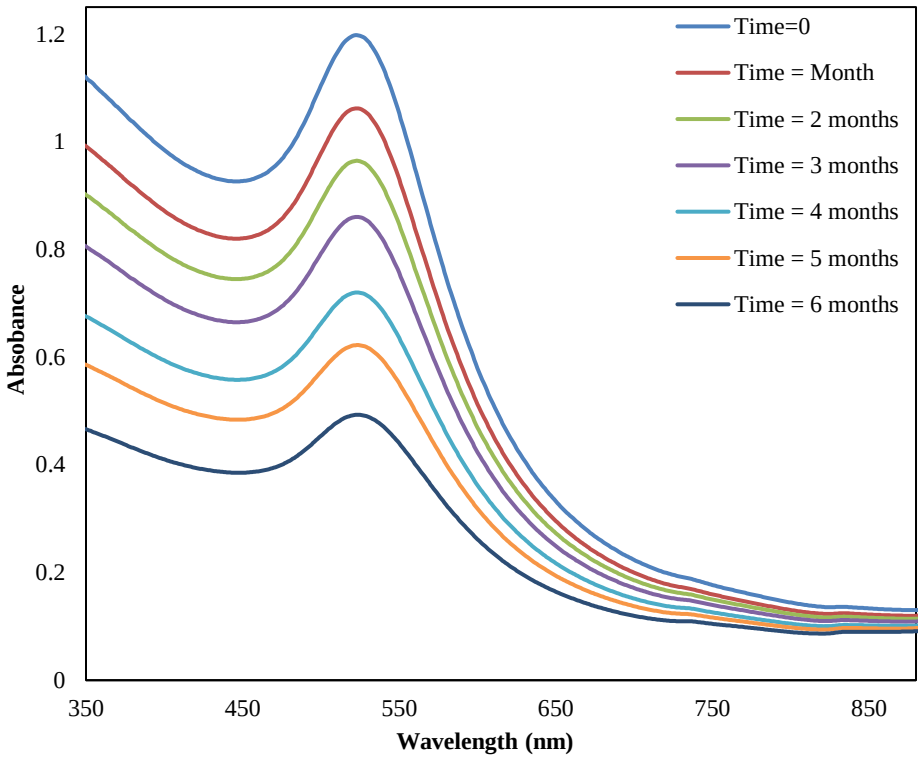

Figure 4.3. UV-Vis for the stability of the **8A**-AuNPs dispersed in H_2O/DMSO, using $NaBH_4$ as reducing agent at time = 0, 1, 2, 3, 4, 5, and 6 months respectively. Where time = 0 is the initial time of the **8A**-AuNPs preparation.

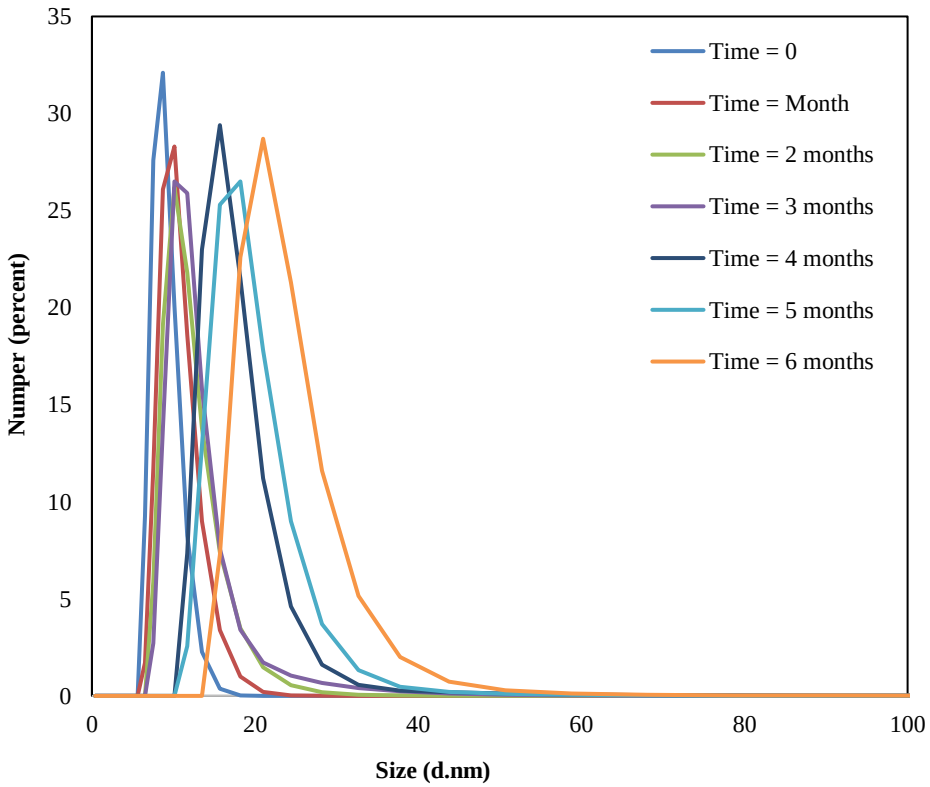

Figure 4.4. The size and standard deviation of each diameter range taken at a different time value for **8A**-AuNPs, using $NaBH_4$ as reducing agent by using DLS.

These results were confirmed by DLS as shown in Table 4.1. Whereas, **8D**, **8A**, **9D** and **9A**-AuNPs sizes diameter were in the range of 32 ± 2 nm, 8.8 ± 1.6 nm, 6.9 ± 1.3 nm and 33 ± 2.2 respectively. Figures 4.1 displays the UV-Visible spectra of fresh AuNPs solutions (time = 0) and the same solutions after 1 and 2 months for **8D**-AuNPs, also **9D**-AuNPs stayed stable for 2 months (see appendix G, Figure G4.1, G4.2). Figure 4.3 shows **8A**-AuNP stay stable for 0, 1, 2, 3, 4, 5, 6 months respectively, and **9A**-AuNP stays stable for 8 weeks as well (see appendix G, Figures G4.3, G4.4). With no sign of degradation or aggregation through DLS or UV-Visible absorption spectroscopy analysis for all these AuNPs solutions, this indicates that the particle sizes were not changed over this period.

It was expected that the $NaBH_4$ synthesised AuNPs would be smaller than the ascorbic acid synthesised nanoparticles owing to $NaBH_4$ being a stronger reducing agent [12].

From Chapter 2, it can be seen that, AuNPs functionalised by **4C**, **5** and **4** ligands using $NaBH_4$ as reducing agent have bands centred at 519 (Figure 2.1, see UV-visible spectrum at time = 0), 519 (Figure 2.2, see UV-visible spectrum at time = 0) and 529 nm (Figure 2.3, see UV-visible spectrum at time 0) respectively.

In contrast, as shown in the UV–Vis spectra (see table 4.2, Figures 4.5, 4.7 and appendix G, Figure G4.5), when the ascorbic acid is used as reducing agent, the maximum absorptions of **4C**, **5**, **4**-AuNPs are centred at 542, 575 (see Figures 4.5 - 4.8) and 557 nm respectively (see appendix G, Figures G4.5, G4.6).

Table 4.1. **8D**, **8A**, **9D** and **9A**-AuNPs solutions in H_2O/DSMO using $NaBH_4$ with the UV-Vis and DLS studies. All these types of AuNPs prepared as described in experimental section.

Name of AuNPs	Peak wavelength (nm)	Diameter size (nm)
8D-AuNP	532 nm	32 ± 2 nm
8A-AuNP	523 nm	8.8 ± 1.6 nm
9D-AuNP	516 nm	6.9 ± 1.3 nm
9A-AuNP	535 nm	33 ± 2.2 nm

For **8B**-AuNP, there was not a lot of difference between the two methods. The absorbance centred at 522 nm using $NaBH_4$ and at 528 nm using ascorbic acid as reducing agent, (see Table 4.2 and appendix G, Figure G4.7).

The stabilities of AuNPs used ascorbic acid in this Chapter were low compared with AuNPs used $NaBH_4$. AuNPs prepared by ascorbic acid appear to have higher wavelength than for $NaBH_4$. This was also confirmed by DLS results with the AuNPs diameter being smaller when $NaBH_4$ was used as reducing agent. The most commonly weak reducing agent used to reduce many metal ions in the solution phase is L-ascorbic acid, which forms complexes with comparatively low stability constants [38].

It is having been identified that the reducing potential of the ascorbic acid depends on the pH of the solution. The ascorbic acid exists in the protonated form, ($AscH_2$) at pH below 4.1. With increasing of the pH, it transforms into ascorbate form, $AscH^-$. However, at pH above 11.6, it is completely deprotonated to form, (Asc^{2-}) [39].

Table 4.2. Comparison between the **4C**, **5**, **4** and **8B**-AuNPs solutions according to the UV-Vis, TEM and DLS measurements. The results were in the case of ascorbic acid [40] and in the case of $NaBH_4$ as reducing agents.

Name of AuNPs	Peak wavelength (nm)		TEM		Diameter size (nm)	
	$NaBH_4$	AA	$NaBH_4$	AA	$NaBH_4$	AA
4C-AuNP	519 nm	542 nm	11±1 nm		8.7± 1.2 nm	17 ± 1.5 nm
5-AuNP	519 nm	575 nm	8 ±1 nm		7.3 ± 2 nm	74 ± 3.9 nm
4-AuNP	529 nm	557 nm	10±1 nm	11±1.8 nm	9.6 ± 2 nm	36.3± 2 nm
8B-AuNP	522 nm	528 nm	7±1.2 nm	8±1.6 nm	9.2 ± 0.9 nm	13 ± 1.2 nm

Therefore, the ascorbic acid has different reducing power with regard pH. Spherical AuNPs can be produced with high mono-dispersity when initial pH of the ascorbic acid solution is indeed controlled [41]. Au NPs with averages diameter of 18, 10 and 7 nm, were generated from a $HAuCl_4$ / ascorbic acid mixture with low poly-dispersity indices of 0.4, 0.3 and 0.2 at a pH of 10.2, 10.7, and 11.1 respectively [39]. Furthermore, AuNPs were generated by using ascorbic acid as reducing agent with different size. UV-vis showed different absorbance at 540, 542, 545, 547, and 550 nm, relating to different sizes of indicating AuNPs diameter [8]. The goal of adding NaOH into the ascorbic reaction system in our experimental was to change the acidity of AuNPs solution because AuNPs are not stable at low pH as mentioned in the literature, also study reports have clearly indicated the influence of pH on the growth of the nanoparticles [42].

Sau, TK.,et al., illustrated that, ascorbic acid was not enough to reduce of Au(III) ions to AuNPs and for this reason NaOH combined ascorbic as mixture reducing agent [43]. In addition, it is noted that, ascorbic acid was a weak reducing agent and unable to reduce the silver ion in order to produce AgNPs. However, with increased the pH of the solution *via* adding NaOH, which increase the reducing power of ascorbate. Where this result confirmed that Ag ions are not reduced under (lower pH when using weaker reducing agent) reaction conditions [44].

It was proposed that in comparison between ascorbic acid and ascorbate, where the latter is a stronger reducing agent than ascorbic acid. For instance, ascorbic acid's pka is 4.1. Also at pH higher than 4.1, most of ascorbic acid, turn into ascorbate. More ascorbate in the solution indicates faster reduction of Au ion to atomic Au on the tip facets. Usually having a pH higher than 4.1 lead to form longer Au nanorods [45].

It was not possible to achieve a synthesis of phenyl- and tolyl-phosphine with six carbons functionalised AuNPs in comparison with tris(2,4,6-trimethoxyphenyl) containing ligands. Using ascorbic acid became this reducing agent is not as strong as $NaBH_4$, which was used previously. The lack of success could also be due to other factors such as alkyl chain length, monolayer quality and the nature of the substrate [46].

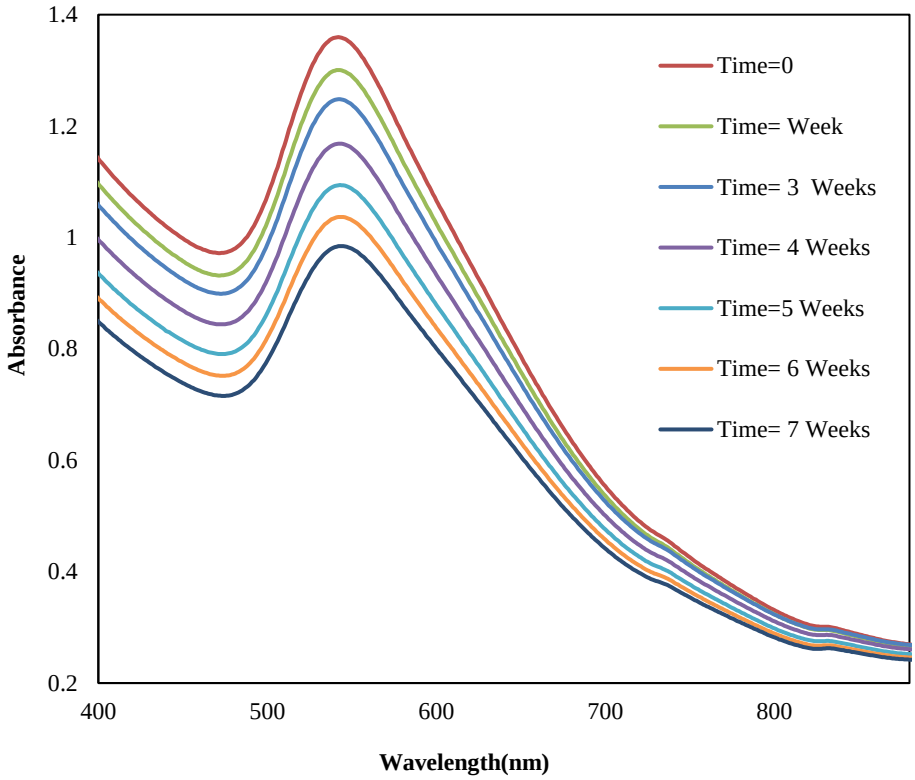

Figure 4.5. UV-Vis for the stability of the **4C**-AuNPs dispersed in aqueous solution at time = 0, 1, 3, 4, 5, 6, and 7 weeks respectively. Using ascorbic acid as reducing agent.

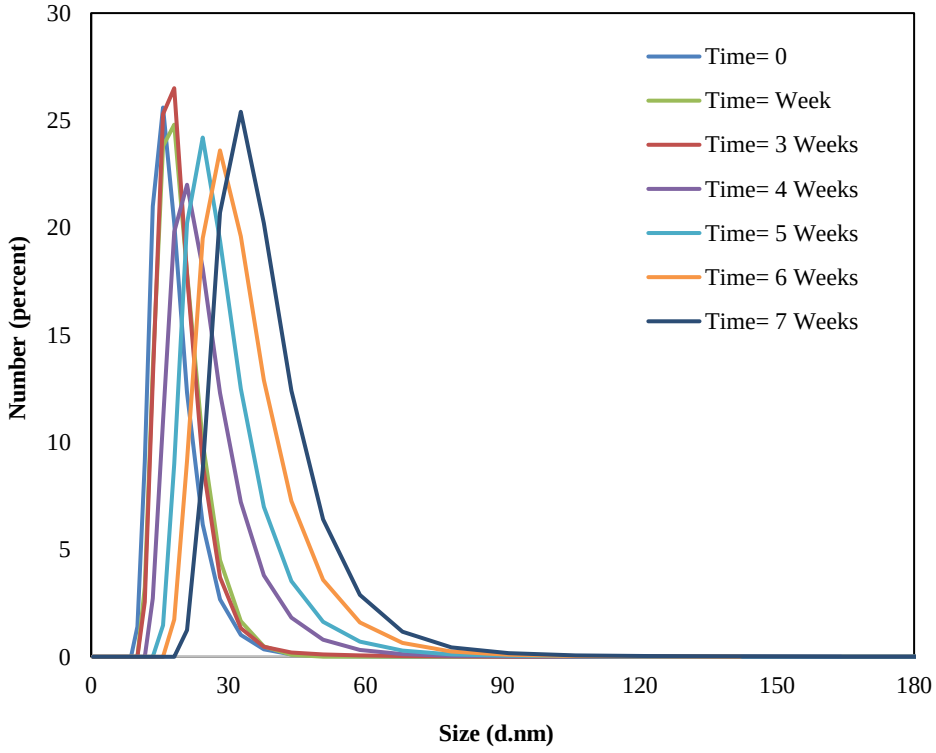

Figure 4.6. The size and standard deviation of each diameter range taken at a different time value for **4C**-AuNPs as reported by DLS study. Using ascorbic acid as reducing agent.

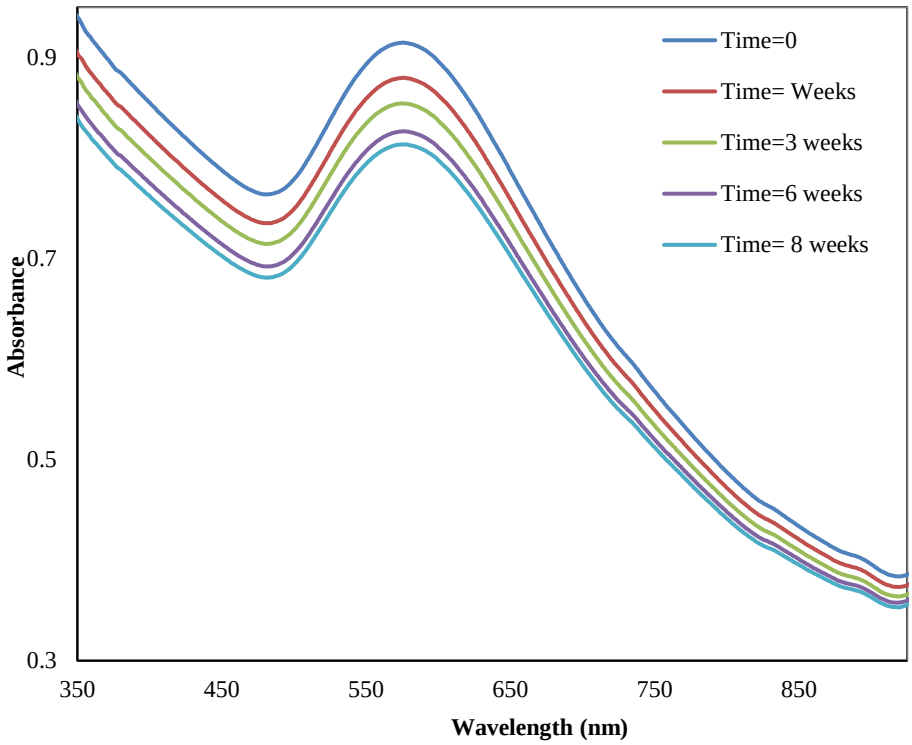

Figure 4.7. UV-Vis study for the stability of the **5**-AuNPs dispersed in aqueous solution at time = 0, 1, 3, 6, and 8 weeks respectively. Using ascorbic acid as reducing agent.

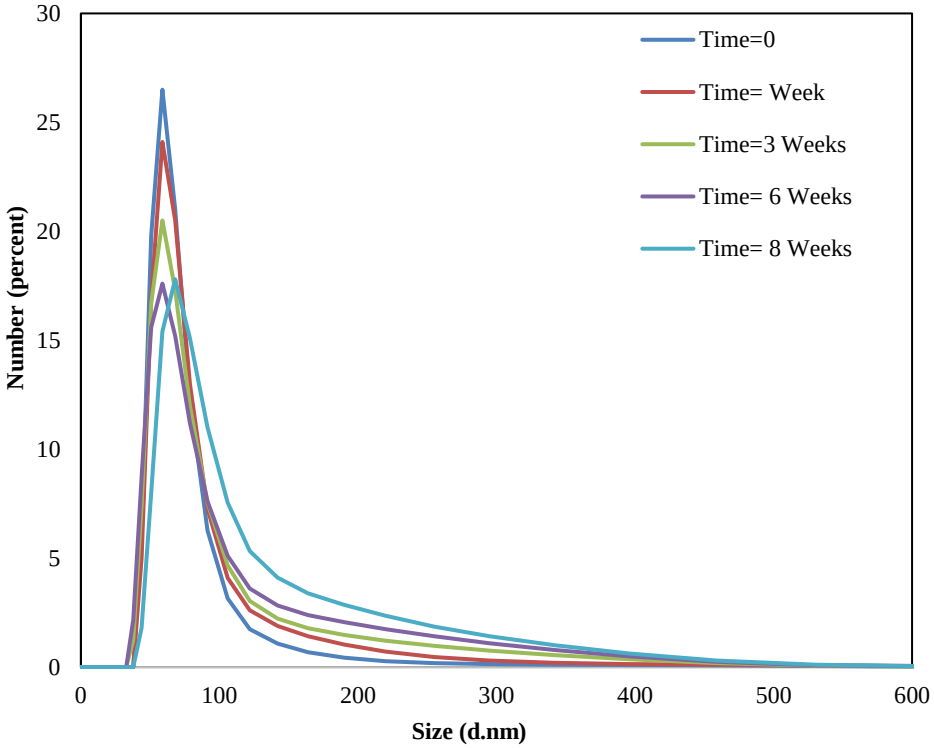

Figure 4.8. The size and standard deviation of each diameter range taken at a different time value for **5**-AuNPs as reported by DLS study. Using ascorbic acid as reducing agent.

The only ligands containing tris(2,4,6-trimethoxyphenyl)phosphine derivatives were able to functionalise AuNPs. According to Fevre, MV., et al., tris(2,4,6-trimethoxyphenyl) phosphine was used as an organic catalyst for the Group Transfer Polymerization (GTP) of methyl methacrylate (MMA) and tert-butyl acrylate (tBA). Only tris(2,4,6-trimethoxyphenyl)-phosphine (TTMPP) was able to bring about the controlled GTP of both monomers at room temperature in contrast with trialkylphosphines and tributyl-phosphine [47]. In addition, the GTP of MMA could also be performed in bulk, whilst maintaining good control over molar masses and dispersity. This is because of the moderate activity of the TTMPP catalyst compared to other nucleophiles, such as N-heterocyclic carbenes, ligands containing this group have previously been confirmed as successful [47].

Moreover, TTMPP is considered are good catalyst precursor in important reactions such as hydrogenation, hydroformylation, and polymerization became both oxygen and phosphorus atoms in its structure which are good donors [48]. TTMPP is a relatively strongly basic phosphine (pKa = 11.2) [47, 48] compared, for instance to triphenyl-phosphine, Ph_3P (pKa in CH_3NO_2 = 2.73) [49]. As well as, it was given an order of decreasing basicity of $P(4\text{-}CH_3OC_6H_4)$, > $P(4\text{-}CH_3C_6H_4)$, > $P(4\text{-}C1C_6H_4)_3$ > $P(C_6H_5)_3$. Because donate groups such as a (OCH_3) raising the apparent basicity's of the phosphines, and causing large changes in the basicities of these phosphines [49]. Furthermore, modification ligands such as thiol ligands contain (methoxy-benzene groups) modified AuNPs found to be most stable compared to other thiol compounds contain (Benzene or Toluene) [50].

4.4.2.1 Characterisation of AuNPs using transmission electron microscopy

The TEM is considered the perfect device for the characterisation of structural and chemical at the nanoscale, which can be easily producing information about nanostructured materials [51]. The colloidal solutions of AuNPs functionalised using **8B** (Figure 4.9, TEM4.1) when $NaBH_4$ was used as reducing agent. While, (Figure 4.9, TEM4.2) and (Figure 4.9, TEM4.3), show **4**, **8B** as protecting ligands for AuNPs in case ascorbic acid used as reducing agent, whereas all analysed by TEM. Micrographs of all three AuNPs samples showed spherical or semi-spherical shaped particles. Then, particle sizes for samples TEM4.1, TEM4.2 and TEM4.3 were obtained by analysing at least 150 particles per sample from several images taken.

It is known that, in order to determine the larger particles is formed due to the aggregation of small particles or as result to the growth of separated particles, TEM used for this reason according to the literature [17].

In this Chapter, TEM shows that most of the AuNPs are spherical in shape and a mono-dispersional state without obvious aggregations. Furthermore, TEM image of **8B**-AuNP analysis results are presented in Figure 4.9 (TEM4.1), which shows size and size distributions for **8B**-AuNP when $NaBH_4$ used and were approximately 7 ± 1.2 nm in size and the shape is almost spherical as mention in the previous study [40]. Similarly, the size of **8B**-AuNP was detected by DLS 9.2 ± 0.9 nm. The average size of **8B**-AuNP increased to 8 ± 1.6 nm according to TEM results when pH of the solution was changed *via* using ascorbic acid as reducing agent. The size became bigger compare in the case of $NaBH_4$ with less stability as mentioned above (see Table 4.2, TEM4.3).

According to Sun, K., et al., the AuNPs prepared in aqueous solution using an ascorbic acid as reducing agent was nearly spherical and the average sizes were about 7 – 8 nm. Which also confirmed by using UV-Vis, where a strong absorption peak occurred at roughly 540 nm indicates the formation of AuNPs [8]. While, according to Khan, Z., et al., monodispersed spherical gold particles prepared (shape ranging from 80 nm to 5 mm) *via* reducing Au(III) with iso-ascorbic acid at 20°C [14].

It is well known that, the reduction by iso-ascorbic acid is equivalent in reducing properties with ascorbic acid but biologically is considered inactive [52]. Furthermore, iso-ascorbic acid (an isomer) has also utilised instead of ascorbic acid. However, reports of stabilisation without any other surface functionalisation are scarce [50].

Similar results were collected of **8B**-AuNP by DLS, where give 13 ± 1.2 nm in the case of ascorbic acid. The size was observed to increase slightly with time as illustrated in UV–Vis spectrophotometer results. However, remained almost unchanged a lot when $NaBH_4$ was used. While some aggregation to larger particles occurs when ascorbic acid was used, which demonstrated big size with less stability. This may be explained due to reduce the stability of a weak reducing agent, which is not efficient enough to reduce efficiently lead to low pH as illustrated in the literature [10, 40]. As well as, **4**-AuNPs illustrated small size when $NaBH_4$ used in comparison in the case of ascorbic acid, as observed by TEM where size was 10 ± 1 nm in the case of $NaBH_4$, and DLS also

confirmed the size which was 9.6 ± 2 nm. It is found that AuNPs when produced using ascorbic acid have a narrow size distribution (31 ± 5, 36 ± 6, and 40 ± 5 nm) and can be readily stabilised *via* adjusting the initial pH of the reaction solutions [50].

Same situation in **8B**-AuNP was noted when ascorbic acid used in case **4**-AuNP, size increase to 11 ± 1.8 nm and DLS was 36.3 ± 2 nm. Aggregates, which observed after many weeks in DLS and UV results of samples taken during early stages of the preparation and weekly.

Many experiments carried out to understand effect of ascorbic acid as reducing agent through AuNPs preparation. For example, AuNPs synthesised by using ascorbic acid as a reducing agent occurred spectrum consist a single SRP band at 550 nm in the whole UV–visible region (350 – 800 nm), where the peak at 550 nm is shifted to higher wavelength nearly to 600 nm when a higher ascorbic acid concentration used. The intensity of SRP band also declines with increase in ascorbic acid concentration [14]. Kim, F., et al., illustrated that, ascorbic acid / $HAuCl_4$ ratio play a significant role during the growth of AuNPs [14, 53]

In addition, as mentioned early, smaller AuNPs are normally produced by using stronger reducing agents such as $NaBH_4$, phosphorus, tetrakis(hydroxymethyl)phosphonium chloride. While, larger size particles (diameter 25–110 nm) were produced by using ascorbic acid [43] as reductant which confirm our results in this Chapter.

According to DLS results, **4**-AuNPs changed from 36.3 ± 2 nm to 50 ± 2.2 after 10 weeks in the case of ascorbic acid. **8B**-AuNP changed from 13 ± 1.2 nm to 31 ± 2 after 10 weeks. However, **8B**-AuNP changed from 9.2 ± 0.9 nm to 20.4 ± 1.7 nm after 11 weeks when $NaBH_4$ used. In addition, **4C**-AuNP and **5**-AuNP with ascorbic acid were changed from 17 ± 1.5 nm and 74 ± 3.9 nm to 39 ± 2.1 nm (after 7 weeks) and 101 ± 12 nm (after 8 weeks) respectively. AuNPs have shown larger sizes based aggregates are present after several weeks from the synthesis of AuNPs, thus confirming a low stabilising potential in ascorbic acid solution. While AuNPs are often stable for long periods of time in the case of $NaBH_4$. According to the previous study, DLS results can be less accurate in case poly-disperse or agglomerated NPs where DLS is more sensitive to bigger particles [35]. In addition, a single TEM image may not be totally representative of the entire sample. [54].

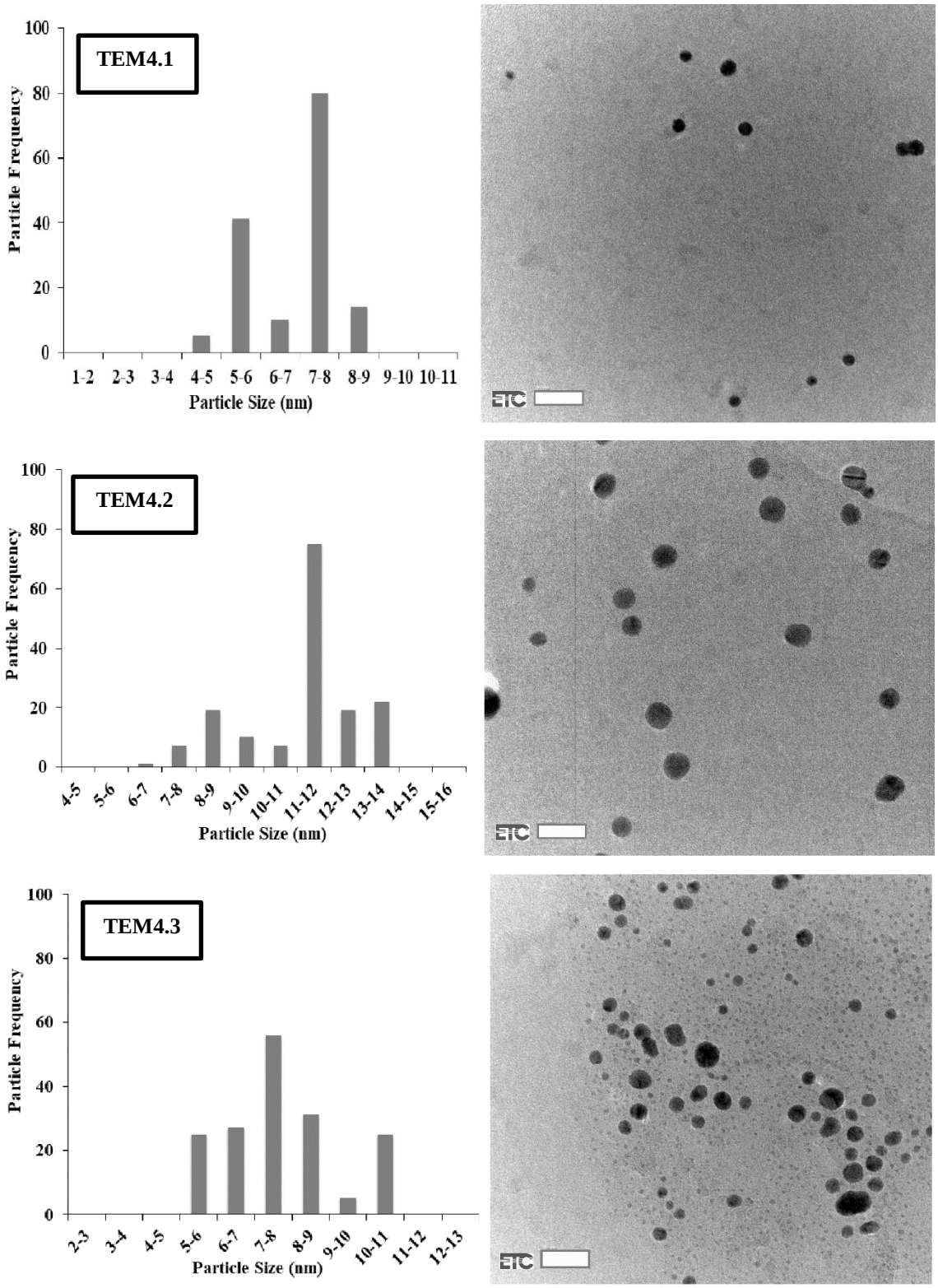

Figure 4.9. TEM micrographs of cationic phosphonium **8B**-AuNPs using $NaBH_4$ as reducing agent (TEM4.1), **4**-AuNP (TEM4.2), and **8B**-AuNP (TEM4.3) as protecting ligands in case ascorbic acid had used, and corresponding particle size histograms.

Moreover, literature data showed that, it is observed a very good agreement between some analysis technic used to characterise AuNPs such as the electron microscopy and disc centrifuging data. While, DLS was slightly larger diameters compared with mentioned technic, which explained to that, DLS measures the hydrodynamic diameter rather than the natural one of the AuNPs [35]. In general, DLS data presented in this Chapter were in agreement with TEM images to some extent.

4.5 Conclusion

In summary, ascorbic acid is an essential nutrient for humans and some other animal species also having antioxidant properties. It is well to know that redox chemistry of ascorbic acid plays a significant role in human nutrition as well as in the synthesis of advanced nanomaterials of noble metal. For this reason, the studies on the mechanism of redox reactions of ascorbic acid in biological systems has become important to bio-, inorganic-, and surface-chemists nowadays [14].

In this work, we present the size-controlled synthesis of AuNPs by chemical reduction method using ascorbic acid and $NaBH_4$ as reducing agent. The AuNPs were produced directly and simply by the reduction of Au (III) with two different reducing agents, including sodium borohydride and ascorbic acid. All of these methods can successfully produce AuNPs regardless of a type of reducing agents. This study shows that there are fundamental differences between two methods with several different properties of AuNPs. Based on these observations, clear evidence of the reduction of gold (III) to gold (0) and formation of colloidal AuNPs were obtained, as a maximum absorbance at 519, 519 and 529 nm was observed in the corresponding UV-Visible spectra for **4C**, **5** and **4**-AuNPs respectively when $NaBH_4$ was used.

The stability study carried out over time. According to the UV and DLS results, with a sample of the functionalised AuNPs showed that, the AuNPs synthesised by using $NaBH_4$ was stable for a long time (nearly up to 6 months), compared to **4C**, **5** and **4**-AuNPs used ascorbic acid as reducing agent, which stay stable maximum for 10 weeks at 542 nm, 575 and 557 nm respectively. DLS was in the range of 17 ± 1.5 nm, 74 ± 3.9 and 36.3 ± 2 respectively. With no sign of degradation or aggregation through DLS or UV-Visible absorption spectroscopy analysis where. The particles show good shape and size

uniformity in addition to good long-term stability. The two reducing agents lead to the low poly-dispersity and the formation of only spherical particles.

Tables 4.1, 4.2 summarises all the results of varying the reducing agent in this Chapter. By using three complementary techniques (TEM, DLS and UV-Vis), AuNPs over a size range of 7.3 ± 2 to 9.6 ± 2 nm (diameter) were prepared by $NaBH_4$ as reducing agent. The AuNPs were associated with a larger size in the case when a weak reducing agent (ascorbic acid) was used, where size range was 13 ± 1.2 nm to 74 ± 3.9 nm.

Different preparation of colloidal AuNPs is essential to produce different sizes and offer different stabilities, because biocompatible AuNPs have increased significant attention in current years for potential applications in bio-diagnostics, and nano-medicine as result of their interesting size-dependent [55].

Development of more environmentally friendly and biocompatible synthetic methods is one of the main goals to contribute in biomedical applications. Green methods used to synthesis AuNPs by using ascorbic acid as bio-reducing agent was important nowadays, especially within the biological cells due to its low toxicity [50].

In final, TEM, DLS, and UV characterisation suggest that AuNPs can be obtained *via* using bio-reducing agent (ascorbic acid) and $NaBH_4$ as well.

4.6 References

1. Malassis, L., Dreyfus, R., Murphy, RJ., Hough, LA., Donnio, B and Murray, CB, *One-step green synthesis of gold and silver nanoparticles with ascorbic acid and their versatile surface post-functionalization.* RSC Advances, 2016. **6**(39): p. 33092-33100.

2. Nalawade, P., Mukherjee, T and Kapoor, S, *Green synthesis of gold nanoparticles using glycerol as a reducing agent.* Advances in Nanoparticles, 2013. **2**(02): p. 78-86.

3. Elia, P., Zach, R., Hazan, S., Kolusheva, S., Porat, ZE and Zeiri, Y, *Green synthesis of gold nanoparticles using plant extracts as reducing agents.* International journal of nanomedicine, 2014. **9**: p. 4007-21.

4. Lin, SM., Geng, S., Li, N., Li, NB and Luo, HQ, *D-penicillamine-templated copper nanoparticles via ascorbic acid reduction as a mercury ion sensor.* Talanta, 2016. **151**: p. 106-113.

5. Cao, Y., Zheng, R., Ji, X., Liu, H., Xie, R and Yang, W, *Syntheses and characterization of nearly monodispersed, size-tunable silver nanoparticles over a wide size range of 7–200 nm by tannic acid reduction.* Langmuir, 2014. **30**(13): p. 3876-3882.

6. Zhou, J., Ralston, J., Sedev, R and Beattie, DA, *Functionalized gold nanoparticles: synthesis, structure and colloid stability.* Journal of Colloid and Interface Science, 2009. **331**(2): p. 251-262.

7. Saffi, J., Sonego, L., Varela, QD and Salvador, M, *Antioxidant activity of L-ascorbic acid in wild-type and superoxide dismutase deficient strains of Saccharomyces cerevisiae.* Redox Report, 2006. **11**(4): p. 179-184.

8. Sun, K., Qiu, J., Liu, J and Miao, Y, *Preparation and characterization of gold nanoparticles using ascorbic acid as reducing agent in reverse micelles.* Journal of materials science, 2009. **44**(3): p. 754-758.

9. Nadagouda, MN and Varma, RS, *A greener synthesis of core (Fe, Cu)-shell (Au, Pt, Pd, and Ag) nanocrystals using aqueous vitamin C.* Crystal Growth and Design, 2007. **7**(12): p. 2582-2587.

10. Mudabuka, B., Ondigo, D., Degni, S., Vilakazi, S and Torto, N, *A colorimetric probe for ascorbic acid based on copper-gold nanoparticles in electrospun nylon.* Microchimica Acta, 2014. **181**.

11. Darroudi, M., Ahmad, MB., Abdullah, AH., Ibrahim, NA and Shameli, K, *Effect of accelerator in green synthesis of silver nanoparticles.* International journal of molecular sciences, 2010. **11**(10): p. 3898-3905.

12. Luty-Błocho, M., Fitzner, K., Hessel, V., Löb, P., Maskos, M., Metzke, D., Pacławski, K and Wojnicki, M, *Synthesis of gold nanoparticles in an interdigital*

micromixer using ascorbic acid and sodium borohydride as reducers. Chemical engineering journal, 2011. **171**(1): p. 279-290.

13. Jayalakshmi, K., Ibrahim, M and Rao, KV, *Effect of pH on the size of gold nanoparticles.* Int. J. Electron. Electr. Eng, 2014. **7**: p. 159-64.

14. Khan, Z., Singh, T., Hussain, JI and Hashmi, AA, *Au (III)–CTAB reduction by ascorbic acid: Preparation and characterization of gold nanoparticles.* Colloids and Surfaces B: Biointerfaces, 2013. **104**: p. 11-17.

15. Goia, D and Matijević, E, *Tailoring the particle size of monodispersed colloidal gold.* Colloids and Surfaces A: Physicochemical and Engineering Aspects, 1999. **146**(1): p. 139-152.

16. Wang, S., Qian, K., Bi, X and Huang, W, *Influence of speciation of aqueous HAuCl4 on the synthesis, structure, and property of Au colloids.* The Journal of Physical Chemistry C, 2009. **113**(16): p. 6505-6510.

17. Ziegler, C and EychmüLler, A, *Seeded growth synthesis of uniform gold nanoparticles with diameters of 15− 300 nm.* The Journal of Physical Chemistry C, 2011. **115**(11): p. 4502-4506.

18. Jana, NR, *Gram-scale synthesis of soluble, near-monodisperse gold nanorods and other anisotropic nanoparticles.* Small, 2005. **1**(8-9): p. 875-882.

19. Ju-Nam, Y., Bricklebank, N., Allen, DW., Gardiner, PH., Light, ME and Hursthouse, MB, *Phosphonioalkylthiosulfate zwitterions—new masked thiol ligands for the formation of cationic functionalised gold nanoparticles.* Organic & biomolecular chemistry, 2006. **4**(23): p. 4345-4351.

20. Ju-Nam, Y., Allen, DW., Gardiner, PH and Bricklebank, N, *ω-Thioacetylalkylphosphonium salts: Precursors for the preparation of phosphonium-functionalised gold nanoparticles.* Journal of organometallic chemistry, 2008. **693**(23): p. 3504-3508.

21. Sun, Y and An, C, *Shaped gold and silver nanoparticles.* Frontiers of Materials Science, 2011. **5**(1): p. 1-24.

22. Capek, I, *Preparation and Functionalization of Gold Nanoparticles.* J. Surf. Sci. Technol, 2013. **29**: p. 1-18.

23. Shamaila, S., Zafar, N., Riaz, S., Sharif, R., Nazir, J and Naseem, S, *Gold nanoparticles: an efficient antimicrobial agent against enteric bacterial human pathogen.* Nanomaterials, 2016. **6**(4): p. 1-10.

24. Frens, G, *Controlled Nucleation for Regulation of Particle-Size in Monodisperse Gold Suspensions*. 1973.Vol. 241. p 20-22

25. Daniel, M-C and Astruc, D, *Gold nanoparticles: assembly, supramolecular chemistry, quantum-size-related properties, and applications toward biology, catalysis, and nanotechnology.* Chemical reviews, 2004. **104**(1): p. 293-346.

26. Keunen, R., Macoretta, D., Cathcart, N and Kitaev, V, *Stable ligand-free stellated polyhedral gold nanoparticles for sensitive plasmonic detection.* Nanoscale, 2016. **8**(5): p. 2575-2583.

27. Qin, Y., Ji, X., Jing, J., Liu, H., Wu, H and Yang, W, *Size control over spherical silver nanoparticles by ascorbic acid reduction.* Colloids and Surfaces A: Physicochemical and Engineering Aspects, 2010. **372**(1): p. 172-176.

28. Gottlieb, HE., Kotlyar, V and Nudelman, A, *NMR chemical shifts of common laboratory solvents as trace impurities.* The Journal of organic chemistry, 1997. **62**(21): p. 7512-7515.

29. Fulmer, GR., Miller, AJ., Sherden, NH., Gottlieb, HE., Nudelman, A., Stoltz, BM., Bercaw, JE and Goldberg, KI, *NMR chemical shifts of trace impurities: common laboratory solvents, organics, and gases in deuterated solvents relevant to the organometallic chemist.* Organometallics, 2010. **29**(9): p. 2176-2179.

30. Kuo, SC., Huang, LJ and Nakamura, H, *Studies on heterocyclic compounds. 6. Synthesis and analgesic and antiinflammatory activities of 3, 4-dimethylpyrano [2, 3-c] pyrazol-6-one derivatives.* Journal of medicinal chemistry, 1984. **27**(4): p. 539-544.

31. Bellam, M., Gundluru, M., Sarva, S., Chadive, S., Netala, VR., Tartte, V and Cirandur, SR, *Synthesis and antioxidant activity of some new N-alkylated pyrazole-containing benzimidazoles.* Chemistry of Heterocyclic Compounds, 2017. **2**(53): p. 173-178.

32. Yavari, I and Beheshti, S, *ZnO nanoparticles catalyzed efficient one-pot three-component synthesis of 2, 3-disubstituted quinalolin-4 (1H)-ones under solvent-free conditions.* Journal of the Iranian Chemical Society, 2011. **8**(4): p. 1030-1035.

33. Hampton, C., Demoin, D and Glaser, RE, *Vibrational spectroscopy tutorial: sulfur and phosphorus.* University Of Missouri, Fall, 2010.

34. Kononova, O., Shatnykh, K., Prikhod'ko, K and Kashirin, D, *Ion-exchange recovery of gold (I) and silver (I) from thiosulfate solutions.* Russian Journal of Physical Chemistry A, Focus on Chemistry, 2009. **83**(13): p. 2340-2345.

35. García, CP., Sumbayev, V., Gilliland, D., Yasinska, IM., Gibbs, BF., Mehn, D., Calzolai, L and Rossi, F, *Microscopic analysis of the interaction of gold nanoparticles with cells of the innate immune system.* Scientific Reports, 2013.

36. Martin, MN., Basham, JI., Chando, P and Eah, S-K, *Charged gold nanoparticles in non-polar solvents: 10-min synthesis and 2D self-assembly.* Langmuir, 2010. **26**(10): p. 7410-7417.

37. Brust, M., Fink, J., Bethell, D., Schiffrin, D and Kiely, C, *Synthesis and reactions of functionalised gold nanoparticles.* Journal of the Chemical Society, Chemical Communications, 1995(16): p. 1655-1656.

38. Zümreoglu-Karan, B, *A rationale on the role of intermediate Au (III)–vitamin C complexation in the production of gold nanoparticles.* Journal of Nanoparticle Research, 2009. **11**(5): p. 1099-1105.

39. Rahman, MT and Rebrov, EV, *Microreactors for gold nanoparticles synthesis: from Faraday to flow.* Processes, 2014. **2**(2): p. 466-493.

40. Kalliola, S., Repo, E., Sillanpää, M., Arora, JS., He, J and John, VT, *The stability of green nanoparticles in increased pH and salinity for applications in oil spill-treatment.* Colloids and Surfaces A: Physicochemical and Engineering Aspects, 2016. **493**: p. 99-107.

41. Jun, H., Fabienne, T., Florent, M., Coulon, P-E., Nicolas, M and Olivier, S, *Understanding of the size control of biocompatible gold nanoparticles in millifluidic channels.* Langmuir, 2012. **28**(45): p. 15966-15974.

42. Ji, X., Song, X., Li, J., Bai, Y., Yang, W and Peng, X, *Size control of gold nanocrystals in citrate reduction: the third role of citrate.* Journal of the American Chemical Society, 2007. **129**(45): p. 13939-13948.

43. Sau, TK., Pal, A., Jana, N., Wang, Z and Pal, T, *Size controlled synthesis of gold nanoparticles using photochemically prepared seed particles.* Journal of Nanoparticle Research, 2001. **3**(4): p. 257-261.

44. Jana, NR., Gearheart, L and Murphy, CJ, *Seed-mediated growth approach for shape-controlled synthesis of spheroidal and rod-like gold nanoparticles using a surfactant template.* Advanced Materials, 2001. **13**(18): p. 1389-1393.

45. Busbee, BD., Obare, SO and Murphy, CJ, *An Improved Synthesis of High-Aspect-Ratio Gold Nanorods.* Advanced Materials, 2003. **15**(5): p. 414-416.

46. Ju-Nam, Y., Chen, Y-S., Ojeda, JJ., Allen, DW., Cross, NA., Gardiner, PH and Bricklebank, N, *Water-soluble gold nanoparticles stabilized with cationic phosphonium thiolate ligands.* RSC Advances, 2012. **2**(27): p. 10345-10351.

47. Fevre, MV., Vignolle, J., Heroguez, VR and Taton, D, *Tris (2, 4, 6-trimethoxyphenyl) phosphine (TTMPP) as potent organocatalyst for group transfer polymerization of alkyl (meth) acrylates.* Macromolecules, 2012. **45**(19): p. 7711-7718.

48. Chen, S and Dunbar, K, *Synthesis and characterization of Rh2 (O2CCH3) 3 [{C6H2 (OMe) 3} 2P {C6H2 (OMe) 2O}](MeOH) with a novel tridentate ligand derived from tris (2, 4, 6-trimethoxyphenyl) phosphine.* Inorganic Chemistry, 1990. **29**(4): p. 588-590.

49. Allman, T and Goel, RG, *The basicity of phosphines.* Canadian Journal of Chemistry, 1982. **60**(6): p. 716-722.

50. Tyagi, H., Kushwaha, A., Kumar, A and Aslam, M, *pH-dependent synthesis of stabilized gold nanoparticles using ascorbic acid.* International Journal of Nanoscience, 2011. **10**(04n05): p. 857-860.

51. Smith, DJ, *Characterization of Nanomaterials Using Transmission Electron Microscopy.* 2015.

52. Aziz, MA and Oyama, M, *Thermal-driven attachment of gold nanoparticles prepared with ascorbic acid onto indium tin oxide surfaces.* Journal of Nanoparticle Research, 2013. **15**(5). 1618.

53. Kim, F., Sohn, K., Wu, J and Huang, J, *Chemical synthesis of gold nanowires in acidic solutions.* Journal of the American Chemical Society, 2008. **130**(44): p. 14442-14443.

54. Robertson, JD., Rizzello, L., Avila-Olias, M., Gaitzsch, J., Contini, C., Magoń, MS., Renshaw, SA and Battaglia, G, *Purification of nanoparticles by size and shape.* Scientific reports, 2016. **6**: 27494.

55. Kumar, SV and Ganesan, S, *Preparation and Characterization of Gold Nanoparticles with Different Capping Agents.* International Journal of Green Nanotechnology, 2011. **3**(1): p. 47-55.

Chapter 5: Synthesis AuNPs functionalised by phosphine oxide derivatives in DMSO

5.1 Abstract

Several nano-particulate carrier systems including polymeric nanoparticles, dendrimers, liposomes, metal and magnetic nanoparticles are being widely investigated especially for drug delivery of siRNA, gene, tumour targeting therapy, bio-imaging and bio-sensing [1]. The chemistry of phosphorus, and organic phosphonium salts are considered to act as lipophilic cations, which are accumulated in the cell's mitochondria. AuNPs functionalised by phosphonium were accumulated by cells and TEM confirmed that, they are localised in the mitochondria [2].

In the past few decades important progress have been made in controlling AuNPs *via* using thiol / phosphine ligands as protecting ligands. AuNPs stabilised by phosphine ligands offer broad applications such as catalysis, sensing, imaging, and new therapeutic approaches including biological imaging, and immunoassay. In addition, these nanoparticles have been used as staining agents in labelling of biological molecules such as proteins. For example, the use of a phosphine ligand as a stabiliser enables easy replacement by thiolated surfactants, which may extend the solubility of the nanoparticles in aqueous media for nano-biotechnology.

In this Chapter, AuNPs have been stabilised through using protecting ligands such as phosphine oxide derivative ligands. These ligands include (3-thioacetylpropyl)di-(*p*-tolyl)phosphine oxide (**12A)**, (3-thioacetylpropyl)diphenylphosphine oxide (**12D)**, (3-thioacetylpropyl)thiodiphenylphosphine oxide (**15)** and (3-thioacetyl-N-ethylmethylamine)diphenylphosphine oxide (**18)** *via* $NaBH_4$ as reducing agent in DMSO which is reported for the first time in this Chapter. Stability of AuNPs solutions has been measured using UV/ Vis and DLS devices. All samples were stable for 5 months. UV-Vis absorbance of AuNPs functionalised by these ligands **12A**, **12D**, **15** and **18** were centred at 542, 530, 527 and 529 nm respectively. DLS confirmed UV results and sizes were 26 ± 3.5 nm, 10.2 ± 2.7 nm, 7.9 ± 1.7 nm, 9.6 ± 1.9 nm. **12A-**AuNP was produced with different reducing agents.

When biocompatible ascorbic acid was used as a reducing agent, **12A**-AuNP offered slightly different results in comparison with when $NaBH_4$ was used, the stability was less than in the case of $NaBH_4$ and only remind for a few weeks with obvious aggregation being noted. The SPB centred at 544 nm of **12A**-AuNPs (in the case of ascorbic acid) and the size was 28 ± 2.2 nm, which changed to 47 ± 2 nm after nearly 8 weeks. In addition, AuNPs functionalised by ligand **15,** which contains a dithiol group, has the smallest size compared to other ligands in this Chapter with high stability for approximately 5 months, indicating the dithiol group enhances colloidal stability of AuNPs as shown in the previous literature. AuNPs have different applications based on their sizes and function groups used [3].

Diphenylphosphine derivatives functionalised AuNPs were used against bacteria. For instance, 1,1,1-tris(diphenylphosphinomethyl)ethane [$CH_3C(CH_2PPh_2)_3$] and 1,1,1-tris-(diphenylphosphinomethyl)ethanetrisulphide [$CH_3C(CH_2P(S)Ph_2)_3$] used for stabilisation of small AuNPs, where the AuNPs were more active against Gram (+) bacteria, such as., *Staphylococcus aureus* compared with Gram (−) bacteria. Among the two AuNPs, the ligand [$CH_3C(CH_2PPh_2)_3$] stabilised AuNPs shown higher activity [4]. Thus, there is an important need in order to provide new AuNPs, based on original ligands, to give access to an increased variety of applications.

5.2 Introduction

The protection and surface modification of AuNPs from the environmental impact are important requirements for many applications especially in bio-applications [5]. Recently, AuNPs have become more popular because of the possibility of them being used in photothermal therapy. The light collected on the surface of AuNPs is emitted by several processes, including electron-electron scattering and electron-lattice vibrations, with the concomitant production of heat [6]. However, problems with the core-shell particle structure include that of the development of biological ligands for effectively detecting specific tumour cells, and conjugating them to the metal. There is, therefore, a need for metal NPs that can selectively detect various cancer cells.

It is important to stress that, nanotechnology is an emerging field that is potentially changing the way diseases are treated *via* drug delivery with curcumin. Recent investigations have established several approaches in order to improve the bioavailability,

and to increase the plasma concentration, also to enhance the cellular permeability processes of curcumin [7].

The Au-sulphur interaction is the common studied organo-Au system, due to a strong bonding between Au-thiolate. Also weakly binding such as nitrogen-Au, phosphine-Au where the monolayer in this case can be removed for further applications [8]. The past few decades have been important progress in controlling AuNPs by using thiol / phosphine ligands as protecting ligands [9].

In addition, there are some protection groups such as S-acetyl, S-cyano, and S-(N-ethylcarbamoyl) that have been used to functionalise AuNPs [10-13].

Furthermore, α, ω-thiolates or aromatic thiol, which is used in order to prepare Self-assembled monolayers (SAMs) are more sensitive to air oxidation and form disulphides and other oxidised products. Oxidation of thiols leads to forming thiolate radicals *via* loss of the sulphur-bound H atoms. However, thiocyanates were easily synthesised stable thiol derivatives, which assembled directly on Au surfaces without any additional support reagents required [14-16]. Furthermore, thioacetate derivatives were a more stable alternative to thiols due to de-protection in situ of the corresponding thiolate *via* reaction with a small amount of base such as aqueous ammonium solution, which then forms a SAMs on the gold substrates [14]. According to Piotrowski. P., et al., the deprotected aromatic S acetyl-derivatives were used in order to modify both a gold electrode and AuNPs surfaces, which play an important part in controlling the thickness of the self-assembled fullerene layer [17].

Moreover, according to Vorfalt, T., et al., the thioacetate was used as a protective group in the Cavitands compounds which undergo cleavage in the presence of reducing agents such as $LiAlH_4$ leading to the formation of the corresponding hemi-carcerands and SH groups [18]. From the literature, the study has been shown that AuNPs functionalised with cavitands contain two thiols were very stable. In contrast, two amine-functionalised cavitands with AuNPs tended to aggregate within a day [19], which confirm our results in this chapter.

Furthermore, Maya, F., et al., [15] illustrated that Au substrates could be linked with thioacetate tail groups without prior conversion to the analogical thiolate. Also, similar

coverage of the relative surfaces has been shown by literatures [15, 20], such studies used a higher concentration of thioacetate ligands with longer adsorption time, which in this case, ammonium hydroxide is not needed. It should also, be acknowledged that, the self-assembly of alkanethiols such as ($HS(CH_2)_nX$) or disulphides ($S(CH_2)_nX_2$) where (X) is CO_2 -, SO_3 -, PO_3^{-2}, OH, $N(CH_3)_3^+$, CH_3) have by far the most studied processer, using Au as the solid substrate [21, 22]. Mixed SAMs of alkane thiolates on Au have been shown to resist non-specific adsorption of proteins [23, 24]. Also, SAMs were used for covalent immobilisation of biomolecules such as antibodies onto the surface of AuNPs [21, 25].

The principle of using SAMs is uncomplicated: whereas, an alkane chain of 10-18 units, is equipped with a head group of the thiol (S-H) with a strong preferential adsorption to the substrate, Au(ш). The (S-H) head groups have been bound to the Au as a thiolate (Au-S-$(CH_2)_nX$), in order to form a well-structured monolayer with the tail groups formulating a carriage outwards from the surface. In addition, several varities of functional groups can be used on the surface under the following limitations: firstly, they do not compete with the thiol in the case of adsorption to the substrate; secondly, they should also not react with thiols; and finally, they are not too bulky thus permitting close packing of the hydrocarbon chains [26]. In addition, secondary phosphine oxides (SPOs), have been used to functionalise AuNPs, with different electronic properties which were synthesised by using $NaBH_4$ as a reducing agent to get small NPs (size 1.2–2.2 nm) [27].

According to Cano, I.,. et al., who used SPOs in the first time as stabilising ligands for AuNPs, where generated stable and homogeneous AuNPs 1.24 ± 0.16 nm, and have used in particular for catalysis hydrogenation, which was very little precedent. Where the SPO plays a fundamental role in granting the highest activity and selectivity in the catalytic hydrogenation of α,β-unsaturated aldehydes by NPs where phosphines directly attached to the AuNP surface, by a Au−$P(O)R_2$ binding mode [28], and SPOs ligands are more donating than many trialkylphosphines [29]. In the same way, the AuNPs functionalised by aryl-substituted SPOs were more active catalysts for the highly chemo-selective hydrogenation of substituted aldehydes in contrary, with AuNPs containing alkyl SPOs that showed low activity and selectivity. This was because aromatic SPOs ligated to AuNPs present a strong polarity in their P=O bonds [30]. Moreover, the complex [tBu(naphthalen-1-yl)-$P(OH)AuCl]_2$ used as a precursor for AuNPs that proved to be very

active catalysts used for the hydrogenation of substituted aldehydes, which confirms SPO ligands were successfully coordinated to gold (I) salt [31].

Synthesis of phosphine oxide can be extremely useful by interacting with biomolecules *via* hydrogen bonds. For example, 11-mercaptoundecanylphosphonic acid, R-P(O)$(OH)_2$ have a wid range of biological activity such as enzyme inhibitors. In the same way, phosphonic acid groups can be acting as hydrogen-bond donor *via* groups of P-OH and as electron acceptors through oxygen in P=O [32]. Moreover, those phosphonic acids were quite useful for introducing pendant polar functional groups into metal oxide surfaces [33]. While, bi-functional molecular linkers, such as the mercaptopropionic acid (MPA) has used in order to attach the QDs to metal oxides for getting the best control in a specific manner. However, some materials such as ZnO are not compatible with these molecules as a result of their pH sensitivity [34].

In addition, an air-stable and homogeneous AuNPs functionalised by tert-butyl(naphthalen-1-yl)phosphine oxide as a supporting ligand *via* $NaBH_4$ as a reducing agent. AuNPs were found to be highly active catalysts for the hydrogenation of substituted aldehydes, giving high conversions and chemo-selectivity for a wide type of substrates [28].

This Chapter gaves a description of the stabilisation of AuNPs through using protecting ligands such as the phosphine oxide/thiol derivatives ligands, which also promotes interactions with biomolecules through hydrogen bonds. Ligands contain phosphine have been used to functionalise AuNPs and offered significant bio applications. For example, 1,1,1-tris (diphenylphosphinomethyl) ethane [$CH_3C(CH_2PPh_2)_3$] and 1,1,1-tris-(diphenylphosphino methyl)ethane trisulphide [$CH_3C(CH_2P(S)Ph_2)_3$] used for stabili**s**ing AuNP**s** and produced small core diameter. These AuNPs were more active against Gram (+) bacteria, such as, *Staphylococcus aureus* compared to Gram (−) bacteria. Among these two AuNPs, the AuNPs ligand [$CH_3C(CH_2PPh_2)_3$] displayed higher activity [4]. Ligands combining phosphorus centres and sulfur centres are especially interesting. Both phosphorus and sulfur are excellent ligand donor atoms for a wide range of metals, Phosphinothiols contain a phosphine group and a thiol function separated by an organic bridge, such as phosphinothioformamides were used in catalytic applications [35].

Thioacetate ligands have recently been used as an alternative to thiols acting as masked thiolate ligands for the function of AuNPs. Chapter 5 will describe the synthesis of phosphonioalkylthioacetate ligands and phosphine oxide derivative ligands with their stabilities. The stability of colloidal AuNPs is of great importance for their practical applications in many fields such as Nano-optoelectronics, catalysis and bioassays. For this reason, many ligands have chosen to stabilise AuNPs including thiol, disulfide, phosphine, phosphine oxide, amine, and carboxylate [36].

The biggest exploited side of phosphine derivatives is their ability to bind transition metals. The ligands were selected due to their ability to stabilise an especially wide variety of metal centres, for example, the secondary phosphine oxides present a notable dichotomy in their coordination method [37].

5.3 Materials and Methods

All chemicals used were purchased from Sigma-Aldrich and Fisher Scientific Ltd. All reagents were used as received without further purification. All solutions were prepared with redistilled water. All the glassware was washed with aqua regia solution (HCl / HNO_3, 3:1), following being rinsed thoroughly with deionised water before used.

5.3.1 Cationic phosphonium ligand synthesis

The synthesis of the (3-thioacetylpropyl)diphenylphosphine oxide (**12D**) was prepared according to a reported procedure [38, 39]. While, the (3-thioacetylpropyl)di-(*p*-tolyl)-phosphine oxide (**12A**), (3-thioacetylpropyl)thio-diphenylphosphine oxide (**15**), and (3-thioacetylethyl-N-methylamine)diphenylphosphine oxide (**18**) synthesis and characterisation are reported for the first time in this Chapter. The synthetic protocols used to produce the four ligands are outlined in this section.

5.3.1.1 Synthesis of (3-thioacetylpropyl)di-(*p*-tolyl)phosphine oxide(12A) and (3-thioacetylpropyl)diphenylphosphine oxide (12D)

The synthesis of the (**12A**) phosphine oxide and (**12D**) are shown in Scheme 1. The compounds were prepared *via* alkaline hydrolysis of hydroxypropylphosphonium salt (**2**) in the first stage in order to get the (hydroxypropyl)di(*p*-tolyl)phosphine oxide and (hydroxypropyl)diphenylphosphine oxide (**10 A**, **D**) respectively. Hydroxylpropylphos-phonium salt (**2 A**, **D**, 1mmol) was dissolved in approximately 1.5 mL of ethanol, and the

mixtures were heated with 2mL of 20% aqueous NaOH solution .In the next stage, the (**10 A**, **D**) were dissolved in hydrobromic acid (48%, 5mL) and refluxed for five hours to obtain the corresponding bromopropylphoshine oxide (**11 A**, **D**). The final stage, involved bromopropylphoshine oxide (**11 A**, **D**, 2 mmol) reacted with potassium thioacetate (3 mmol) in a mixture of aqueous ethanol (4 mL). The mixture as a solution was stirred at room temperature in order to get the (**12 A**, **D**). The reaction mixture was left stirring overnight under nitrogen. TLC is used to observe the progress of the reaction by using 10 % CH_3OH: 90 % DCM as a mobile phase. The (**12 A**, **D**) were purified by diethyl ether and ethanol to generate a brown powder and yellow oil respectively.

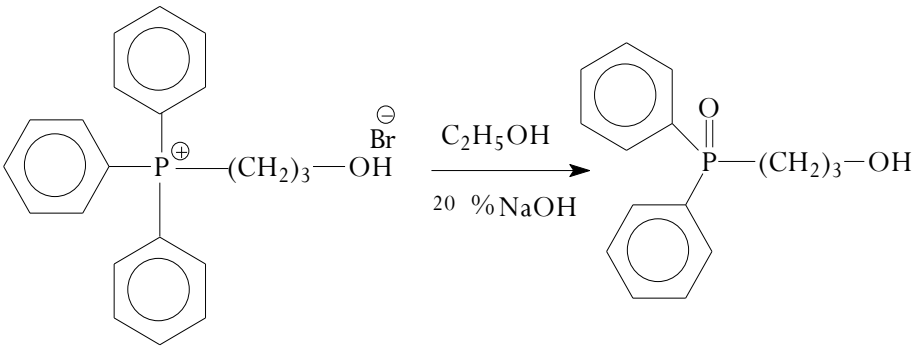

(2) **Reaction 1** (10)

A= 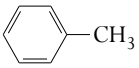

D= 

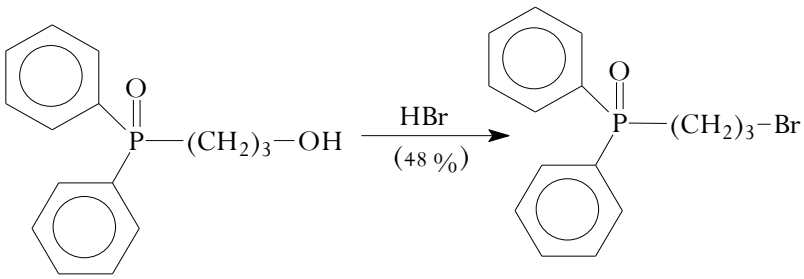

(10) **Reaction 2** (11)

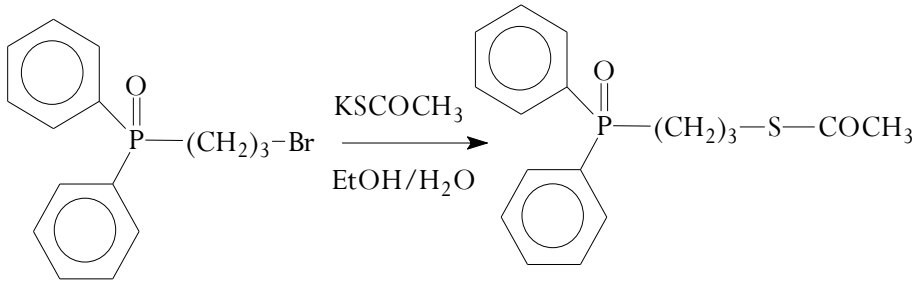

(11) **Reaction 3** (12)

Scheme 1

5.3.1.2 Synthesis of (3-thioacetylpropyl)thio-diphenylphosphine oxide (15)

The synthesis of compound **15** was carried out following the reactions showed in Scheme 2. In a round bottom flask with a reflux condenser a mixture of diphenylphosphinic chloride (**13**) (0.71 ml) (3.8 mmol) with approximately (0.331ml) (15 mmol) from 3-chloro-1-propanthiol in 5 ml DCM under reflux 7 hours. The corresponding a white precipitate has occurred (**14**) and it's mp was 170 °C. Then the salt (**14**) (2 mmol) (0.6 gm) was reacting with potassium thioacetate (0.34 gm) (3 mmol) in an aqueous ethanol (10 mL). The reaction mixture was left stirring over night at room temperature under nitrogen. TLC was used to monitor the progress of the reaction, using 10 % methanol: 90 % DCM as a mobile phase. Compound **15** was obtained after extracted by using DCM (10 mL, 3 times) of the reaction mixture and all the extracts were combined and dried with $MgSO_4$ and rotary evaporated. The precipitate formed **15** was collected by filtration, and purified by diethyl ether to yield a cream coloured powder.

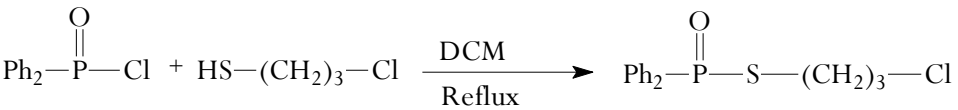

(13) **Reaction 1** (14)

Ph=

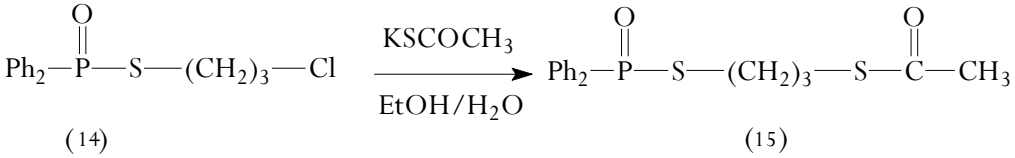

(14) (15)

Reaction 2

Scheme 2

Reaction Mechanism

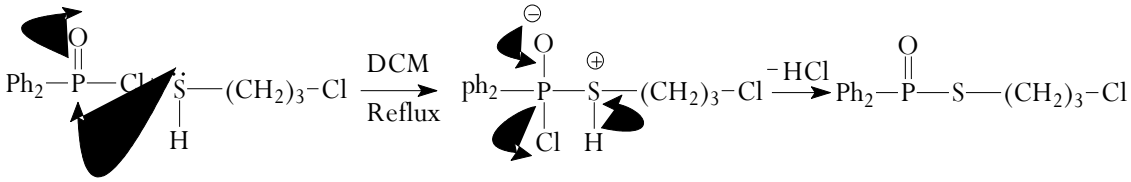

(13) **Reaction 1** (14)

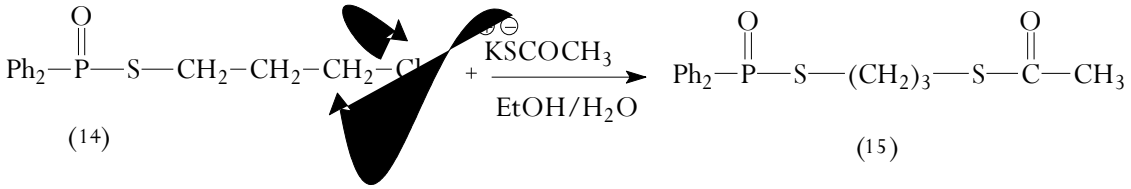

(14) (15)

Reaction 2

5.3.1.3 Synthesis of (3-thioacetylethyl-N-methylamine)diphenylphosphine oxide (18)

In a round bottom flask with a reflux condenser a mixture of diphenylphosphinic chloride (**13**) (0.71ml) (3.8 mmol) and approximately (1.63 ml) (15 mmol) from (2-methoxyethyl)methylamine (**16**) in 5 ml DCM was reflux for six hours. The corresponding a a yellow precipitate occurred **17** as shown in Scheme 3. Then the salt **17** (2mmol) (0.57gm) was reacting with potassium thioacetate (0.34 gm) (3 mmol) in aqueous ethanol (10 mL) and the reaction mixture was left stirring over night at room temperature under nitrogen. TLC was used to monitor the progress of the reaction, using 10 % methanol: 90 % DCM as a mobile phase. Compound **18** was obtained after being extracted by DCM (10 mL, three times) of the reaction mixture and all the extracts were

combined and dried with magnesium sulphate anhydrous $MgSO_4$, and rotary evaporated. The product **18** was purified by ethanol to give a yellow powder.

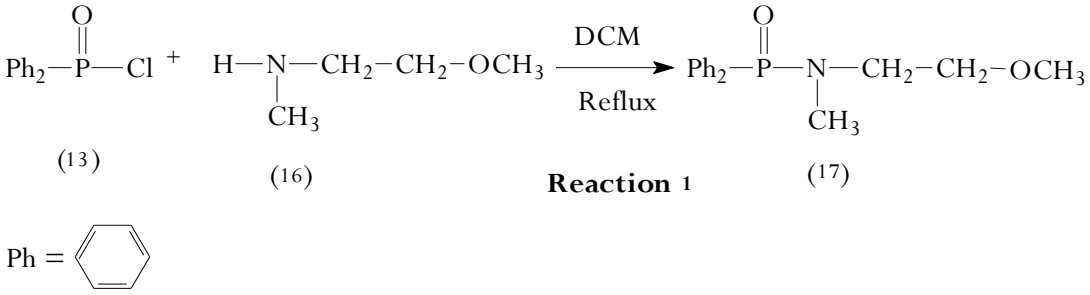

(13) (16) **Reaction 1** (17)

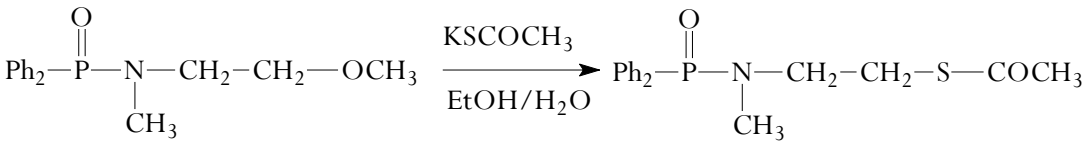

(17) **Reaction 2** (18)

Scheme 3

Reaction Mechanism

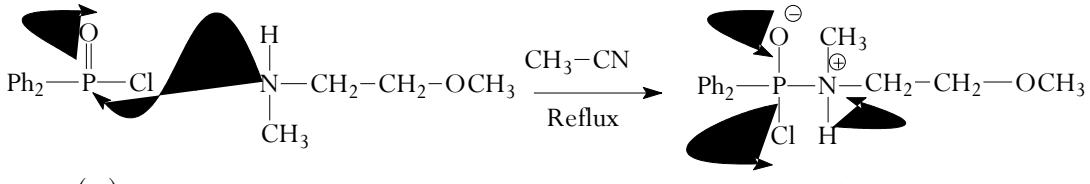

(13) (16) **Reaction 1** (17)

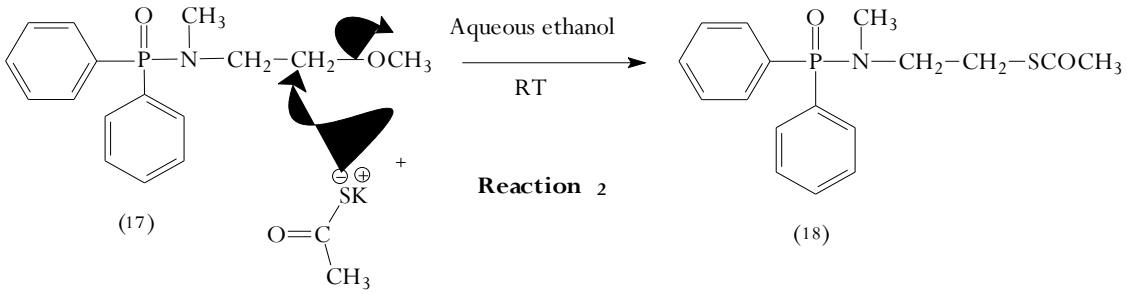

Reaction 2

5.3.2 Synthesis of phosphine oxide gold nanoparticles derivatives in DMSO using $NaBH_4$ as reducing agent

The method for the synthesis of colloidal cationic phosphonium AuNPs with our ligands in DMSO in this chapter is reported for the first time and was developed, similarly as the previous methods [38].

In order to prepare the colloidal AuNPs in DMSO, solutions of the phosphonium ligands derivatives, including, **12A**, **12D**, **15** and **18** (0.57 mmol), (0.4 mmol), (0.6 mmol), (0.8 mmol) respectively, were prepared in DMSO 25 ml. A solution of potassium tetrachloroaurate (0.8 mmol) in H_2O (10 mL) was also prepared. Then both, ligands and gold salt solutions were mixed and vigorously stirred for roughly 4 hours at room temperature until the colure was changed from yellow to colourless. The reduction was carried out by adding 5 mL of a freshly prepared aqueous solution of sodium borohydride 0.4 M to the DMSO mixture. In order to remove the excess of ligands in each one of the gold colloidal solutions prepared, liquid-liquid extractions were carried out using diethyl ether.

5.3.3 Synthesis AuNPs using (3-thioacetylpropyl)di(*p*-tolyl)phosphine oxide, in aqueous solution using ascorbic acid as reducing agent

Several attempts were made to functionalise AuNPs by **12D**, **15** and **18** in aqueous solution with ascorbic acid without any good results, despite changed ligands / Au salt ratio and ascorbic acid concentration. A possible explanation is the poor solubility of these ligands in the aqueous solution. However, good results were collected when **12A** was used to functionalised AuNPs in aqueous solution. The detailed synthesis of the AuNPs in aqueous solution with ascorbic acid was shown in experimental section / Chapter 4.

5.4 Results and Discussion

ATR-FTIR, ^{31}P, ^{1}H NMR and ESI-MS techniques have been used to characterise all the ligands that were prepared in this Chapter before being used to functionalise AuNPs. Stability of **12** (A, D)-AuNPs, **15**-AuNPs and **18**-AuNPs are confirmed *via* using UV-visible absorption spectroscopy and DLS. The measurements of AuNPs solution are taken regularly to see any changes such agglomeration / aggregation which may occur.

5.4.1 Synthesis of 12A and 12D

The synthesis of **12A** and **12D** are shown in Scheme1 including three stages with two intermediates. The first compound was generated by an alkaline hydrolysis of hydroxylpropylphosphonium salt (**2**) as the first stage to obtain (hydroxylpropyl)di-(*p*-tolyl)phosphine oxide and (hydroxylpropyl)diphenyl-phosphine oxide (**10 A, D**) respectively [39]. The (**10 A**, **D**) were then treated with (48 %) HBr in order to generate the corresponding bromopropylphosphine oxide (**11 A**, **D**). **12A** and **12D** were then obtained *via* reaction of the latter (**11 A, D**, 2 mmol) with potassium thioacetate (3 mmol) in aqueous ethanol (5ml) at room temperature. The reaction mixture was left stirring overnight. The resulting products (**12 A, D**) were purified by trituration using diethyl ether. The final product was powder, brown coloured with a melting point at 119-120°C and yellow oil respectively. The yield was 70 % and 67 % respectively.

When **12 A** and **12D** studied by ESI-MS in positive ion mode, ion corresponding to $[M+Na]^+$ and $[M + H]^+$ were observed at 369.10 *m/z* and 319.09 *m/z* respectively. Expected MW **12A** and **12D** are 346 g/mol, 318 g/mol respectively.

IR spectrum of (**12A**) showed absorption bands at the regions of 725 – 720 cm^{-1} (ν CH_2), 1738 cm^{-1} (ν C=O), 1345 cm^{-1} (C-S-), 1217 cm^{-1} (ν P=O) and 3100 – 3000 cm^{-1} (ν CH-Aromatic). NMR: $\delta^{31}P$ (CD_2CL_2) = 32.0 ppm, ^{1}H NMR showed the distinctive chemical shift at δ 2.6 (2H, t, P-$\underline{CH_2}$-CH_2-CH_2), δ 2.3 (2H, t, P-CH_2-CH_2-$\underline{CH_2}$), δ 1.9 (2H, m, P-CH_2-$\underline{CH_2}$-CH_2), δ 3.3 (3H, s, Ph-$\underline{CH_3}$), δ 3.4 (3H, s, Ph-$\underline{CH_3}$), δ 2.4 (3H, s, CO-$\underline{CH_3}$), 5.6 (1H, s, CD_2CL_2 (solvent)) [40], and at 7.4 - 7.8 (8H, m, Aromatic H) ppm. Where IR of (**12D**) showed absorption bands at the regions IR spectrum at the regions of 699 – 710 cm^{-1} (ν CH_2), 1739 cm^{-1} (ν C=O), 1340 cm^{-1} (C-S-), 1217 cm^{-1} (ν P=O) and 3100 – 3000 cm^{-1} (ν CH-Aromatic). NMR: (DMSO), ^{1}H NMR spectrum gave signals at 3.6 (2H, t, P-

$\underline{CH_2}$-CH_2-CH_2), δ 3.4 (2H, t, $\underline{CH_2}$-S-CO), δ 1.9 (2H, m, P-CH_2-$\underline{CH_2}$-CH_2), δ 2.4 (3H, s, CO-$\underline{CH_3}$), δ 2.5 (1H, s, DMSO-(solvent)) [41], and at 7.4 – 7.8 (10H, m, Aromatic H) ppm.

The evidence to generate compounds **12A** and **12D** are occurring carbonyl group (C=O) in IR at 1738 cm^{-1} and 1739 cm^{-1} respectively. In addition, (ν P=O) [42], stretching absorption appeared at 1217 cm^{-1} for **12A** and **12D**. In the same hand, it is noted that there are singles in ^{1}H NMR at δ 2.4 for (3H, s, CO-$\underline{CH_3}$) in both **12A** and **12D** respectively which confirmed the literature [43, 44]. ^{31}P NMR ($CDCl_3$) analysis provided a single sharp peak at 32 ppm conforming producing the **12A** compound. According to Jeong, K., et al., ^{31}p has changed from 24 ppm to 39 ppm as result of oxidation and hydrogenation whereas peak shifted up-field and down-field respectively [42].

5.4.2 Synthesis of (3-thioacetylpropyl)thio-diphenylphosphine oxide (15)

Synthesis NPs in organic solvents have been published for a wide range recently [45]. Stability of NPs, depend on the environment and are fundamentally adjusted by the ligands. It is well known that disulfide ligands enhanced colloidal stability of AuNPs compared to monothiols [45-47]. For example, it has been found that peptides with mono-, dithiol and amine ended were more stable compared to peptides with no thiol groups in their structure. In addition, QDs containing S and Se were unstable in the case of presence of a mono-dentate thiol, while poly-thiol ligands were effectively employed as capping agents. Similarly the poly(methacrylic acid) (PMAA) was incorporated with a thioether group in order to the stabilising cobalt NPs to be stored for up to eight weeks in comparison when pure PMAA (without thioether group) used which were stable for up to 11 days. This indicates the significance of thiol groups in stabilising metal NPs [45, 48, 49].

The synthesis of the compound **15** is shown in Scheme 2 in two stages. The first compound was generated *via* reaction of diphenylphosphinic chloride (**13**) with 3-chloro-1-propanthiol to generate salt (**14**) as the first stage, which was reacting with potassium thioacetate in aqueous ethanol (5 ml) at room temperature. The reaction mixture was stirring overnight. The resulting product **15** was purified by trituration using diethyl ether. The final product was a powder, creamy coloured with a melting point at 219-220°C. The

yield was 77 %. When the compound studied by ESI-MS in positive ion mode, ion corresponding to $[M + H]^+$ was observed at (351.06). Expected MW **15** is 350 g/mol.
IR spectrum for **15** showed absorption bands at the regions of 722 cm^{-1} (ν CH_2), 1685 cm^{-1} (ν C=O), 1306 cm^{-1} (C-S-), 1191 cm^{-1} (ν P=O) and 3070 – 3000 cm^{-1} (ν CH-Aromatic). NMR: ^{1}H NMR spectrum gave signals at δ 5.6 (1H, s, CD_2CL_2 (solvent) [40]. δ 2.4 (3H, s, CO-$\underline{CH_3}$), δ 3.4 (2H, m, $\underline{CH_2}$-), δ 3.5 (2H, t, P- S-$\underline{CH_2}$-), δ 3.2 (2H, t, $\underline{CH_2}$-S-CO) and at 7.4 – 7.8 (10H, m, Aromatic H) ppm. These protons are affected by an electron withdrawing groups such as phosphine oxide. Protons of a methyl group in ($COCH_3$) has weaker shielding effect than those between thiol and thiol groups as expected [42, 50].

5.4.3 Synthesis of (3-thioacetyl-N-ethylmethylamine)diphenylphosphine oxide (18)

Ligand-NP affinity is greatly dependent on the natural of NP surface and the ligand head group. Other sulfur functional groups such as thiocarbamates (O-thiocarbamates, ROC(=S)NR2) and S-thiocarbamates, RSC(=O)NR2) can be used as ligands for a variety of transition metal-based NPs. However, they have lower affinity toward the NP surface than thiols [45, 51, 52].

Stabilisation of metal NPs by suitable organic groups such as amines derivatives have been widely used. The main difference between function by thiols or amines is the stability of the NPs. Metal NPs have bigger sizes when functionalised by amines than in the case of thiol ligands, as a result there is weaker bonding between NPs and amines. While, both of them can be complementary. For instance, peptides are linked to AgNPs *via* both the thiol and amine functions [53].

The synthesis of compound **18** is shown in Scheme 3. The first compound was generated *via* reaction of diphenylphosphinic chloride (**13**) with (2-methoxyethyl)methylamine (**16**) to produce salt **17** as the first stage, which was reacting with potassium thioacetate in aqueous ethanol (5ml) at room temperature. The resulting product **18** was purified by trituration using diethyl ether. The final product was powder; yellow coloured with a melting point at 248-250 °C. The yield was 85 %. When studied by ESI-MS in positive ion mode, ion corresponding to $[M\text{-}COCH_3]^+$ was observed at 290.13 *m/z*. While expected MW for **18** is 333 g/mol. IR spectra showed absorption bands at the regions of 726 – 720

cm^{-1} (ν CH_2), 1737 cm^1 (ν C=O), 1375 cm^{-1} (C-S-), 1177cm^{-1} (ν P=O) and 3100 – 3000 cm^{-1} (ν CH-Aromatic). NMR: $\delta^{31}P$ ($CDCL_3$) = 30.0 ppm. ^1H NMR spectrum gave signals at δ 1.8 (1H, s, H_2O of $CDCL_3$ solvent) [40]. δ 2.4 (3H, s, CO-$\underline{CH_3}$), 3.3 (3H, s, N-$\underline{CH_3}$), δ 3.0 (2H, t, $\underline{CH_2}$-N-), δ 3.5 (2H, t, $\underline{CH_2}$-S-) and at 7.6 - 7.8 (10H, m, Aromatic H) ppm.

All these ligands were soluble in methanol, ethanol, DMSO, chloroform, and DCM. ^{31}P NMR ($CDCl_3$) analysis provided a single sharp peak at 30 ppm conforming producing compound **18**. Sharp single peaks indicate the high purity of compound **18** [42]. As well as, carbonyl peaks showed at 1737 cm^{-1} (C=O asymmetric stretching) and 1728cm^{-1} (C=O symmetric stretching) and 716 cm^{-1} (C=O banding), with the C–N peak at 1373 cm^{-1} suggesting complete **18** compound [42]. ^1H NMR introduced further evidence to ensure compound **18** was produced. For instance, present 4H of $(CH_2)_2$ at δ 3.0-3.5 ppm, which was absent in start meterial (**13**).

5.4.4 Stability of gold nanoparticles using (12A), (12D), (15), and (18) in DMSO by using $NaBH_4$ and ascorbic acid as reducing agents

Secondary phosphine oxide ligands were used as NP stabilisers, where synthesis of air-stable and uniform AuNPs was generated using these ligands, which showed high catalytic activity. In a similar way, aryl secondary phosphine oxide presents a strong polarity of the P=O bond, and this ability is lost compared with aliphatic phosphine oxides ligands used to functionalise AuNPs [28]. The synthesised AuNPs primarily confirmed by a colour change from colourless to blushing red, were further systematically characterised by using UV/ Vis spectroscopy and DLS.

AuNPs can be synthesised in different sizes and various media according to the desired application and can easily be functionalised with small drug molecules, polymers, and biomaterials for many potential applications [54]. AuNPs are chemically highly active towards biological molecules and have the potential to alter the fate of chemical reactions inside cells and modulate cellular signalling pathways and cellular function according to the size effect. The TEM imaging demonstrated that AuNPs were spherical in nature and can pass *via* the cell membrane due to their intrinsic properties to bind to carbon-bonded sulfhydryl (–C–SH or R–SH) group [55].

In this Chapter, DMSO was used for dissolving these ligands due to their poor solubility in water. However, these hydrophobic ligands have shown their ability to functionalise and stabilise the surface of AuNPs in DMSO for more than 6 months. Their interaction with AuNPs surface, cause them to a penetrate into the lipophilic cell wall. Due to reduction conditions which could be removing acetyl groups from the original structure of the ligands to form $Ph_2P{=}O(CH_2)_3S^-$ in the solution which can form a strong covalent bond to the AuNPs surface [38].

Several attempts of synthesising phosphonium AuNPs were carried out by using current ligands as the stabilising ligand with the two phase DCM / water method [38], but the attempts were unsuccessful despite adjusting synthetic conditions such as variety in concentrations of ligands and gold salts. In contrast, aggregations and coagulate to bulk gold occurred immediately after a reducing agent ($NaBH_4$) was added to the mixture solutions. This aggregation may have been due to poor affinity to water or dichloromethane (DCM), the nature of the ligands not only caused stability of the AuNPs but also effected their properties such as solubility in polar or nonpolar solvents [56].

Colloidal AuNPs were prepared in DMSO, a reduction of Au (III) to Au (0) was carried out in the presence of **12**(**A, D**), **15** and **18**, in DMSO, using $NaBH_4$ as the reducing agent. With this reducing method using DMSO as the dispersing solvent, a red coloured colloidal solution of AuNPs functionalised with all ligands was obtained which stayed stable for nearly six months with no clear evidence for aggregation.

5.4.5 UV-Visible and DLS studies

Evidence for formation of colloidal AuNPs was observed in the UV- visible spectrum of the fresh and ageing solutions. A broad band was shown at 520 nm, which indicated a reduction of Au (III) to Au (0) and the size of the particles were in the range 5-10 nm according to the values for similar thiolate-capped AuNPs reported in the literature [38]. Furthermore, AuNPs were characterised by a peak at 520 – 535 nm in the UV–Vis spectrum which was 12 ± 2 nm [57]. Figures (5.1, 5.2, 5.3, and 5.4) show the stability of AuNPs at nearly six months. Evidence for the formation of AuNPs using the reduction method in DMSO was shown by UV-Visible spectroscopy technique. DMSO was used as the blank. Bands centred at 542 (Figure 5.1, see UV-visible spectrum at time = 0), 530 nm (Figure 5.2, see UV-visible spectrum at time 0), 527 (Figure 5.3, see UV-visible

spectrum at time = 0), and 529 nm (Figure 5.4, see UV-visible spectrum at time 0). They were observed in the resulting UV spectra corresponding to the Burgundy AuNPs colloidal solutions prepared by **12A**, **12D**, **15** and **18** respectively.

When the compared, the UV spectra of all the colloidal solutions of AuNPs functionalised with **12A**, **12D** and **15** in DMSO (Figures 5.1, 5.2 and 5.3, see UV-visible spectra at time = 0), they did not show a significant changes in the wavelengths.

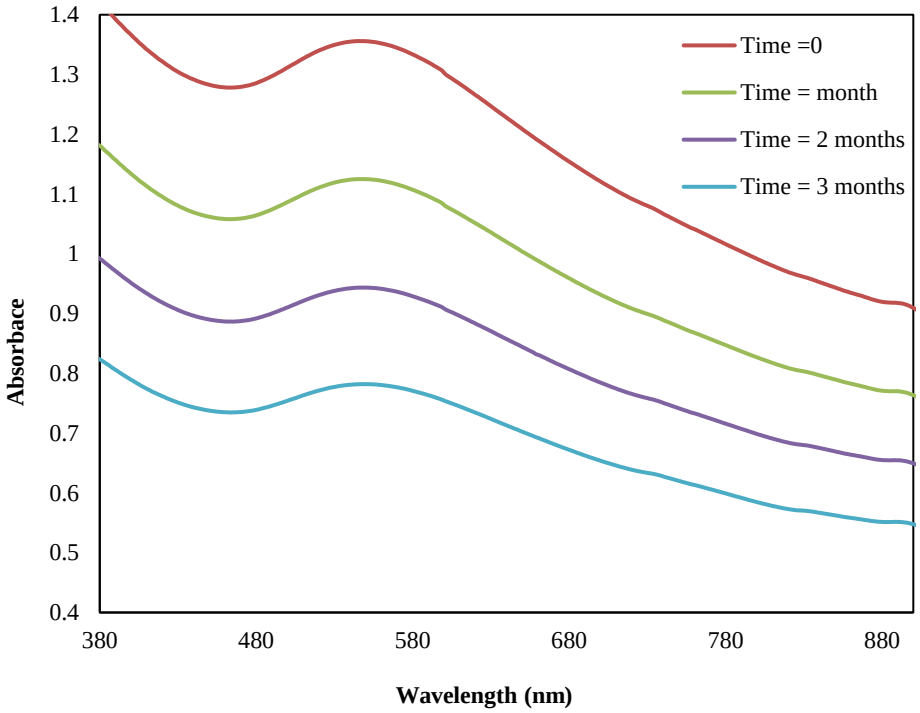

Figure 5.1. UV-visible absorption spectra of the colloidal solutions of AuNPs functionalised using **12A** as protecting ligand. The different UV-visible spectra represent these AuNPs dispersed in DMSO at time = 0, 1, 2, and 3 months. Solutions prepared using different dilution factors.

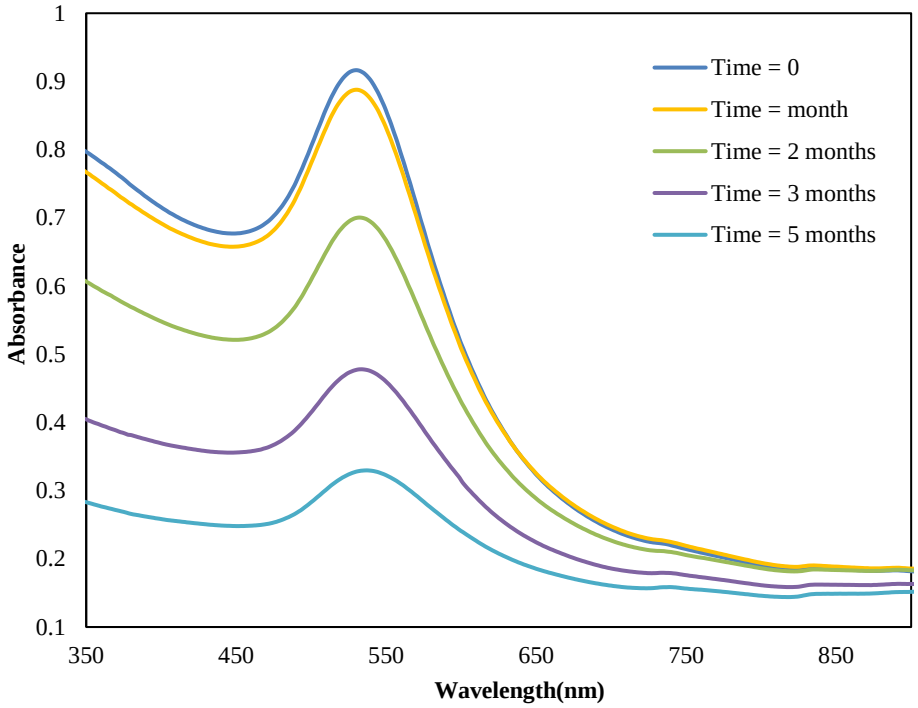

Figure 5.2. UV-visible absorption spectra of the colloidal solutions of AuNPs functionalised using **12D** as protecting ligand. The different UV-visible spectra represent these nanoparticles dispersed in DMSO at time = 0, 1, 2, 3, and 5 months respectively. Solutions prepared using different dilution factors.

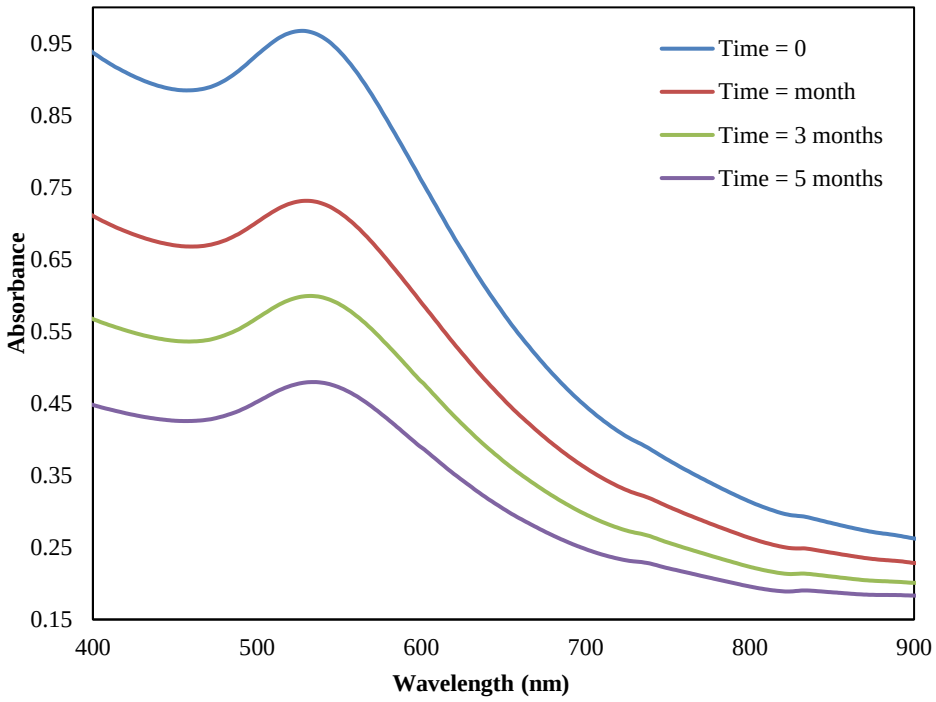

Figure 5.3. UV-visible absorption spectra of the colloidal solutions of AuNPs functionalised using **15** as protecting ligand. The different UV-visible spectra represent these AuNPs dispersed in DMSO at time = 0, 1, 3, and 5 months. Solutions prepared using different dilution factors.

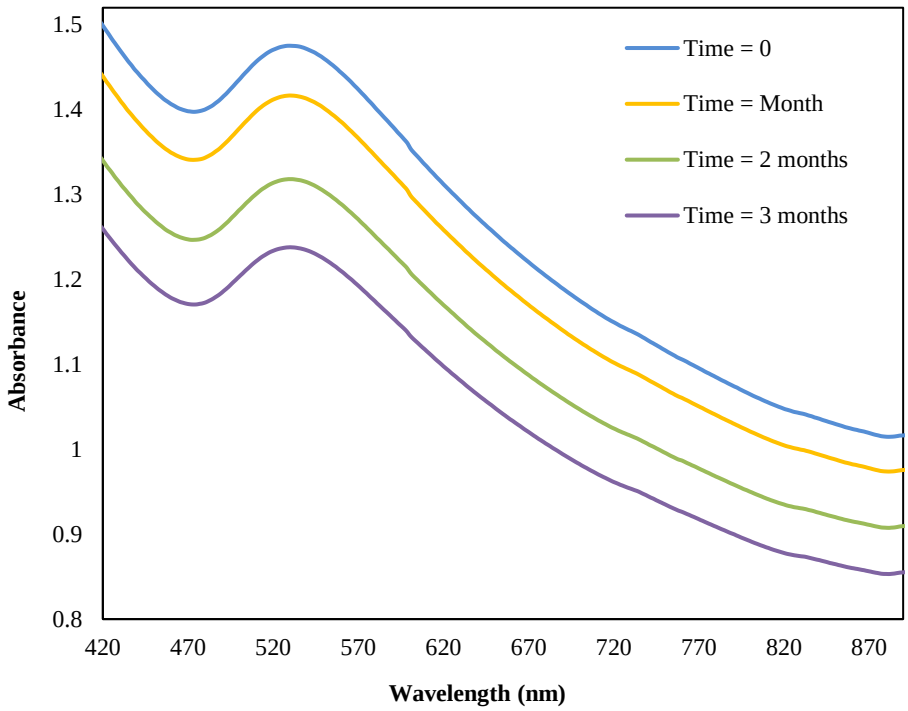

Figure 5.4. UV-visible absorption spectra of the colloidal solutions of AuNPs functionalised using **18** as protecting ligand. The different UV-visible spectra represent these AuNPs dispersed in DMSO at time = 0, 1, 2, and 3 months respectively. Solutions prepared using different dilution factors.

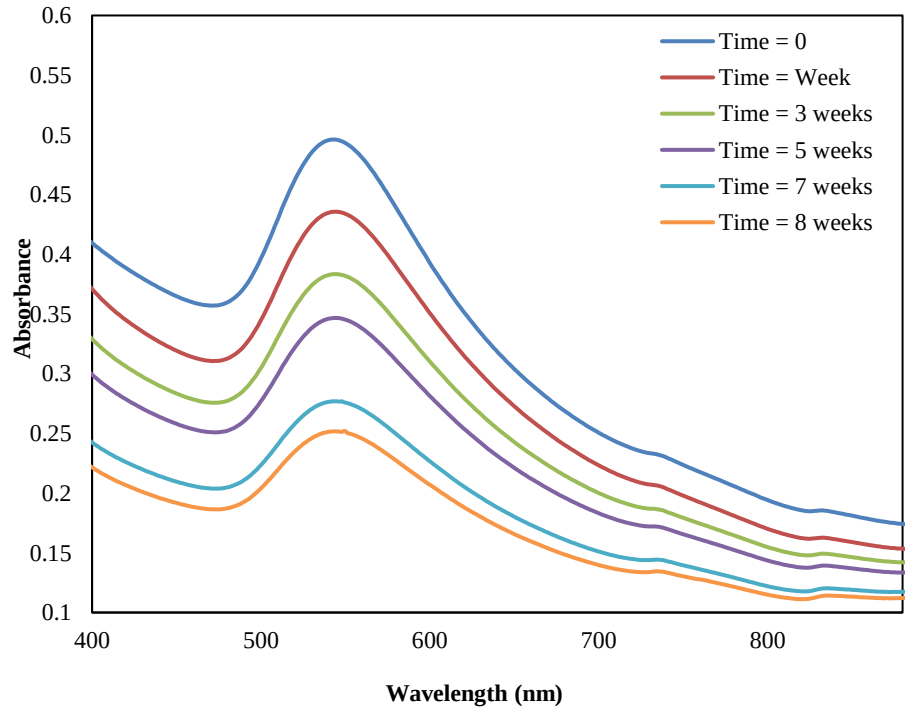

Figure 5.5. UV-visible absorption spectra of the colloidal solutions of AuNPs functionalised using **12A** as protecting ligand using **ascorbic acid** as reducing agent. The different UV-visible spectra represent these AuNPs dispersed in aqueous solution at time = 0, 1, 3, 5, 7 and 8 weeks respectively. Solutions prepared using different dilution factors.

In this study, the refractive index of the solvent DMSO has not shown to induce a shift of the SPB of AuNPs as suggested in the literature [38]. Slight differences in wavelengths (542 and 530 nm 527 nm, respectively) can be observed when ligands change in structure (see Figures 5.1, 5.2 and 5.3). However, **18**-AuNP gave a wavelength of 529 nm (Figure 5.4) which contains a nitrogen atom instead of S atom in its structure has not offered any important differences with other ligands contain S atoms. However, time of stability was only a maximum of 3 months compared with **12A**, **12D** and **15**-AuNPs, most of which are stable until the fifth month, this may be due to the tertiary amine containing ligand-coated AuNPs which are no longer protonated and cause aggregation faster than ligands contain thiol as demonstrated in previous researches [58]. Existence a tolyl group in **12A** has not a lot of advantages for stability AuNPs using sodium borohydride as reducing agent compared with other ligands, however, it is played significant difference for the stability of AuNPs when ascorbic acid has used as a reducing agent (see Figure 5.5), which is illustrated in this Chapter.

The colloidal solutions of AuNPs functionalised using **12A**, **12D**, **15** and **18** as protecting ligands were all analysed by DLS as well. Then, particle sizes for samples were obtained by analysing at least 253 particles per sample from several results taken. All four AuNPs samples showed spherically shaped particles. AuNPs functionalised by ligand **15,** which contains dithiol group has the smallest size in this Chapter with high stability for 5 months, indicates to significant dithiol group to enhanced colloidal stability for AuNPs as shown in the literature [58, 59].

Mean diameters obtained for the samples **12A**, **12D**, **15**, **18-AuNPs** analysed were as follows: 26 ± 3.5 nm, 10.2 ± 2.7 nm, 7.9 ± 1.7 nm, 9.6 ± 1.9 nm, respectively. It can be shown that the DLS results of AuNPs are similar to the corresponding UV-Visible spectra results, which confirmed each other. The corresponding UV-Visible spectrum showed that the SPB of AuNPs functionalized by **12A** is centred at 542 nm, which is slightly larger than those where other ligands have been used to functionalise AuNPs in this Chapter and when $NaBH_4$ was used as reducing agent. Similar size has been measured for **12A**-AuNP when ascorbic acid was used as reducing agent instead $NaBH_4$ and the

SPB was centred at 543 nm with a red shift is observed after 8 weeks at 550 nm indicating to lose the colloidal stability and form aggregates.

However, the stability of **12A**-AuNP used $NaBH_4$ was greater than in case where ascorbic acid was used, whereas the **12A**-AuNP was stable for nearly to 4 months with no obvious aggregation noted in UV and DLS results. While with ascorbic acid the solution stays stable just for 8 weeks with clearly in changing in its size, where it was 28 ± 1.5 nm (pink coloured) in initial preparation and became 47 ± 2 after 8 weeks, which indicated clearly to aggregation. In contrast, **12A**-AuNP was 26 ± 1.5 nm in the case of $NaBH_4$, and changed to 38 ± 2.2 nm illustrated to big size occurred after four months indicated to agglomeration (loosely bonded between NPs) but no evidence for any aggregation (strongly bonded between nanoparticles) was happened. These results confirming to big size of AuNPs solution can be produced when ascorbic acid used as reducing agent in comparison in the case of $NaBH_4$ which produce a small sizes as mentioned in the literature [60].

5.5 Conclusion

Derivatives of phenyl phosphine such as triphenyl phosphine have been used to increase the stability of AuNPs *via* their phenyl range, which provides high stability to AuNPs as result to oxidation resistance to the phosphine itself. For this reason, phenyl phosphine derivatives have chosen in this chapter to functionalise AuNPs [61-63]. The fabrication of phosphine oxide AuNPs using (**12A**), (**12D**), (**15**), and (**18**) as protecting ligands which consider a newly masked thiol, also the reduction method in DMSO is reported here for the first time.

It has been shown that these ligands are strongly stabilised to air oxidation, as a result, to strongly bound to the AuNPs surface, which may be due to high solubility in DMSO. Also, these ligands functionalised AuNPs gave good stability in DMSO due to poor solubility in aqueous solution. It is seen that, different sizes and different stability of AuNPs were noted with changing in structure of protected ligands, such as changing a phenyl group head in **12D** to tolyl group in **12A**. Also, present dithiol group in **15** and amine group in **18** showed a slightly different in the stability of AuNPs as demonstrated in the discussion section. All of these properties of these ligands would promise smart AuNPs in DMSO to be a new efficient agent for cancer targeting or photothermal therapy.

While in most cases of AuNPs that are not stabilised by these ligand molecules in water, due to often poor stability to external factors is observed, and only **12A** has been generated in aqueous solution and ascorbic acid as reducing agent. Control of AuNPs size is an important factor for many applications, especially in bio-applications.

5.6 References

1. Dreaden, EC., Austin, LA., Mackey, MA and El-Sayed, MA, *Size matters: gold nanoparticles in targeted cancer drug delivery.* Therapeutic delivery, 2012. **3**(4): p. 457-478.

2. Lalwani, N., Chen, Y-S., Brooke, G., Cross, NA., Allen, DW., Reynolds, A., Ojeda, J., Tizzard, GJ., Coles, SJ and Bricklebank, N, *Triphenylarsonium-functionalised gold nanoparticles: potential nanocarriers for intracellular therapeutics.* Chemical Communications, 2015. **51**(19): p. 4109-4111.

3. Woehrle, GH., Brown, LO and Hutchison, JE, *Thiol-functionalized, 1.5-nm gold nanoparticles through ligand exchange reactions: Scope and mechanism of ligand exchange.* Journal of the American Chemical Society, 2005. **127**(7): p. 2172-2183.

4. Borah, BJ., Yadav, A and Dutta, DK, *Au-nanoparticles: Control size and morphology stabilized by tripodal phosphine based ligands and their antimicrobial activity.* Journal of biomedical nanotechnology, 2011. **7**(1): p. 152-153.

5. Jin, P., Dai, Z and Chang, T, *The Role of Bis (p-Sulfonatophenyl) Phenylphosphine in Stabilizing Gold Nanoparticles*. in *AASRI International Conference on Industrial Electronics and Applications*. 2015.

6. Sortino, S, *Photoactivated nanomaterials for biomedical release applications.* Journal of Materials Chemistry, 2012. **22**(2): p. 301-318.

7. Ghalandarlaki, N., Alizadeh, AM and Ashkani-Esfahani, S, *Nanotechnology-applied curcumin for different diseases therapy.* BioMed research international, 2014. **2014**.

8. Mollenhauer, D, *Nitrogen-and phosphine-binding ligands in interaction with gold atoms, clusters, nanoparticles and surfaces.* Chemical Modelling, 2015. **12**: p. 293-350.

9. Jin, S., Du, W., Wang, S., Kang, X., Chen, M., Hu, D., Chen, S., Zou, X., Sun, G and Zhu, M, *Thiol-Induced Synthesis of Phosphine-Protected Gold Nanoclusters with Atomic Precision and Controlling the Structure by Ligand/Metal Engineering.* Inorganic Chemistry, 2017.

10. Éll, AH., Csjernyik, G., Slagt, VF., Bäckvall, JE., Berner, S., Puglia, C., Ledung, G and Oscarsson, S, *Synthesis of Thioacetate‐Functionalized Cobalt (II) Porphyrins and Their Immobilization on Gold Surface–Characterization by X‐ray Photoelectron Spectroscopy.* European journal of organic chemistry, 2006. **2006**(5): p. 1193-1199.

11. Lee, MH., Yang, Z., Lim, CW., Lee, YH., Dongbang, S., Kang, C and Kim, JS, *Disulfide-cleavage-triggered chemosensors and their biological applications.* Chemical reviews, 2013. **113**(7): p. 5071-5109.

12. Singh, R and Whitesides, GM, *Thiol-disulfide interchange.* S. Patai, and Z. Rappoport, Z.(eds.), Supplement S: The Chemistry of Sulphur-containing Functional Groups, 1993: p. 633-658.

13. Badia, A., Demers, L., Dickinson, L., Morin, F., Lennox, R and Reven, L, *Gold–Sulfur Interactions in Alkylthiol Self-Assembled Monolayers Formed on Gold Nanoparticles Studied by Solid-State NMR.* Journal of the American Chemical Society, 1997. **119**(45): p. 11104-11105.

14. Ashwell, GJ., Chwialkowska, A and High, LH, *Au-SC n H 2n-Q3CNQ: self-assembled monolayers for molecular rectification.* Journal of Materials Chemistry, 2004. **14**(15): p. 2389-2394.

15. Maya, F., Flatt, AK., Stewart, MP., Shen, DE and Tour, JM, *Formation and analysis of self-assembled monolayers from U-shaped oligo (phenylene ethynylene) s as candidates for molecular electronics.* Chemistry of materials, 2004. **16**(16): p. 2987-2997.

16. Ciszek, JW., Stewart, MP and Tour, JM, *Spontaneous assembly of organic thiocyanates on gold sufaces. Alternative precursors for gold thiolate assemblies.* Journal of the American Chemical Society, 2004. **126**(41): p. 13172-13173.

17. Piotrowski, P., Pawłowska, J., Pawłowski, J., Opuchlik, LJ., Bilewicz, R and Kaim, A, *Fullerene modification of gold electrodes and gold nanoparticles based on application of aromatic thioacetate-functionalized C 60.* RSC Advances, 2014. **4**(109): p. 64310-64318.

18. Vorfalt, T and Plenio, H, *Facile syntheses of cavitands with sulfur-containing functional groups.* Synthesis, 2007. **2007**(04): p. 565-571.

19. Samanta, SR., Kulasekharan, R., Choudhury, R., Jagadesan, P., Jayaraj, N and Ramamurthy, V, *Gold nanoparticles functionalized with deep-cavity cavitands: Synthesis, characterization, and photophysical studies.* Langmuir, 2012. **28**(32): p. 11920-11928.

20. Ashwell, GJ., Tyrrell, WD and Whittam, AJ, *Molecular rectification: self-assembled monolayers of a donor–(π-bridge)–acceptor chromophore connected via a truncated Au–S–(CH 2) 3 bridge.* Journal of Materials Chemistry, 2003. **13**(12): p. 2855-2857.

21. Liedberg, B and Cooper, J, *Bioanalytical applications of self-assembled monolayers.* Immobilized Biomolecules in Analysis: A practical approach. The practical approach series PAS, Oxford, 1998. **198**: p. 55-78.

22. Aizenberg, J., Black, AJ and Whitesides, GM, *Oriented growth of calcite controlled by self-assembled monolayers of functionalized alkanethiols supported on gold and silver.* Journal of the American Chemical Society, 1999. **121**(18): p. 4500-4509.

23. Chapman, RG., Ostuni, E., Yan, L and Whitesides, GM, *Preparation of mixed self-assembled monolayers (SAMs) that resist adsorption of proteins using the*

reaction of amines with a SAM that presents interchain carboxylic anhydride groups. Langmuir, 2000. **16**(17): p. 6927-6936.

24. Ostuni, E., Yan, L and Whitesides, GM, *The interaction of proteins and cells with self-assembled monolayers of alkanethiolates on gold and silver.* Colloids and Surfaces B: Biointerfaces, 1999. **15**(1): p. 3-30.

25. Laibinis, P., Palmer, B., Lee, S-W and Jennings, G, *The synthesis of organothiols and their assembly into monolayers on gold.* THIN FILMS-NEW YORK-ACADEMIC PRESS-, 1998. **24**: p. 2-43.

26. Whitesides, GM., Bain, CD., Troughton, E., Tao, Y-T and Evall, J, *Formation of monolayer films by the spontaneous assembly of organic thiols from solution onto gold*. Journal of the American Chemical Society, 1989. **111**(1): p. 321-335.

27. Cano, I., Huertos, MA., Chapman, AM., Buntkowsky, G., Gutmann, T., Groszewicz, PB and Van Leeuwen, PW, *Air-stable gold nanoparticles ligated by secondary phosphine oxides as catalyst for the chemoselective hydrogenation of substituted aldehydes: a remarkable ligand effect.* Journal of the American Chemical Society, 2015. **137**(24): p. 7718-7727.

28. Cano, I., Chapman, AM., Urakawa, A and Van Leeuwen, PW, *Air-stable gold nanoparticles ligated by secondary phosphine oxides for the chemoselective hydrogenation of aldehydes: crucial role of the ligand.* Journal of the American Chemical Society, 2014. **136**(6): p. 2520-2528.

29. Wellala, NP and Guan, H, *A diphenyl ether derived bidentate secondary phosphine oxide as a preligand for nickel-catalyzed C–S cross-coupling reactions.* Organic & biomolecular chemistry, 2015. **13**(44): p. 10802-10807.

30. Cano, I., Martínez-Prieto, LM., Fazzini, PF., Coppel, Y., Chaudret, B and Van Leeuwen, PW, *Characterization of secondary phosphine oxide ligands on the surface of iridium nanoparticles.* Physical Chemistry Chemical Physics, 2017. **19**(32): p. 21655-21662.

31. SchröDer, F., Tugny, C., Salanouve, E., Clavier, H., Giordano, L., Moraleda, D., Gimbert, Y., Mouries-Mansuy, V., Goddard, J-P and Fensterbank, L, *Secondary Phosphine Oxide–Gold (I) Complexes and Their First Application in Catalysis.* Organometallics, 2014. **33**(15): p. 4051-4056.

32. Fiurasek, P and Reven, L, *Phosphonic and sulfonic acid-functionalized gold nanoparticles: A solid-state NMR study.* Langmuir, 2007. **23**(5): p. 2857-2866.

33. Pawsey, S., Yach, K and Reven, L, *Self-assembly of carboxyalkylphosphonic acids on metal oxide powders.* Langmuir, 2002. **18**(13): p. 5205-5212.

34. Aldakov, D., Sajjad, MT., Ivanova, V., Bansal, AK., Park, J., Reiss, P and Samuel, ID, *Mercaptophosphonic acids as efficient linkers in quantum dot sensitized solar cells.* Journal of Materials Chemistry A, 2015. **3**(37): p. 19050-19060.

35. Dilworth, JR and Wheatley, N, *The preparation and coordination chemistry of phosphorus- sulfur donor ligands.* Coordination Chemistry Reviews, 2000. **199**(1): p. 89-158.

36. Zhou, J., Ralston, J., Sedev, R and Beattie, DA, *Functionalized gold nanoparticles: synthesis, structure and colloid stability.* Journal of Colloid and Interface Science, 2009. **331**(2): p. 251-262.

37. Achard, T, *Advances in Homogeneous Catalysis Using Secondary Phosphine Oxides (SPOs): Pre-ligands for Metal Complexes.* CHIMIA International Journal for Chemistry, 2016. **70**(1): p. 8-19.

38. Ju-Nam, Y., Bricklebank, N., Allen, DW., Gardiner, PH., Light, ME and Hursthouse, MB, *Phosphonioalkylthiosulfate zwitterions—new masked thiol ligands for the formation of cationic functionalised gold nanoparticles.* Organic & biomolecular chemistry, 2006. **4**(23): p. 4345-4351.

39. Ju-Nam, Y., Allen, DW., Gardiner, PH and Bricklebank, N, *ω-Thioacetylalkylphosphonium salts: Precursors for the preparation of phosphonium-functionalised gold nanoparticles.* Journal of organometallic chemistry, 2008. **693**(23): p. 3504-3508.

40. Fulmer, GR., Miller, AJ., Sherden, NH., Gottlieb, HE., Nudelman, A., Stoltz, BM., Bercaw, JE and Goldberg, KI, *NMR chemical shifts of trace impurities: common laboratory solvents, organics, and gases in deuterated solvents relevant to the organometallic chemist.* Organometallics, 2010. **29**(9): p. 2176-2179.

41. Gottlieb, HE., Kotlyar, V and Nudelman, A, *NMR chemical shifts of common laboratory solvents as trace impurities.* The Journal of organic chemistry, 1997. **62**(21): p. 7512-7515.

42. Jeong, K., Kim, J-J and Yoon, T-H, *Synthesis and characterization of novel polyimides containing fluorine and phosphine oxide moieties.* Polymer, 2001. **42**(14): p. 6019-6030.

43. Hampton, C., Demoin, D and Glaser, RE, *Vibrational spectroscopy tutorial: sulfur and phosphorus.* University Of Missouri, Fall, 2010.

44. Kononova, O., Shatnykh, K., Prikhod'ko, K and Kashirin, D, *Ion-exchange recovery of gold (I) and silver (I) from thiosulfate solutions.* Russian Journal of Physical Chemistry A, Focus on Chemistry, 2009. **83**(13): p. 2340-2345.

45. Thanh, NT and Green, LA, *Functionalisation of nanoparticles for biomedical applications.* Nano Today, 2010. **5**(3): p. 213-230.

46. Yonezawa, T., Yasui, K and Kimizuka, N, *Controlled formation of smaller gold nanoparticles by the use of four-chained disulfide stabilizer.* Langmuir, 2001. **17**(2): p. 271-273.

47. Letsinger, R., Elghanian, R., Viswanadham, G and Mirkin, C, *Use of a steroid cyclic disulfide anchor in constructing gold nanoparticle− oligonucleotide conjugates.* Bioconjugate chemistry, 2000. **11**(2): p. 289-291.

48. Medintz, IL., Uyeda, HT., Goldman, ER and Mattoussi, H, *Quantum dot bioconjugates for imaging, labelling and sensing.* Nature materials, 2005. **4**(6): p. 435.

49. Uyeda, HT., Medintz, IL., Jaiswal, JK., Simon, SM and Mattoussi, H, *Synthesis of compact multidentate ligands to prepare stable hydrophilic quantum dot fluorophores.* Journal of the American Chemical Society, 2005. **127**(11): p. 3870-3878.

50. Kim, D., Salman, S., Coropceanu, V., Salomon, E., Padmaperuma, AB., Sapochak, LS., Kahn, A and Brédas, J-L, *Phosphine oxide derivatives as hosts for blue phosphors: A joint theoretical and experimental study of their electronic structure.* Chemistry of materials, 2009. **22**(1): p. 247-254.

51. Ulman, A, *Formation and structure of self-assembled monolayers.* Chemical reviews, 1996. **96**(4): p. 1533-1554.

52. Tzhayik, O., Sawant, P., Efrima, S., Kovalev, E and Klug, J, *Xanthate capping of silver, copper, and gold colloids.* Langmuir, 2002. **18**(8): p. 3364-3369.

53. Neouze, M-A and Schubert, U, *Surface modification and functionalization of metal and metal oxide nanoparticles by organic ligands.* Monatshefte für Chemie/Chemical Monthly, 2008. **139**(3): p. 183-195.

54. Alexiou, C, *Biomedical nanotechnologies.* Nanotechnol Rev, 2013. **2(4)**(379).

55. Singh, M., Chandrasekaran, N., Mukherjee, A., Kumar, M and Kumaraguru, A, *Cancerous cell targeting and destruction using pH stabilized amperometric bioconjugated gold nanoparticles from marine macroalgae, Padina gymnospora.* Bioprocess and biosystems engineering, 2014. **37**(9): p. 1859-1869.

56. Sperling, RA and Parak, W, *Surface modification, functionalization and bioconjugation of colloidal inorganic nanoparticles.* Philosophical Transactions of the Royal Society of London A: Mathematical, Physical and Engineering Sciences, 2010. **368**(1915): p. 1333-1383.

57. Ganapuram, BR., Alle, M., Dadigala, R., Dasari, A., Maragoni, V and Guttena, V, *Catalytic reduction of methylene blue and Congo red dyes using green synthesized gold nanoparticles capped by salmalia malabarica gum.* International Nano Letters, 2015. **5**(4): p. 215-222.

58. Nam, J., Won, N., Jin, H., Chung, H and Kim, S, *pH-induced aggregation of gold nanoparticles for photothermal cancer therapy.* Journal of the American Chemical Society, 2009. **131**(38): p. 13639-13645.

59. Hofmann, A., Schmiel, P., Stein, B and Graf, C, *Controlled formation of gold nanoparticle dimers using multivalent thiol ligands.* Langmuir, 2011. **27**(24): p. 15165-15175.

60. Luty-Błocho, M., Fitzner, K., Hessel, V., Löb, P., Maskos, M., Metzke, D., Pacławski, K and Wojnicki, M, *Synthesis of gold nanoparticles in an interdigital*

micromixer using ascorbic acid and sodium borohydride as reducers. Chemical engineering journal, 2011. **171**(1): p. 279-290.

61. Mckenzie, LC., Zaikova, TO and Hutchison, JE, *Structurally similar triphenylphosphine-stabilized undecagolds, Au11 (PPh3) 7Cl3 and [Au11 (PPh3) 8Cl2] Cl, exhibit distinct ligand exchange pathways with glutathione.* Journal of the American Chemical Society, 2014. **136**(38): p. 13426-13435.

62. Daniel, M-C and Astruc, D, *Gold nanoparticles: assembly, supramolecular chemistry, quantum-size-related properties, and applications toward biology, catalysis, and nanotechnology.* Chemical reviews, 2004. **104**(1): p. 293-346.

63. Häkkinen, H., Walter, M and Grönbeck, H, *Divide and Protect: Capping Gold Nanoclusters with Molecular Gold− Thiolate Rings.* The Journal of Physical Chemistry B, 2006. **110**(20): p. 9927-9931.

Chapter 6: Antimicrobial activities of novel gold nanoparticles agent against *Escherichia coli* and *Staphylococcus aureus* bacteria

6.1 Abstract

Escherichia coli (E. coli) and *Staphylococcus aureus* (*S. aureus*) are among the major cause of diarrheal infections for a human. These bacterial infections have been treated using different types of antibiotic drugs. In contrary, antibiotic resistant bacteria are the reason why new antimicrobials need to be developed. It is better to explore new antibacterial agents instead of tradition antibiotics with reduced unwanted side effects.

In this Chapter, we used non-pathogenic bacteria including (*E. coli* NCIB 8277 and *S. aureus* ATCC 6538P) which do not cause disease for human or any another organism. The development of multi-drug-resistant (MDR) bacteria has become dangerous to community health [1]. Where, antibiotic resistant bacteria cause millions of infections. That leads to thousands of deaths every year in the U.S., according to a report published by the U.S [1].

Additionally, due to significant continuously decrease in the number of approved antibiotics in the past decade, an urgent need for discovery a novel antibacterial and strategies of treatment are an important goal nowadays [1, 2]. That is why AuNPs were chosen in this Chapter and used for this purpose. AuNPs exhibit novel chemical and physical properties due to their unique properties such as small size and high surface area to volume ratio. Currently, modern researches have been made an attempt to examine the bactericidal efficacy of AuNPs on bacteria in particle on non-pathogenic bacteria.

The main achievement of this Chapter is presented the effect of functionalised AuNPs on non-pathogenic bacteria, where different affects were noted depending on different functional groups used to modify AuNPs. AuNPs with average size from 8.0-17 nm were used and surface modified using different ligands including triphenylphosphoniopropylthiosulfate (**4C**), (6-thioacetylhexyl)tris(2,4,6-trimethoxy-phenyl)-phosphonium bromide (**8B**), tris(2,4,6-trimethoxyphenyl)-

phosphoniopropylthiochloride (**2C**) and (3-thioacetylpropyl)tri(*p*-tolyl)phosphonium bromide (**4A**).

Different doses of these AuNPs including four concentrations for the 4 µL (low dose) solution contained 0.181 µg AuNPs, 8 µL contained 0.363 µg AuNPs, 15 µL contained 0.68 µg AuNPs, and 30 µL (high dose) contained 1.36 µg AuNPs, were utilised in order to check the antibacterial mechanism against two non-pathogen bacteria. Then, from these doses, the zones of inhibition were studied by the Agar well diffusion method and IC50 have been calculated. The stabilised AuNPs with high concentration (30 µL) exhibited excellent antibacterial sensitivity to both *E. coli* and *S. aureus,* which may be suitable choice of overcoming bacterial resistance, and should be tested on clinical isolates in the future.

6.2 Introduction

Staphylococcus aureus and *Escherichia coli* are the most common species of gram-positive and gram-negative bacteria, respectively. Nowadays, the emergence of resistant *S. aureus* and *E. coli* strains against many of antibiotics has been observed worldwide. Many researchers have tried to develop new, effective antimicrobial reagents at low cost and free of resistance [3-5].

Antimicrobial drug resistance is considered one of the most serious threats to global health to appear in the 21st century. For example, in the USA approximately 11,000 people die annually as result to methicillin-resistant *S. aureus* (MRSA) infections [6]. Furthermore, there are over 1.3 million deaths each year due to *Mycobacterium tuberculosis* (TB) infections according to the World Health Organisation (WHO), with roughly 17,0000 deaths because of multidrug resistant (MDR) strains [7]. In September 2013, extensively-drug resistant (XDR) TB accounted for 10 % of all MDR-TB diagnoses, with 92 countries having about one or more reported cases [8]. Additionally, about 300 million cases of severe illness have caused annually around the worldwide, due to bacterial infections, also the threat generated by bacterial infections have been increased by MDR bacteria due to infections [9]. For this reason, novel strategies are needed in order to discover antimicrobial compounds may contribute to the limited acute infection associated with *E. col* and *S. aureus* with avoiding any resistance drugs may happen.

Metal NPs have been utilised in therapeutic applications, and also in fundamental studies on bacterial behaviour. Furthermore, it has been pointed that, to various NPs causing to differences in toxic responses between Gram-negative (such as *E. coli*), and Gram-positive (like *S. aureus*) bacteria. Many studies have shown a remarkably higher toxicity of NPs to Gram-positive bacteria compared to Gram-negative ones [10-13]. It is demonstrated that cationic AuNPs possessed toxicity against bacteria [9, 14]. In addition, NPs functionalised with non-antibiotic molecules have antimicrobial activity, which depended upon their composition on the surface. NPs surfaces displays a great potential for antimicrobial therapy [9, 15]

The NPs have an antibacterial effect through their direct interaction with the cell and causing the weakness of basic metabolic functions [12, 16]. Also, nanomaterials are considered medical revolution recently, to give new promising drugs in order to control resistant bacteria infections [17, 18].

Biomedical applications of AuNPs have been rapidly increased with great attention currently, and broadly used as a catalyst for medical therapy, gene therapy, diagnostic and biological purposes [19-21]. For example, triphenylphosphinegold (I) complexes were used for the treatment of cancer tumours, psoriasis, HIV infections and also shown considerable antimicrobial activity [22].

AuNPs have to be valued in the development of antimicrobial agent. For instance, AuNPs functionalised with 5-fluorouracil (5-FU, an anti-leukemic drug) are used as antimicrobial activity against Gram-Positive such as (*S. aureus*) and Gram-Negative Bacteria such as (*E. coli*). Also, it investigated that, AuNPs have more effect on Gram Negative (*E. coli* and *Pseudomonas aeruginosa*) than Gram Positive (*Staphylococcus aureus*, *Micrococcus luteus*), which explained to their easier incorporation into bacteria of gram negative [23, 24].

Moreover, Lima, E., et al in 2013 illustrated that 5 nm sized AuNPs have used as an antimicrobial effect on *E.coli* and *S. aureus* types bacteria and reported that about 90-95% of both bacterial colonies habitation have reduced due to AuNPs effective [24, 25]. In addition, the smallest NPs possess the strongest antimicrobial effect compared with larger size ones, due to their ability to interact easily with bacteria cells, where, bacteria are 50 up to 5000 times bigger than NPs [17].

In addition, it is noted that the average particle size of AuNPs decreased after conjugation with antibiotics such as ampicillin, this was suggested to be due to the combined reducing property of both antibiotics and borohydride during synthesis AuNPs [26]. Furthermore, AuNPs may be appropriate for the formulation of new types of bactericidal materials equivalent to the antibiotics against microbial infections. AuNPs with a small size offers a significant bactericidal effect due to become easier to interact with the microorganisms [27].

As mentioned earlier, antibacterial activity is also influenced by both concentration and size of metal nanoparticles. For example, 5 nm DNPs (diamond nanoparticles) were more effective against *E. coli* compared to 50 nm DNPs. TEM was used to observe the interactions of DNPs with bacterial cells. For instant, 5 nm DNPs accumulates on *E. coli* cells and aggregated cause affecting of the cell, also, bacterial membranes exhibit some defects compared to untreated control cells. However, the effect of 50 nm DNPs was much less obvious than 5 nm DNPs. Furthermore, larger aggregates, > 200 nm, do not have any effect on the bacteria cells because it cannot be penetrating inside cells [12]. Furthermore, the bactericidal properties of the AgNPs are size-dependent. For example, previous studies have confirmed that AgNPs have a diameter of ∼1–10 nm found inside of Gram-negative bacteria including *E.coli* due to their ability to interaction the bacterial cells [28].

In addition, the surface modifications and size of AuNPs can affect their antibacterial activity levels [29, 30]. AuNPs show low toxicity to biological systems compared with other NPs whether on the bacteria, animal, or human, as result of its unique elemental properties [31, 32].

AuNPs are generally used in both *in vitro* and *in vivo* investigation due to the uniqueness of their properties as mentioned early, also they have a high chemical stability compared to various nanomaterials, which have encouraged and attracted great interest in drug development [33, 34].

According to Zhou, Y., et al., low concentrations of citrate AuNPs have a larger inhibitory effect on bacterial growth in comparison to high concentrations and that maybe due to smaller aggregates exist at lower AuNPs concentrations and that causes further damage through interacting with bacterial cells.

It is useful to mention that, the effect of AuNPs on bacteria is dependent on their concentration and their affinities for cell surfaces [34, 35]. However, AgNPs have different effects with different concentrations on the *E.coli* in comparison with AuNPs, whereas the highest concentration has the biggest effect on the bacteria [24].

In addition, functionalised AuNPs have biological and chemical activity with high antibacterial efficacy which reinforces their ability to target different bacterial structures [27, 36]. Using a stabiliser groups for NPs can be enhancing dispersion and steric hindrance [37], for instance, carbohydrates can act as a stabiliser and reducing agent in the same time which, leads to the creation of noble metal NPs, and conjugated water soluble NPs with potential antimicrobial applications [38]. As well, the gold(I)–PPh_3 complexes have shown noticeable biological activities: in specific, effective antimicrobial activities against Gram-positive bacteria [39].

It is noted that around 120 different mixed thiols–AuNPs conjugates were shown to be potent growth inhibitors of some types of bacteria including, *E. coli*, *S. aureus*, and *Klebsiella pneumoniae*. thiol–AuNPs conjugates AuNPs activity depended upon the specific combination of ligands attached to the particle surface, it is found that the AuNPs are more potent toward *E. coli* inhibition compare with several small-molecule antibiotics, like ampicillin (11 μM), gentamicin (1 μM), and chloramphenicol (12 μM). Moreover, it is shown that *E. coli* develops resistance against the small-molecule drug chloramphenicol far faster than the AuNPs [8].

In agreement with Chwalibog et al., it is investigated that, the interaction between *S. aureus* and AuNPs were trapped *via* biofilm and the substances which were released by cells and causing distortion of the cell wall [27, 40]. Also, AuNPs can bind closely to the surface of the microorganisms leading to visible damage to the cells membrane. It can lower the treatment period and reduce any side effects of drugs after coated with AuNPs and became highly effective against tested isolates [41]. All negative metal nanoparticles had cell damaging properties. For example, both AgNPs and PtNPs showed the properties of self-organization with the cells, where cells death was observed as a result to holes in the cell wall due to nanoparticles leading to leakage of cell contents. While, AuNPs did not create a system with microorganisms of self-organization, but it causes damage to fungal cells and bacteria due to interaction between the AuNPs and microorganisms [40].

Taylor, E. and Webster, TJ, [42] illustrated that Nanostructures were more safely recommended as some microorganisms were extra resistance against traditional antibiotics than from NPs [17, 42]. As reported by Saha, B., et al., AuNPs conjugated with antibiotics had more antibacterial activity compared to the equivalent free antibiotics without AuNPs, and it is noted that the interaction between AuNPs and antibiotics were based on the adsorption of the antibiotic molecules on the surfaces of AuNPs. It is provided that AuNPs conjugated antibiotics were more stable compared to antibiotic free [26, 41].

In the same way, spherical AuNPs (22–52 nm) functionalised by Cefaclor is used as an antibiotic drug used to treat some infections that is caused by bacteria. Cefaclor which contains a primary amine group which acts as both the capping agent and a reducing agent for the synthesis of AuNPs, leaving the β-lactam ring of Cefaclor available due to its activity against microbes. Antimicrobial results showed that Cefaclor reduced AuNPs have a strong antimicrobial activity against both Gram-negative (*E. coli*) bacteria and Gram-positive (*S. aureus*) compared to Cefaclor or AuNPs alone [43].

Cell surfaces in Gram-negative bacteria are negatively charged as result of phosphate groups and carboxylate groups present in sugar acids. Cell surfaces in Gram-positive bacteria are also negatively charged, mainly due to the teichoic acid polymeric chains, that contain anionic phosphate groups in the glycerol phosphate repeat units [35, 44]. PAH functionalised AuNPs and were synthesised by polyelectrolyte. Poly(allylamine hydrochloride) (PAH) are positively charged and have high toxicity on the Gram-negative and Gram-positive bacteria. Charge densities of AuNPs are correlated directly to ligand densities. For instance, PAH-AuNPs have more positively charged surfaces and higher charge densities cause to stronger electrostatic interactions between cationic PAH-AuNPs and the surfaces of bacterial negatively charged [35].

6.3 Experimental Section

6.3.1 Materials and Methods

All chemicals, including used potassium tetrachloroaurate ($KAuCl_4$ 98%) and $NaBH_4$ were purchased from Sigma-Aldrich and Fisher Scientific Ltd. All solutions were prepared in deionised water. The experiments for antibacterial activity were carried out using different bacterial strains. Non-pathogenic bacteria including (*E. coli* NCIB 8277 and *S. aureus* ATCC 6538P) were provided by the Department of Biosciences, Swansea University / UK. Nutrient media was utilised for evaluating bacterial growth in liquid broth culture. An absorbance of bacterial growth was measured by spectrophotometer at 625 nm.

6.3.2 Antibacterial activity

The antibacterial activity of cationic phosphonium AuNPs against both Gram positive and Gram negative bacteria was confirmed in this Chapter. AuNPs were tested in four different dilutions and the results are summarised in following sections (see Table 6.1). To observe the minimum inhibitory concentration (MIC) of different cationic phosphonium AuNPs, MIC was defined as the lowest concentration of a chemical that prevents the visible growth of a bacterium, and the following procedure was carried out. A 96-well plate (Greiner-Dio-one) and absorbance measured using BioTek Synergy H1 multi-mode reader spectrophotometer was used to measure the effect of AuNPs on the bacterial growth. Nutrient Broth Dehydrated powder was used to make the nutrient broth (NB) medium. All glassware and NB medium were sterilised by incubating for 24 h at 37 °C.

In the tubes (5mL) of the transparent NB media were filled and sterilised by autoclave for 15 min at 121 °C [33, 45]. The bacterial culture was prepared *via* shifting a known Gram-positive bacterial culture (*S. aureus*), and Gram-negative bacteria (*E. coli*) into different tubes including NB media. The positive control (test tubes having AuNPs with nutrient broth media without adding inoculum and a negative control (test tube having inoculum and nutrient broth media, free from AuNPs) incorporated in the experiment. The absorbance values for tubes (containing nutrient broth media, inoculum and AuNPs) were corrected by subtle acting discounting the corresponding absorbance values for the positive controls. All the experiments were confirmed in four replicates.

AuNPs solution were filtered through 30 µm Millipore syringe filters to remove any impurities before use, and were planned with four concentrations for the 4 µL (low dose) solution contained 0.181 µg AuNPs, 8 µL contained 0.363 µg AuNPs, 15 µL contained 0.68 µg AuNPs, and 30 µL (high dose) contained 1.36 µg AuNPs. Four tubes of each dose were prepared and incubated at 37 °C for 24 h. The spectrophotometer was used to observe each micro-well plate which contains 200 µL from each tube [33].

The micro-plate reader was provided with the values of optical density (OD) which were taken in absorption mode with obscured the bacterial growth for each sample, and then both mean and standard deviation were calculated based on four values of OD for every single sample.

Diffusion method was used in order to calculate the inhibition zone *via* using Agar plates, both bacteria *E. coli* and *S. aureus* have developed on the nutrient Agar plate and maintained at 4°C overnight, and then used in the experiments [33, 46]. These two bacterial non-pathogens were coated over the Agar plate by using the sterile swab of cotton and these plates were left to dry. After that, four wells were bored by a sterile well cutter of 6.0 mm diameter in each agar plate. Subsequently, the suspension of AuNPs (30 µL, 15 µL, 8 µL and 4 µL) was poured into wells named 1, 2, 3, and 4 respectively. The initial concentration of AuNPs is 45.34 µg/ml [33].

The plates were placed to dry for 1 h in order to complete diffusion, and after that incubated at 37°C for 24 h. The zones of inhibition were measured. The mean surface area of each inhibition zone (mm) square millimetre was calculated from the mean diameter of each tested antibiotic. The percentage of increase in the inhibition zone areas for different AuNPs bacteria was calculated as $(b^2 - a^2)/a^2 \times 100$ where a is the inhibition zone without AuNPs, while b represents the inhibition zone in the presence of AuNPs [22].

6.3.3 Antimicrobial mechanism of cationic phosphonium AuNPs

The experiments for antibacterial activity were carried out using two kinds of bacterial strains. Nutrient media was used in order to evaluate bacterial growth in liquid broth culture, and the spectrophotometer was used for measuring absorbance of bacterial growth at 625 nm, (the absorbance of AuNPs is zero when compared to suspended bacteria at 625 nm) [47]. The antibacterial effect of each dose of AuNPs was also

calculated statistically. Moreover, estimated value with the standard error were obtained. All the experiments were confirmed four times. Furthermore, all the data of experiments were also analysed through applying ANOVA test ($p < 0.05$).

6.3.4 Synthesis of tris(2,4,6-trimethoxyphenyl)phosphoniopropylthio-chloride zwitterion (2C)

In a round bottom flask with a reflux condenser a mixture of tris(2,4,6-trimethoxyphenyl)-phosphine (**1B**) (3.8mmol) with 3-Chloro-1-propanethiol (15 mmol) were refluxed for five hours in acetonitrile (0.03 mmol) and the white precipitate (**2C**) was collected and re-crystallised from ethanol (see Reaction 1, Scheme 1).

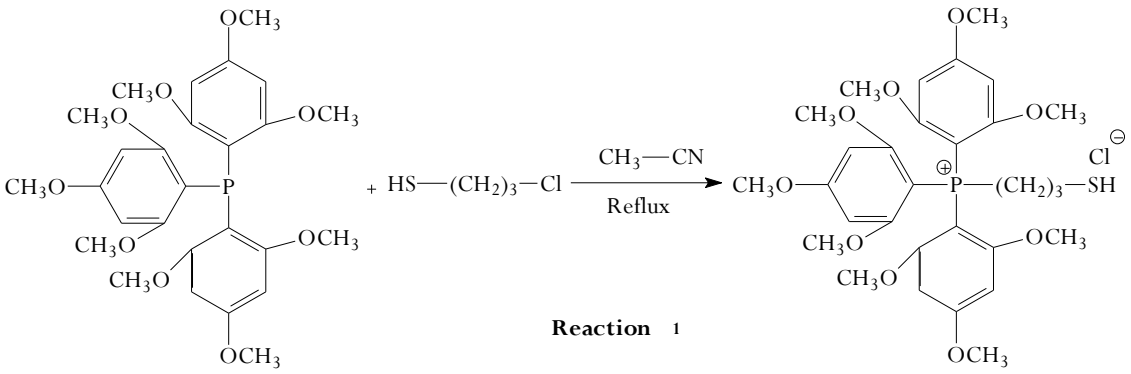

(1B) (2C)

Reaction 1

Scheme 1

6.3.5 Synthesis of (6-thioacetylhexyl)tris(2,4,6-trimethoxyphenyl)-phosphonium bromide ligands zwitterion (8B)

The syntheses of **8B** is shown in Scheme 2 The compound was synthesised *via* reaction of tris(2,4,6-trimethoxyphenyl)phosphine (**1B**) (3.8mmol) with approximately bromo-hexanol (15 mmol) in a round bottom flask with a reflux condenser were refluxed for five hours in acetonitrile (0.024 mmol), a brown solid was collected and re-crystallised from diethyl ether (Reaction 1, Scheme 2).

The resulting salt (**6B**) was dissolved in hydrobromic acid (0.18 mmol, 10 ml) (48%) in a round bottom under reflux five hours (Reaction 2, Scheme 2). Then a mixture of ω-

bromohexyl-tris(2,4,6-trimethoxyphenyl)phosphonium bromide (**7B**) (2 mmol) and potassium thioacetate (3 mmol) were stirring overnight at room temperature in aqueous ethanol (1:1, 10ml) (Reaction 3, Scheme 2). The compounds looked as a brown precipitate **8B**. TLC has used to monitor the reactions by using 20 % methanol: 80 % DCM (dichloromethane) as a mobile phase. The ligand **8B** were achieved by DCM extraction of the mixture of reaction and purified by diethyl ether.

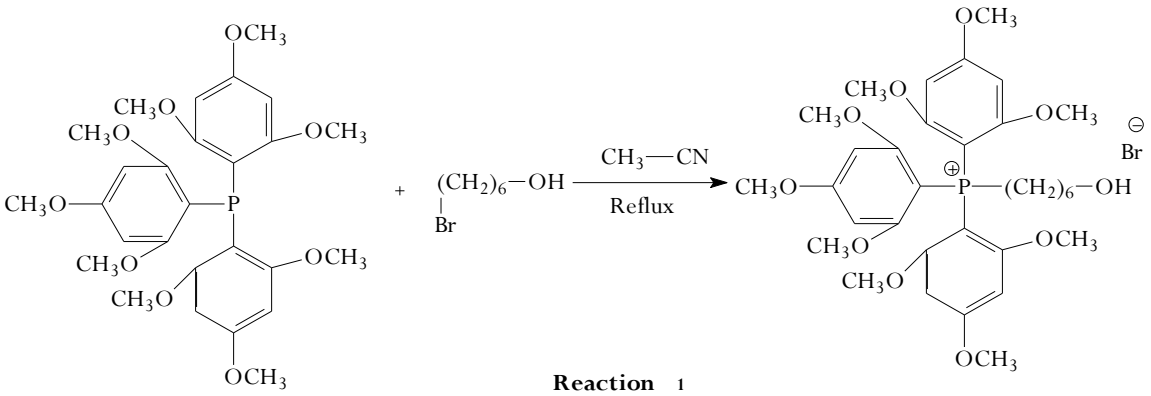

Reaction 1

(1B) (6B)

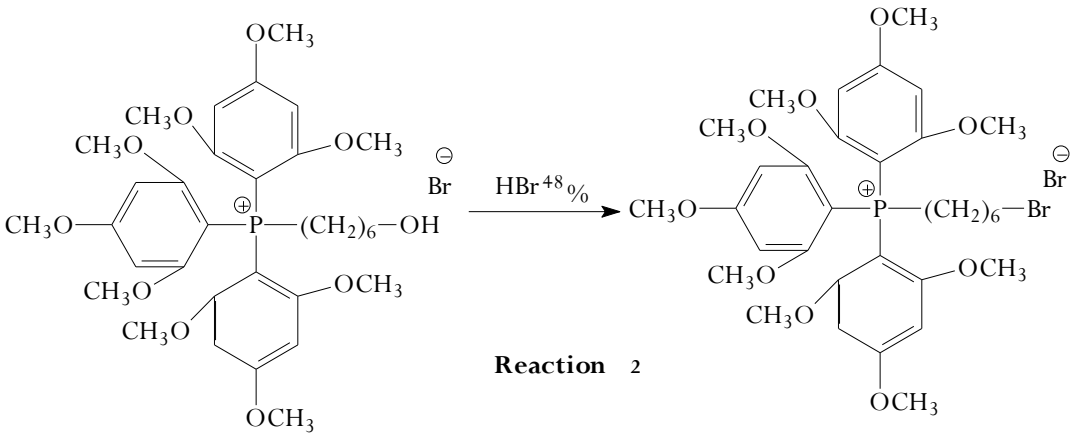

Reaction 2

(6B) (7B)

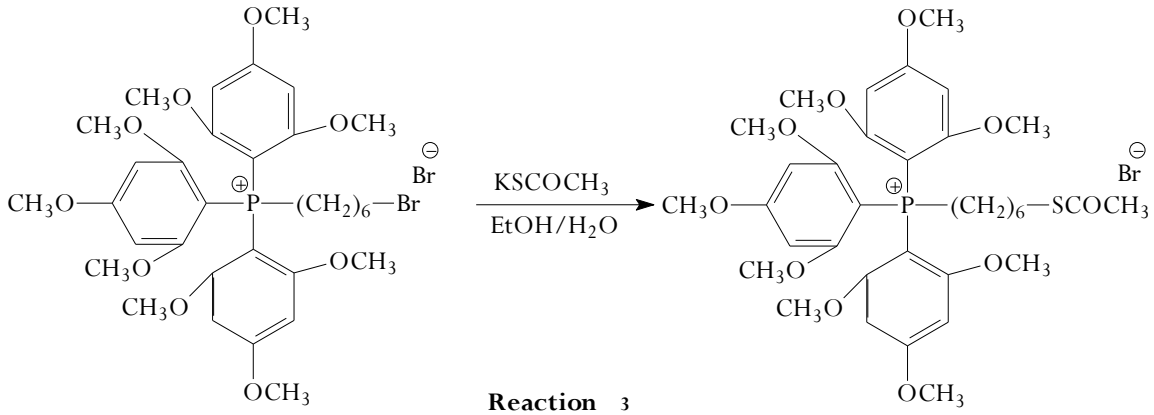

(7B) (8 B)

Reaction 3

Scheme 2

This Chapter is restricted to in vitro experiments. Our attention is focused on evaluating the results against non-pathogens of a small AuNPs with different compositions and surface modifications, also AuNPs were chosen to have slightly similar sizes and shapes.

6.3.6 Synthesis gold nanoparticles

AuNPs have synthesised with good controlled and well-characterized surface chemistries by using triphenylphosphoniopropylthiosulfate (**4C**) and (3-thioacetylpropyl)tri(*p*-tolyl)phosphonium bromide (**4A**) compounds which have been mentioned in Chapters (2 and 3 respectively). However, (6-thioacetylhexyl)tris(2,4,6-trimethoxyphenyl)-phosphonium bromide (**8B**) and tris(2,4,6-trimethoxyphenyl)-phosphoniopropylthiochloride (**2C**) as protected ligands to preventing AuNPs from forming aggregates as will describe below. UV-Vis with DLS measurement were taken continuously to measure stabilities of AuNPs. The surface plasmon resonance of the AuNPs was recorded for nearly four months. The data were presented in Figures 6.9-6.12 below. SPR of the particles remained stable to some extent throughout this period of time indicating that the AuNPs particles behaved in a quite stable manner when functionalised by these ligands.

All these ligands have the same preparation technique. **2C** and **8B** were prepared in DMSO (0.16 mmol, 0.30 mmol respectively). The volume used for these solutions was 30 mL. A solution of potassium tetrachloroaurate (0.12 mmol) in DMSO (10 mL) was also prepared. Then both, ligands and gold salt solutions were mixed and stirred. The

reduction was carried out by adding 5 mL of a freshly prepared aqueous solution of sodium borohydride (2.0 mmol) to the DMSO mixture. Liquid-liquid extractions were carried out by using diethyl ether in order to remove the excess of ligands in each one of the colloidal AuNPs solutions.

6.4 Results and Discussion

The AuNPs were characterised by UV-Vis spectroscopy and DLS. While, the ligands characterised by ATR, ESI-MS and NMR. The effect of AuNPs functionalised by **4A** and **2C** on *E.coli* cells were found to be significantly more sensitive than AuNPs functionalised by **4C** and **8B**.

However, all these compounds in this Chapter have enormous influence on *S. aureus*. AuNPs functionalised with **8B** exhibited high antibacterial resistance to both Gram positive and Gram-negative bacteria, perhaps due to its chemical structure when compared to other compounds. *E. coli* was inhibited 13% at 0.181 µg and 24 % at 0.181 µg (low dose), by AuNPs functionalised by **2C** and **4A** respectively. While, *S. aureus* was inhibited 12% at 0.36 µg (third dose), 14% at 0.68 µg (second dose) and 76% at 0.181 µg (low dose), by AuNPs functionalised by **4C**, **2C** and **4A** respectively, (see Figures 6.1, 6.2).

AuNPs stabilised by **4A** exposed the accompanying reduction in growth. For example, at high concentration (1.63 µg-30 µL), the growth of *S. aureus* reducing to 93.71%. While 76% was calculated, when low concentration (0.181 µg-4 µL) used. However, *E. coli* with a maximum reducing in its growth was 95.3% and was become up to 24.2% in low concentration (0.181 µg-4 µL), at the third concentration (0.363 µg-8 µL) was 79%. Thus, for complete inhibition of *S. aureus*, a smaller dose (0.181 µg-4 µL) is required, whereas the third dose (0.363 µg-8 µL) is required in case of *E. coli*, as Figure 6.8 shown. Based on these results, AuNPs functionalised by **4A** exhibited highest antibacterial sensitivity to both kinds of bacteria.

AuNPs functionalised by **2C** has a slightly lower effect than **4A**-AuNPs but more effect than **4C**-AuNPs. In contrast, AuNPs functionalised with **8B** had no influence on both types of bacteria, maybe due to increase in length of the side chain in this compound compared with above ones. Percentage influence of AuNPs was different according to a

variety of ligand stabilisers as is given in Table 6.1. Selvaraj, V., and Alagar, M, found that AuNPs citrate-capped offer 27 mm for the inhibition zone of *E. coli* [48]. In contrast, Nazari, ZE., et al., counted 14 mm and 13 mm for the inhibition zones for both *E. coli* and *S. aureus* respectively [22]. Whereas Shamaila, S., et al., revealed that the inhibition zones were different with a variety of AuNPs size, for instance, AuNPs with size 7–34 nm against *E. coli* and *S. aureus* were ~31 mm and 22 mm respectively. Inhibition zones were about 35 mm and 25 mm in AuNPs sized 20–40 nm, respectively [33].

In this Chapter, the zone of inhibition for AuNPs stabilised by compounds **4C**, **2C** and **4A** against *S. aureus* were found to be 16, 8.5 and 23 mm respectively, in contrast, the inhibition zone was 22 mm and 21 mm on *E. coli* for AuNPs stabilised by compound **2C** and **4A** respectively. However, AuNPs were stabilised by compounds **4C** and **8B** did not have any remarkable effect on *E. coli*. These differences appear to be based on the basic distinction between the ligands coated of AuNPs which may be leading to different affinity of AuNPs to cells of the bacterial species used. According to Rotello, VM., et al., uptake and removal of NPs in cells / tissues are reliant on upon their physiochemical properties. For instance, cationic NPs have higher uptake and a slower rate of exocytosis in cells compared to their anionic NPs [9].

Moreover, AuNPs functionalised with 3-mercaptopropionic acid (MPA) have the lowest toxicity on bacterial strains, while AuNPs functionalised with PAH have the highest cell death due to its strong affinity between bacteria cell and the cationic polyelectrolyte coating on this PAH–AuNPs. This evidence may guide future studies of ligands functionalised NPs [35]. Cationic AuNPs might be effective adjuvants to identified antibiotics, as they were shown to modify the cell surface; also, the multi-drug-resistant infections can be treated *via* surface-binding NPs [49]. Positively charged molecules have been chosen as ligands of AuNPs in order to increase the permeability of the outer membrane of bacteria [47].

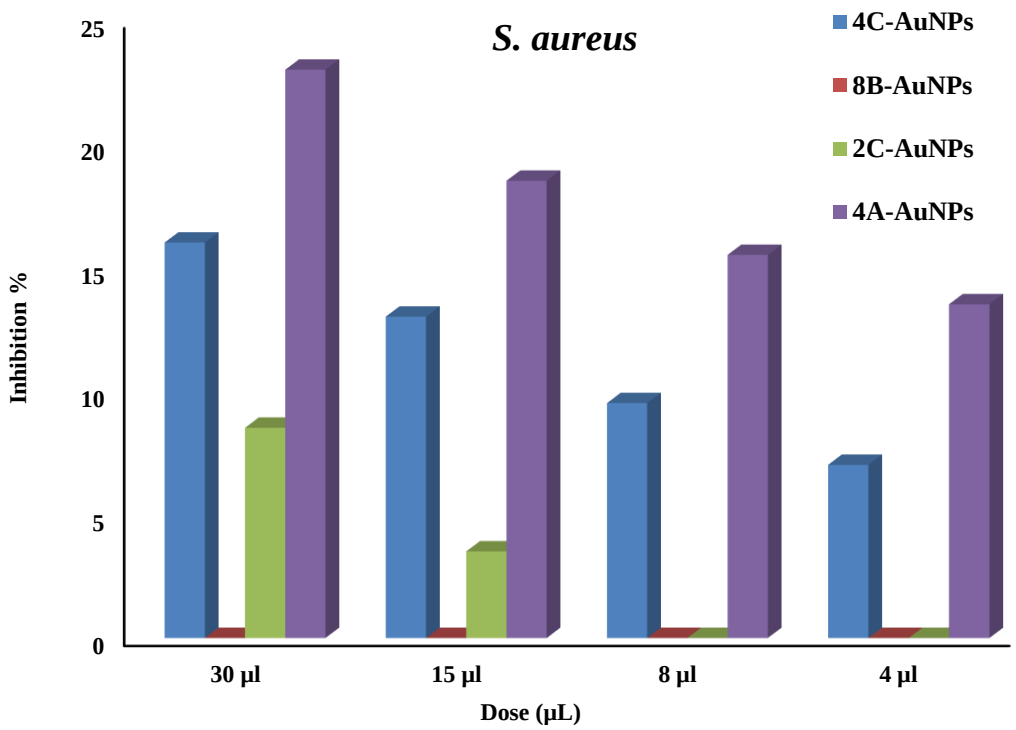

Figure 6.1. Percentage of inhibition of S. aureus, which treated by **4C**-AuNPs, **8B**-AuNPs, **2C**-AuNPs, and **4A**-AuNPs at different, concentrations (1.36 µg-30 µL), (0.63 µg-15 µL), (0.363 µg-8 µL), and (0.181 µg-4 µL) respectively.

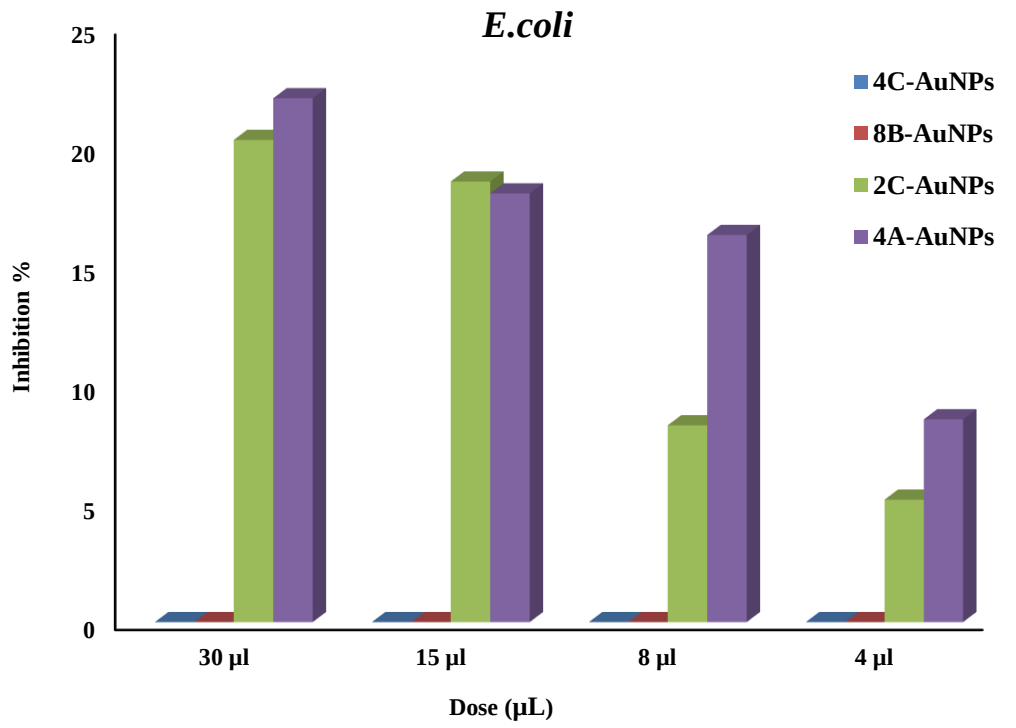

Figure 6.2. Percentage of inhibition of *E. coli*, which treated by **4C** -AuNPs, **8B**- AuNPs, **2C**-AuNPs, and **4A**-AuNPs at different, concentrations (1.36 µg-30 µL), (0.63 µg-15 µL), (0.363 µg-8 µL), and (0.181 µg-4 µL) respectively.

Figure 6.1 and 6.2 show analysis results of percent's inhibition for all AuNPs against *S. aureus* and *E. coli*. The inhibition percentages were zero when **8B**-AuNP tested on both of bacteria. While, significant increase inhibition percentages of *S. aureus* and *E. coli* showed when **4A**-AuNP tested.

According to Kirby-Bauer test for antibiotic susceptibility, the zone diameter interpretation (see Table 6.1) is as follows: (R) Resistant: 13 mm or less; (I) Intermediate: 14-16 mm; and (S) Susceptible: 17 mm or more [50]. From Table 6.1, *E. coli* isolate is reading as susceptible to **4A**-AuNPs and **2C**-AuNPs at the high and second dose. However, *S. aureus* is reading as resistant to **2C**-AuNPs and as intermediate to **4C**-AuNPs.

For **4A**-AuNPs, both *E. coli* and *S. aureus* were susceptible at the high and second dose. In addition, *E. coli* resisted at different concentrations of **4C**-AuNPs, whereas the growth-inhibitory effects on *S. aureus* were mild. **8B**-AuNPs has shown no activity toward both *E. coli* and *S. aureus*.

In previous studies, reduction of growth inhibition effect of AuNPs on different types of bacteria was reported [51, 52]. In this study, it found that **2C**, **4C**, **4A** and **8B**-AuNPs with sizes in range from 8-17 nm and $NaBH_4$ used as reducing agent have remarkable effect on the *E. coli* and *S. aureus* bacteria as mentioned above. While the effect of 15 nm citrate capped AuNPs on the growth of *E. coli* was indicated that there was no important toxic effect caused by AuNPs as mentioned in the literature [52]. According to the literature, sizes based toxicity of AuNPs are reported, it has been found that smaller particles possess some degree of toxicity more than the bigger particles. It was expected that smaller NPs can easily penetrate in the bacteria cells and affect their growth [53], and that confirms our results in this Chapter which showed bacteria growth were affected by small AuNPs.

Furthermore, current results showed that bacterial growth curve decreased constantly with increasing AuNPs concentration. Also, AuNPs with the highest concentration showed almost slightly growth of *E. coli* NCIB 8277 and *S. aureus* ATCC 6538P. In addition, *S. aureus* and *E. coli* display clearly different inhibition zone according to variety of AuNPs with different concentration as explained in current study (see Figures 6.3 and 6.4).

Table 6.1. Illustrates calculation of zone of inhibition of two types of bacteria at different concentrations, (1.36 µg-30 µL, 0.63 µg-15 µL, 0.363 µg-8 µL, 0.181 µg-4 µL) of **4C**-AuNPs, **8B**-AuNPs, **2C**-AuNPs, and **4A**-AuNPs.

Micro Organism	**Organism Category**	**Concentration µg/ml**		**Control**	**Zone of inhibition (mm).**			
		Dose µl	Au. µg		**4C-AuNPs**	**8B -AuNPs-**	**2C -AuNPs**	**4A-AuNPs**
S. aureus	Gram Positive	30	1.36	0	16	Nil	9	23
		15	0.68	0	13	Nil	4	19
		8	0.363	0	10	Nil	Nil	16
		4	0.181	0	7	Nil	Nil	14
E.coli	Gram Negative	30	1.36	0	Nil	Nil	21	22
		15	0.68	0	Nil	Nil	18.5	18
		8	0.363	0	Nil	Nil	9	17
		4	0.181	0	Nil	Nil	5	9

The toxicity of the NPs on the bacteria is believed to be caused as a result of interaction between NPs and bacteria cells, where dissolved ions of NPs can easily penetrate the cell membrane and showing their toxicity in the cytoplasm [54, 55].

Toxicity of the AuNPs was supported by the data presented in this Chapter, which demonstrated significant inhibition of the bacteria growth after the high concentration of AuNPs applied.

Several MIC and zone diameter values confirmed each other and from the data presented, the diameters of inhibition zones (in millimetre) were calculated based on the content of

AuNPs producing clear zone of inhibition at different concentration after 24h at 37°C [22], and it appears that no antibacterial activity was observed for **8B**-AuNPs at different concentrations against both bacteria. However, **4A**-AuNPs have the higher antibacterial effect on *E. coli* and *S. aureus* and the inhibition zones were 22 mm and 23 mm at high concentration, respectively. While at lower concentration (0.181 µg/ 4µL) were 9 mm and 14 mm. **2C**-AuNPs had a slightly smaller zone of inhibition than **4A**-AuNPs and was 21 mm on *E. coli* at high and 5 mm at low concentrations (0.181 µg/ 4µL), but the results are not significant for the zone of inhibition in the case of *S. aureus* which showed only 9 mm and 0.2 mm at high and third concentrations with no effect at lower concentration. The maximum inhibition zones are an extra support to confirm the data of MICs calculations as illustrated in Table 6.1 and Figures 6.3-6.8.

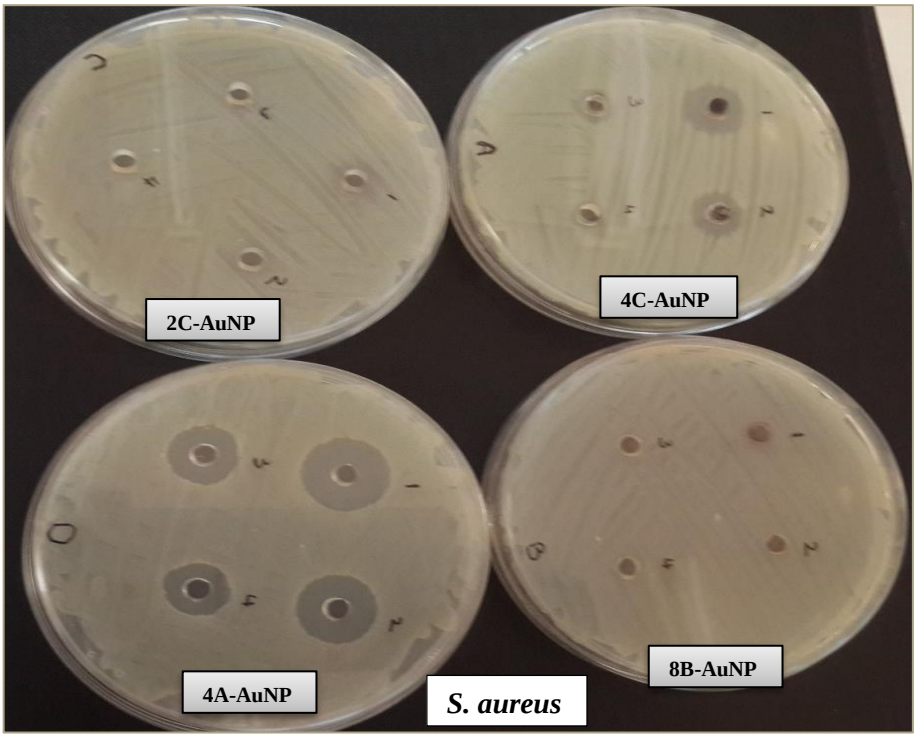

Figure 6.3. An antibacterial activity of four kinds of AuNPs against *S. aureus*. Where **A** = **4C**-AuNPs, **B** = **8B**-AuNPs, **C** = **2C**-AuNPs and **D** = **4A**-AuNPs. 1, 2, 3, 4 are represent, concentrations (1.36 µg-30 µL, 0.63 µg-15 µL, 0.363 µg-8 µL, 0.181 µg-4 µL respectively).

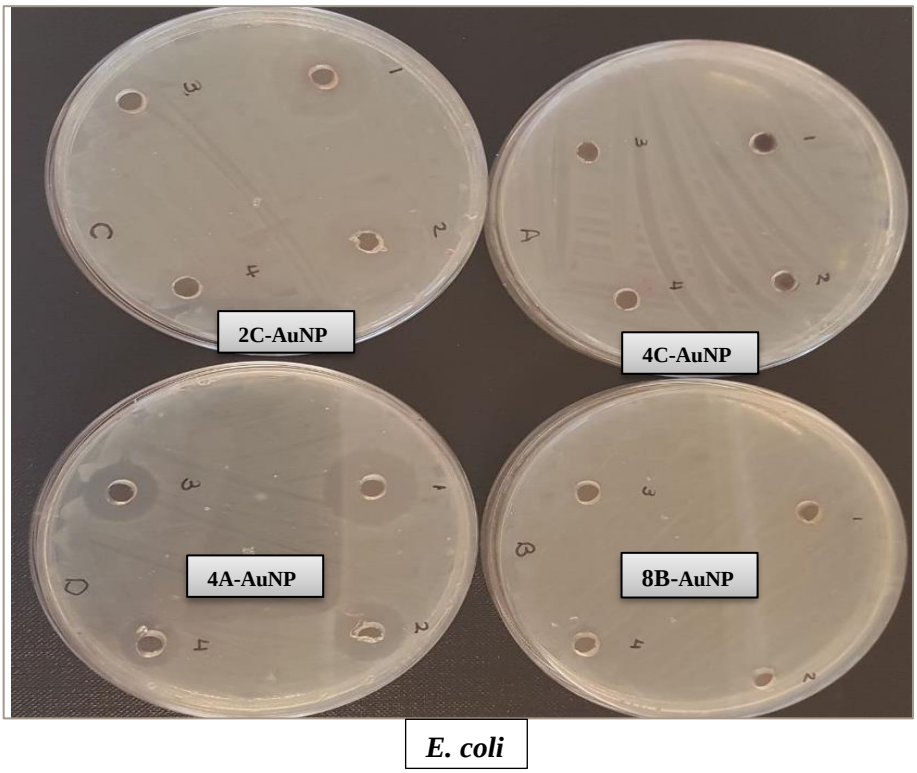

Figure 6.4. An antibacterial activity of four kinds of AuNPs against *E. coli*, where **A** = **4C**-AuNPs, **B** = **8B**-AuNPs, **C** = **2C**-AuNPs and **D** = **4A**-AuNPs. 1, 2, 3, 4 are represent, concentrations (1.36 µg-30 µL, 0.63 µg-15 µL, 0.363 µg-8 µL, 0.181 µg-4 µL respectively).

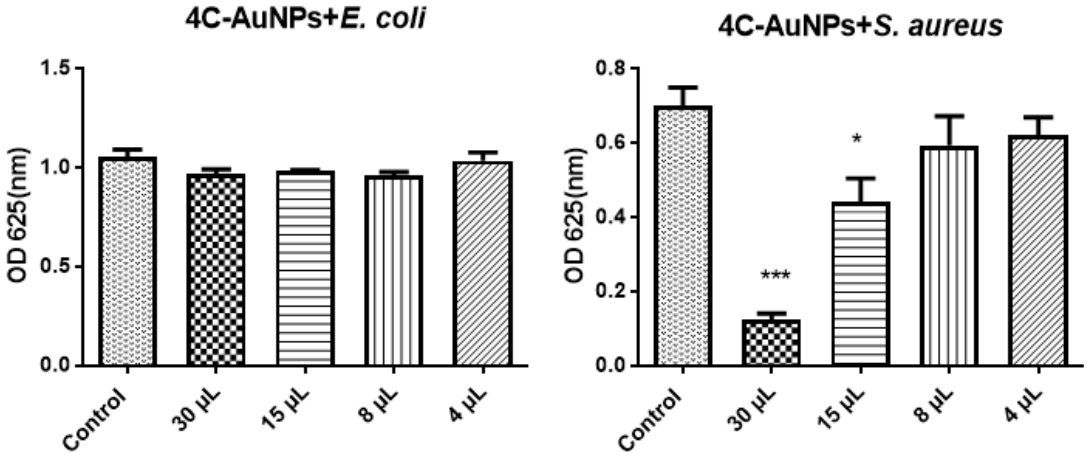

Figure 6.5. An antibacterial activity of **4C**-AuNPs against *E. coli* and *S. aureus* bacteria, at different, concentrations (1.36 µg-30 µL), (0.63 µg-15 µL), (0.363 µg-8 µL), and (0.181 µg-4 µL) respectively. Where, (*** represents $p \leq 0.0001$), (** represents $p \leq 0.001$), (*represents $p \leq 0.05$).

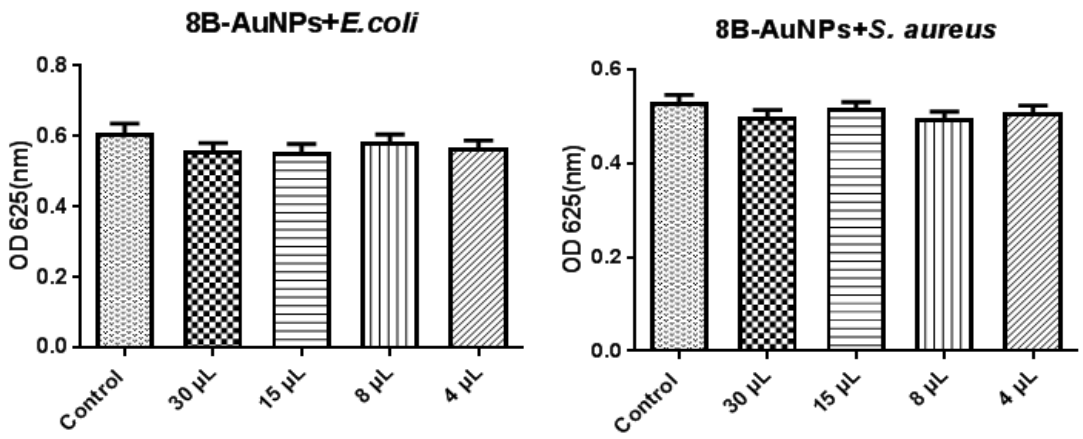

Figure 6.6. An antibacterial activity of **8B**-AuNPs against *E*. coli and *S. aureus* bacteria, at different, concentrations (1.36 µg-30 µL), (0.63 µg-15 µL), (0.363 µg-8 µL), and (0.181 µg-4 µL) respectively.

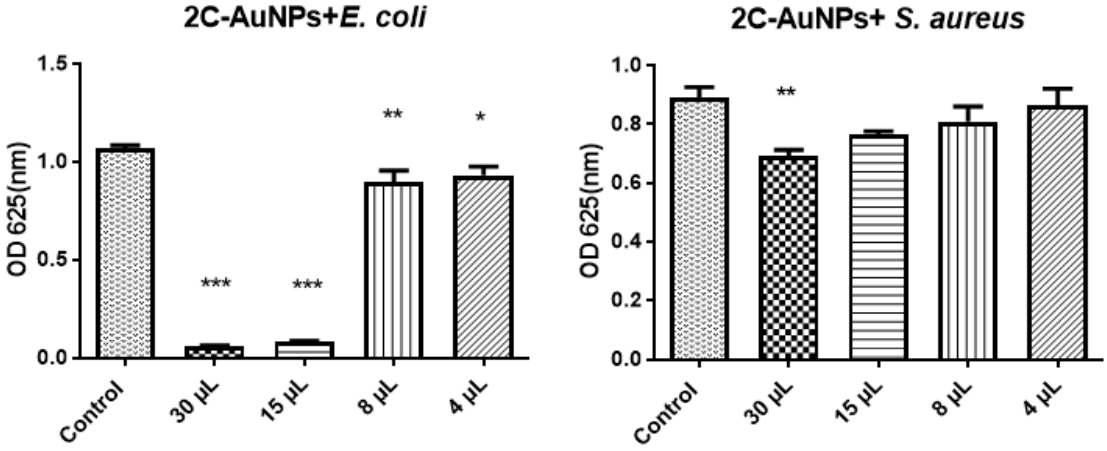

Figure 6.7. An antibacterial activity of **2C**-AuNPs against *E. coli* and *S. aureus* bacteria, at different, concentrations (1.36 µg-30 µL), (0.63 µg-15 µL), (0.363 µg-8 µL), and (0.181 µg-4 µL) respectively. Where (*** represents p-value ≤ 0.0001), (** represents p ≤ 0.001), (*represents p ≤ 0.05).

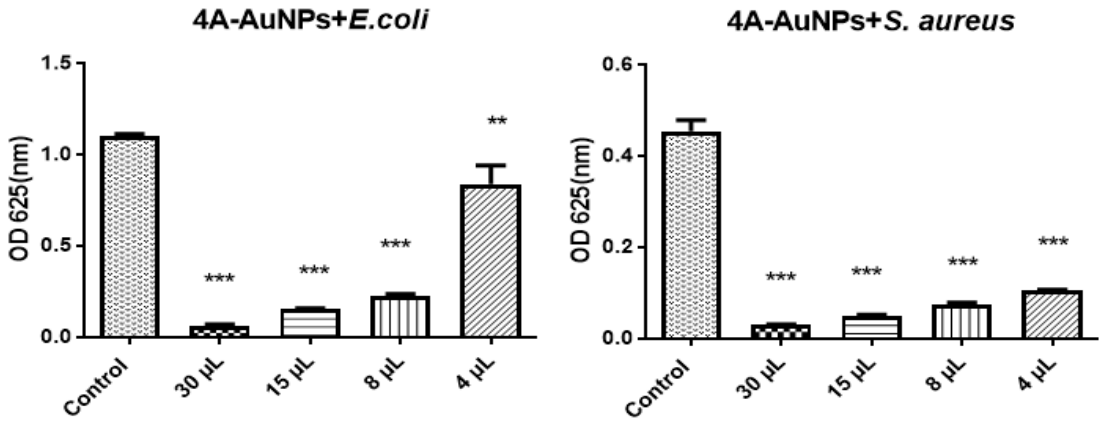

Figure 6.8. An antibacterial activity of **4A**-AuNPs against *E. coli* and *S. aureus* bacteria, at different, concentrations (1.36 µg-30 µL), (0.63 µg-15 µL), (0.363 µg-8 µL), and (0.181 µg-4 µL) respectively. (*** represents p-value ≤ 0.0001), (** represents p ≤ 0.001).

Due to the high surface to volume ratio of NPs, allows incorporation of plentiful functional ligands, enabling multivalency on the surface of NP in order to enhance interactions to target bacteria. For example, NPs conjugated with known antibiotics in order to affect MDR bacteria. The antibiotic molecules can be infused with NPs via noncovalent or covalent bonds interactions [1, 23].

As stated with Li, X., et al., modification of the functional groups on the surface of the cationic monolayer-protected AuNPs (2 nm) increasing it's effective against clinical isolates, such as Gram-negative (*E. coli* CD-2) and Gram-positive (*S. aureus* CD-489), and showed no evidence for bacterial resistance. AuNPs functionalised by different cationic ligands with changing in chain length, nonaromatic and aromatic characteristics with the hydrophobic end group offer antimicrobial efficacy. For example, the results of 2 nm AuNPs with cationic surface properties suggested that cationic AuNPs could be used as antimicrobial agents [1].

Herein, the effects of functionalised AuNPs, on non-pathogenic bacteria were obvious. Different affected were noted based on different functional groups used. For instance, with changing aromatic groups from benzene in **4C**-AuNP, to toluene in **4A**-AuNP, and to trimethoxy-benzene in both **2C**-AuNP and **8B**-AuNP, different results collected. As well as, length carbon chain could offer variety effects on the bacteria. A strong relationship was observed between the structure of AuNPs and their bio-activities. For instance, from Figures 6.3-6.8, the biggest effect on *E coli* and *S. aureus* was from AuNP functionalised by **4A** (see Figures 6.3, 6.4 and 6.8) which was harmfulness to both bacterial cells especially at high concentration (30 µL). The **4A** contains three toluene groups in its structure, which might contribute to increase the bioactivity for AuNPs.

The second effect was noted from **2C**-AuNP, which exhibit clear influence on *E coli* more than in the case of *S. aureus*. It is possible that the structure of the bacteria is also a factor. **2C**-AuNP contains trimethoxy-benzene with 3 carbon chain length. While AuNP functionalised by **8B**-AuNP, which also contains trimethoxy-benzene in its structure. However, **8B**-AuNPs has not offer any effect on both types of bacteria maybe because it contains 6 carbon chain length rather than three carbon atoms like **2C**-AuNP (see Schemes 1, 2 and Figure 6.6).

AuNPs functionalised by **4C** has more effect on *S. aureus* than in the case of *E. coli*, where in the case *E coli* has not any obvious effect despite different concentrations used (see Figures 6.5 and 6.4). In contrast, in the case of the *S. aureus* shown slightly effect at high dose (30 µL) and second dose (15 µL), but no effective showed at the third (8 µL) and low dose (4 µL) as illustrated in Figures 6.3 and 6.5).

Consequently, AuNPs with different functionalised ligands showed different effects on the bacteria growth, which confirm that surface chemistry of the AuNPs is a very important factor in terms of the effect of the AuNPs on the bacterial cells. Moreover, that explained why the bacteria were resisted and not affected when treated by **8B**-AuNP in comparison with other AuNPs in this Chapter as mentioned.

6.4.1 Characterisation of the cationic AuNP functionalised by tris(2,4,6-trimethoxyphenyl)phosphoniopropylthiolchloride zwitterion (2C) and 8B by using UV-Visible and DLS studies

Evidence of the formation of AuNPs functionalised by **2C** was shown by UV-Visible spectroscopy technique.in Figure 6.9. Quartz cell containing DMSO served as a reference, bands centred at 540 nm.

According to DLS results, mean diameters obtained for the AuNP functionalised by **2C** analysed was 17.8 ± 2 nm and changed after 14 weeks to 39.2 ± 3 nm which confirm the UV result as shown wavelength at 540 nm and at 555 nm at time = 0 and 14 weeks respectively. In addition, the evidence of the formation of AuNPs functionalised by **8B** using the reduction method in DMSO was shown by UV-Visible spectroscopy technique.in Figure 6.11. Using the DMSO as the blank, bands centred at 522 nm. These results are also in agreement DLS analysis of AuNPs.

For mean diameters obtained for the **8B**-AuNPs analysed were the followings: 9.2 ± 0.9 nm (Figure 6.12) and changed to 20.4 ± 1.7 nm after 11 weeks. DLS and UV-vis show that all the AuNPs in this Chapter are round and spherical in shape and in a mono-dispersional state without clear obvious aggregations. That is due to electrostatic repulsion and prevents aggregation of AuNPs. According to UV-Visible spectrum results, which showed that the SPB of AuNP functionalised by **2C** is centred at 540 nm and convert to 555 nm after about 14 weeks, and from 522 nm to 524 nm in **8B** after 11 weeks may be due to increase the particle size but there is no evidence for aggregation.

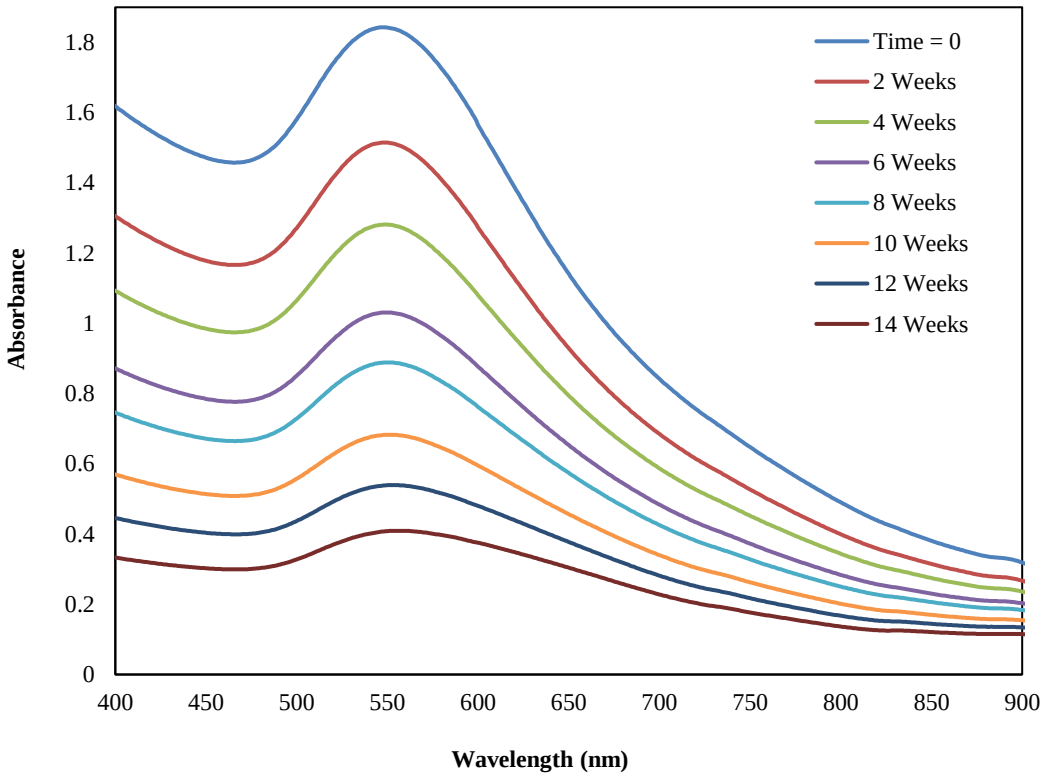

Figure 6.9. UV-visible absorption spectra of the colloidal solutions of AuNPs functionalised using **2C** as protecting ligand. The different UV-visible spectra represent these Au nanoparticles dispersed in DMSO at time = 0, 2, 4, 6, 8, 10, 12 and 14 weeks.

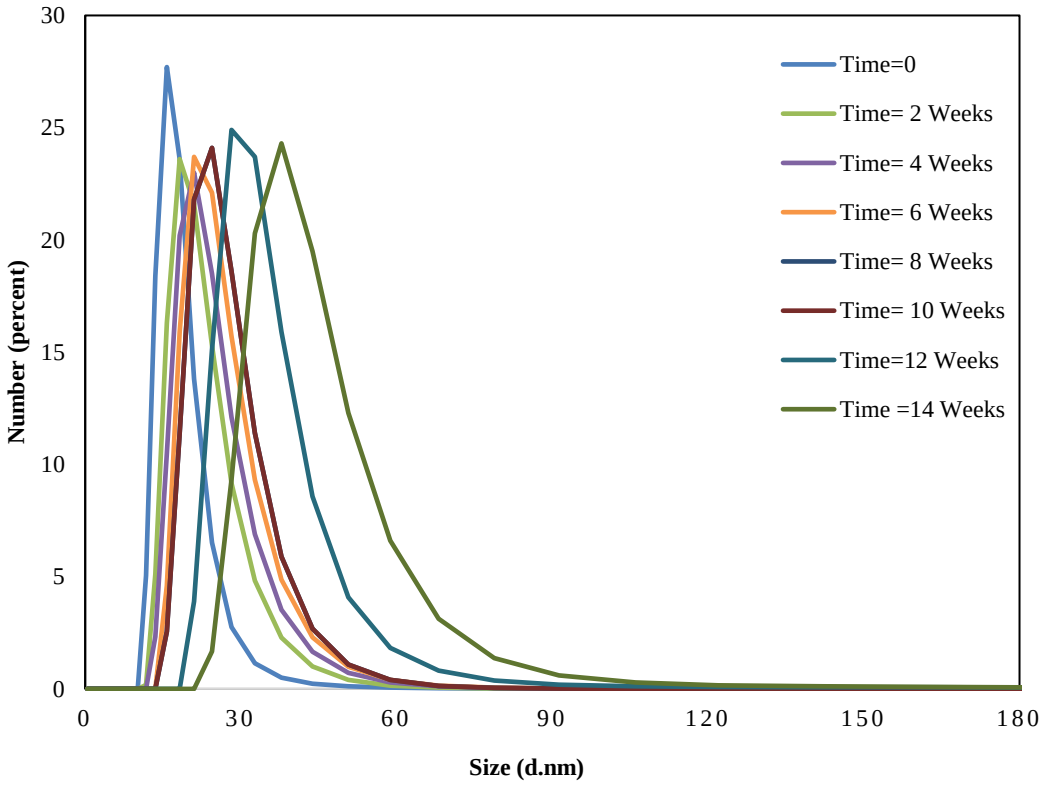

Figure 6.10. DLS for AuNP functionalised by **2C**. Sizes increased as time increased

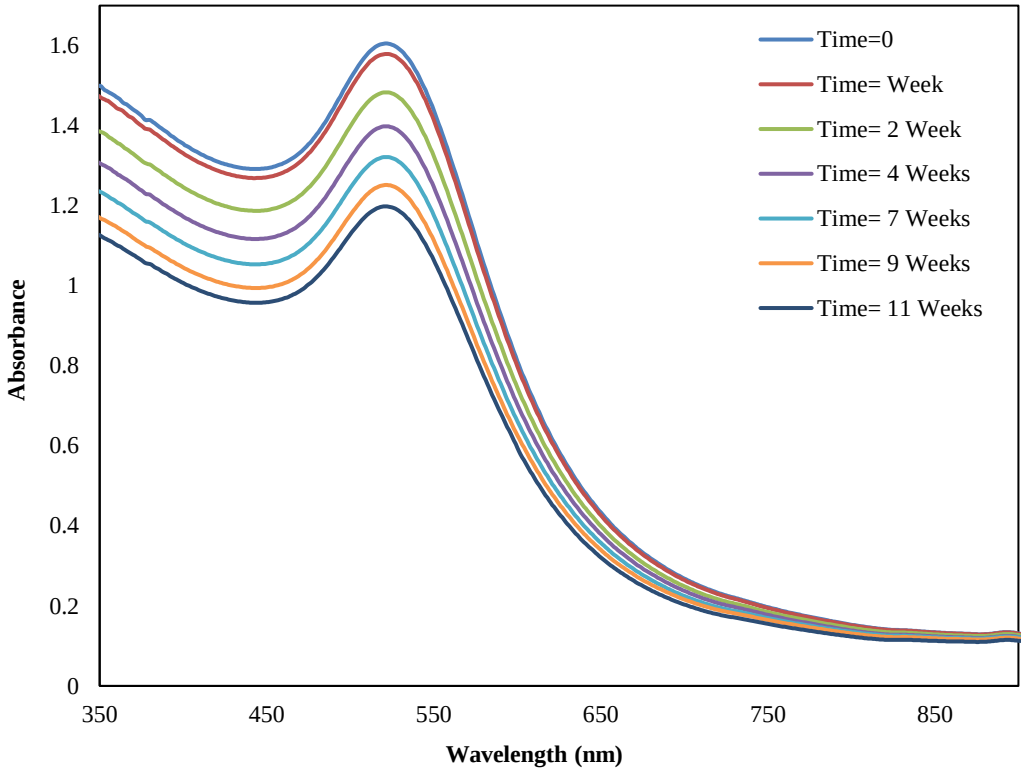

Figure 6.11. UV-visible absorption spectra of the colloidal solutions of AuNPs functionalised using **8B** as protecting ligand. The different UV-visible spectra represent these nanoparticles dispersed in DMSO at time = 0, 1, 2, 4, 7, 9 and 11 weeks.

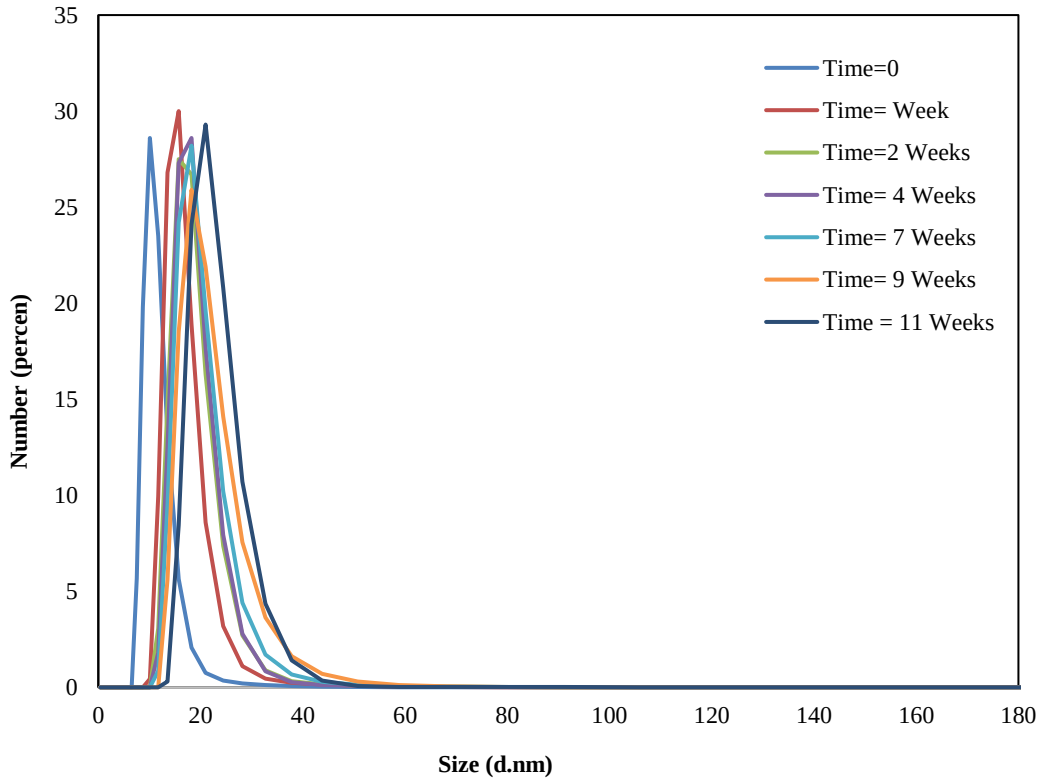

Figure 6.12. DLS of AuNPs synthesised using **8B** as protecting ligand in DMSO, and corresponding particle size histograms.

It is noted that from the literature, the SPR peaks of the AuNPs with a diameter of ~15 nm showed the wavelength at 520 nm and AuNPs with a diameter of ~30 nm exhibited the absorbance peak at wavelength 524 nm [56].

6.4.2 Characterisation of the cationic phosphonium ligands

Several analytical techniques such as TLC, ATR-FTIR, NMR, and ESI-MS techniques were used in order to characterise the ligands in this Chapter before using as protecting ligands for AuNPs.

6.4.3 Tris(2,4,6-trimethoxyphenyl)phosphoniopropylthiochloride zwitterion (2C)

The synthesis of **2C** is shown in Scheme 1. IR, NMR, ESI-MS have used for confirming this ligand is illustrated below.

IR spectrum showed absorption bands at the regions of 800 – 829 cm^{-1} (ν CH_2), 2565 cm^{-1} (ν SH), 1593 cm^{-1} (ν C-O), 1337 cm^{-1} (C-S-) and 3138–3065 cm^{-1} (ν CH-Aromatic). NMR: ^{1}H NMR = ($CDCL_3$) spectrum gave signals at 3.4 (2H, t, -$\underline{CH_2}$-P), δ 3.3-3.7 (27H, s, Ph-$\underline{OCH_3}$), δ 2.4 (2H, m, -$\underline{CH_2}$-), δ 2.1 (2H, t, -$\underline{CH_2}$-SH), δ 1.5 (1H, s, SH), and at 6.3 – 6.5 (6H, m, Aromatic H) ppm. ESI-MS 607.20 $[M\text{-}Cl]^+$. The yield of **2C** was 85%. Melting point: 120-122 °C.

6.4.4 (6-thioacetylhexyl)-tris(2,4,6-trimethoxyphenyl)phosphonium bromide zwitterion (8B)

IR spectrum for **8B** showed absorption bands at 800–829 cm^{-1} (ν CH_2), 1739 cm^{-1} (ν C=O), 1595 cm^{-1} (ν C-O), 1366 cm^{-1} (C-S-), 1146 cm^{-1} (ν P=O) and 3138–3065 cm^{-1} (ν CH-Aromatic). NMR: ^{1}H NMR = (CD_2CL_2) spectrum gave signals at at δ 3.5 (3H, s, CO-$\underline{CH_3}$), δ 4.0 (2H, t, P- $\underline{CH_2}CH_2$-CH_2-), δ3.3 (2H, t, -$\underline{CH_2}$-SCO), δ 2.5 (2H, m, $\underline{CH_2}$-CH_2-SCO), δ 2.0 (2H, m, $CH_2\underline{CH_2}$-CH_2-), δ 1.8 (2H, m, -$\underline{CH_2}$-),δ 1.4 (2H, m, -$\underline{CH_2}$-), δ 5.6-6.2 (27H, s, Ph-$\underline{OCH_3}$) and at 9.7 – 10.6 (6H, m, Aromatic H) ppm. ESI-MS 691.23 $[M - Br]^+$ .The yield of **8B** was 75%. Melting point: 206-208 °C.

The structure of compound **2C** was confirmed from its correct spectral data. Thus, IR spectroscopy detects the vibration characteristics of chemical functional groups of the **2C** showed absorption band at the regions 2565 cm^{-1} which confirm entry of thiol group (ν

SH) to tris(2,4,6-trimethoxyphenyl)phosphine (**1B**). Also, there was a peak at 1593 cm^{-1} bond which corresponded to an ether group (C-O). Also (C-S-) stretching vibration has been assigned to a weak band in the region 621 cm^{-l} in **2C** [57, 58]. For ligand **8B**, there were peaks at 1591 cm^{-1} and 1366 cm^{-1} for (ν C-O) and (C-S) respectively. The important group to confirm conform **8B** is a present peak at 1739 cm^{-1} in IR spectra to indicate to a carbonyl group (ν C=O) [58].

^{1}H NMR spectra provided further evidence for completed reaction for **2C** which confirmed the existence thiol band (1H, s, SH) in **2C,** which appear at δ 1.5 in $CDCl_3$ [59]. In addition, present twelve protons -$(CH_2)_6$ attached to the aromatic ring at chemical shifts from 1.4 - 4.0 ppm to produce compound **8B**, due to absence this group in the start material tris(2,4,6-trimethoxyphenyl)phosphine (**1B**). Furthermore, final products **2C** and **8B** were confirmed by ESI-MS, and ions corresponding to $[M\text{-}Cl]^{+}$ and $[M\text{-}Br]^{+}$ were observed at ESI-MS 607.20 *m/z* for **2C** and 691.23 *m/z* for **8B**, while (expected MW **2C** and **8B** are 642.5 and 770.9 g/mol respectively [60]. Based on these spectral data, compound **2C** and **8B** were assumed to be tris(2,4,6-trimethoxyphenyl)-phosphoniopropylthiochloride and (6-thioacetylhexyl)tris(2,4,6-trimethoxyphenyl)-phosphonium bromide zwitterion respectively.

6.5 Conclusion

In conclusion, novel cationic phosphonium AuNPs with different capping agents were synthesised using methods described in the experimental sections and thoroughly tested. The overall aim was to study the effect of AuNPs on the growth of two kinds of bacteria. It has been confirmed that our AuNPs display significant antibacterial potential for the both Gram negative bacteria (*E. coli*) and the Gram positive bacteria (*S. aureus*) *via* changing AuNPs surface chemistry. AuNPs with similar sizes exhibited different inhibitory effects at the same initial concentration and different doses. The minimum inhibitory content was determined as the lowest content of AuNPs. In addition, the MIC calculations of these AuNPs were also supportive of the results that calculated from the inhibition zones and confirm each other.

AuNPs functionalised by different ligands display different results on the same type of bacteria. For example, AuNPs functionalised by **4A** have the biggest effect on both kind of bacteria compared to other AuNPs used. As result to present tolyl groups in **4A**–AuNP

structure, this increased its effect against the bacteria. **2C** and **8B** have similar chemical structure, where both of them have methoxy benzene groups instead toluene, but AuNPs functionalised by **2C** was more effective than AuNPs functionalised by **8B** which has similar chemical structure except carbon chain length which contains 6 carbon atoms in **8B**-AuNP rather than 3 in comparison with **2C** structure. **4C**-AuNP contains benzene groups in its structure showed a significate effect on the *S.aureus* with no effect on *E.coli*.

Overall, from this present study, it can be concluded that certain cationic phosphonium AuNPs are effective toward two non-pathogenic bacterial strains causing bacterial growth inhibition. Moreover, based on recent findings, it proposes that, because these AuNPs are effective on two non-pathogenic bacteria (*E. coli* NCIB 8277 and *S. aureus* ATCC 6538P), so they maybe offer similar results if they tested on clinical isolates in the future. Maybe to contain promise to reduce diseases in the future *via* reducing or overcome bacterial resistance. Could also, be used for the targeted delivery of traditional antibacterial substances to pathogenic bacteria as a novel antibacterial agent.

AuNPs could act as an effective antibacterial agent and can be proved as an alternative factor in order to develop new antibacterial drugs to fight resistance problem. Also, AuNPs have been used to be an alternate and smart choice for drugs delivery and cancer therapy due to their functional nature and less side effect compared to antibiotics.

The current study is a preliminary test. Quantities test growth curves are needed in order to be more accurate. Mechanism of interaction AuNPs with bacteria also needs more study in the future. An effective of theses AuNPs on other different kinds of bacteria must also, be taken into consideration.

6.6 References

1. Li, X., Robinson, SM., Gupta, A., Saha, K., Jiang, Z., Moyano, DF., Sahar, A., Riley, MA and Rotello, VM, *Functional gold nanoparticles as potent antimicrobial agents against multi-drug-resistant bacteria.* ACS nano, 2014. **8**(10): p. 10682-10686.

2. Alanis, AJ, *Resistance to antibiotics: are we in the post-antibiotic era?* Archives of medical research, 2005. **36**(6): p. 697-705.

3. Bannerman, DD., Paape, MJ., Lee, J-W., Zhao, X., Hope, JC and Rainard, P, *Escherichia coli and Staphylococcus aureus elicit differential innate immune responses following intramammary infection.* Clinical and diagnostic laboratory immunology, 2004. **11**(3): p. 463-472.

4. Doughari, HJ., Ndakidemi, PA., Human, IS and Benade, S, *Virulence factors and antibiotic susceptibility among verotoxic non O157: H7 Escherichia coli isolates obtained from water and wastewater samples in Cape Town, South Africa.* African Journal of Biotechnology, 2011. **10**(64): p. 14160-14168.

5. Kim, JS., Kuk, E., Yu, KN., Kim, J-H., Park, SJ., Lee, HJ., Kim, SH., Park, YK., Park, YH and Hwang, C-Y, *Antimicrobial effects of silver nanoparticles.* Nanomedicine: Nanotechnology, Biology and Medicine, 2007. **3**(1): p. 95-101.

6. Klevens, RM., Morrison, MA., Nadle, J., Petit, S., Gershman, K., Ray, S., Harrison, LH., Lynfield, R., Dumyati, G and Townes, JM, *Invasive methicillin-resistant Staphylococcus aureus infections in the United States.* Jama, 2007. **298**(15): p. 1763-1771.

7. Organization, WH, *Global tuberculosis report 2013*. World Health Organization, 2013.

8. Gifford, JC., Bresee, J., Carter, CJ., Wang, G., Melander, RJ., Melander, C and Feldheim, DL, *Thiol-modified gold nanoparticles for the inhibition of Mycobacterium smegmatis.* Chemical Communications, 2014. **50**(100): p. 15860-15863.

9. Gupta, A., Landis, RF and Rotello, VM, *Nanoparticle-based antimicrobials: Surface functionality is critical.* F1000Research, 2016. **5**.

10. Liu, L., Yang, J., Xie, J., Luo, Z., Jiang, J., Yang, YY and Liu, S, *The potent antimicrobial properties of cell penetrating peptide-conjugated silver nanoparticles with excellent selectivity for Gram-positive bacteria over erythrocytes.* Nanoscale, 2013. **5**(9): p. 3834-3840.

11. Zhao, Y and Jiang, X, *Multiple strategies to activate gold nanoparticles as antibiotics.* Nanoscale, 2013. **5**(18): p. 8340-8350.

12. Beranová, J., Seydlová, G., Kozak, H., Benada, O., Fišer, R., Artemenko, A., Konopásek, I and Kromka, A, *Sensitivity of bacteria to diamond nanoparticles of*

various size differs in gram-positive and gram-negative cells. FEMS microbiology letters, 2014. **351**(2): p. 179-186.

13. Zhang, Y., Peng, H., Huang, W., Zhou, Y and Yan, D, *Facile preparation and characterization of highly antimicrobial colloid Ag or Au nanoparticles.* Journal of colloid and interface science, 2008. **325**(2): p. 371-376.

14. Goodman, CM., Mccusker, CD., Yilmaz, T and Rotello, VM, *Toxicity of gold nanoparticles functionalized with cationic and anionic side chains.* Bioconjugate chemistry, 2004. **15**(4): p. 897-900.

15. Bresee, J., Maier, KE., Boncella, AE., Melander, C and Feldheim, DL, *Growth inhibition of Staphylococcus aureus by mixed monolayer gold nanoparticles.* Small, 2011. **7**(14): p. 2027-2031.

16. Ahmad, A., Wei, Y., Ullah, S., Shah, SI., Nasir, F., Shah, A., Iqbal, Z., Tahir, K., Khan, UA and Yuan, Q, *Synthesis of phytochemicals-stabilized gold nanoparticles and their biological activities against bacteria and Leishmania.* Microbial Pathogenesis, 2017. **110**: p. 304-312.

17. Santos, C., Albuquerque, A., Sampaio, F and Keyson, D, *Nanomaterials with Antimicrobial Properties: Applications in Health Sciences.* Microbial pathogens and strategies for combating them: science, technology and education. Volume,. **4**:(2), 2013.

18. Zhao, Z., Yan, R., Yi, X., Li, J., Rao, J., Guo, Z., Yang, Y., Li, W., Li, Y-Q and Chen, C, *Bacteria-Activated Theranostic Nanoprobes against Methicillin-Resistant Staphylococcus aureus Infection.* ACS nano, 2017.

19. Giasuddin, A., Jhuma, K and Mujibul, HA, *Use of Gold Nanoparticles in Diagnostics, Surgery and Medicine: A Review.* 2012.

20. Jain, S., Hirst, D and O'sullivan, J, *Gold nanoparticles as novel agents for cancer therapy.* The British journal of radiology, 2014.

21. Mesbahi, A, *A review on gold nanoparticles radiosensitization effect in radiation therapy of cancer.* Reports of Practical Oncology & Radiotherapy, 2010. **15**(6): p. 176-180.

22. Nazari, ZE., Banoee, M., Sepahi, AA., Rafii, F and Shahverdi, AR, *The combination effects of trivalent gold ions and gold nanoparticles with different antibiotics against resistant Pseudomonas aeruginosa.* Gold Bulletin, 2012. **45**(2): p. 53-59.

23. Ahangari, A., Salouti, M., Heidari, Z., Kazemizadeh, AR and Safari, AA, *Development of gentamicin-gold nanospheres for antimicrobial drug delivery to Staphylococcal infected foci.* Drug delivery, 2013. **20**(1): p. 34-39.

24. Grumezescu, A, *Nanobiomaterials in Antimicrobial Therapy: Applications of Nanobiomaterials.* . Vol. 6. 2016: Elsevier Science. p:103-152.

25. Lima, E., Diaz, A., Guizar- Sicairos, M., Gorelick, S., Pernot, P., Schleier, T and Menzel, A, *Cryo- scanning x- ray diffraction microscopy of frozen- hydrated yeast.* Journal of Microscopy, 2013. **249**(1): p. 1-7.

26. Saha, B., Bhattacharya, J., Mukherjee, A., Ghosh, A., Santra, C., Dasgupta, AK and Karmakar, P, *In vitro structural and functional evaluation of gold nanoparticles conjugated antibiotics.* Nanoscale Research Letters, 2007. **2**(12): p. 614-622.

27. Prema., P and Thangapandiyan.S, *In-vitro antibacterial activity of gold nanoparticles capped with polysaccharide stabilizing agents.* Int J Pharm Pharm Sci 2013. **Vol 5**(Issue 1): p. 310-314.

28. Morones, JR., Elechiguerra, JL., Camacho, A., Holt, K., Kouri, JB., Ramírez, JT and Yacaman, MJ, *The bactericidal effect of silver nanoparticles.* Nanotechnology, 2005. **16**(10): p. 2346–53.

29. Brayner, R., Ferrari-Iliou, R., Brivois, N., Djediat, S., Benedetti, MF and Fiévet, F, *Toxicological impact studies based on Escherichia coli bacteria in ultrafine ZnO nanoparticles colloidal medium.* Nano Letters, 2006. **6**(4): p. 866-870.

30. Simon-Deckers, A., Loo, S., Mayne-L'hermite, M., Herlin-Boime, N., Menguy, N., Reynaud, C., Gouget, B and Carriere, M, *Size-, composition-and shape-dependent toxicological impact of metal oxide nanoparticles and carbon nanotubes toward bacteria.* Environmental science & technology, 2009. **43**(21): p. 8423-8429.

31. Jin, Y and Zhao, X, *Cytotoxicity of photoactive nanoparticles*, in *Safety of Nanoparticles*. 2009, Springer. p. 19-31.

32. Alkilany, AM and Murphy, CJ, *Toxicity and cellular uptake of gold nanoparticles: what we have learned so far?* Journal of nanoparticle research, 2010. **12**(7): p. 2313-2333.

33. Shamaila, S., Zafar, N., Riaz, S., Sharif, R., Nazir, J and Naseem, S, *Gold Nanoparticles: An Efficient Antimicrobial Agent against Enteric Bacterial Human Pathogen.* Nanomaterials, 2016. **6**(4): p. 1-10.

34. Zhou, Y., Kong, Y., Kundu, S., Cirillo, JD and Liang, H, *Antibacterial activities of gold and silver nanoparticles against Escherichia coli and bacillus Calmette-Guérin.* Journal of nanobiotechnology, 2012. **10**(1): p. 1-19.

35. Feng, ZV., Gunsolus, IL., Qiu, TA., Hurley, KR., Nyberg, LH., Frew, H., Johnson, KP., Vartanian, AM., Jacob, LM and Lohse, SE, *Impacts of gold nanoparticle charge and ligand type on surface binding and toxicity to Gram-negative and Gram-positive bacteria.* Chemical Science, 2015. **6**(9): p. 5186-5196.

36. Gordon, O., Slenters, TV., Brunetto, PS., Villaruz, AE., Sturdevant, DE., Otto, M., Landmann, R and Fromm, KM, *Silver coordination polymers for prevention of implant infection: thiol interaction, impact on respiratory chain enzymes, and*

hydroxyl radical induction. Antimicrobial agents and chemotherapy, 2010. **54**(10): p. 4208-4218.

37. He, F., Zhao, D., Liu, J and Roberts, CB, *Stabilization of Fe− Pd nanoparticles with sodium carboxymethyl cellulose for enhanced transport and dechlorination of trichloroethylene in soil and groundwater.* Industrial & Engineering Chemistry Research, 2007. **46**(1): p. 29-34.

38. Valodkar, M., Rathore, PS., Jadeja, RN., Thounaojam, M., Devkar, RV and Thakore, S, *Cytotoxicity evaluation and antimicrobial studies of starch capped water soluble copper nanoparticles.* Journal of hazardous materials, 2012. **201**: p. 244-249.

39. Nomiya, K., Yamamoto, S., Noguchi, R., Yokoyama, H., Kasuga, NC., Ohyama, K and Kato, C, *Ligand-exchangeability of 2-coordinate phosphinegold (I) complexes with AuSP and AuNP cores showing selective antimicrobial activities against Gram-positive bacteria. Crystal structures of [Au (2-Hmpa)(PPh 3)] and [Au (6-Hmna)(PPh 3)](2-H 2 mpa= 2-mercaptopropionic acid, 6-H 2 mna= 6-mercaptonicotinic acid).* Journal of inorganic biochemistry, 2003. **95**(2): p. 208-220.

40. Chwalibog, A., Sawosz, E., Hotowy, A., Szeliga, J., Mitura, S., Mitura, K., Grodzik, M., Orlowski, P and Sokolowska, A, *Visualization of interaction between inorganic nanoparticles and bacteria or fungi.* Int J Nanomedicine, 2010. **5**(1): p. 1085-1094.

41. Zawrah, M., El-Moez, SA and Center, D, *Antimicrobial activities of gold nanoparticles against major foodborne pathogens.* Life Sci J, 2011. **8**(4): p. 37-44.

42. Taylor, E and Webster, TJ, *Reducing infections through nanotechnology and nanoparticles.* International journal of nanomedicine, 2011. **6**: p. 1463.

43. Rai, A., Prabhune, A and Perry, CC, *Antibiotic mediated synthesis of gold nanoparticles with potent antimicrobial activity and their application in antimicrobial coatings.* Journal of Materials Chemistry, 2010. **20**(32): p. 6789-6798.

44. Silhavy, TJ., Kahne, D and Walker, S, *The bacterial cell envelope.* Cold Spring Harbor perspectives in biology, 2010. **2**(5). a000414.

45. Belliraj, T., Nanda, A and Ragunathan, R, *In-vitro hepatoprotective activity of Moringa oleifera mediated synthesis of gold nanoparticles.* J. Chem. Pharm. Res, 2015. **7**: p. 781-788.

46. Saleh, M., Kumar, G., Abdel-Baki, A-A., Al-Quraishy, S and El-Matbouli, M, *In vitro antimicrosporidial activity of gold nanoparticles against Heterosporis saurida.* BMC veterinary research, 2016. **12**(1): p. 1-10.

47. Zhao, Y., Tian, Y., Cui, Y., Liu, W., Ma, W and Jiang, X, *Small molecule-capped gold nanoparticles as potent antibacterial agents that target Gram-negative*

bacteria. Journal of the American Chemical Society, 2010. **132**(35): p. 12349-12356.

48. Selvaraj, V and Alagar, M, *Analytical detection and biological assay of antileukemic drug 5-fluorouracil using gold nanoparticles as probe.* International journal of pharmaceutics, 2007. **337**(1): p. 275-281.

49. Hayden, SC., Zhao, G., Saha, K., Phillips, RL., Li, X., Miranda, OR., Rotello, VM., El-Sayed, MA., Schmidt-Krey, I and Bunz, UH, *Aggregation and interaction of cationic nanoparticles on bacterial surfaces.* Journal of the American Chemical Society, 2012. **134**(16): p. 6920-6923.

50. Coyle, MB, *Manual of antimicrobial susceptibility testing*. American Society for Microbiology, 2005.

51. Hwang, ET., Lee, JH., Chae, YJ., Kim, YS., Kim, BC., Sang, BI and Gu, MB, *Analysis of the Toxic Mode of Action of Silver Nanoparticles Using Stress-Specific Bioluminescent Bacteria.* Small, 2008. **4**(6): p. 746-750.

52. Amin, RM., Mohamed, MB., Ramadan, MA., Verwanger, T and Krammer, B, *Rapid and sensitive microplate assay for screening the effect of silver and gold nanoparticles on bacteria.* Nanomedicine, 2009. **4**(6): p. 637-643.

53. Pan, Y., Neuss, S., Leifert, A., Fischler, M., Wen, F., Simon, U., Schmid, G., Brandau, W and Jahnen- Dechent, W, *Size- dependent cytotoxicity of gold nanoparticles.* Small, 2007. **3**(11): p. 1941-1949.

54. Ratte, HT, *Bioaccumulation and toxicity of silver compounds: a review.* Environmental Toxicology and Chemistry, 1999. **18**(1): p. 89-108.

55. Sambhy, V., Macbride, MM., Peterson, BR and Sen, A, *Silver bromide nanoparticle/polymer composites: dual action tunable antimicrobial materials.* Journal of the American Chemical Society, 2006. **128**(30): p. 9798-9808.

56. Martínez, J., Chequer, N., González, J and Cordova, T, *Alternative metodology for gold nanoparticles diameter characterization using PCA technique and UV-Vis spectrophotometry.* Nanoscience and Nanotechnology, 2012. **2**(6): p. 184-189.

57. Rao, C., Venkataraghavan, R and Kasturi, T, *Contribution to the infrared spectra of organosulphur compounds.* Canadian journal of chemistry, 1964. **42**(1): p. 36-42.

58. Qian, W and Krimm, S, *Conformation dependence of the SH and CS stretch frequencies of the cysteine residue.* Biopolymers, 1992. **32**(11): p. 1503-1518.

59. Bandyopadhyay, S and Dey, A, *Convenient detection of the thiol functional group using H/D isotope sensitive Raman spectroscopy.* Analyst, 2014. **139**(9): p. 2118-2121.

60. Zhang, T, *The grignard synthesis of triphenylmethanol.* Organic Chemistry: An Indian Journal, 2015. **11**(8): p. 288-292.

Chapter 7: Conclusion of thesis

7.1 Conclusions and future work

The results presented in this thesis were conducted to assess the properties and stability of colloidal AuNPs manufactured for the potential use in alternative biorecognition and drug delivery systems. The phosphonium groups contained within the ligand have a variety of advantages such as ease of synthesis and biocompatibility making them ideal candidates for bio-applications. Phosphonium AuNPs with sizes between 5 nm -11 nm were obtained *via* the reduction of potassium tetrachloroaurate ($KAuCl_4$) in DMSO and in a two-phase DCM / H_2O system with presence of the protecting ligands. Some our phosphonium-AuNPs ligands were shown to have high affinity toward the aqueous phase. While other ligands that have methoxy or tolyl head group have not shown any affinity for the aqueous phase which led to choosing and alternative compatible solvent such as DMSO. UV-visible spectroscopy, DLS and TEM were used to measure the stability of these AuNPs for up to 6 months.

In addition, from the synthesis of functionalised AuNPs, it was clear to see that the most versatile ligands were those containing methoxy groups with alkyl chain lengths of both three and six such as (3-thioacetylpropyl)tris(2,4,6-trimethoxyphenyl)phosphonium bromide and (6-thioacetylhexyl)tris(2,4,6-trimethoxyphenyl)phosphonium bromide compounds ligands produced stable AuNPs, and it was also possible to synthesis AuNPs by using sodium borohydride as a strong reducing agent and ascorbic acid as a weaker reducing agent. Methoxy is an ideal moiety to incorporate into a ligand as it is a donator group and contributes electrons to the phenol group. This changes the stability of the AuNPs within a solution as the electronegative charge is shifted. The shorter chain ligands synthesised produced a more crystalline structure that was easily soluble in water in case ligands contain phenyl or tolyl head groups such as (3-thio-acetylpropyl)tri(phenyl)phosphonium bromide and (3-thioacetylpropyl)tri(*p*-tolyl)-phosphonium bromide making these ligands ideal for use in biological media.

The data collected with regards to the stability of AuNPs over time supported the results proposed in the published literature. It was clear that over the 6 months' period, the stability of some of the AuNPs remained constant with no shift in the peak absorbance

wavelength observed using UV-Vis. As well as, it is imperative that the AuNPs remain stable within the body over longer time for therapeutic reasons. As a results of the pH stability study in this thesis, it was proposed that the optimum pH of the (3-thioacetylpropyl)triphenylphosphonium bromide, (3-thioacetylpropyl)tri(*p*-tolyl)-phosphonium bromide and (3-thioacetylpropyl)tris(2,4,6-trimethoxyphenyl)-phosphonium bromide showed the AuNPs produced stable within pH 9.2 and pH 5.1 with no sign of degradation or aggregation. The stability of the solution at this pH was measured using UV-Vis data which showed that the peak absorbance wavelength observed did not shift, suggesting a consistent size of AuNPs monodispersed within the solution. The stability of the AuNPs elucidated in the acidic pH study suggests that despite the weakly acidic nature of tumorous tissue, it would be possible for the manufactured nanoparticles to selectively enter the cells required and remain stable for a suitable time period for insure a treatment to be completed. This is due to the hydrophobic nature of the synthesised ligands introducing an affinity with the lipophilic cell walls. Not only do the hydrophobic and cationic properties of the surface coating of the AuNPs aid cell penetration, but it also provides a pathway for ion exchange within the biological media of the cell.

The evidence presented for the stability of functionalised AuNPs at lower pH is significant as it is well documented that the pH of cancer cells is weakly acidic. In addition, AuNPs in present study with the similar size exhibited different inhibitory effects toward both Gram-negative bacteria *E. coli* and the Gram-positive bacteria *Staphylococcus aureus* at the same concentration. Also, study was investigated both the bacterial growth and the inhibition effect of the AuNP, where the effect of both size and surface chemistry of the AuNPs on the bacteria was clearly noted. In addition, it was found out that, AuNPs with different coating agents of similar final concentrations showed different effects on the bacteria

From this present study, it can be deduced that AuNPs could act as an effective antibacterial agent and can be proved as an alternative factor for development of new antibacterial drugs with reducing resistance problem and side effects. Whilst the work presented was conducted *in vitro,* future work should include *in vivo* biological test *via* cellular internalisation of the phosphonium ligands coated AuNPs. This analysis could be achieved using a biophysical technique, such as flow cytometry technique which is

usually employed in the diagnosis of various health disorders where the cells are normally suspended in a stream of fluid and passed by an electronic detection apparatus. In order to prepare the samples for cytometry analysis, our cationic phosphonium AuNPs are planned to be internalised by incubation. Functionalised AuNPs have of a significant importance and expected to have a great impact in different areas in particular in the biological and biomedical applications.

Finally, there are seven-step process that makes this research unique and different from many other studies is the described below:

1- Synthesis novel protecting ligands have different properties toward AuNPs with fully characterisation.

2- Synthesis of novel cationic phosphonium AuNPs dispersible in water and dimethylsulfoxide (DMSO) for their potential use in biomedical applications is outlined.

3- Due to poor solubility of some ligands in water, DMSO as biocompatible solvent was used as solvent, because it is the only organic solvent approved by the U.S. Food and Drug Administration (FDA) for drug carrier tests.

4- The functionalised AuNPs (by ligands contain phenyl, tolyl, trimethoxy head group) were subjected to investigate their stability over time at a pH range of 3-11.

5-Synthesis well-constrained AuNPs by different reducing agent used $NaBH_4$ (strong) and ascorbic acid as (weak) biocompatible reducing agent.

6- Completely characterising AuNPs and studying their stability for the related period of time.

7- Effecting the AuNPs on the bacterial growth with different concentrations used.

Appendix

Appendix A2.1

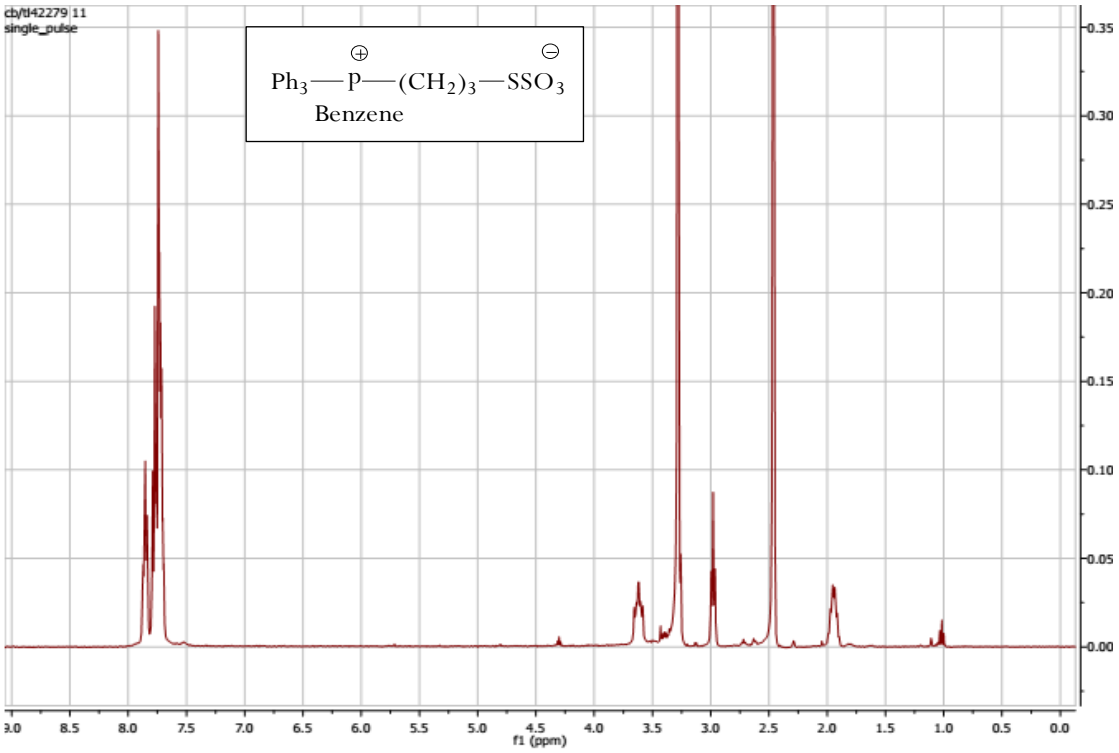

Figure A2.1 ^{1}HNMR of (**4C**). ***Following Chapter 2***

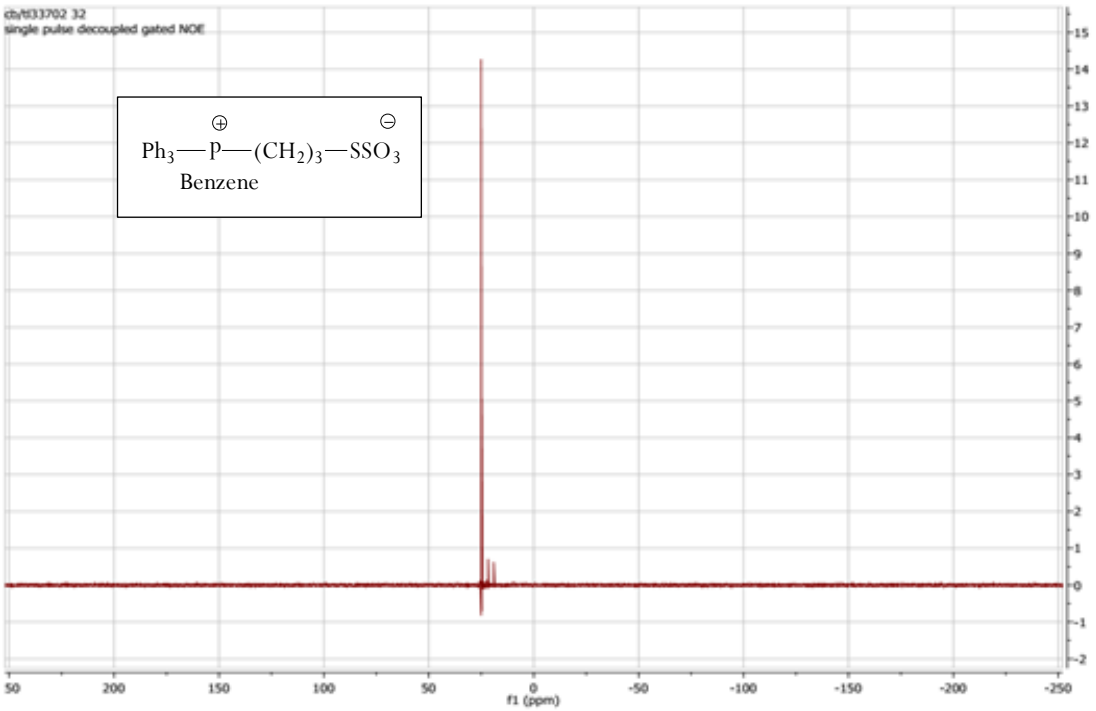

Figure A2.2 ^{13}C-NMR of (**4C**). ***Following Chapter 2***

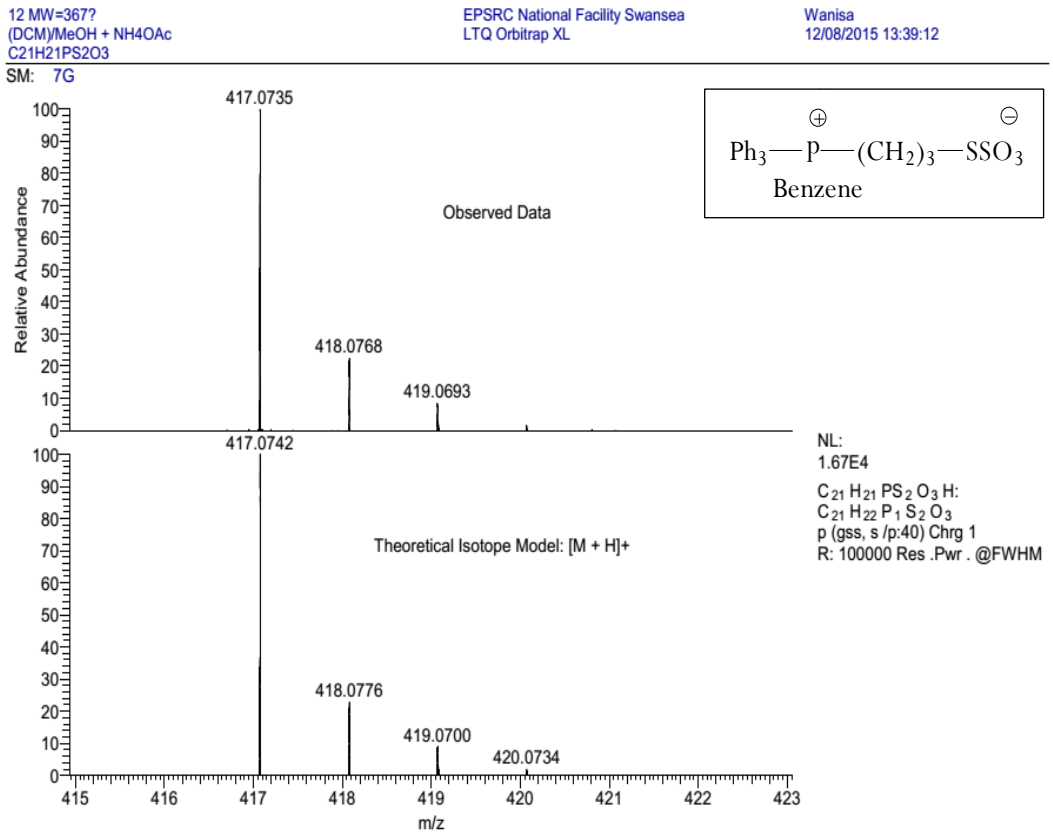

Figure A2.3 ESI-MS of (**4C**). ***Following Chapter 2***

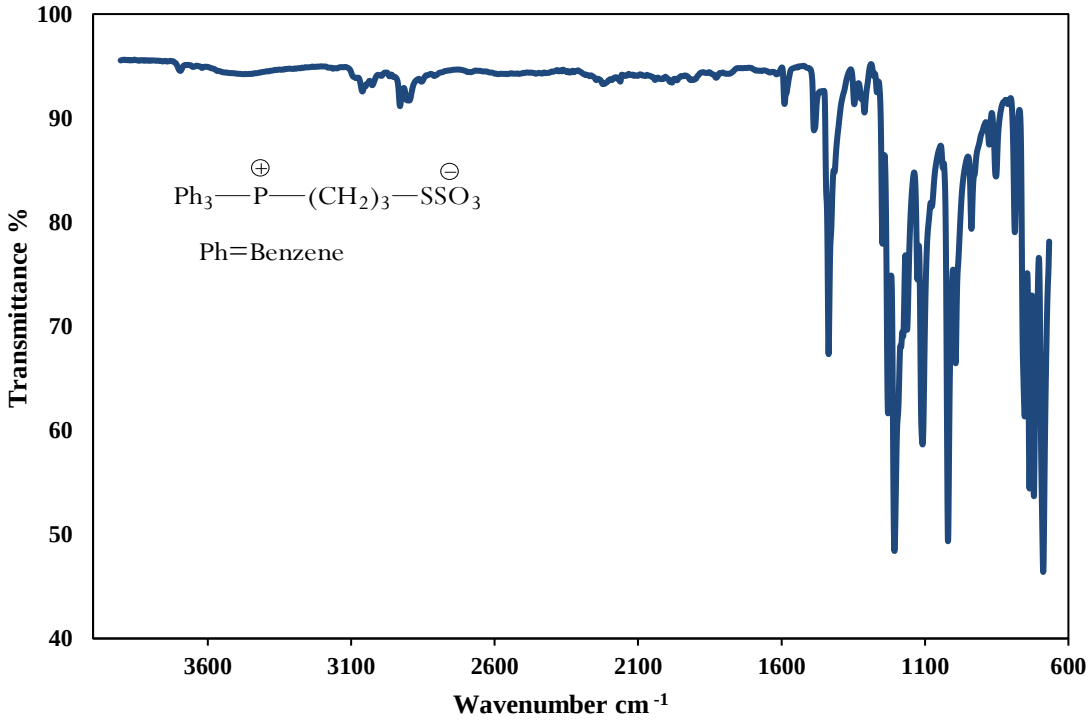

Figure A2.4 ATR-FTIR of (**4C**). ***Following Chapter 2***

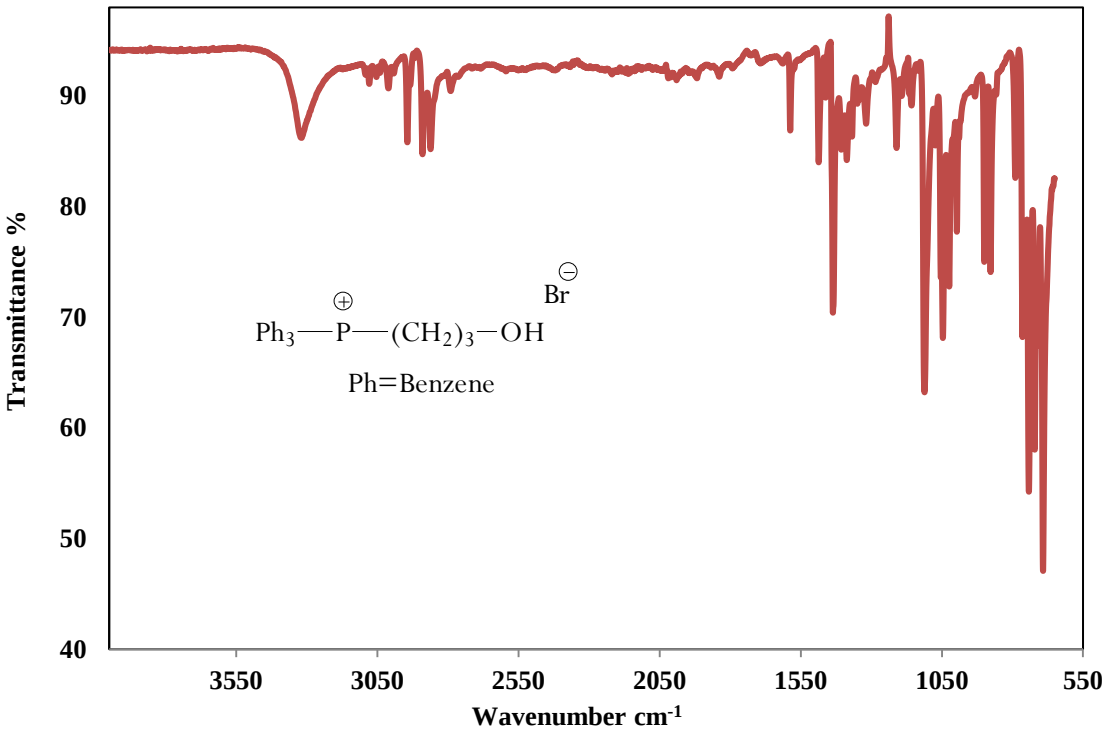

Figure A2.5 ATR-FTIR of Hydroxypropyl-triphenylphosphonium bromide. ***Following Chapter 2***

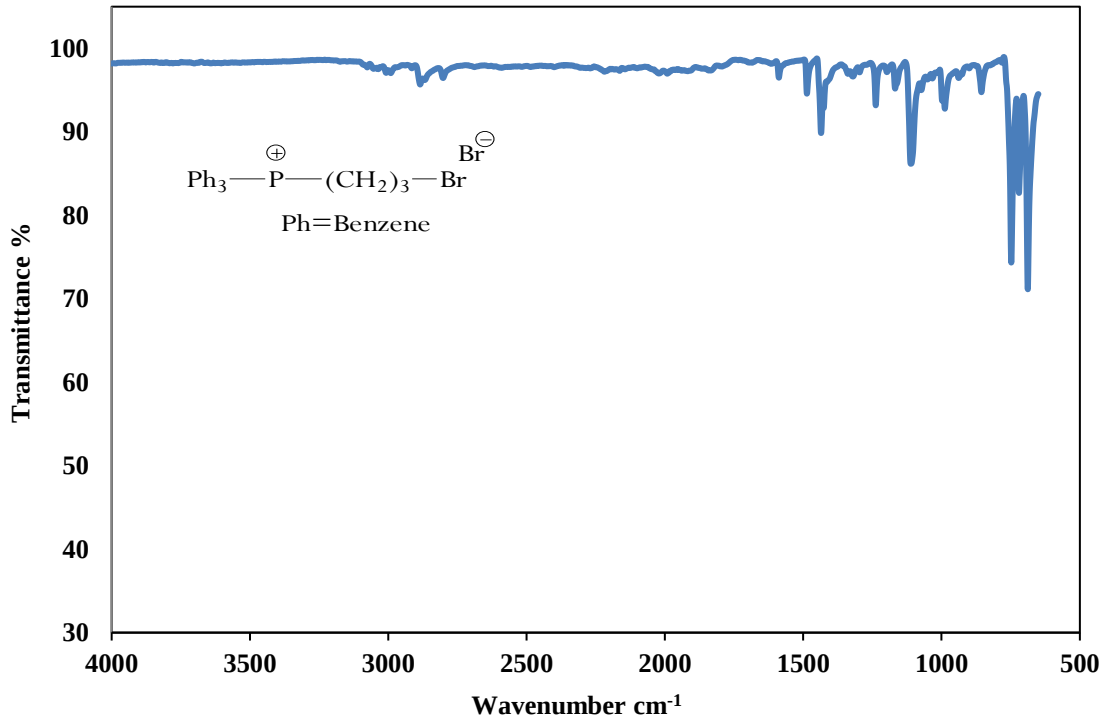

Figure A2.6 ATR-FTIR of ω-bromopropyl-triphenylphosphonium bromide. ***Following Chapter 2***

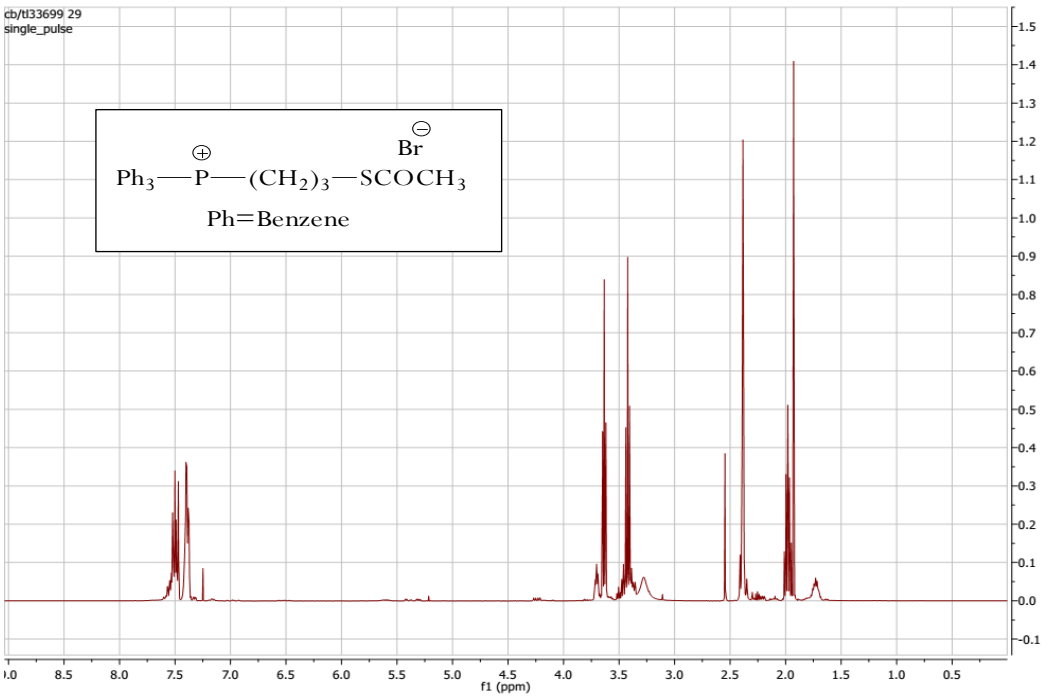

Figure A2.7 ^{1}H-NMR of (**5**). ***Following Chapter 2***

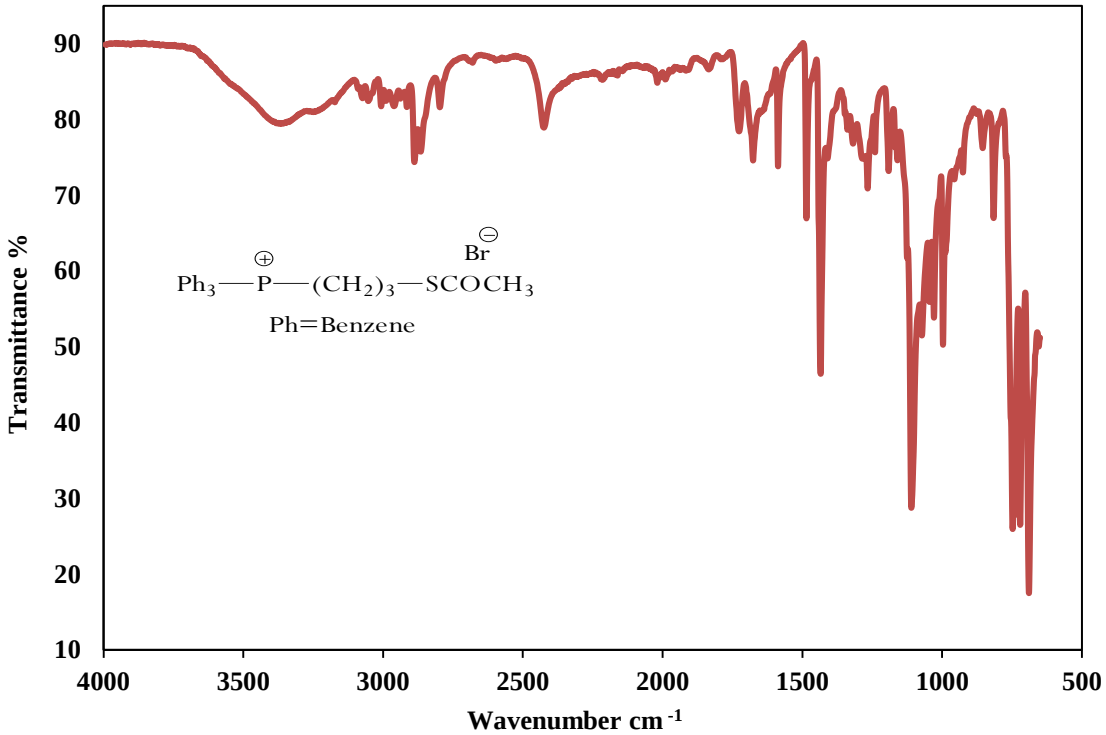

Figure A2.8 ATR-FTIR of (**5**). ***Following Chapter 2***

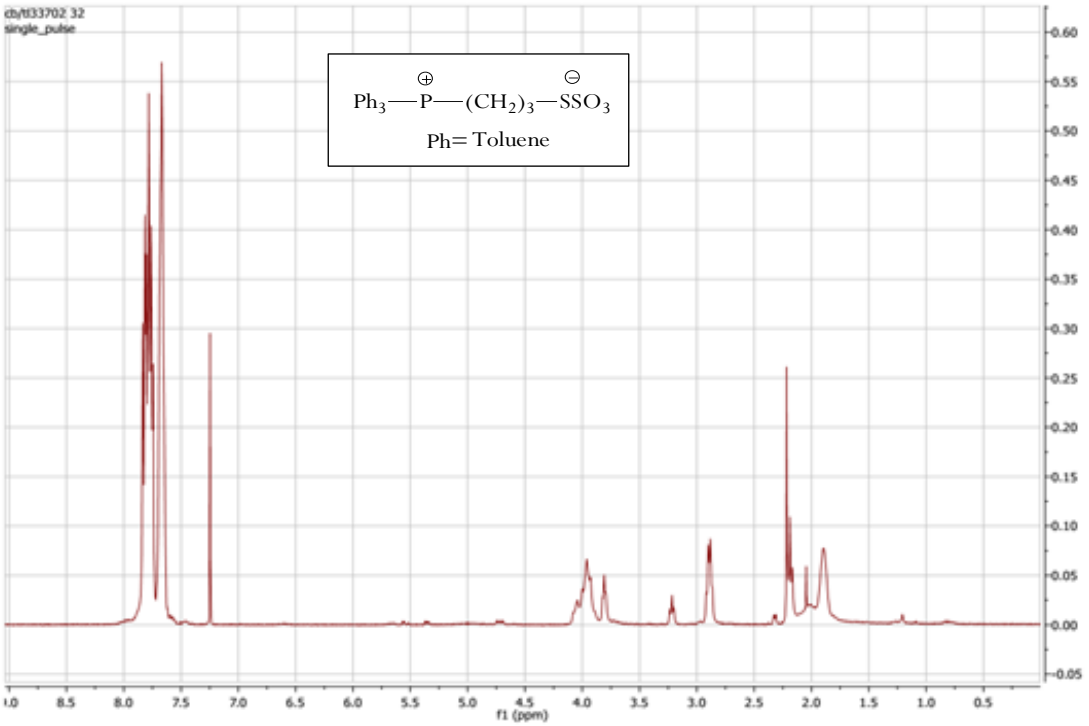

Figure A2.9 ^{1}HNMR of (**4**). ***Following Chapter 2***

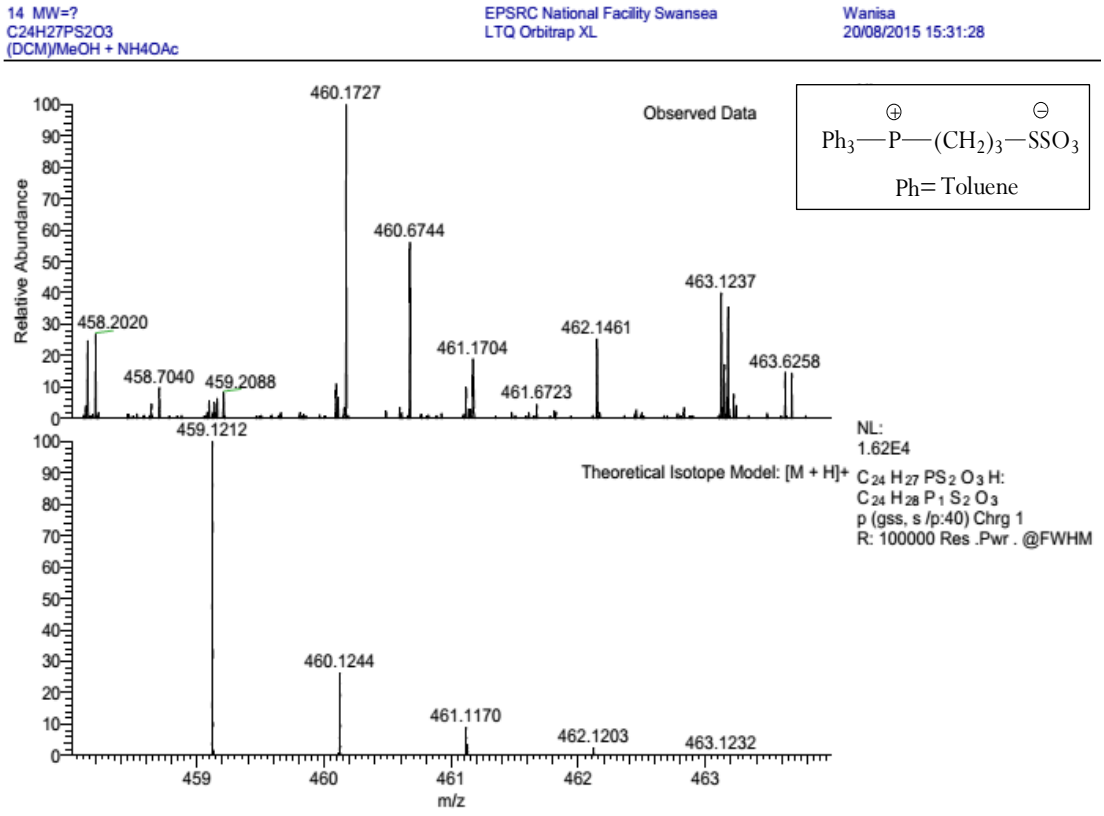

Figure A2.10 ESI-MS of (**4**). ***Following Chapter 2***

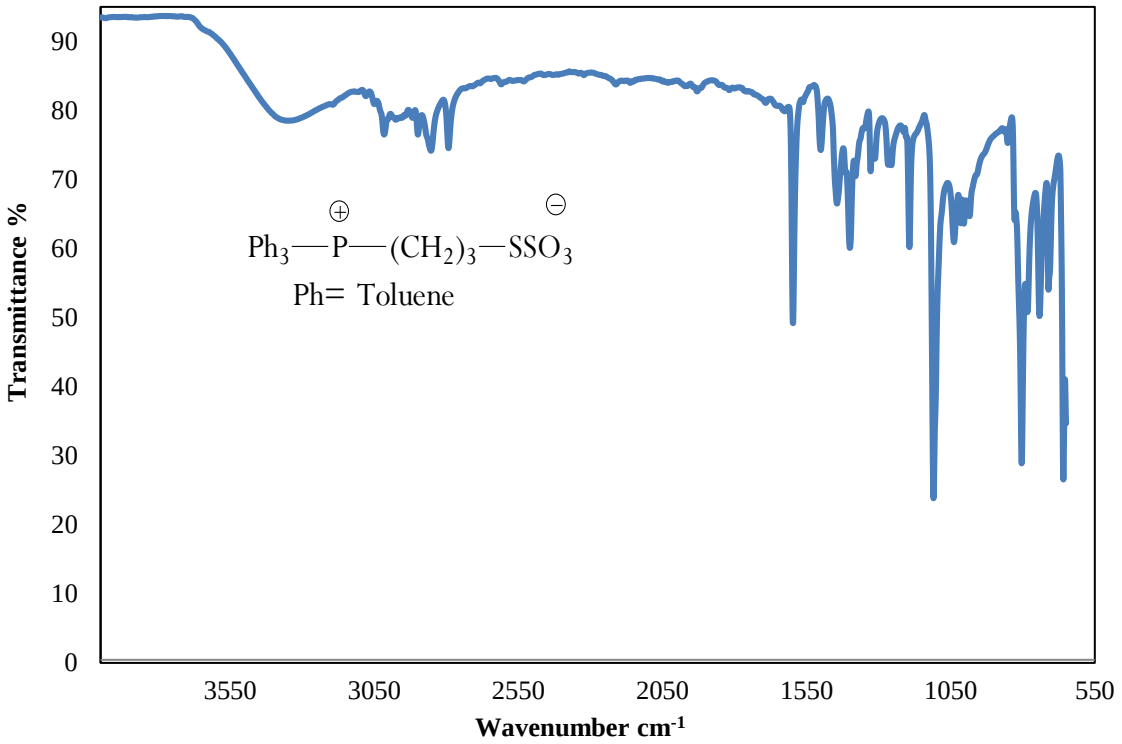

Figure A2.11 ATR-FTIR of (**4**). ***Following Chapter 2***

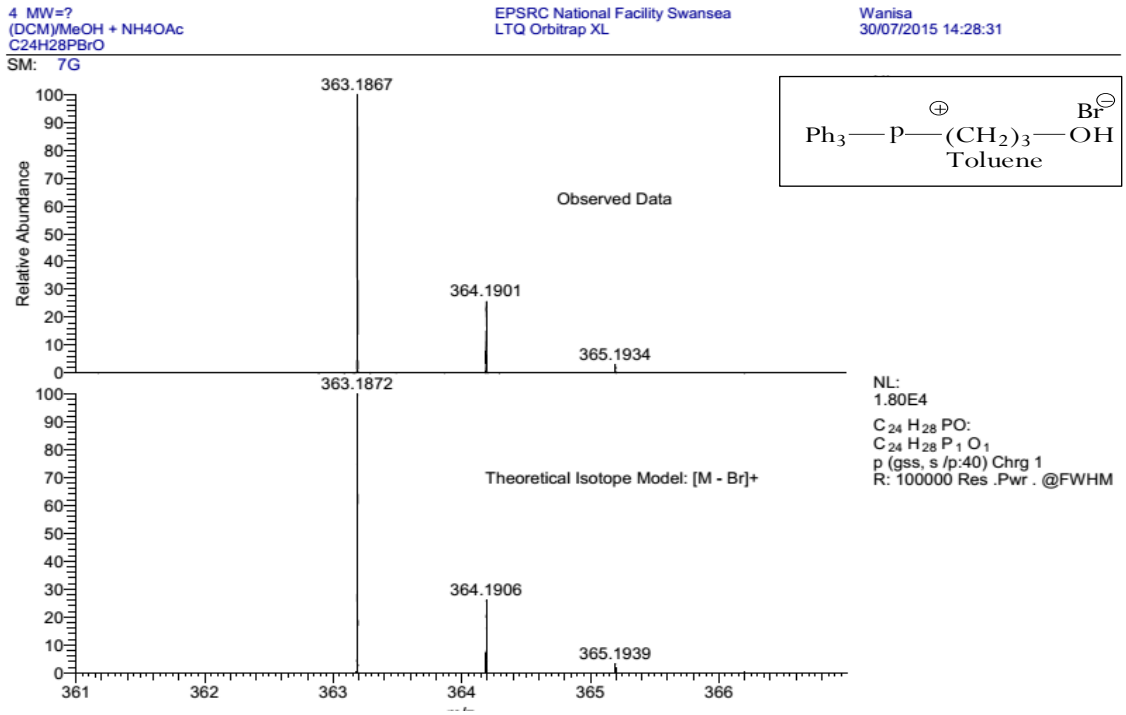

Figure A2.12 ESI-MS of Hydroxypropyl-tri(*p*-tolyl)phenylphosphonium bromide. ***Following Chapter 2***

Appendix B3.1

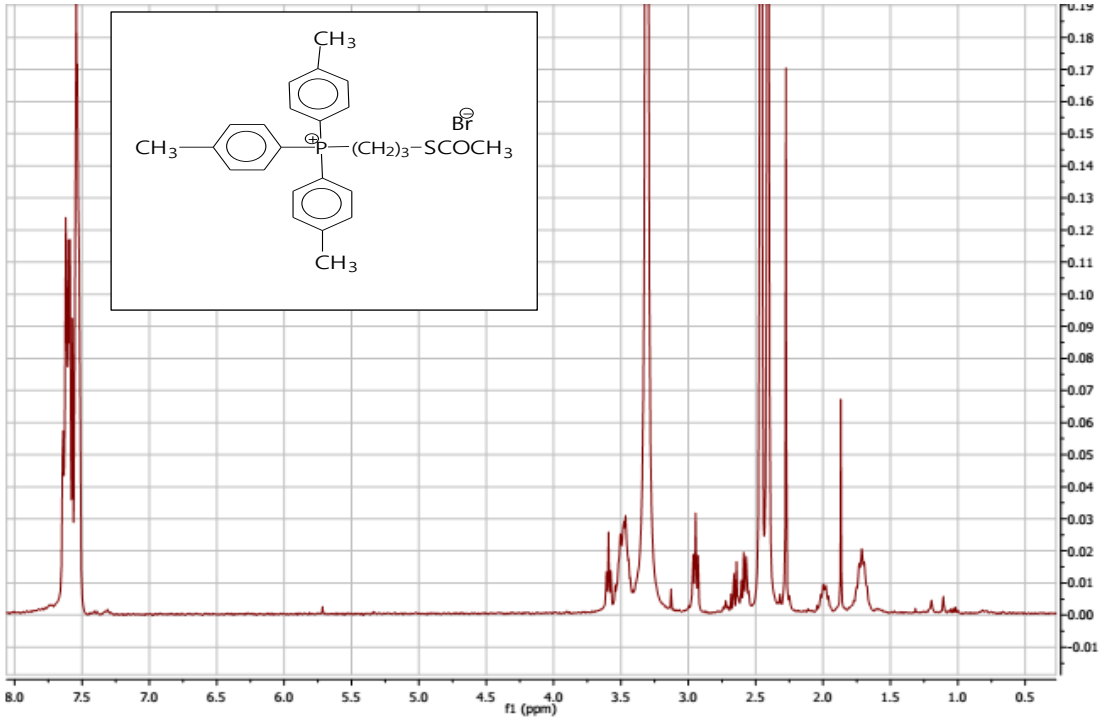

Figure B3.1 ^{1}H-NMR of (**4A**). ***Following Chapter 3***

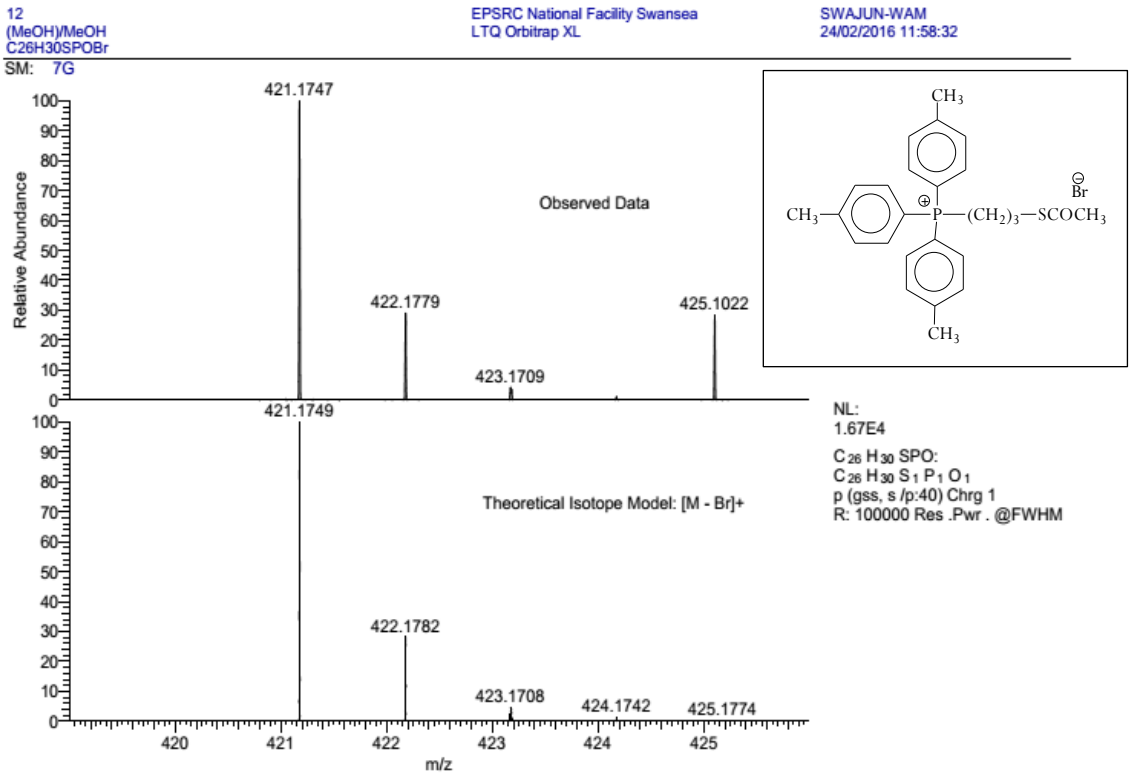

Figure B3.2 ESI-MS of (**4A**). ***Following Chapter 3***

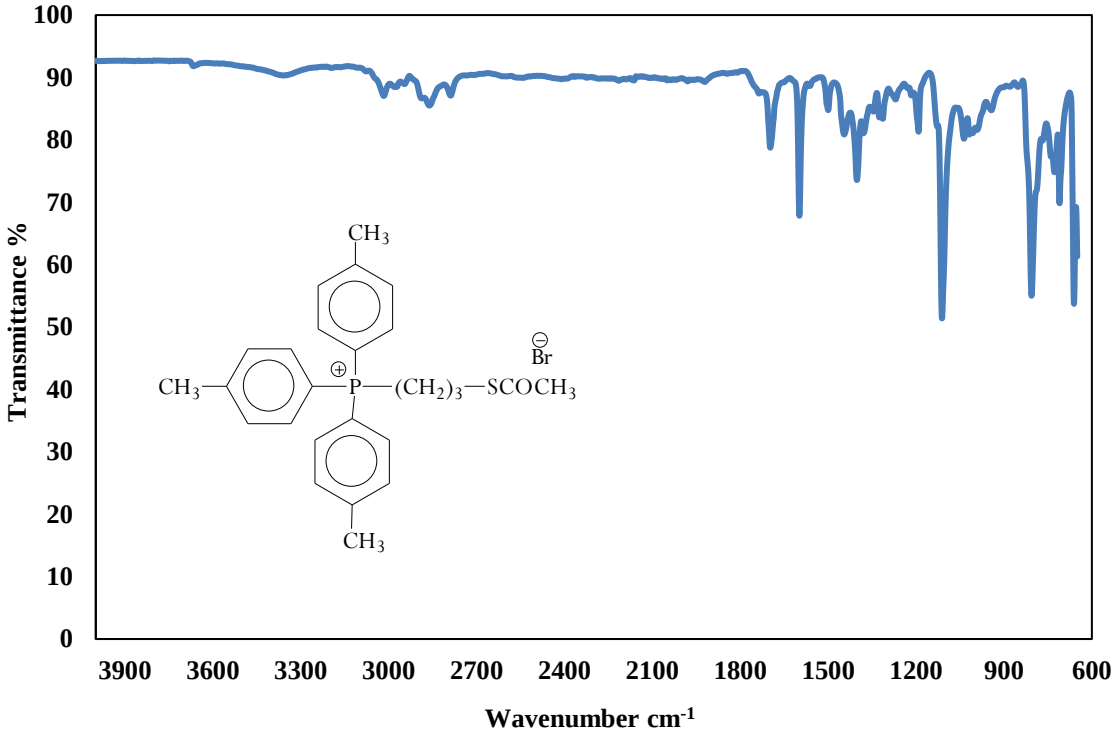

Figure B3.3 ATR-FTIR of (**4A**). ***Following Chapter 3***

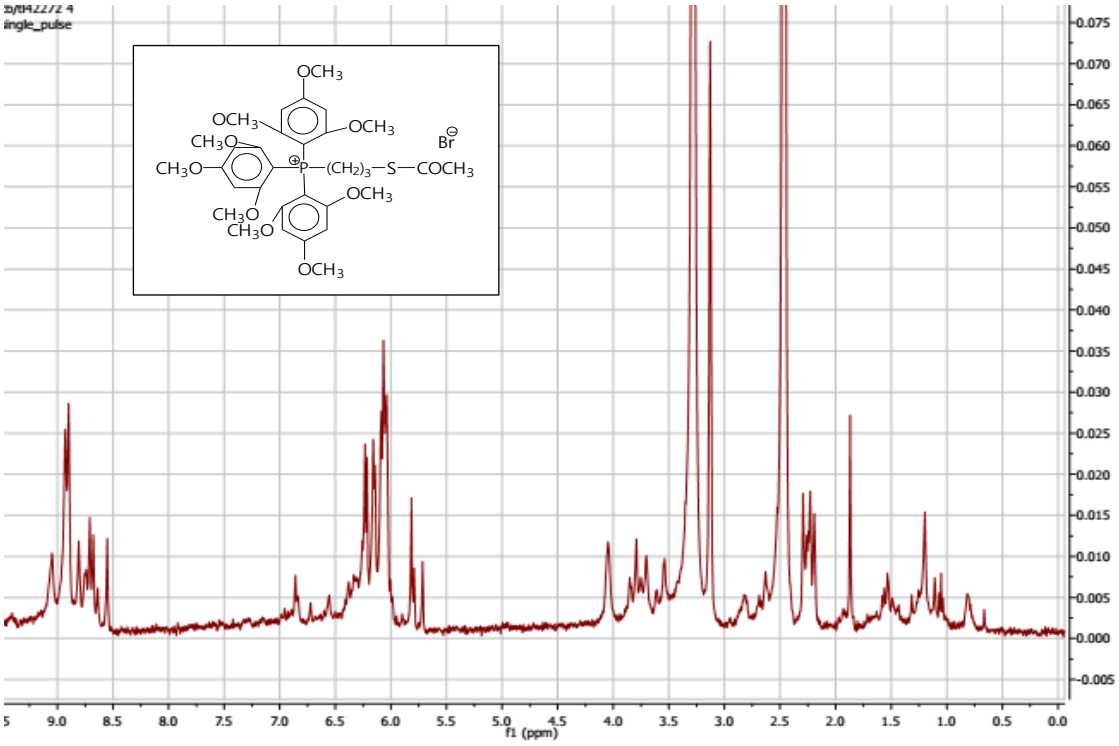

Figure B3.4 ^{1}H-NMR of (**4B**). ***Following Chapter 3***

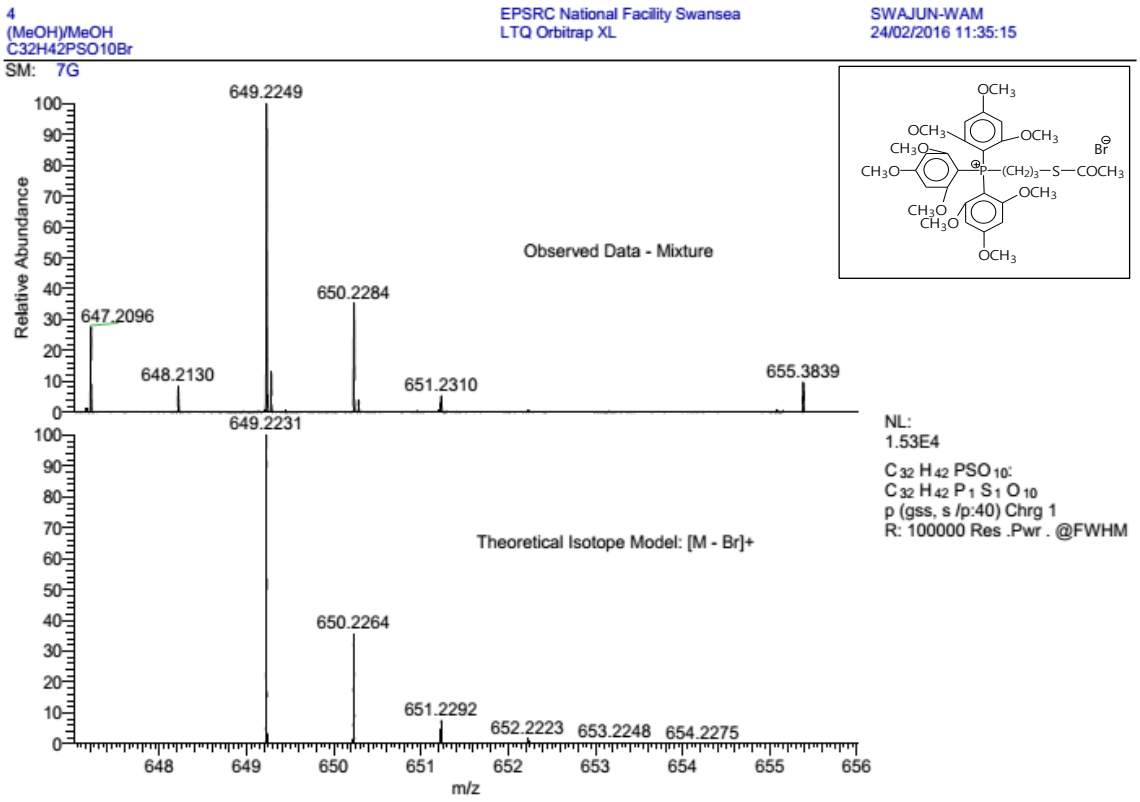

Figure B3.5 ESI-MS of (**4B**). ***Following Chapter 3***

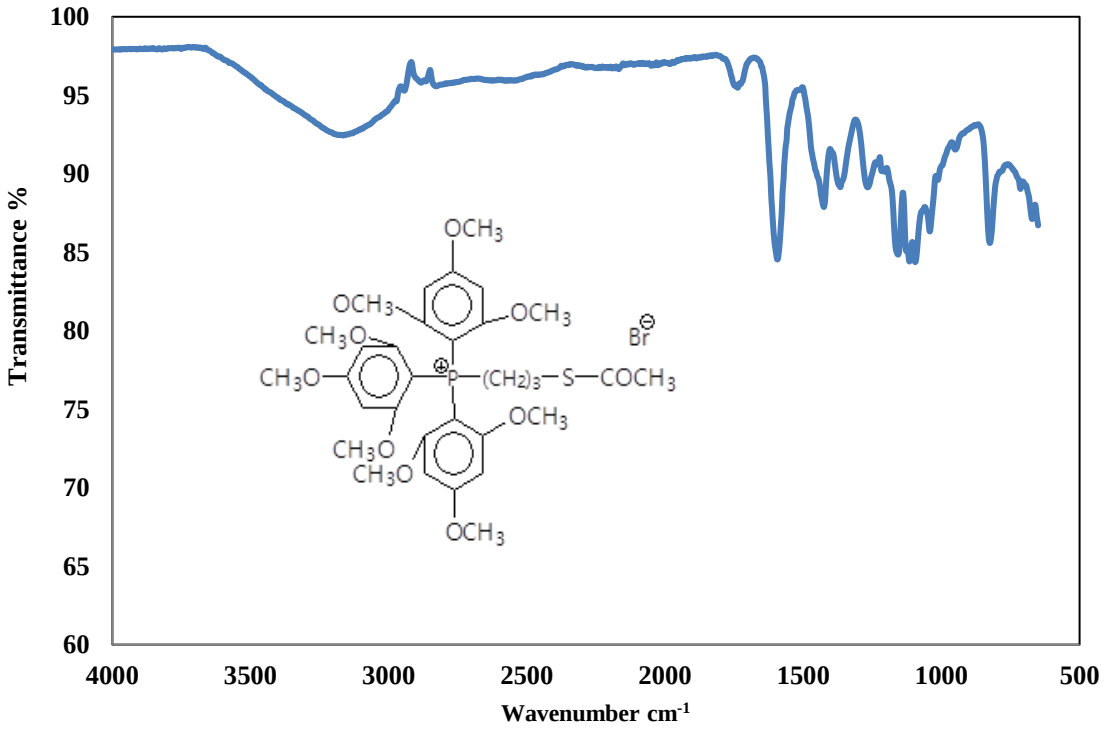

Figure **B3.6** ATR-FTIR of (**4B**). ***Following Chapter 3***

Appendix C4.1

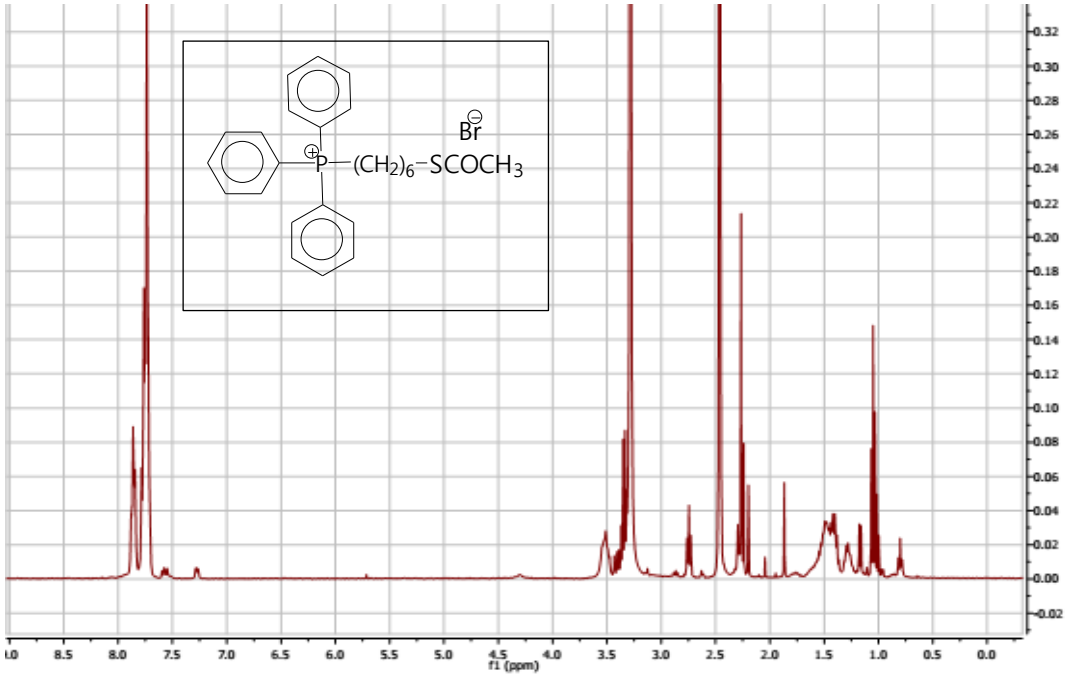

Figure C4.1 ^{1}HNMR of (**8D**). ***Following Chapter 4***

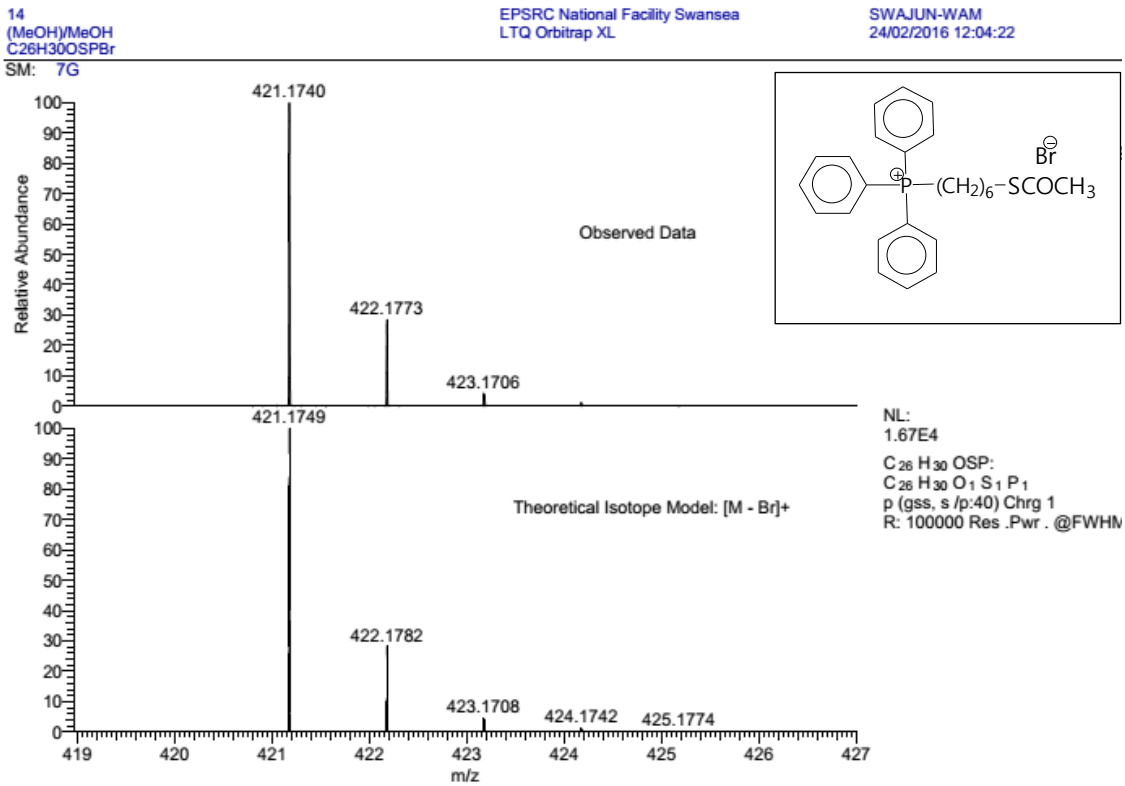

Figure C4.2 ESI-MS of (**8D**). ***Following Chapter 4***

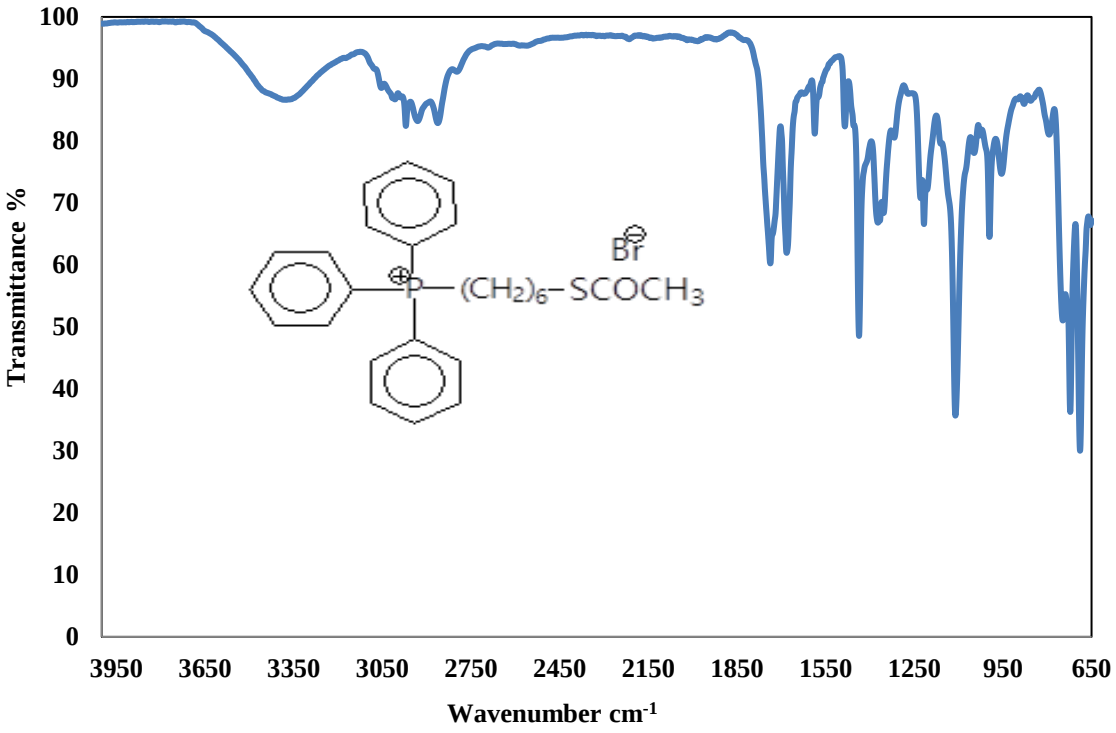

Figure C4.3 ATR-FTIR of (**8D**). ***Following Chapter 4***

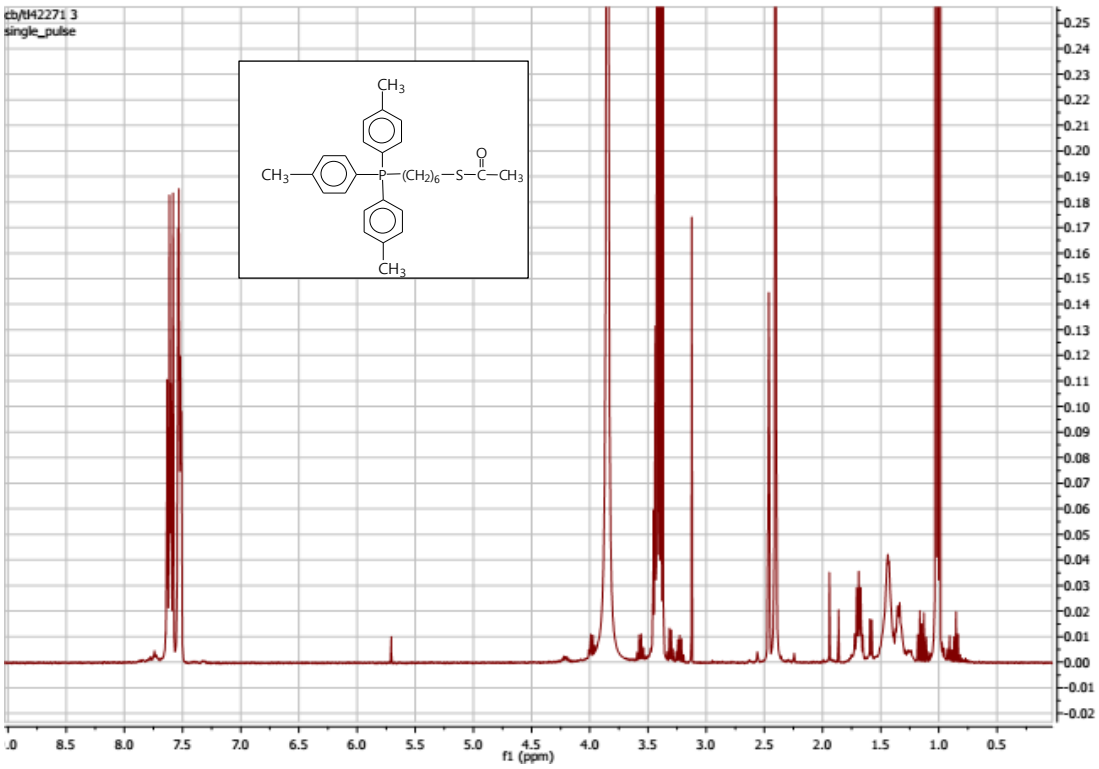

Figure C4.4 ^{1}H-NMR of (**8A**). ***Following chapter 4***

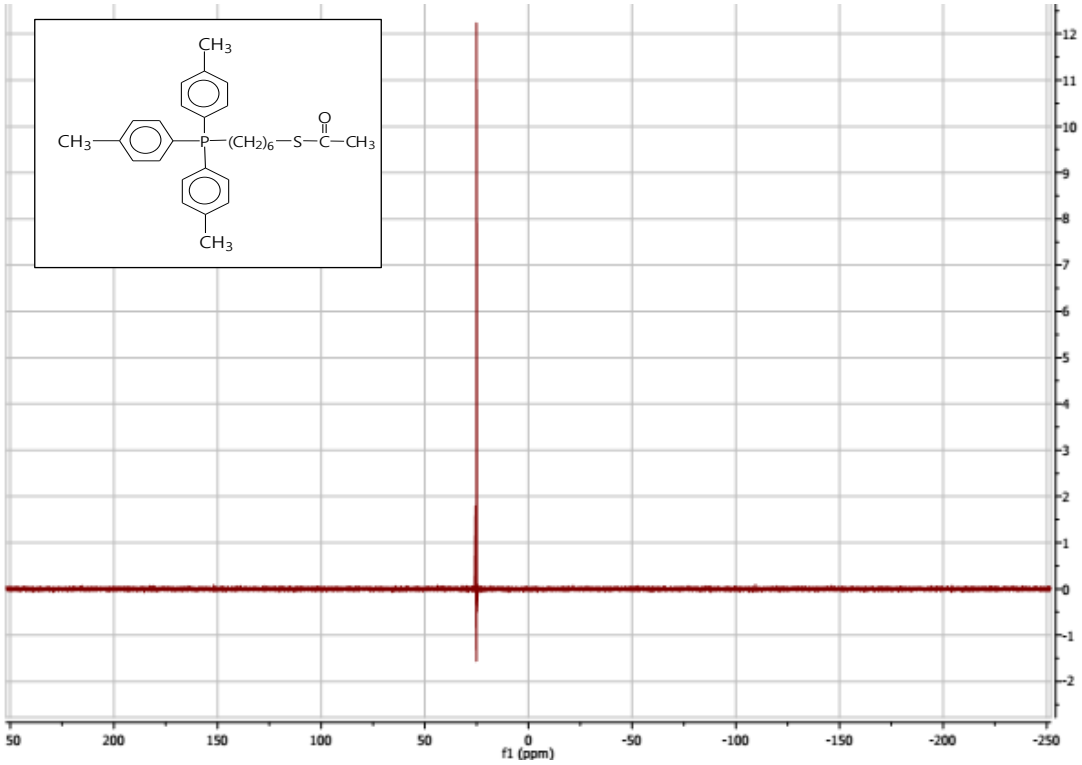

Figure C4.5 ^{13}C-NMR of (**8A**). ***Following Chapter 4***

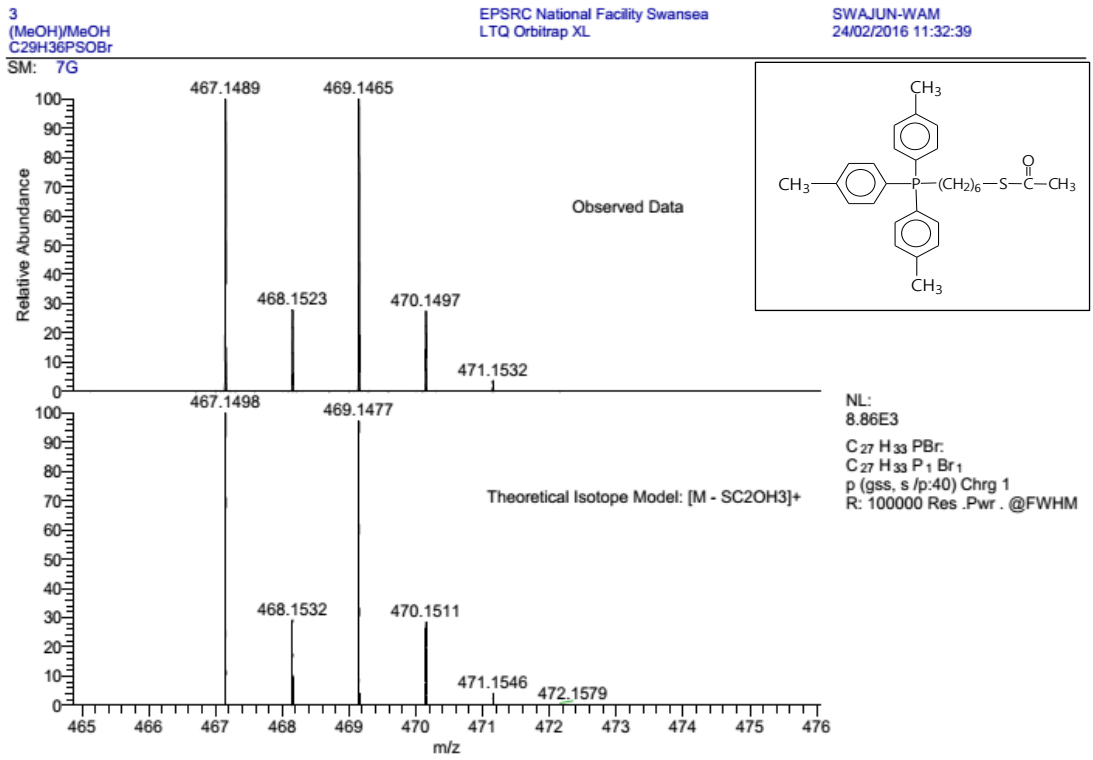

Figure C4.6 ESI-MS of (**8A**). ***Following Chapter 4***

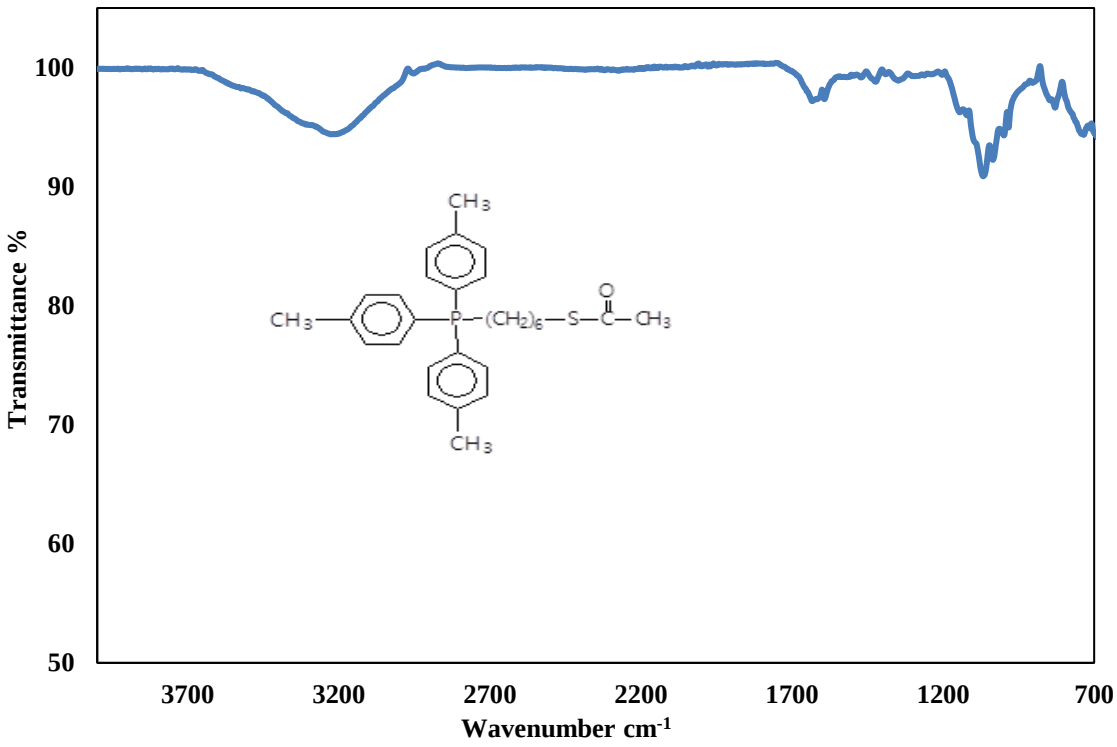

Figure C4.7. ATR-FTIR of (**8A**). ***Following Chapter 4***

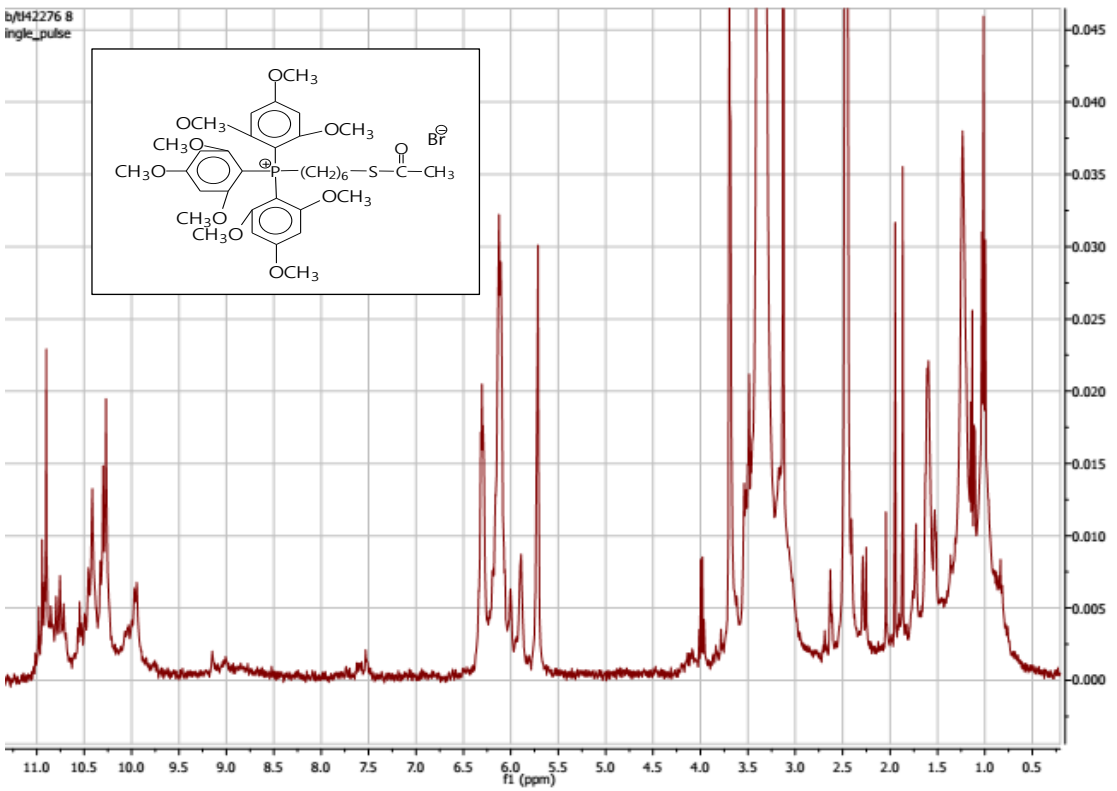

Figure C4.8. ^{1}H-NMR of (**8B**). ***Following Chapters 4 and 6***

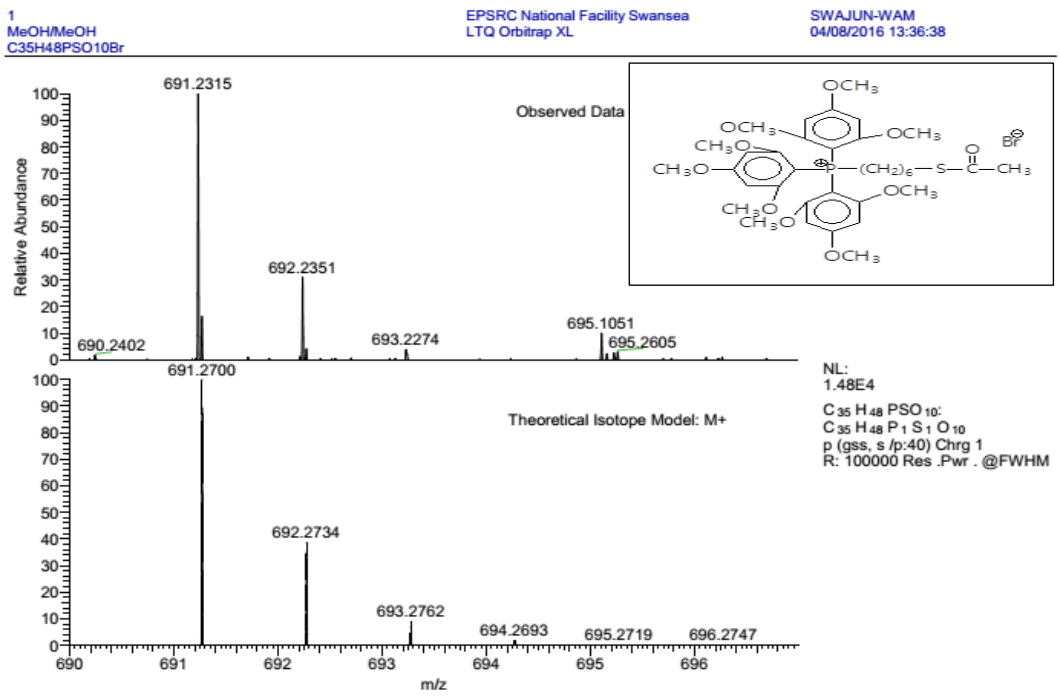

Figure C4.9 ESI-MS of (**8B**). ***Following Chapters 4 and 6***

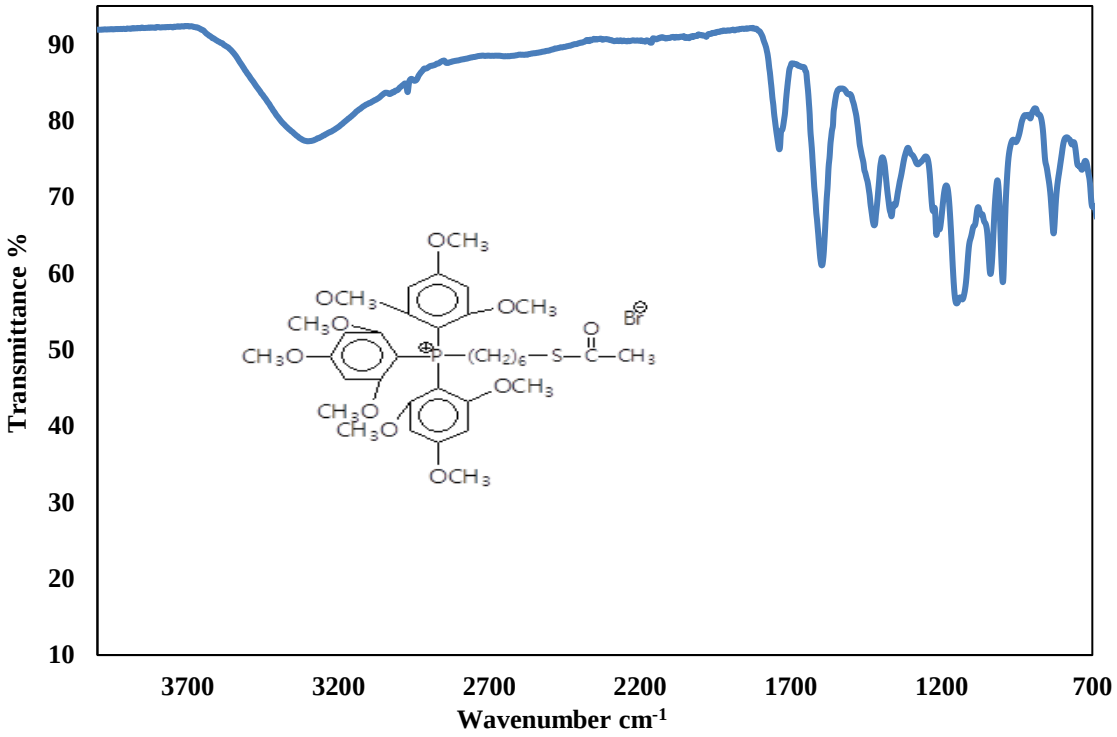

Figure C4.10. ATR-FTIR of (**8B**). ***Following Chapters 4 and 6***

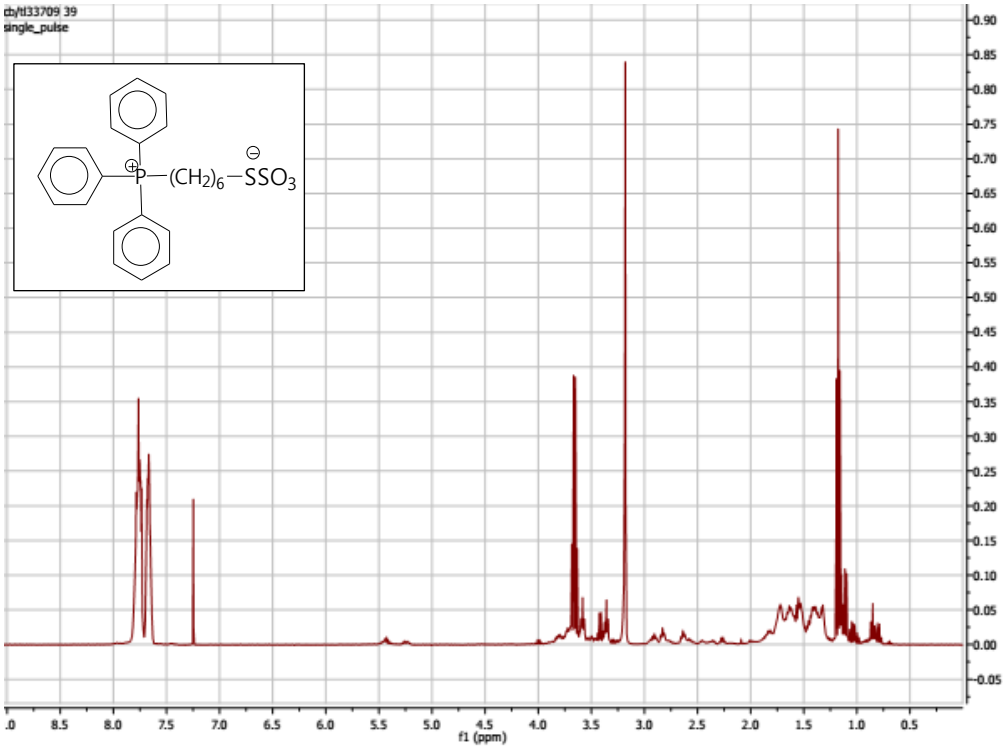

Figure C4.11. ^{1}H-NMR of (**9D**). ***Following Chapter 4***

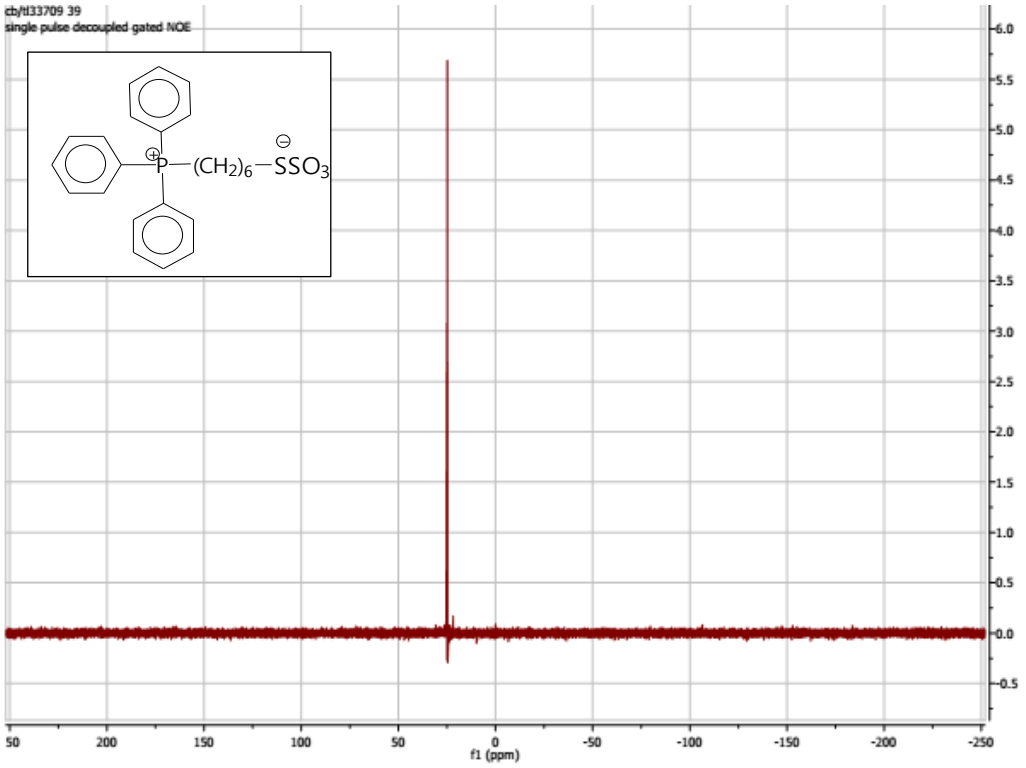

Figure C4.12. ^{13}C NMH of (**9D**). ***Following Chapter 4***

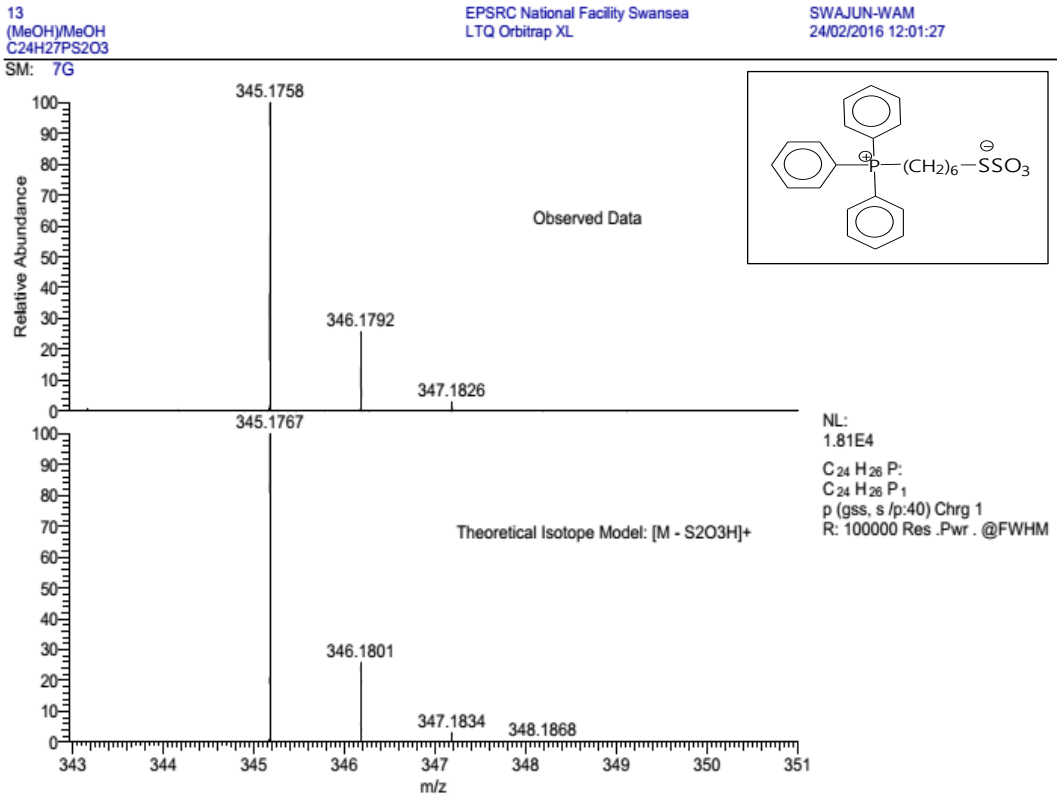

Figure C4.13. ESI-MS of (**9D**). ***Following Chapter 4***

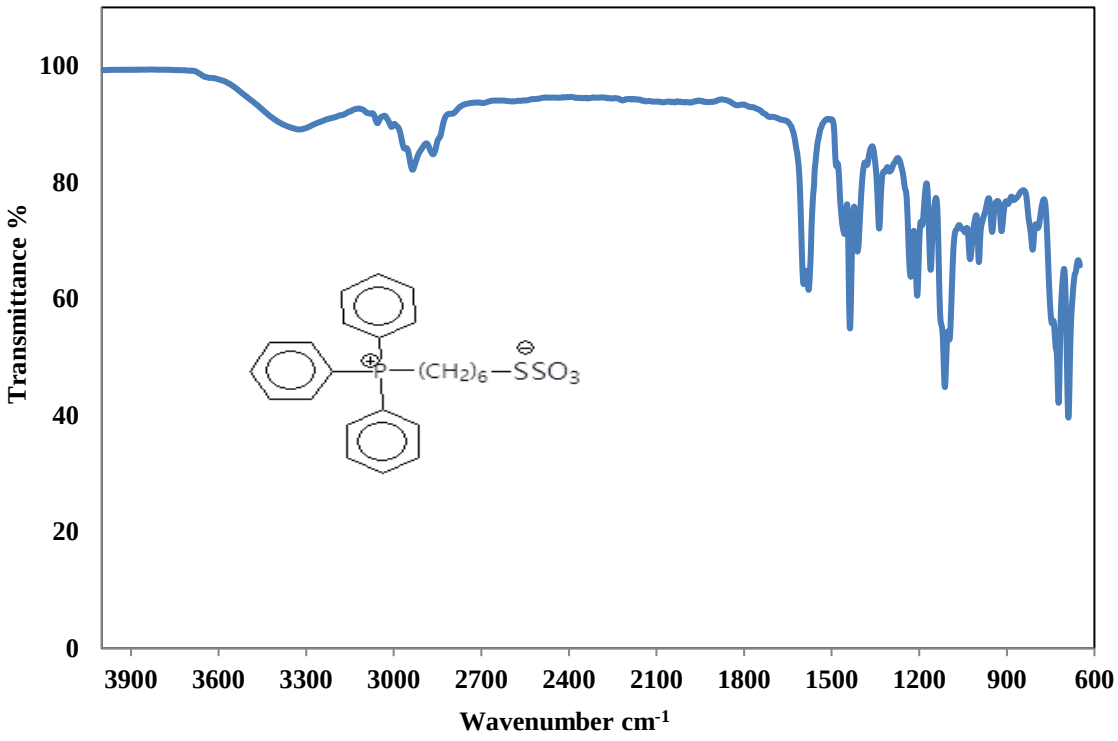

Figure C4.14. ATR-FTIR of (**9D**). ***Following Chapter 4***

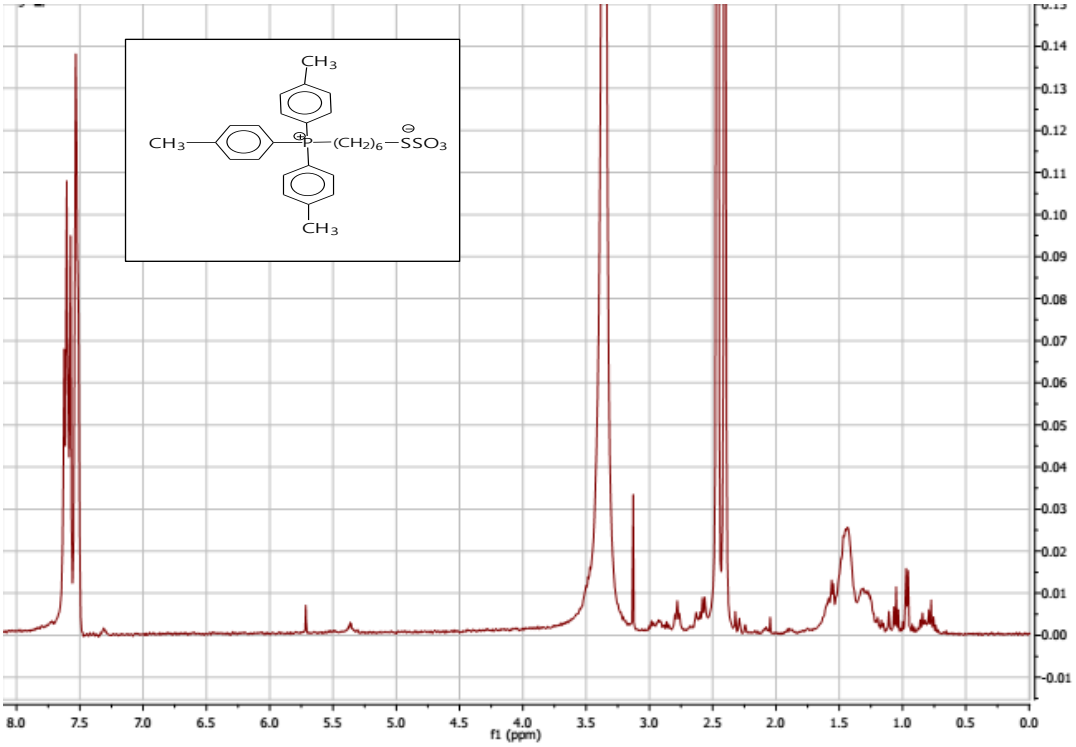

Figure C4.15. ^{1}H-NMR of (**9A**). ***Following Chapter 4***

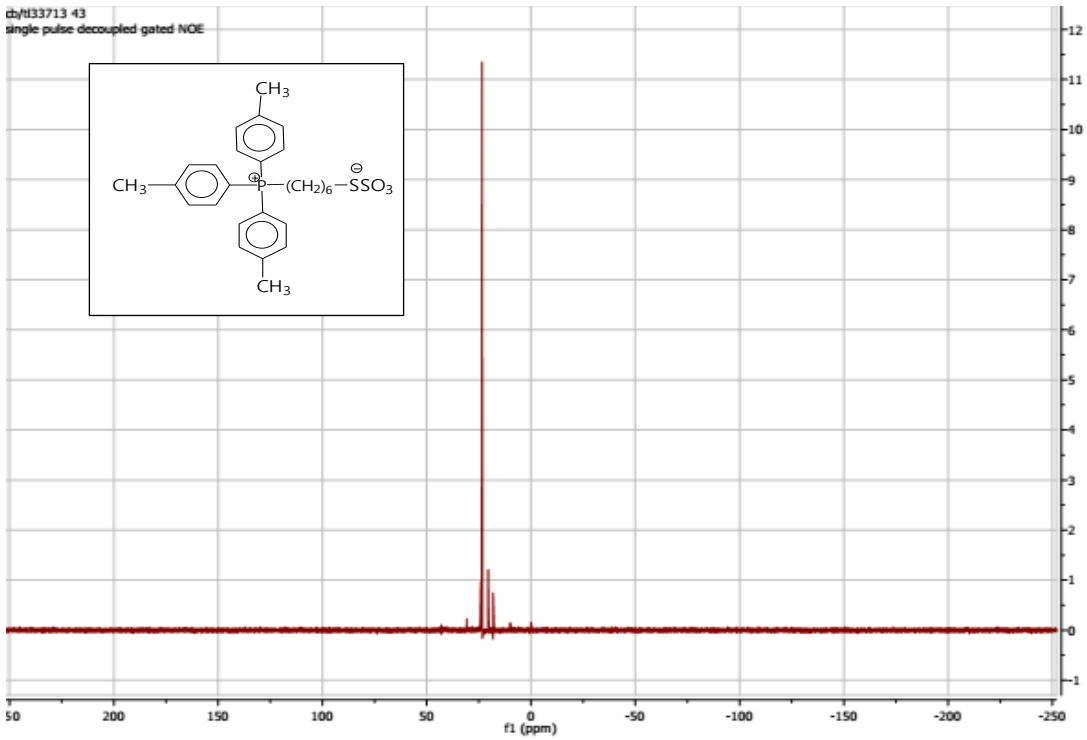

Figure C4.16. ^{13}C-NMR of (**9A**). ***Following Chapter 4***

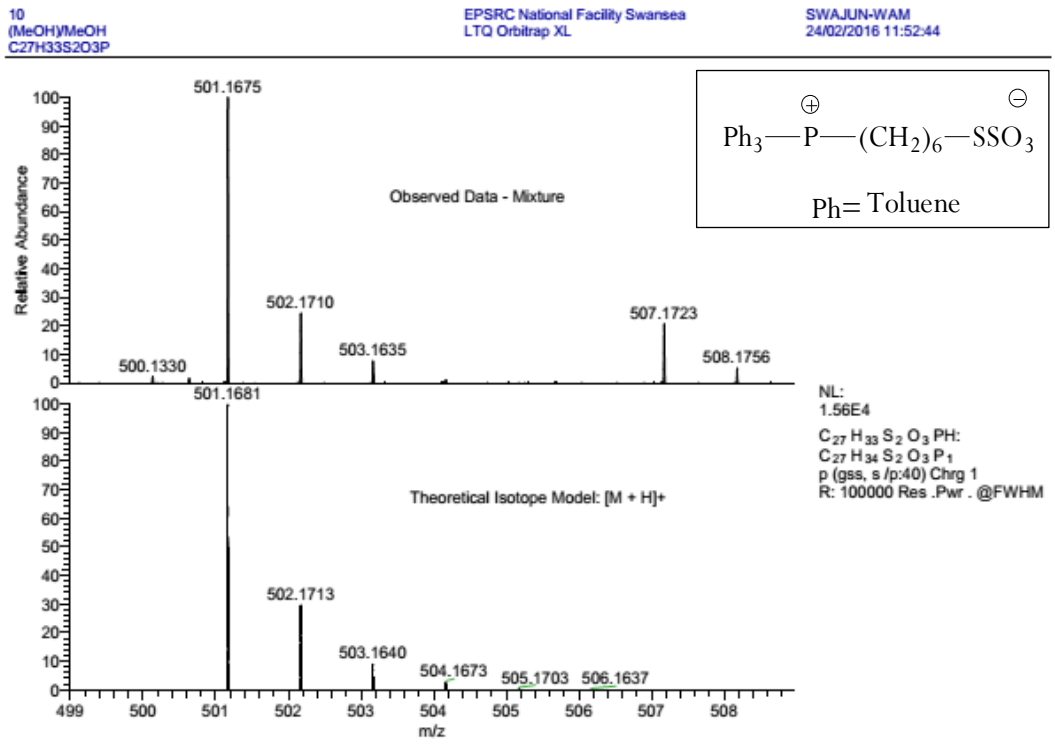

Figure C4.17. ESI-MS of (**9A**). ***Following Chapter 4***

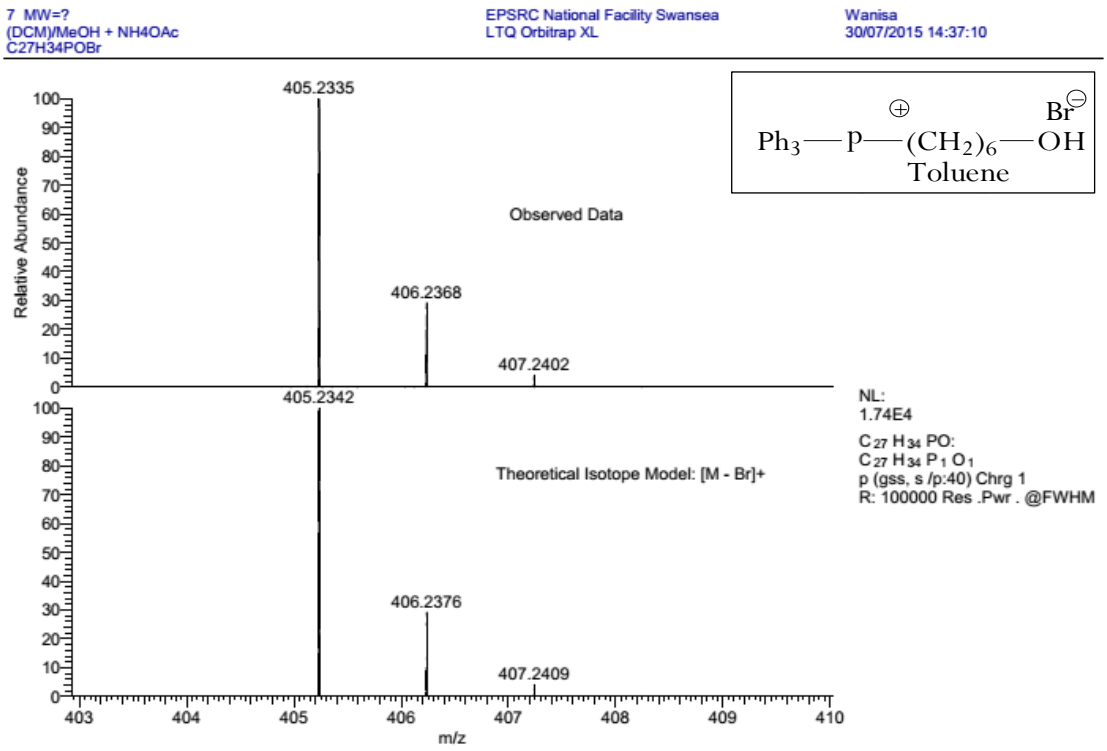

Figure C4.18. ESI-MS of ω-hydroxyhexyltri(*P*-tolyl)phosphonium bromide (**6D**). ***Following Chapter 4***

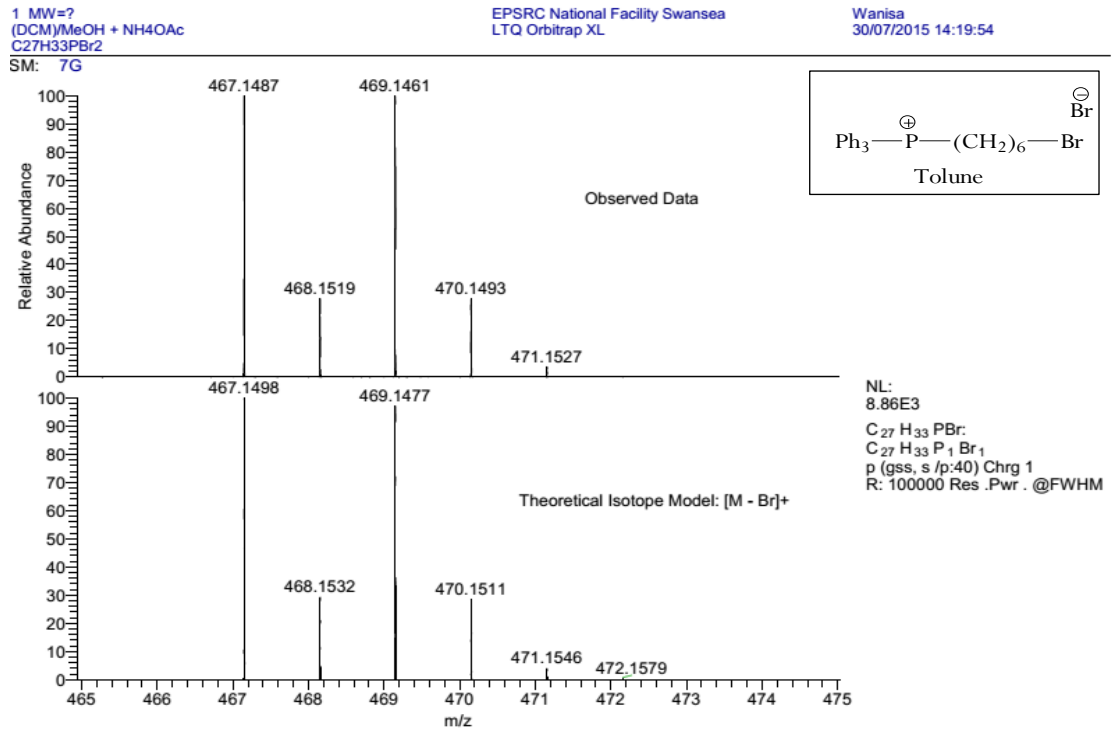

Figure C4.19. ESI-MS of ω-bromohexyl-tri(*P*-tolyl)-phosphonium bromide (**7D**). ***Following Chapter 4***

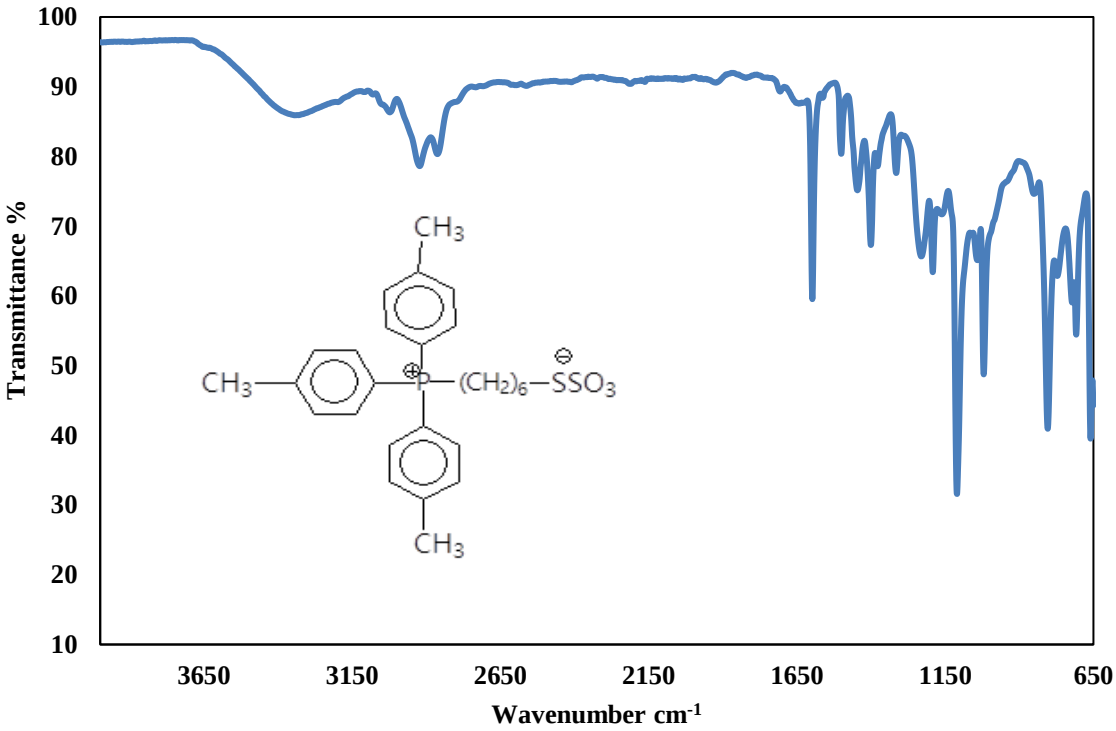

Figure C4.20. ATR-FTIR of (**9A**). ***Following Chapter 4***

Appendix D5.1

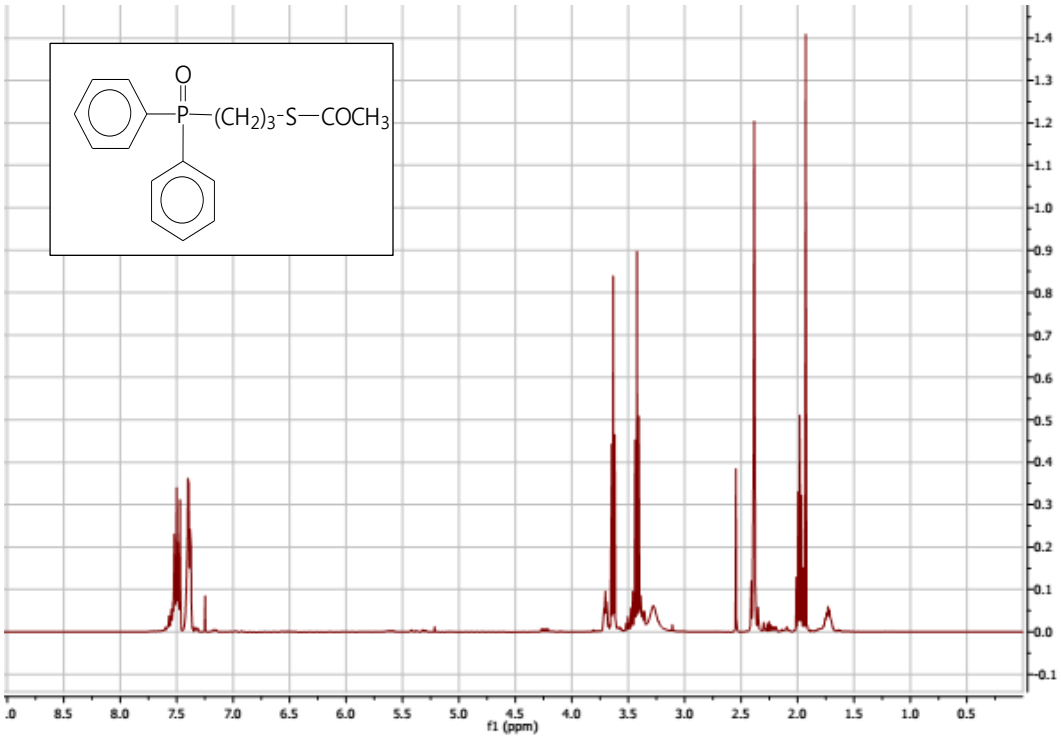

Figure D5.1. ^{1}H-NMR of (**12D**). ***Following Chapter 5***

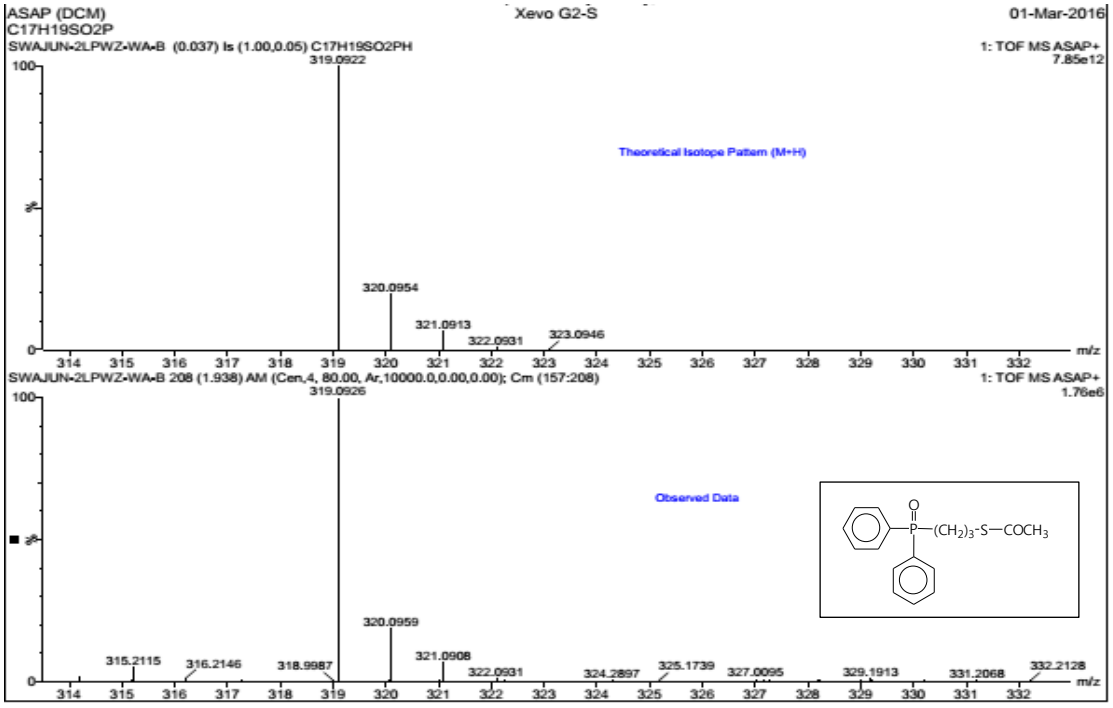

Figure D5.2. ESI-MS of (**12D**). ***Following Chapter 5***

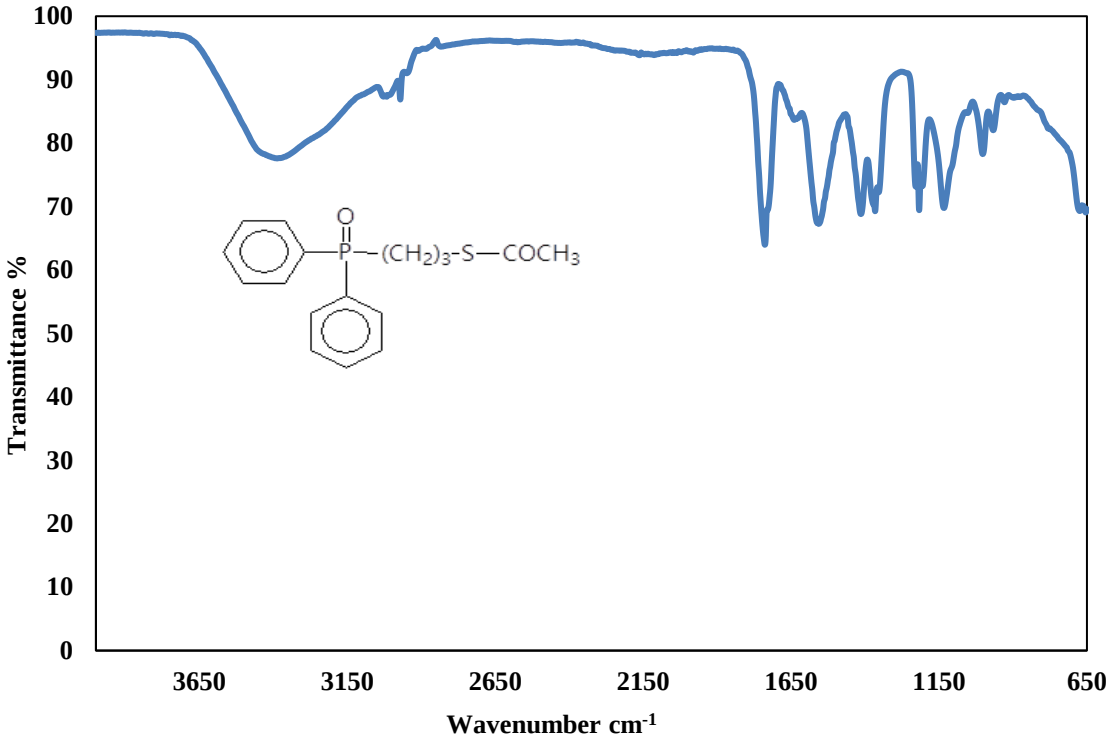

Figure D5.3. ATR-FTIR of (**12D**). ***Following Chapter 5***

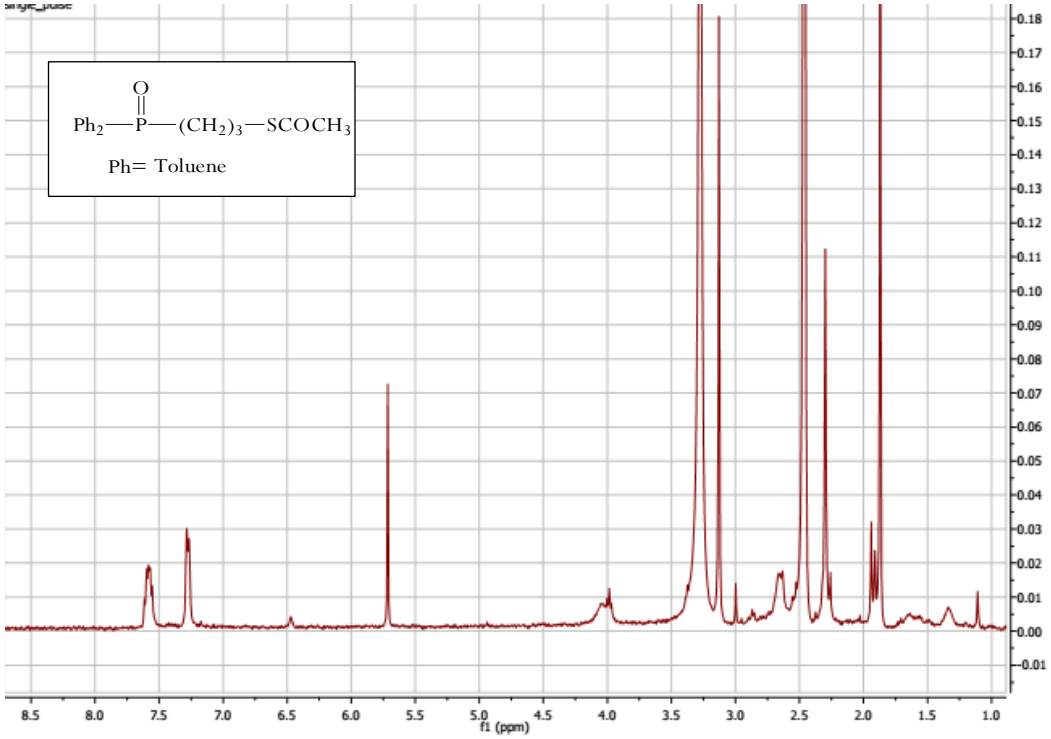

Figure D5.4. ^{1}H-NMR of (**12A**). ***Following Chapter 5***

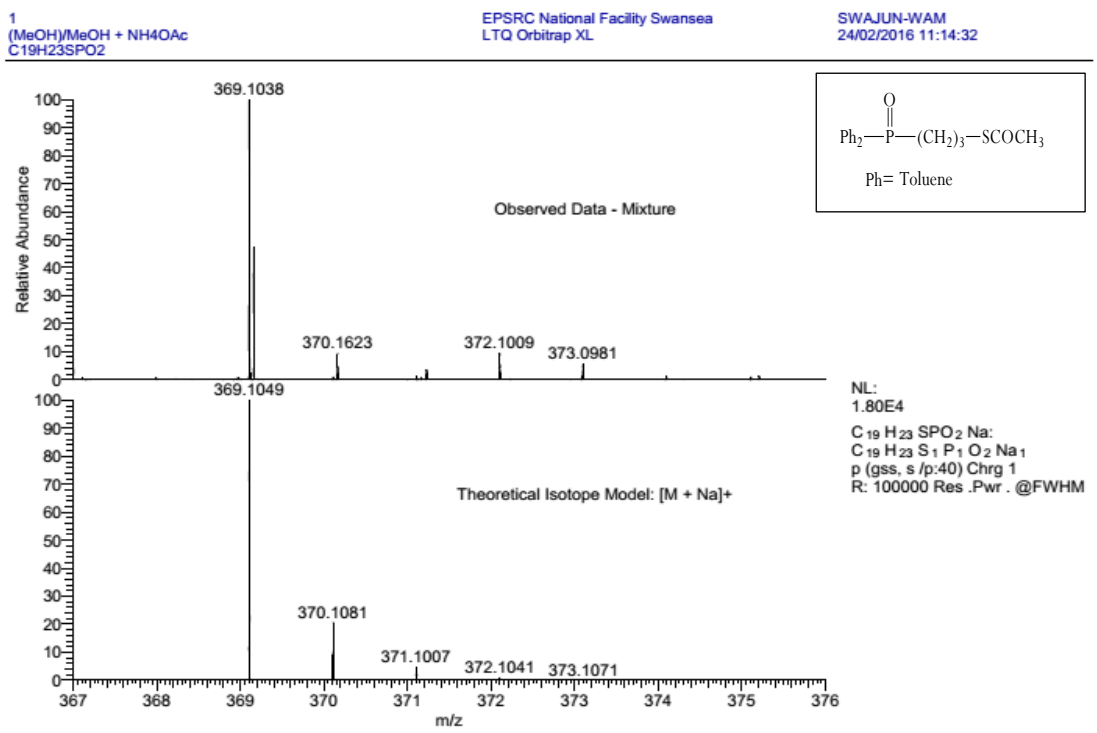

Figure D5.5. ESI-MS of (**12A**). ***Following Chapter 5***

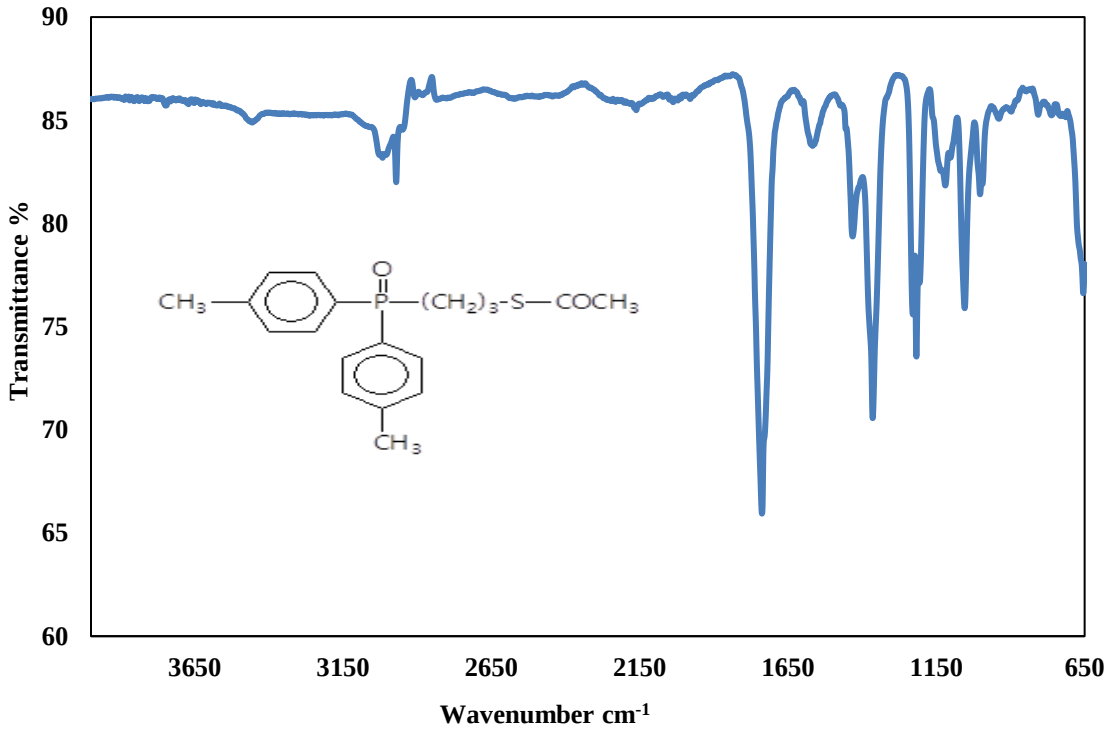

Figure D5.6. ATR-FTIR of (**12A**). ***Following Chapter 5***

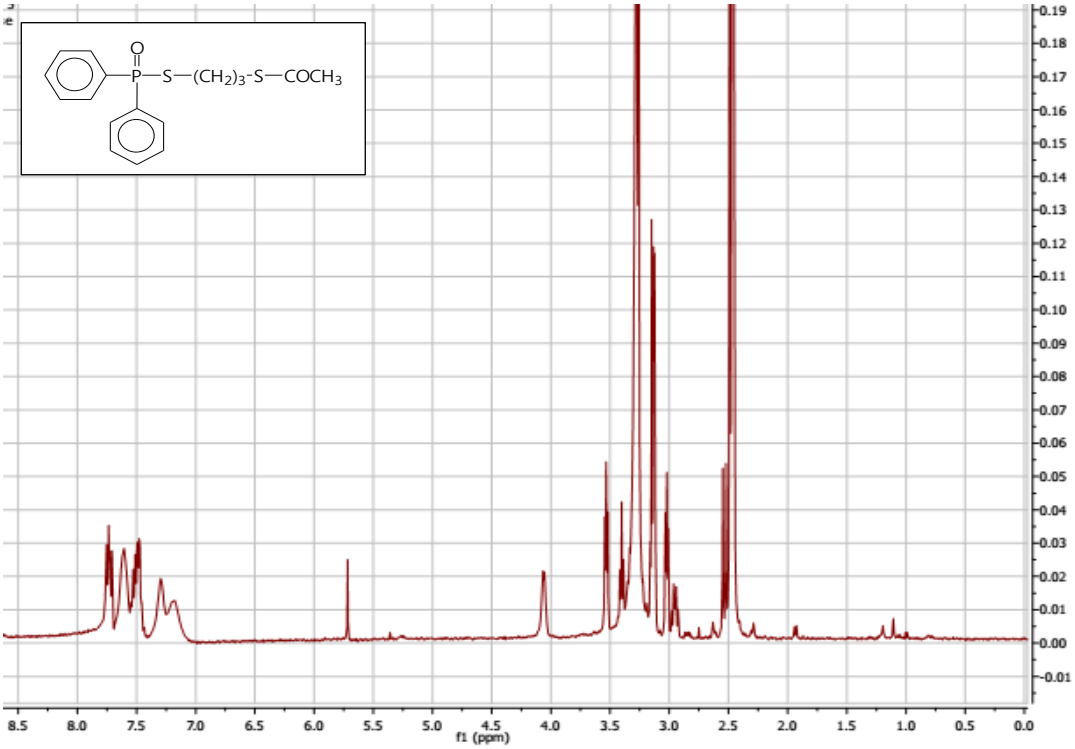

Figure D5.7. ^{1}HNMR of (**15**). ***Following Chapter 5***

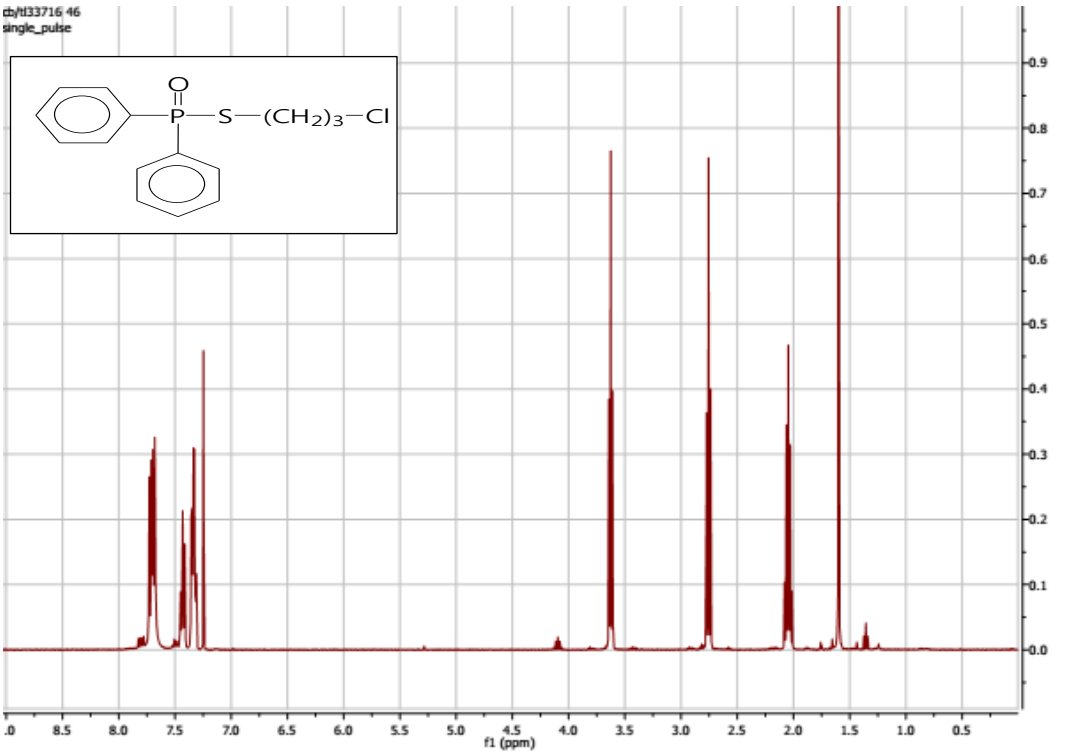

Figure D5.8. ^{1}H-NMR of (**14**). ***Following Chapter 5***

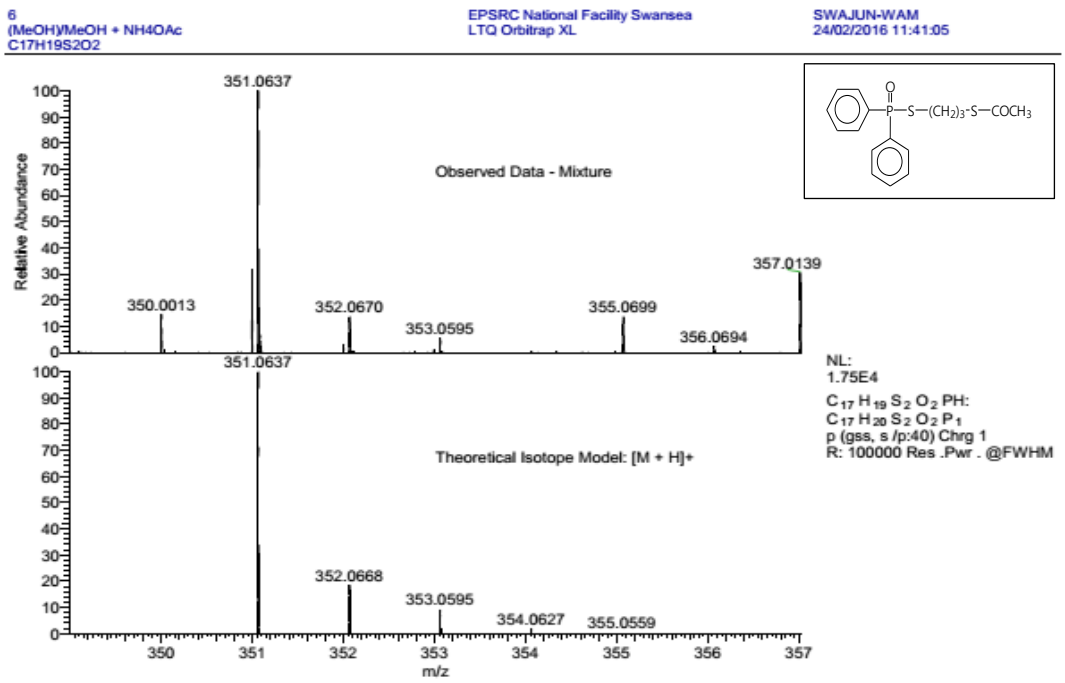

Figure D5.9. ESI-MS of (**15**). ***Following Chapter 5***

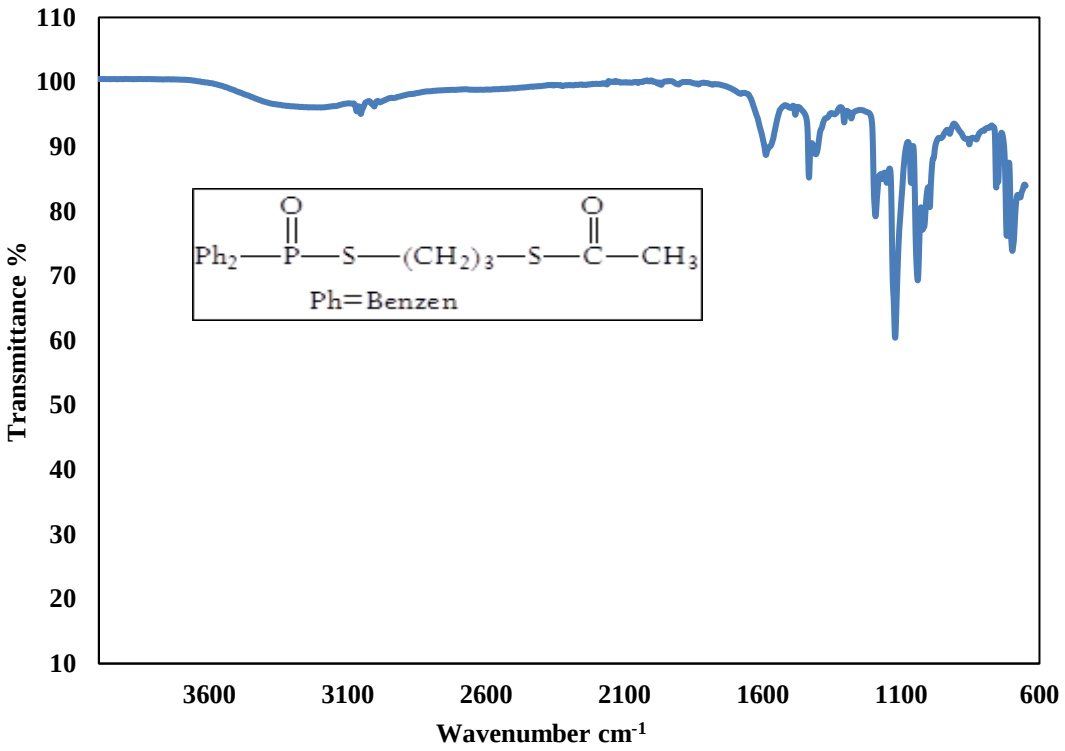

Figure D5.10. ATR-FTIR of (**15**). ***Following Chapter 5***

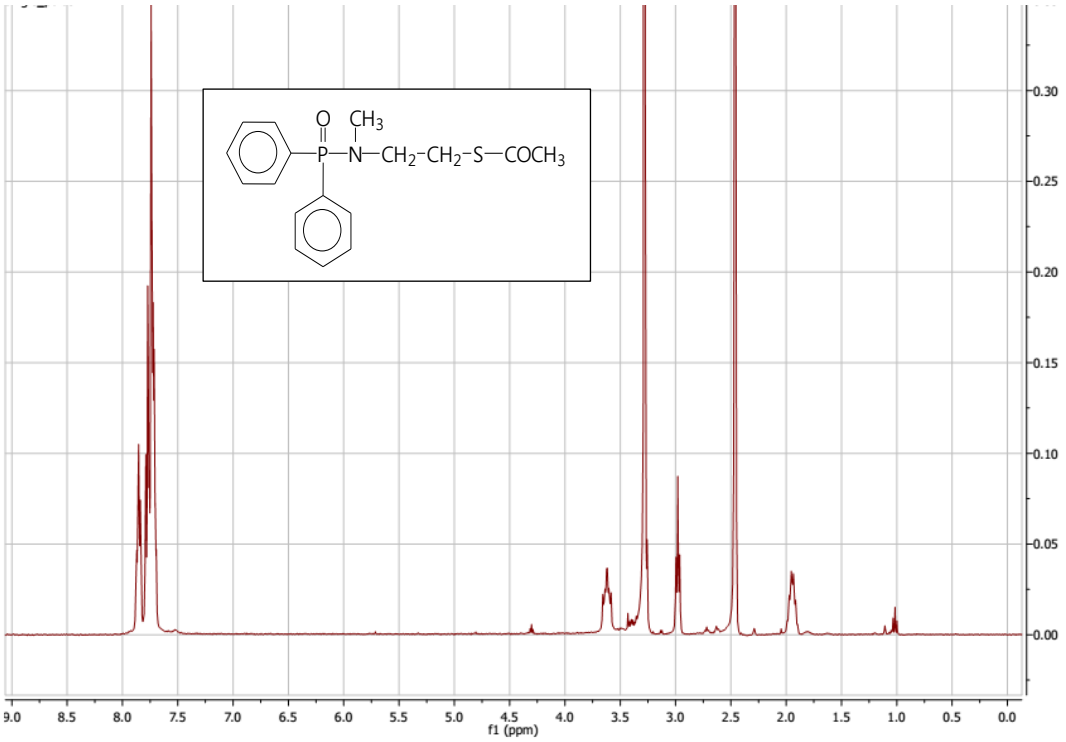

Figure D5.11. ^{1}H-NMR of (**18**). ***Following Chapter 5***

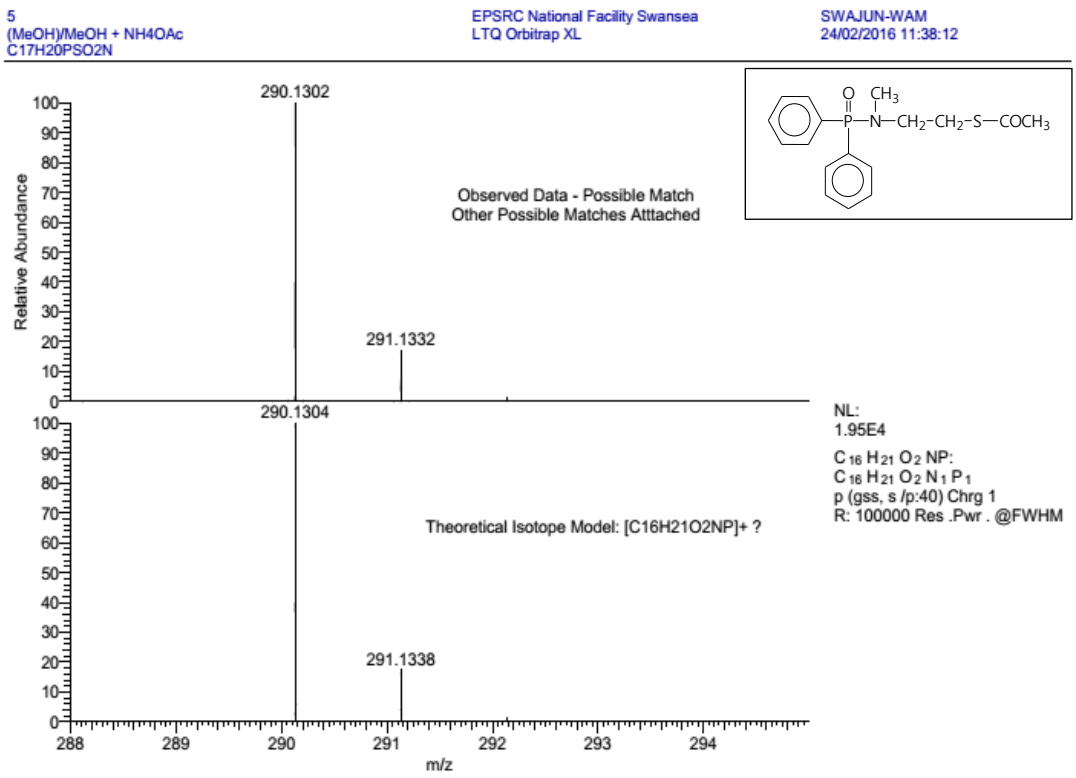

Figure D5.12. ESI-MS of (**18**). ***Following Chapter 5***

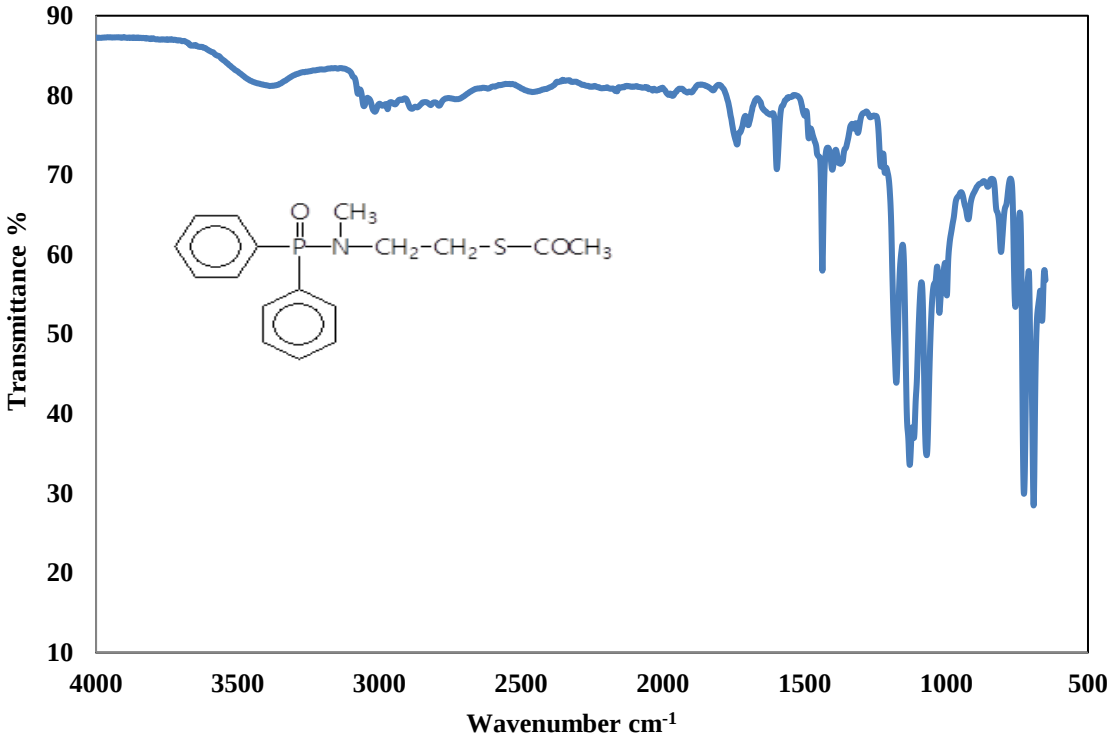

Figure D5.13. ATR-FTIR of (**18**). ***Following Chapter 5***

Appendix E6.1

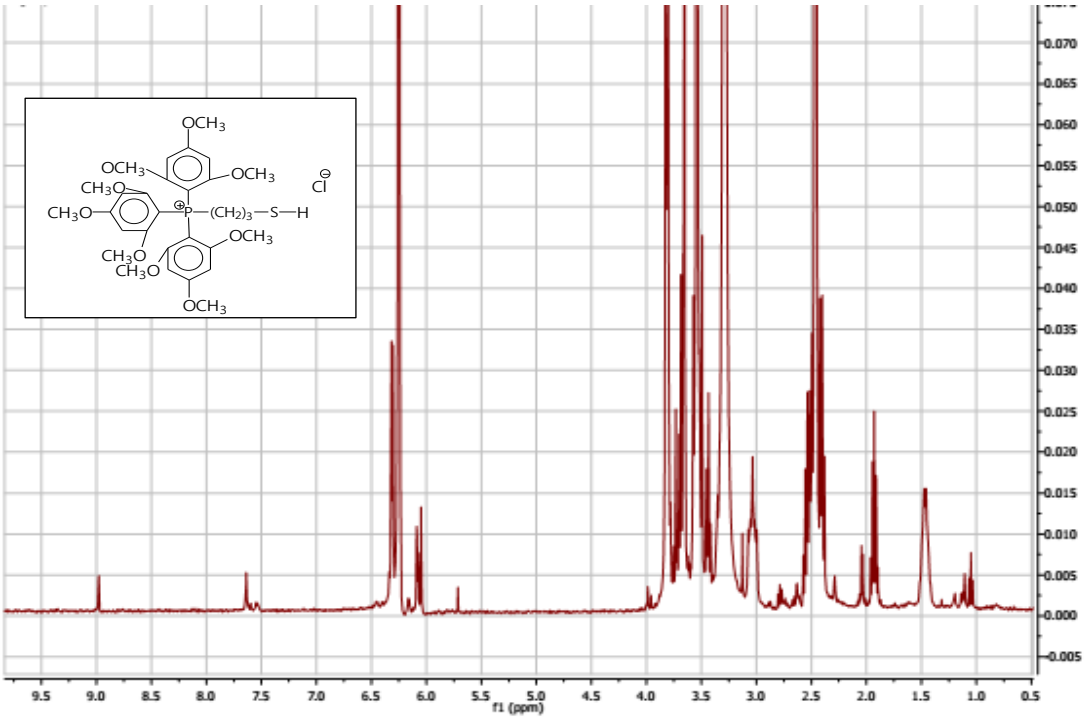

Figure E6.1. ^{1}H-NMR of (**2C**). ***Following Chapter 6***

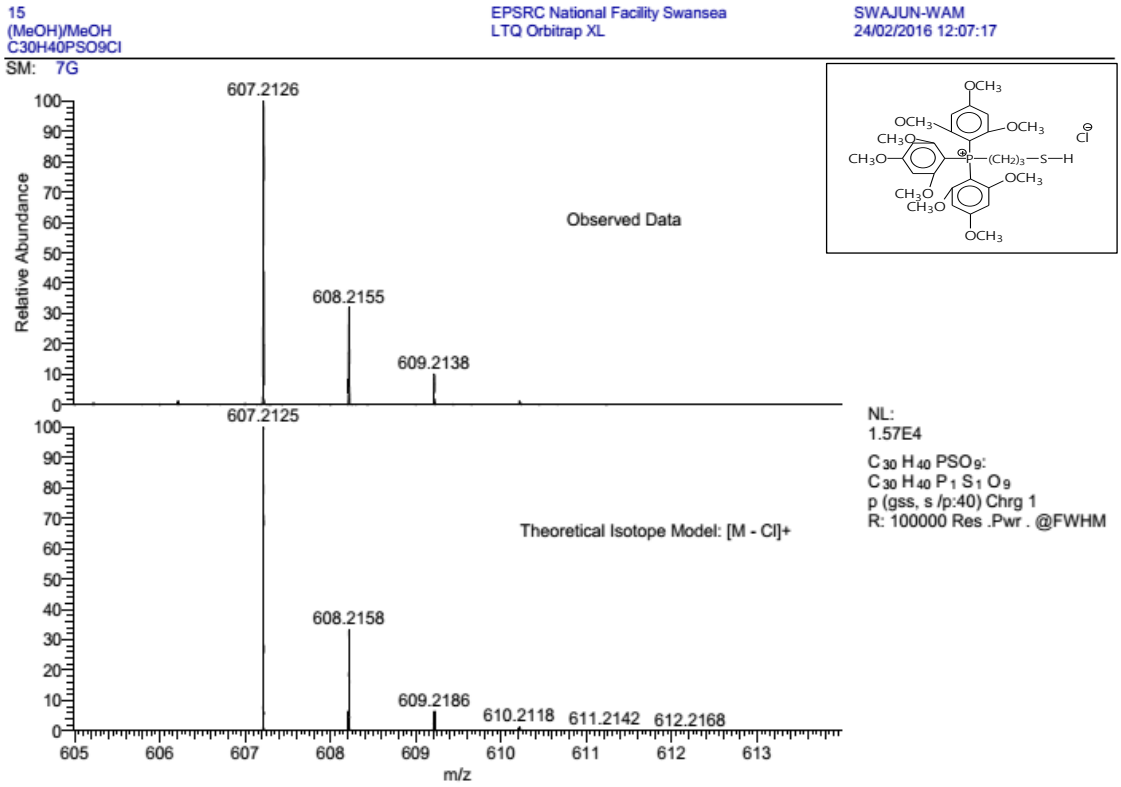

Figure E6.2. ESI-MS of (**2C**). ***Following Chapter 6***

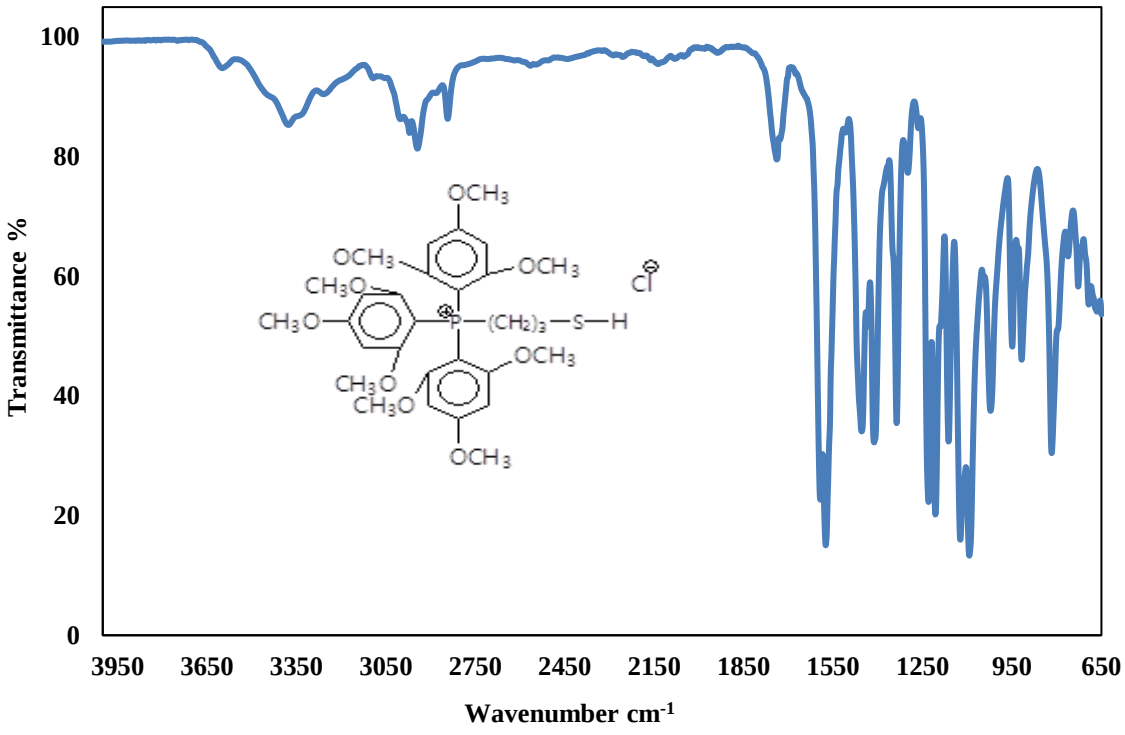

Figure E6.3. ATR-FTIR of (**2C**). ***Following Chapter 6***

Appendix F

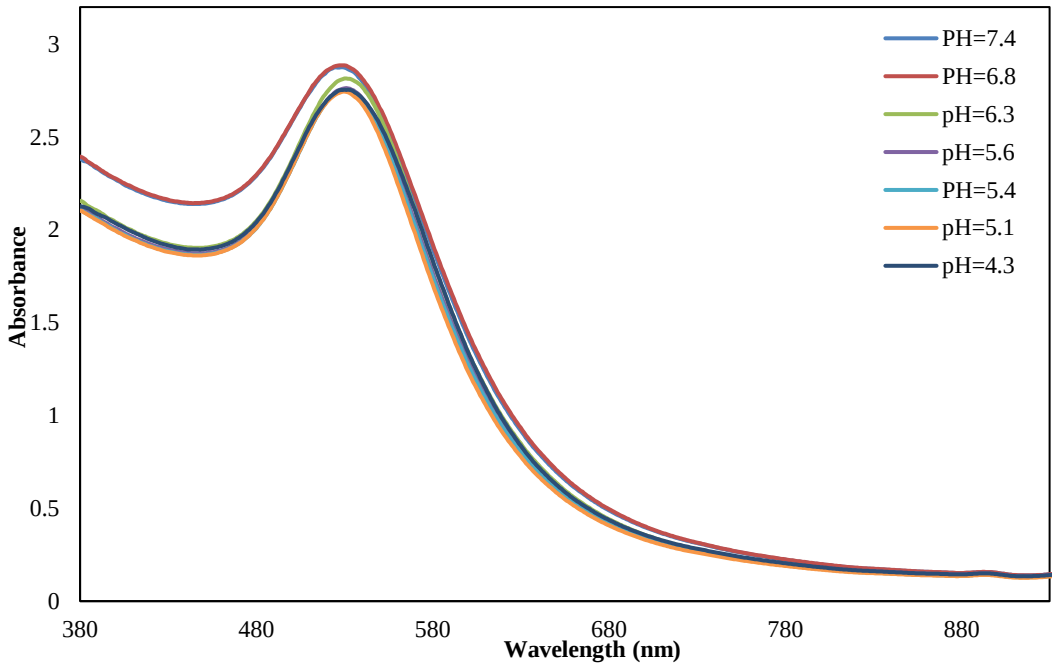

Figure F3.1. Illustrates the data collected through UV-Vis across the pH range produced by adding HCl to (5-30 µL) the AuNPs functionalised by **5**-AuNP solution in (**Run 2**) of the acidic study. ***Following Chapter 3.***

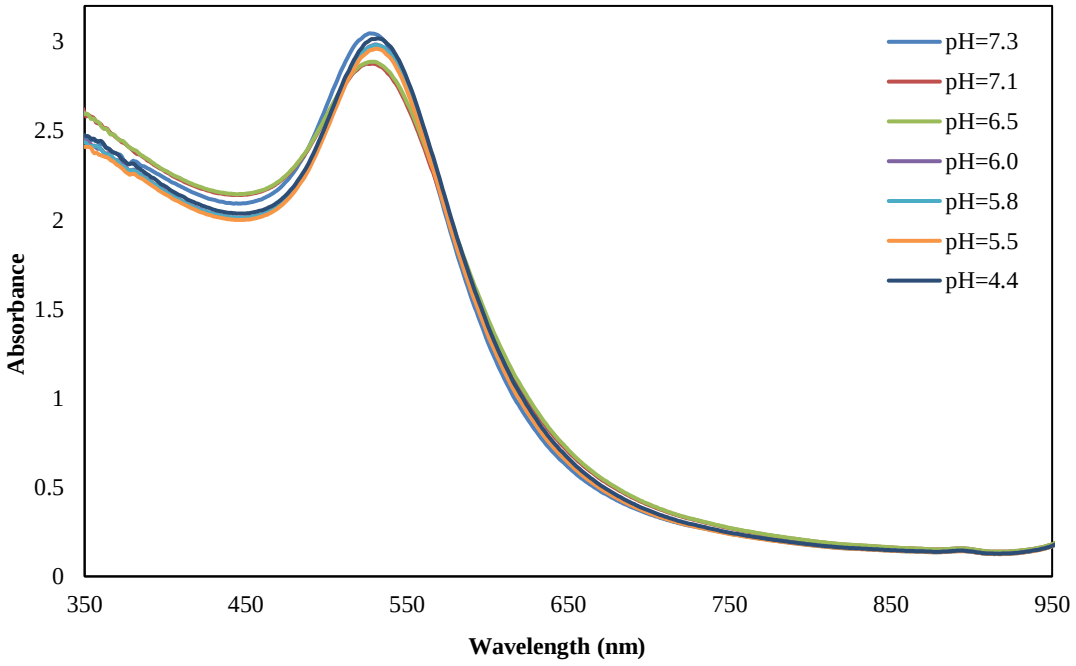

Figure F3.2. Illustrates the data collected through UV-Vis across the pH range produced by adding HCl to (5-30 µL) the AuNPs functionalised by **5**-AuNP solution in (**Run 3**) of the acidic study. ***Following Chapter 3.***

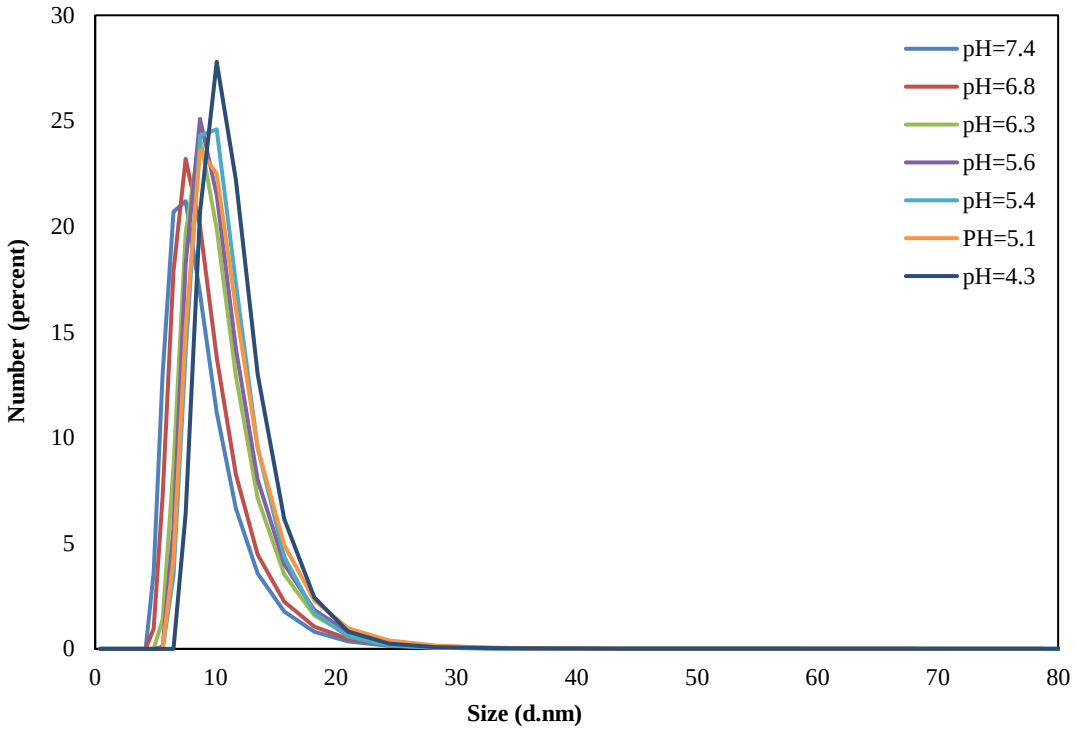

Figure F3.3. Illustrates the data collected of **5**-AuNPs in (**Run 2**) of the acidic pH experiment (pH <7.5) for comparison of DLS results with (Run 1). ***Following Chapter 3.***

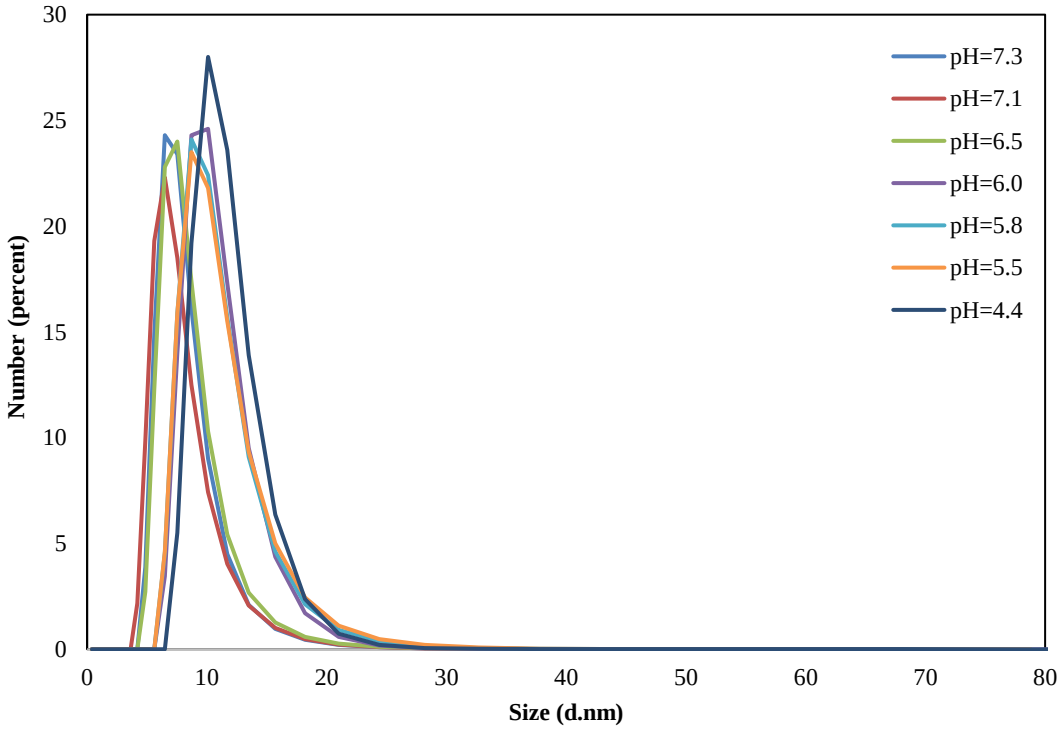

Figure F3.4. Illustrates the data collected of **5**-AuNP in (**Run 3**) of the acidic pH experiment (pH <7.5) for comparison of DLS results with (Run 1) and (Run 2). ***Following Chapter 3.***

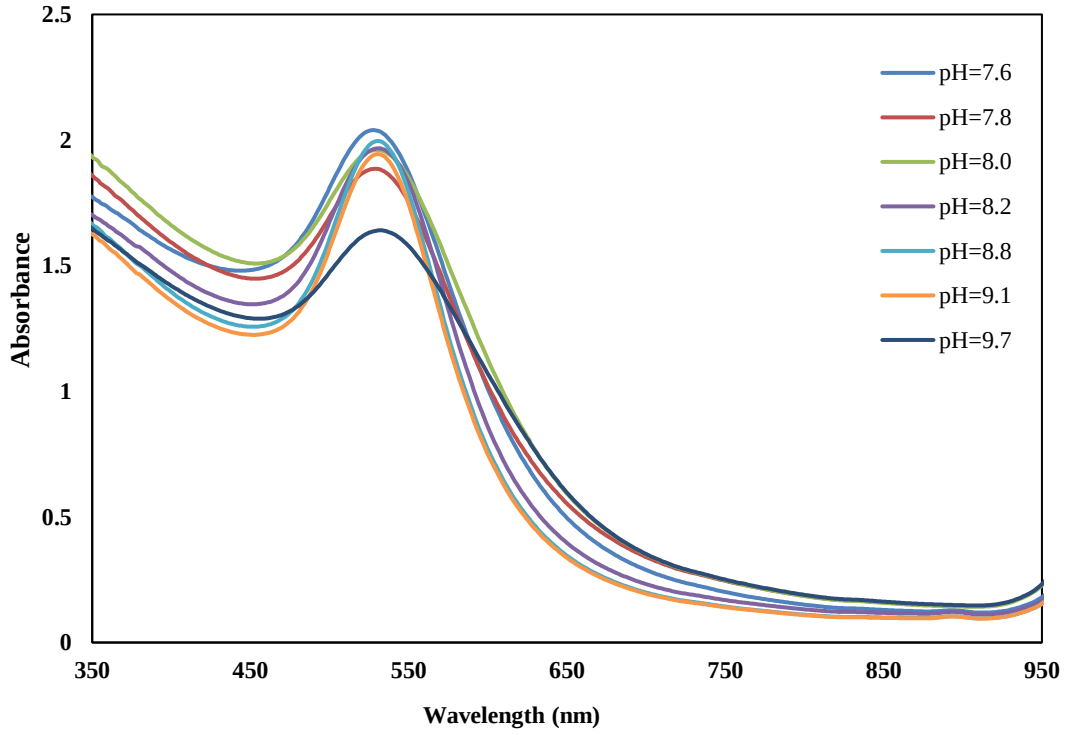

Figure F3.5. Illustrates the UV-Vis data of **5**-AuNP collected for the solutions at increasing pH for (**Run 2**) of the experiment. Where 1M NaOH additions were from (5-30 µL), (pH >7.5). ***Following Chapter 3.***

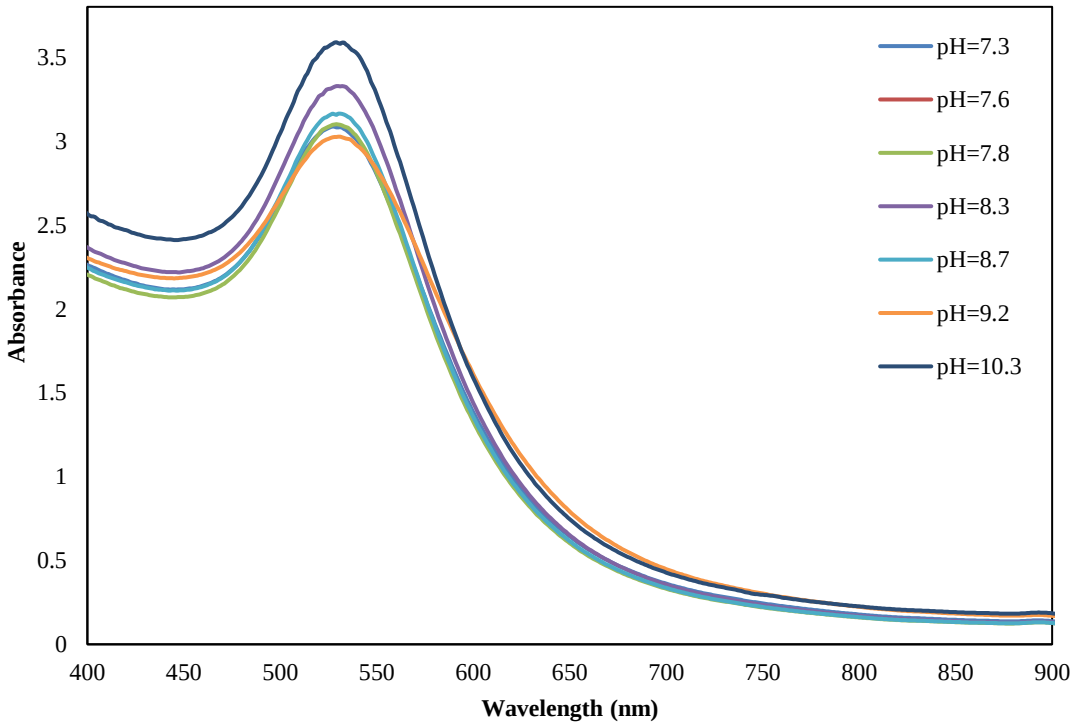

Figure F3.6. Demonstrates the UV-Vis data collected of **5**-AuNP for the solutions at increasing pH for (**Run 3**) of the experiment. Where 1M NaOH additions were from (5-30 µL). ***Following Chapter 3.***

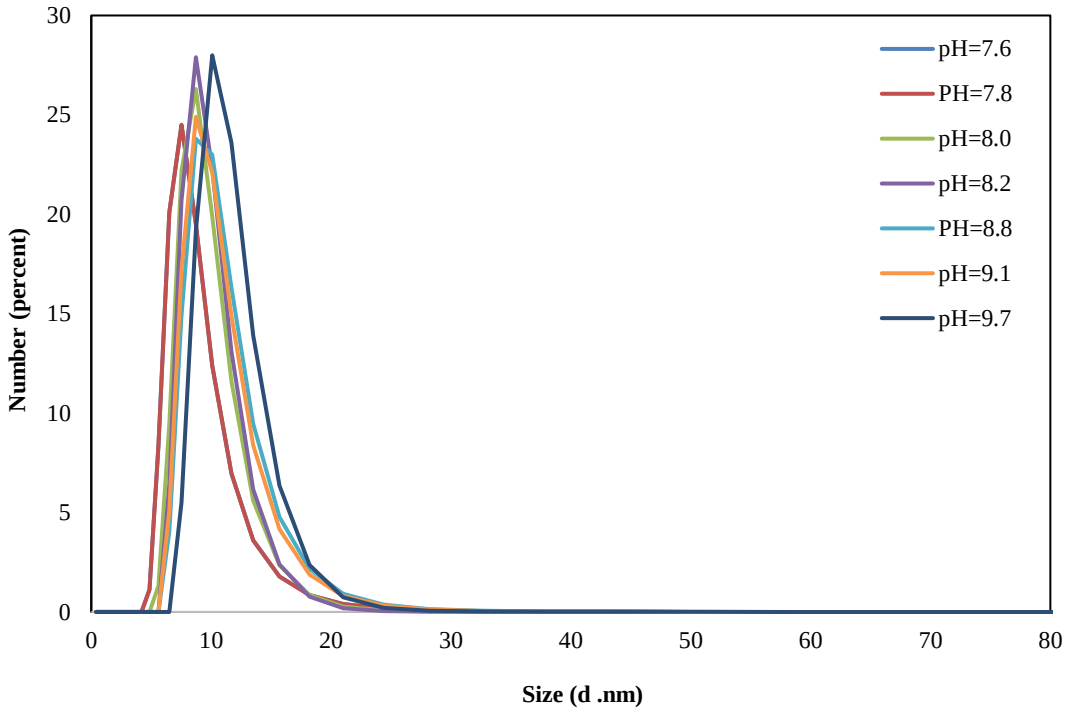

Figure F3.7. Presents the data recorded of **5**-AuNP for the repeat, (**Run 2**), at increasing pH and larger volumes of 1M NaOH (5-30 µL) were added to the AuNPs solution (pH >7.5). ***Following Chapter 3.***

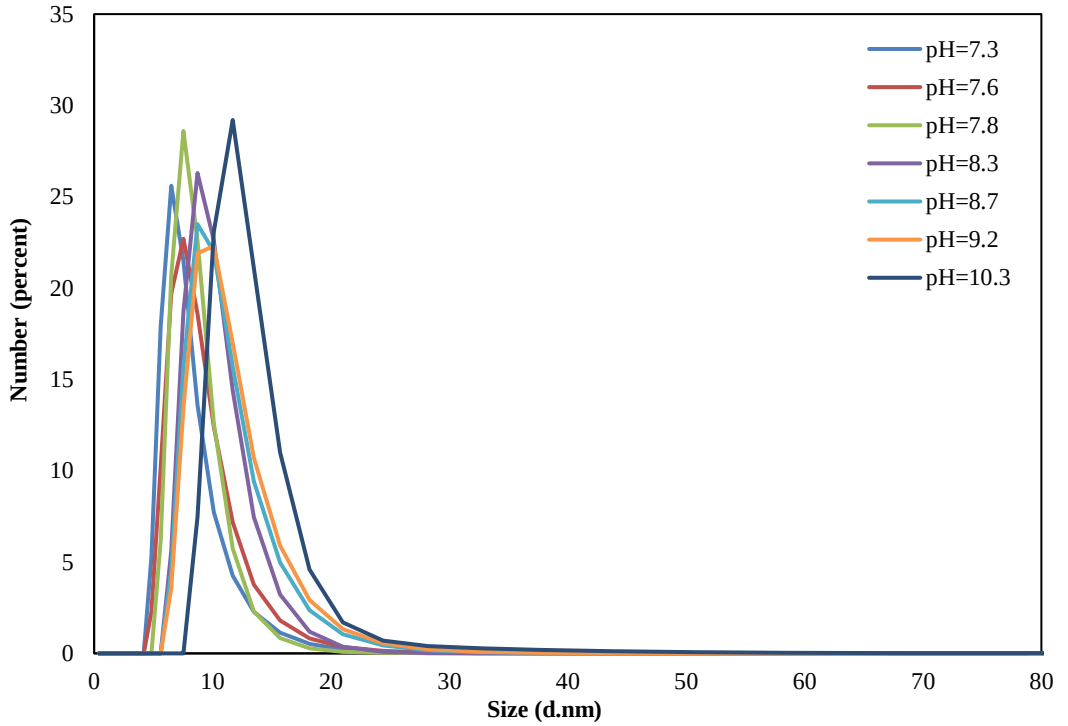

Figure F3.8. Presents the data recorded of **5**-AuNP for the repeat, (**Run 3**), at increasing pH (pH >7.5) and larger volumes of 1M NaOH (5-30 µL) were added to the AuNPs solution. ***Following Chapter 3.***

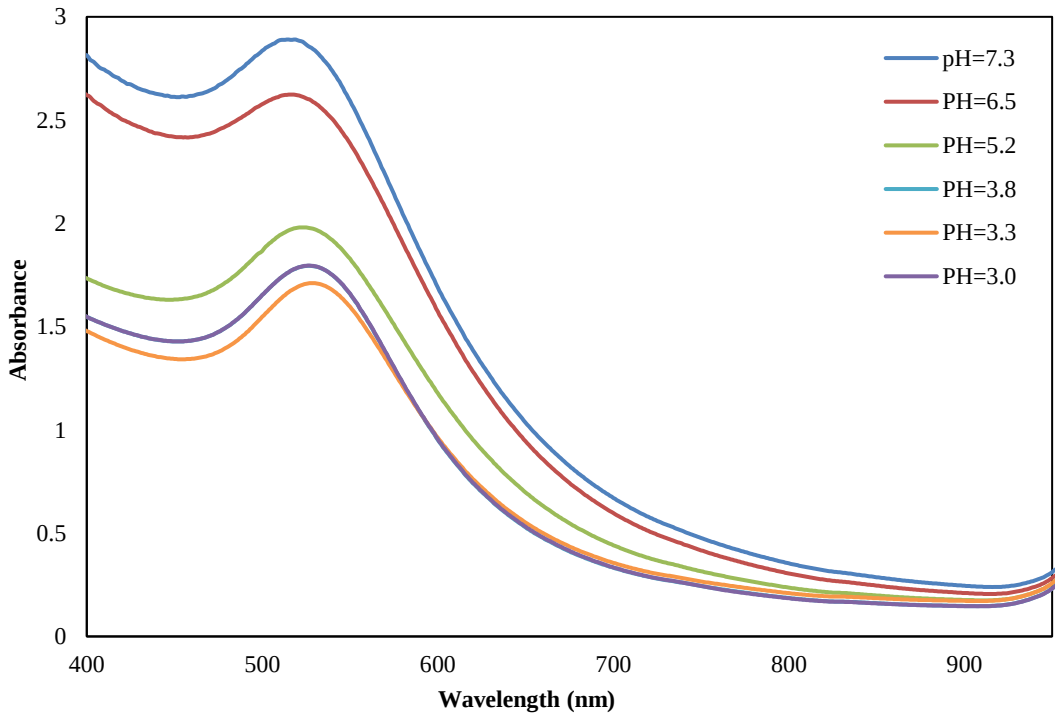

Figure F3.9. Illustrates the data collected through UV-Vis across the pH range produced (pH <7.5) by adding 1M HCl (5-30 µL) to the **4B**-AuNPs solution in (**Run 2**) of the acidic study. ***Following Chapter 3***

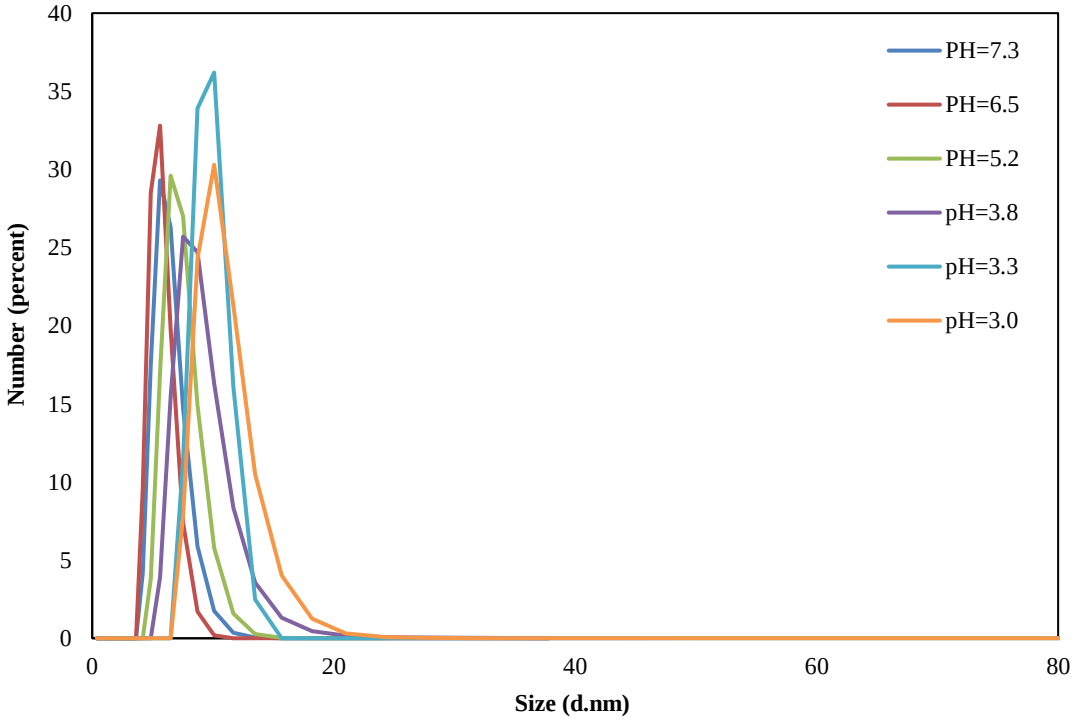

Figure F3.10. Expresses the data collected through DLS analysis of the samples in (**Run 2**) to give the diameter size and standard deviations for each pH range produced by adding 1M HCl (5-30 µL) to the **4B**-AuNPs solution. ***Following Chapter 3.***

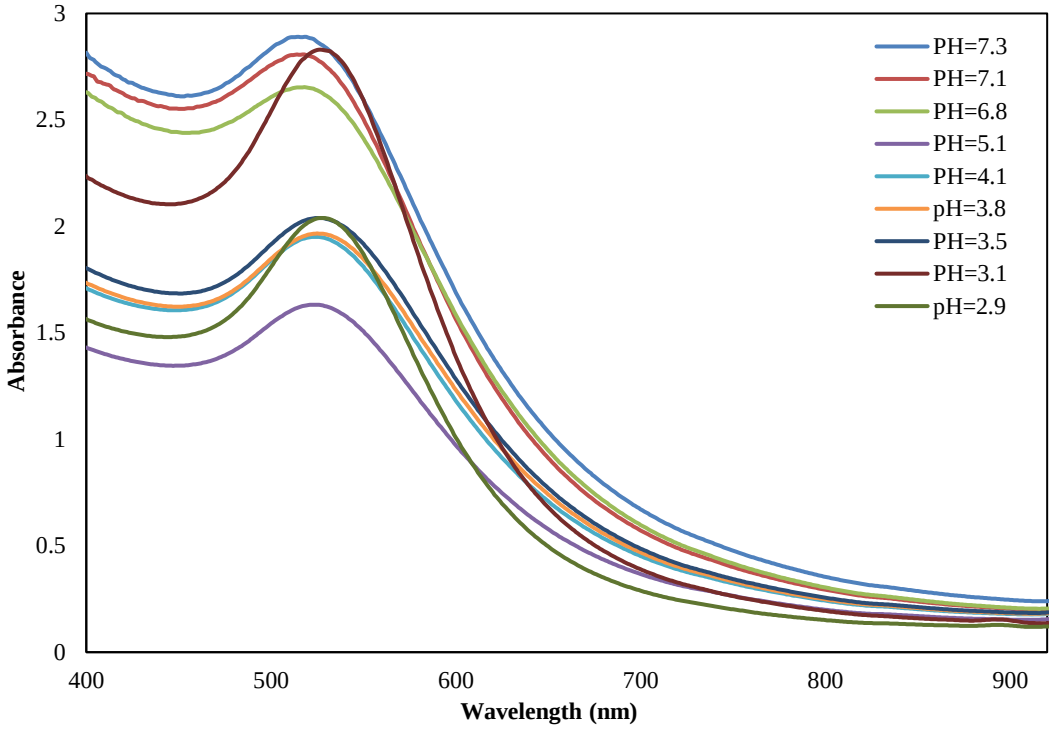

Figure F3.11. Illustrates the data collected through UV-Vis across the pH range produced (pH <7.5) by adding 1M HCl (5-30 µL) to the **4B**-AuNPs solution in (**Run 3**) of the acidic study. ***Following Chapter 3***

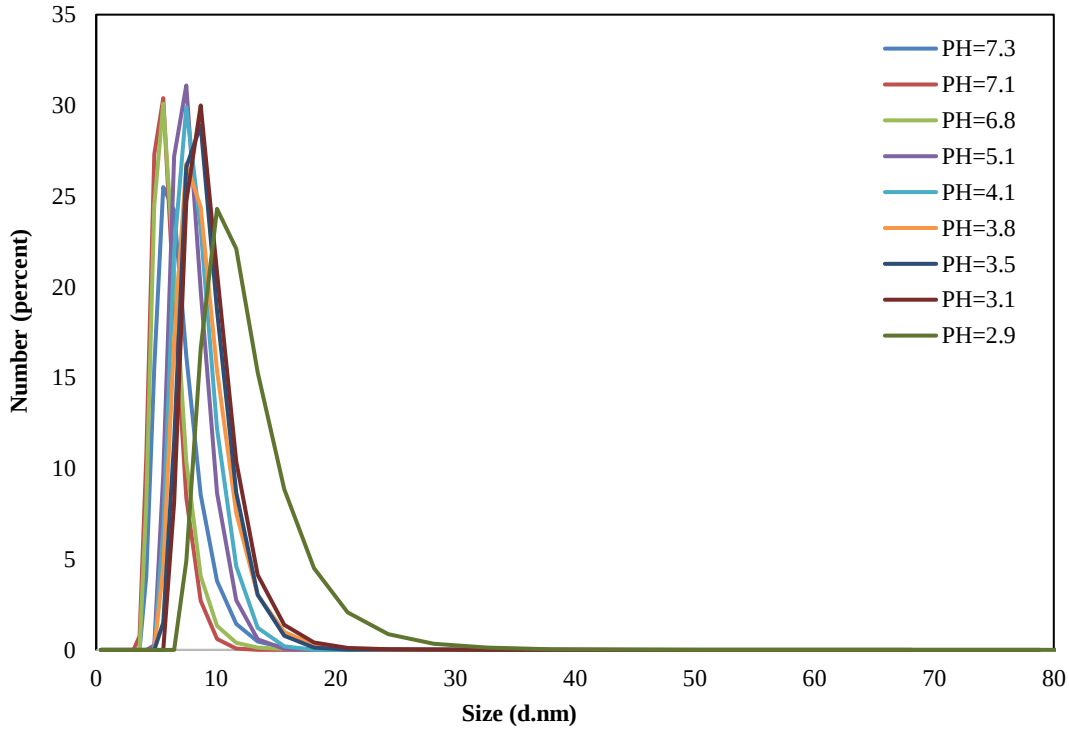

Figure F3.12. Expresses the data collected through DLS analysis of the samples in (**Run 3**) to give the diameter size and standard deviations for each pH range produced by adding 1M HCl (5-30 µL) to the **4B**-AuNPs solution. ***Following Chapter 3.***

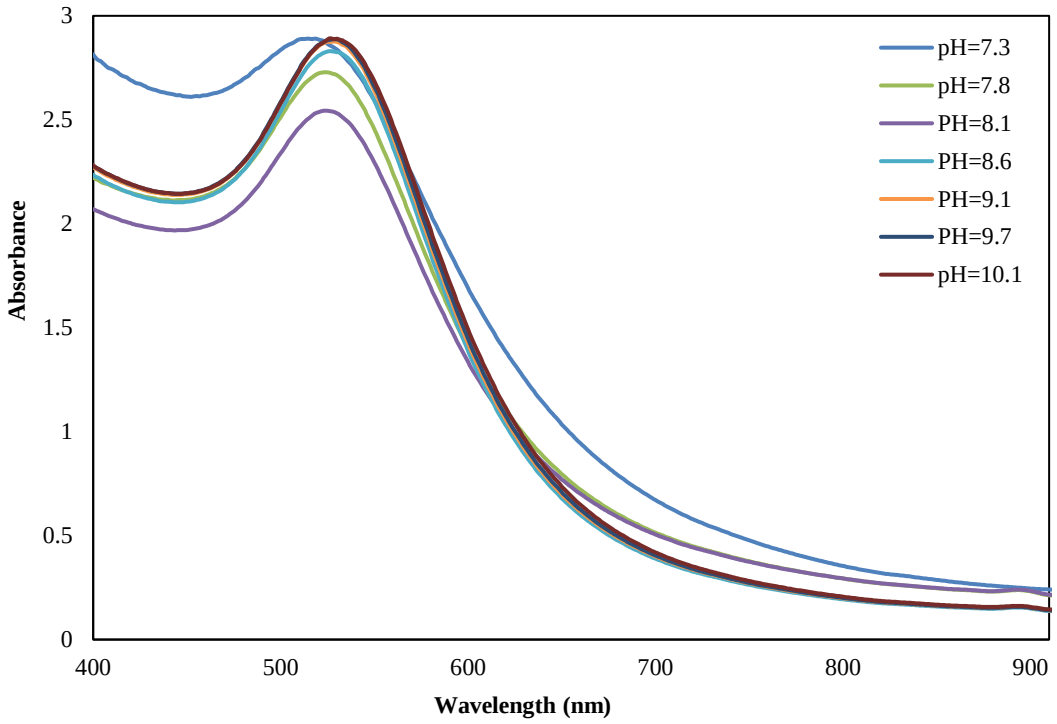

Figure F3.13. Illustrates the data collected through UV-Vis across the pH range produced (pH >7.5) by adding 1M NaOH (5-30 µL) to the **4B**-AuNPs solution in (**Run 1**) of the basic study. ***Following Chapter 3.***

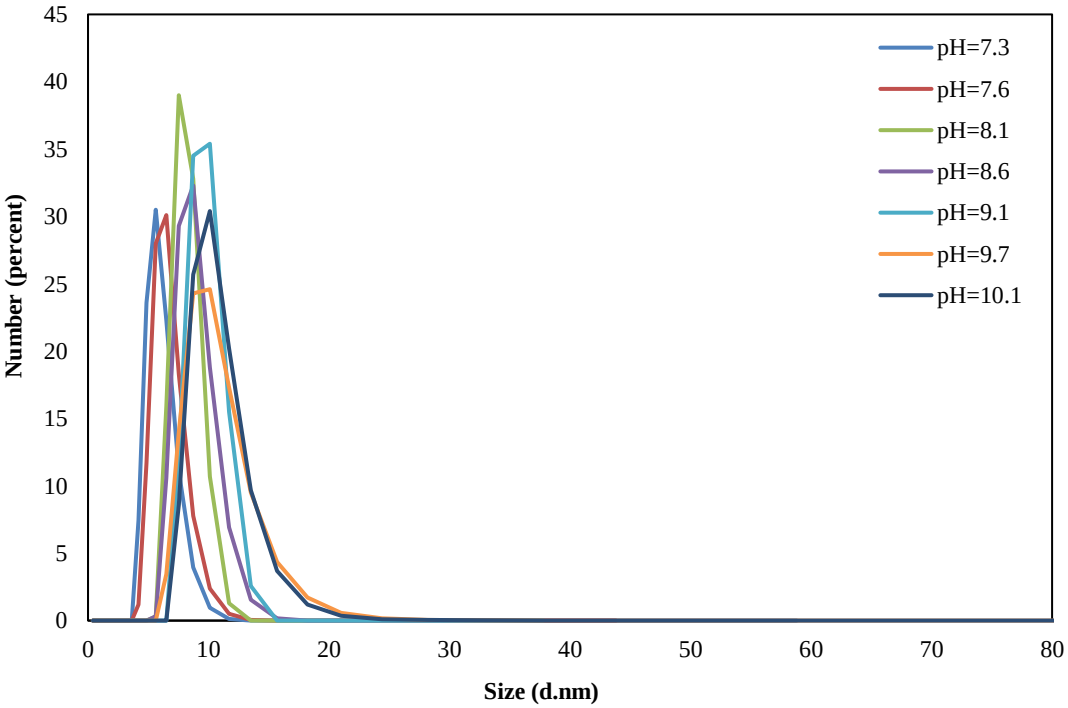

Figure F3.14. Expresses the data collected through DLS analysis of the samples in (**Run 1**) to give the diameter size and standard deviations for each pH range produced by adding 1M NaOH (5-30 µL) to the **4B**-AuNPs solution. ***Following Chapter 3.***

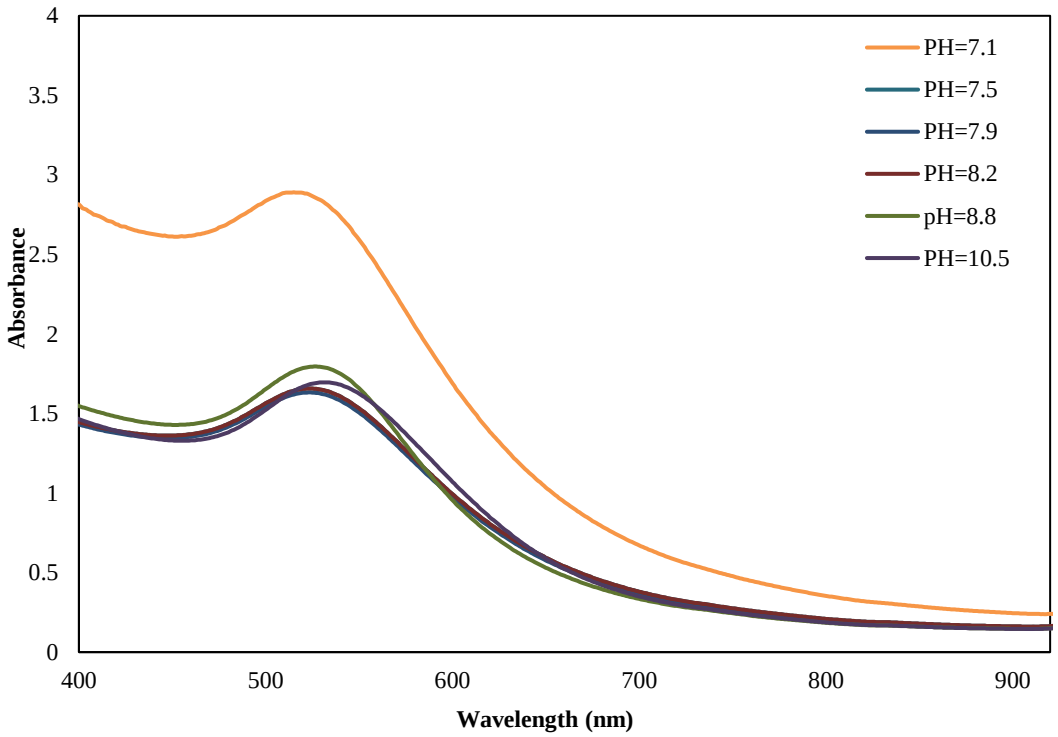

Figure F3.15. Illustrates the data collected through UV-Vis across the pH range produced (pH >7.5) by adding 1M NaOH (5-30 µL) to the **4B**-AuNPs solution in (**Run 3**) of the basic study. ***Following Chapter 3.***

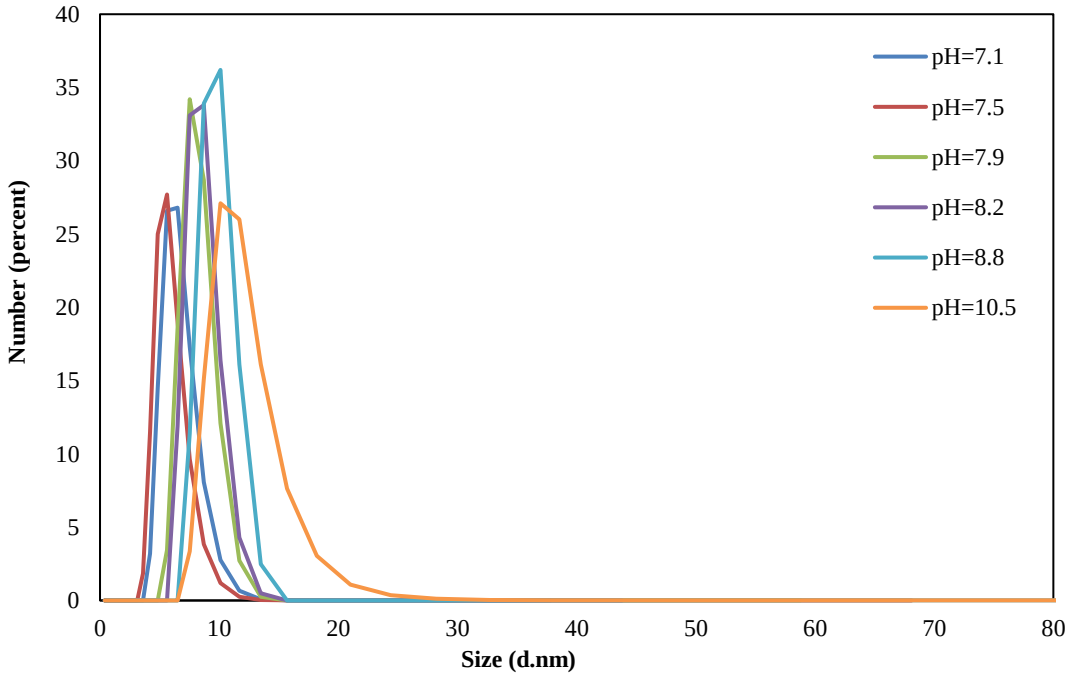

Figure F3.16. Expresses the data collected through DLS analysis of the samples in (**Run 3**) to give the diameter size and standard deviations for each pH range produced by adding 1M NaOH (5-30 µL) to the **4B**-AuNPs solution. ***Following Chapter 3.***

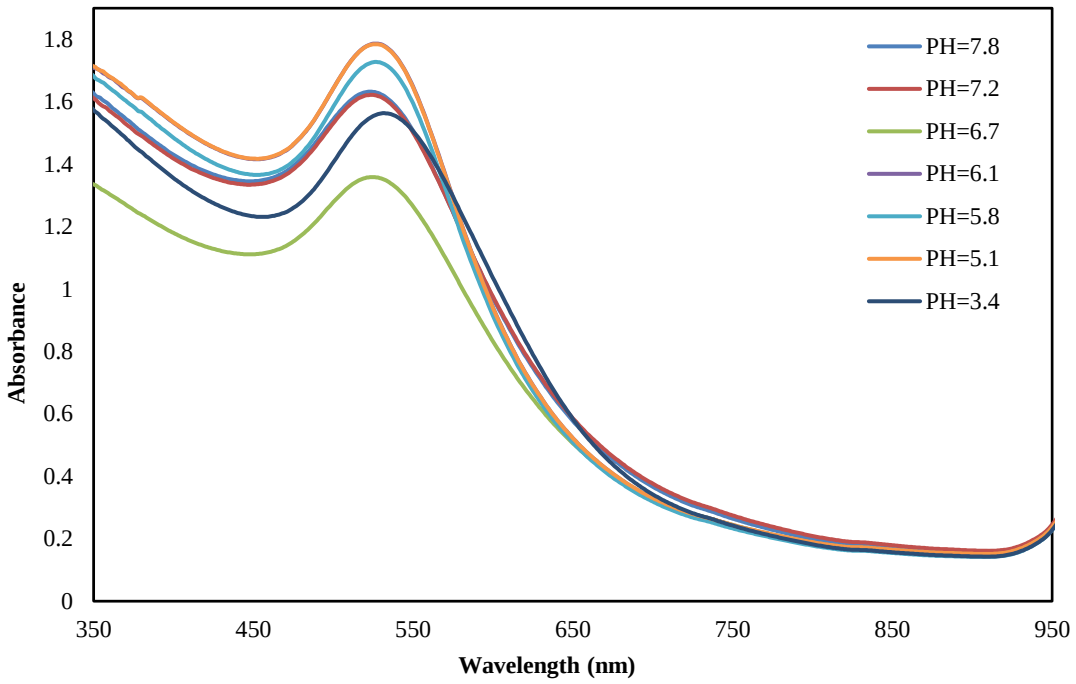

Figure F3.17. Illustrates the data collected through UV-Vis across the pH range produced (pH <7.5) by adding HCl (5-30 µL) to the **4A**-AuNPs solution in (**Run 2**) of the acidic study. ***Following Chapter 3***.

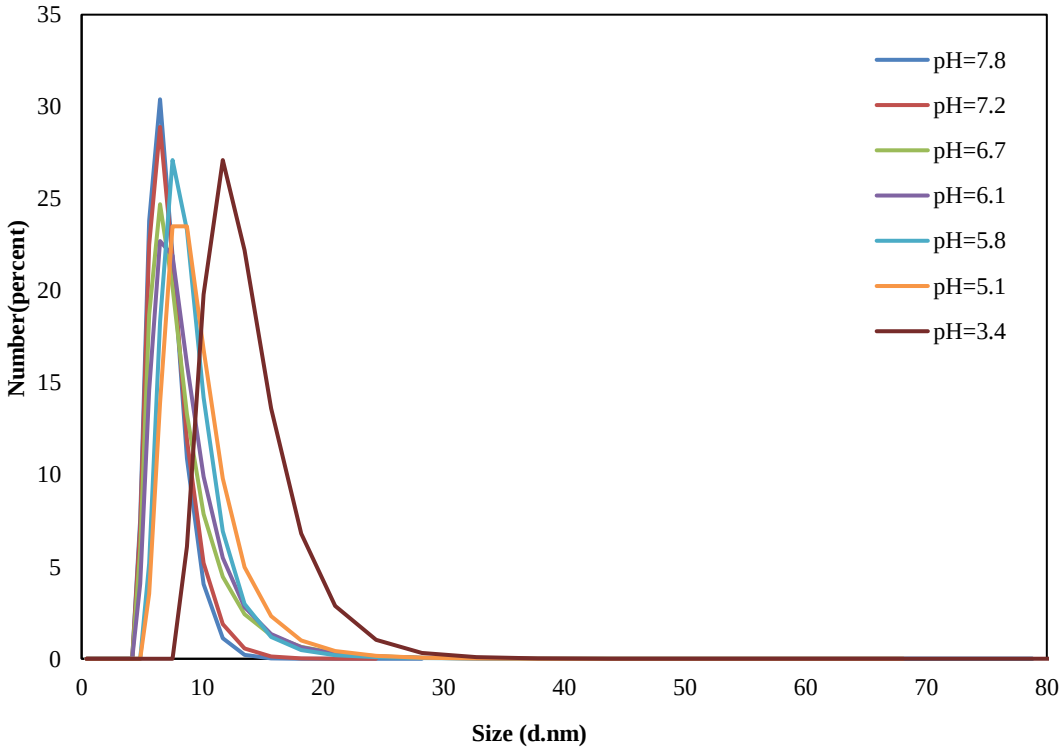

Figure F3.18. Expresses the data collected through DLS analysis of the samples in (**Run 2**) to give the diameter size and standard deviations for each pH range produced (pH <7.5) by adding HCl (5-30 µL) to the **4A**-AuNPs solution. ***Following chapter 3.***

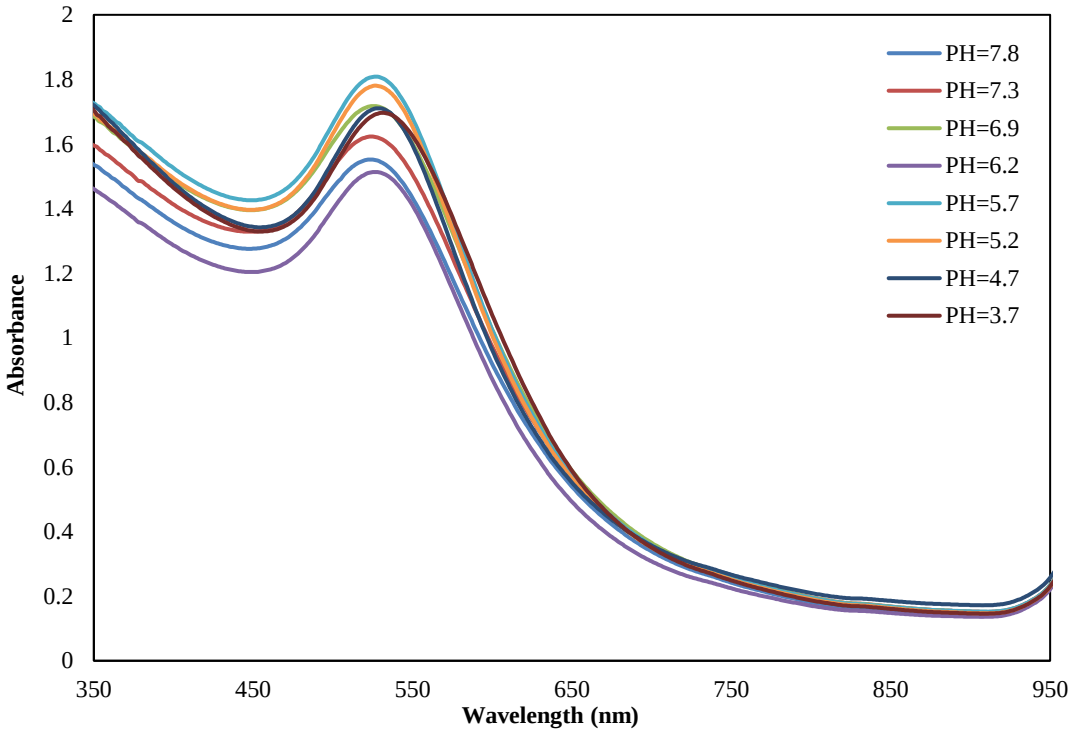

Figure F3.19. Illustrates the data collected through UV-Vis across the pH range produced (pH <7.5) by adding HCl (5-30 µL) to the **4A**-AuNPs solution in (**Run 3**) of the acidic study. ***Following Chapter 3.***

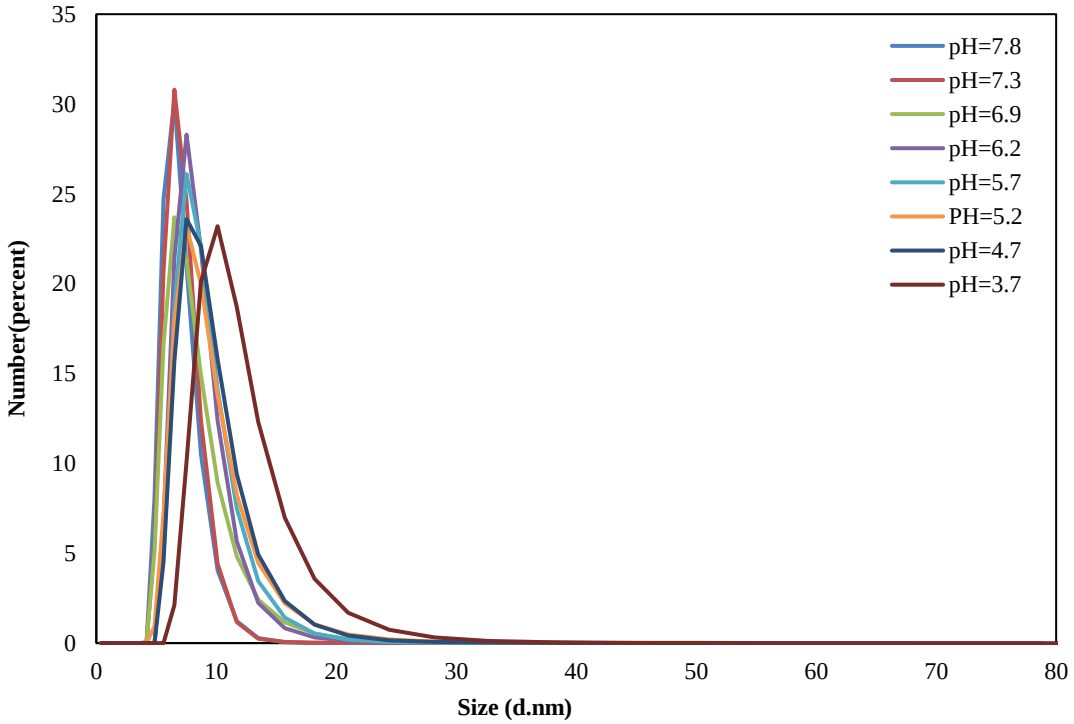

Figure F3.20. Expresses the data collected through DLS analysis of the samples in (**Run 3**) to give the diameter size and standard deviations for each pH range produced (pH <7.5) by adding HCl (5-30 µL) to the **4A**-AuNPs solution. ***Following Chapter 3.***

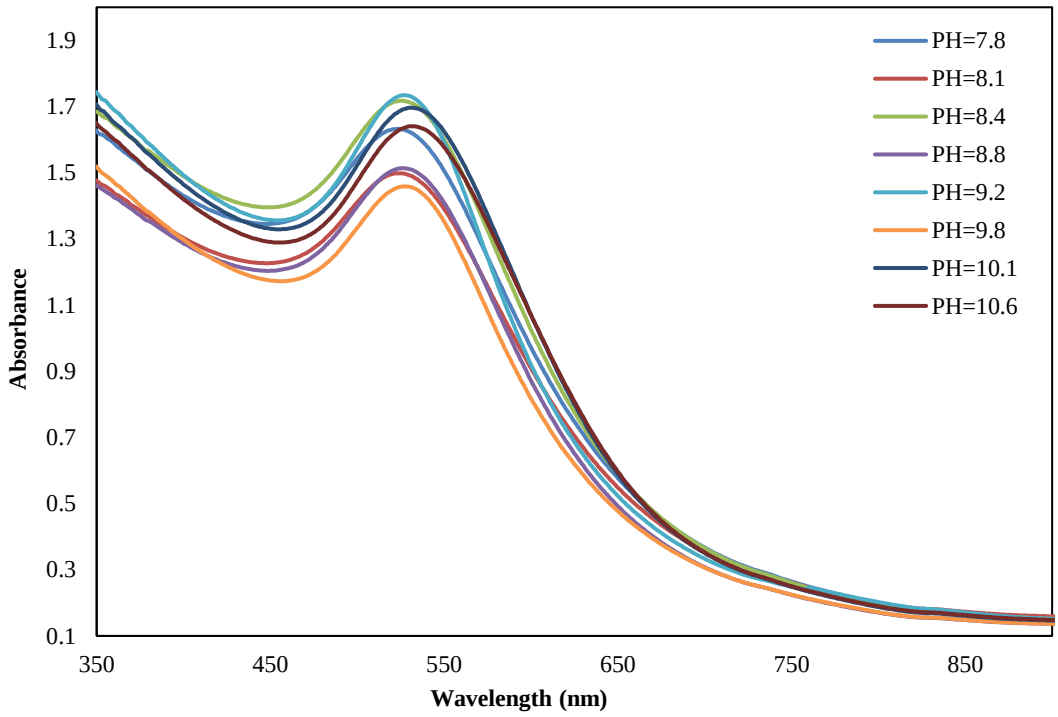

Figure F3.21. Illustrates the data collected through UV-Vis across the pH range produced (pH >7.5) by adding NaOH (5-30 µL) to the **4A**-AuNPs solution in (**Run 1**) of the basic study. ***Following Chapter 3.***

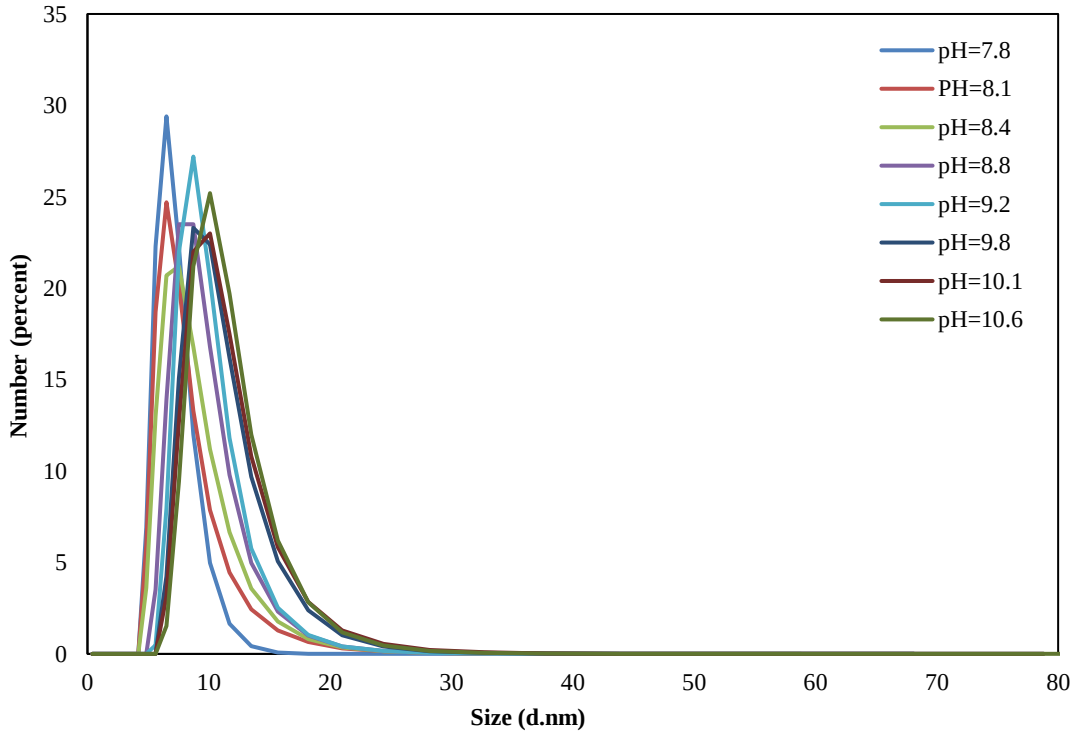

Figure F3.22. Expresses the data collected through DLS analysis of the samples in (**Run 1**) to give the diameter size and standard deviations for each pH range produced by adding NaOH (5-30 µL) to the **4A**-AuNPs solution. ***Following Chapter 3.***

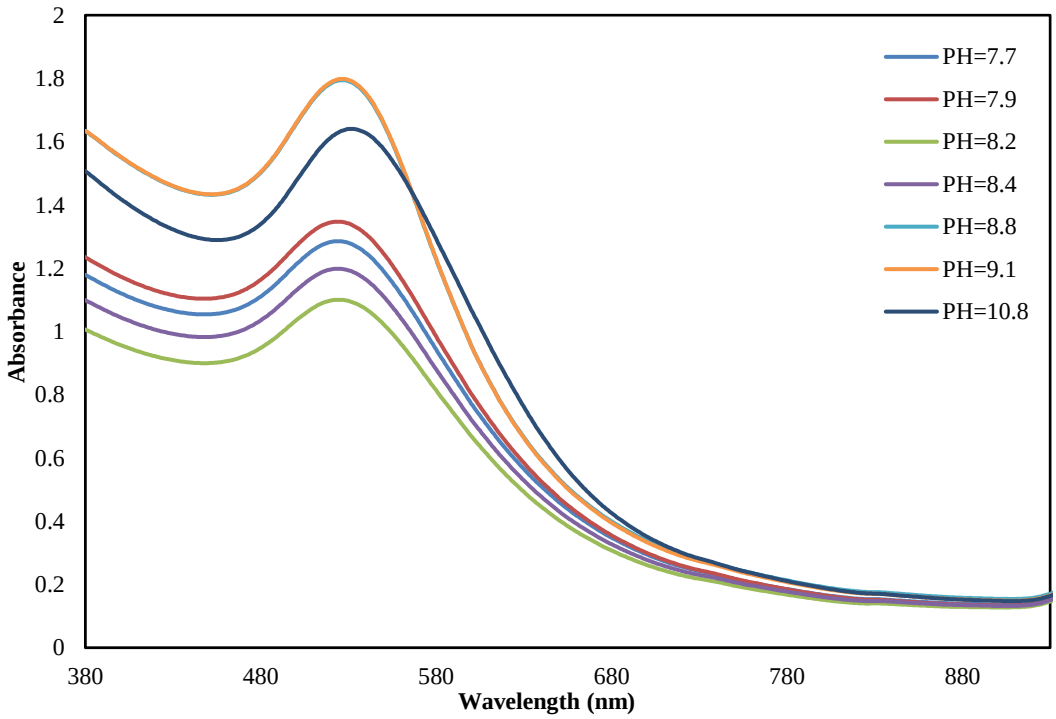

Figure F3.23. Shows the data collected through UV-Vis across the pH range produced (pH >7.5) by adding NaOH (5-30 µL) to the **4A**-AuNPs solution in (**Run 2**) of the basic study. ***Following Chapter 3.***

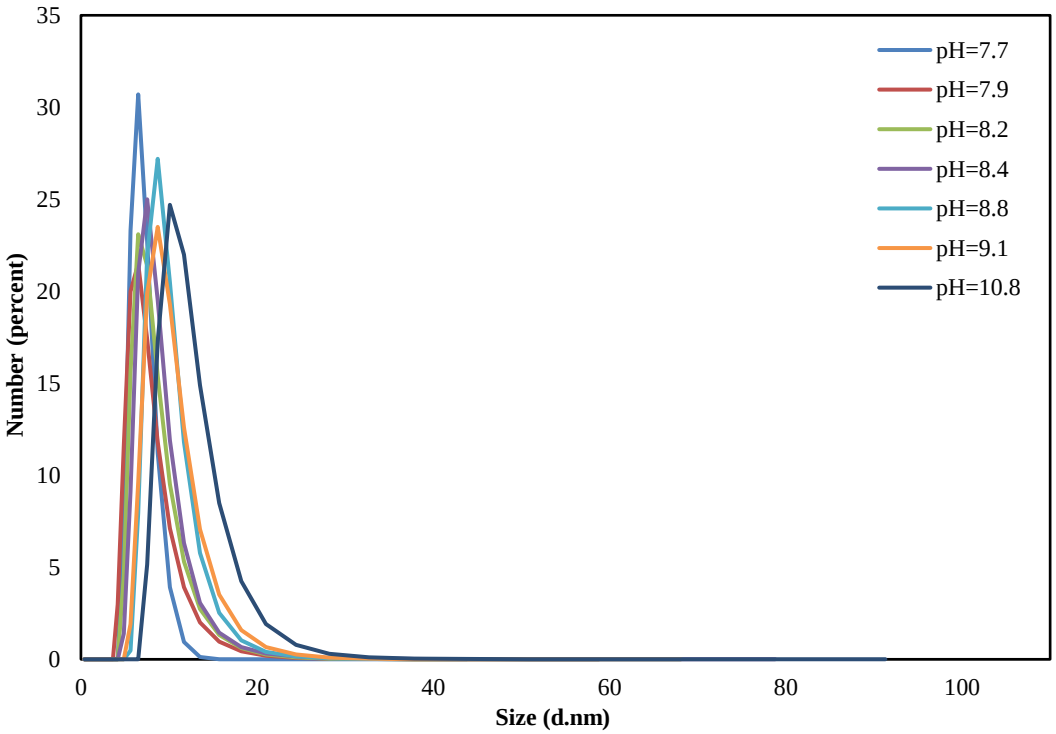

Figure F3.24. Expresses the data collected through DLS analysis of the samples in (**Run 2**) to give the diameter size and standard deviations for each pH range produced by adding NaOH (5-30 µL) to the **4A**-AuNPs solution. ***Following Chapter 3.***

Appendix G

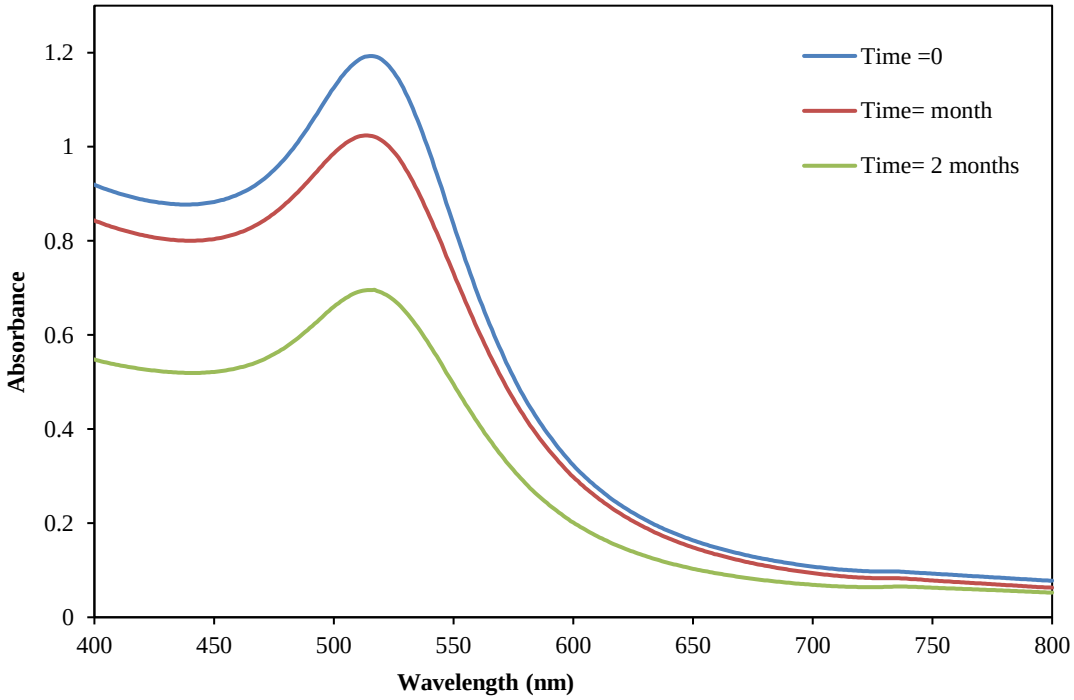

Figure G4.1. UV-Vis for the stability of the **9D**-AuNPs reduced by $NaBH_4$ and dispersed in DMSO at time = 0, 1 and 2 months respectively. ***Follow Chapter 4.***

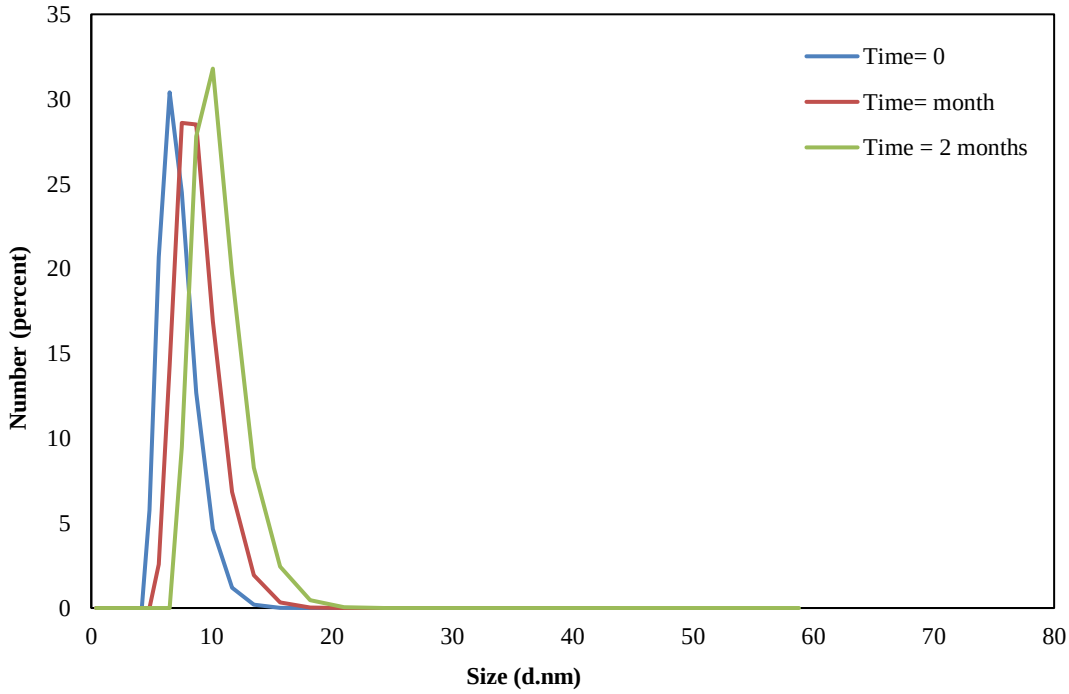

Figure G4.2. The effect of the time on the size disruption and standard deviation of **9D**-AuNPs reduced by $NaBH_4$. The size disruption was determined according to the DLS measurements. ***Follow Chapter 4.***

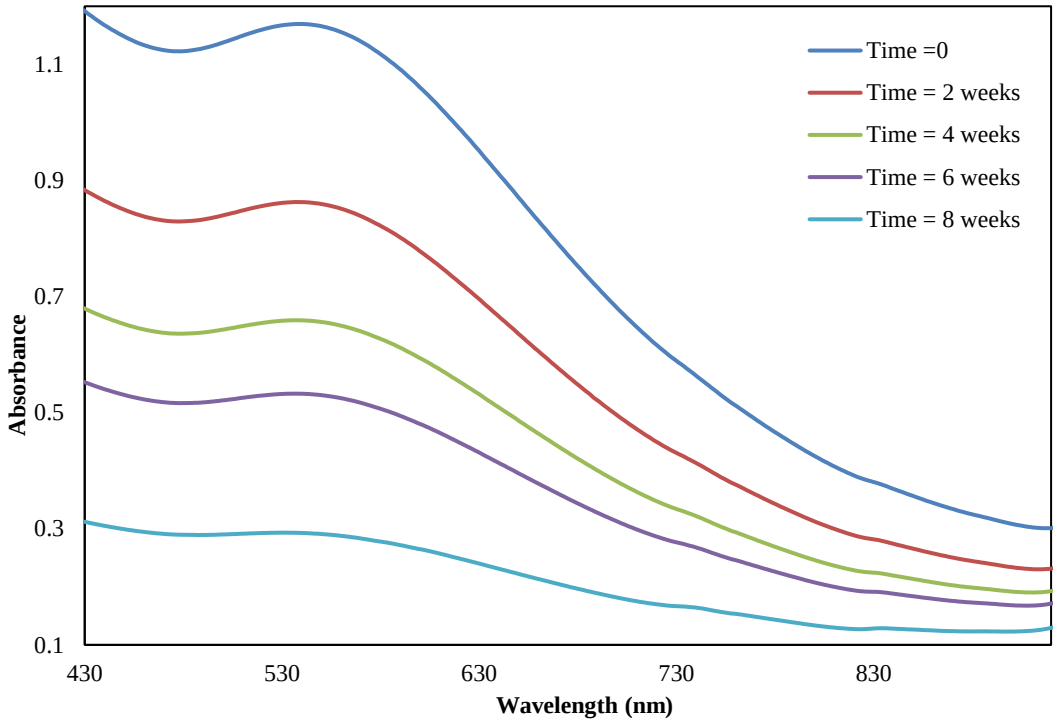

Figure G4.3. UV-Vis for the stability of the **9A**-AuNPs reduced by $NaBH_4$ and dispersed in DMSO at time = 0, 2, 4, 6, and 8 weeks respectively. ***Follow Chapter 4.***

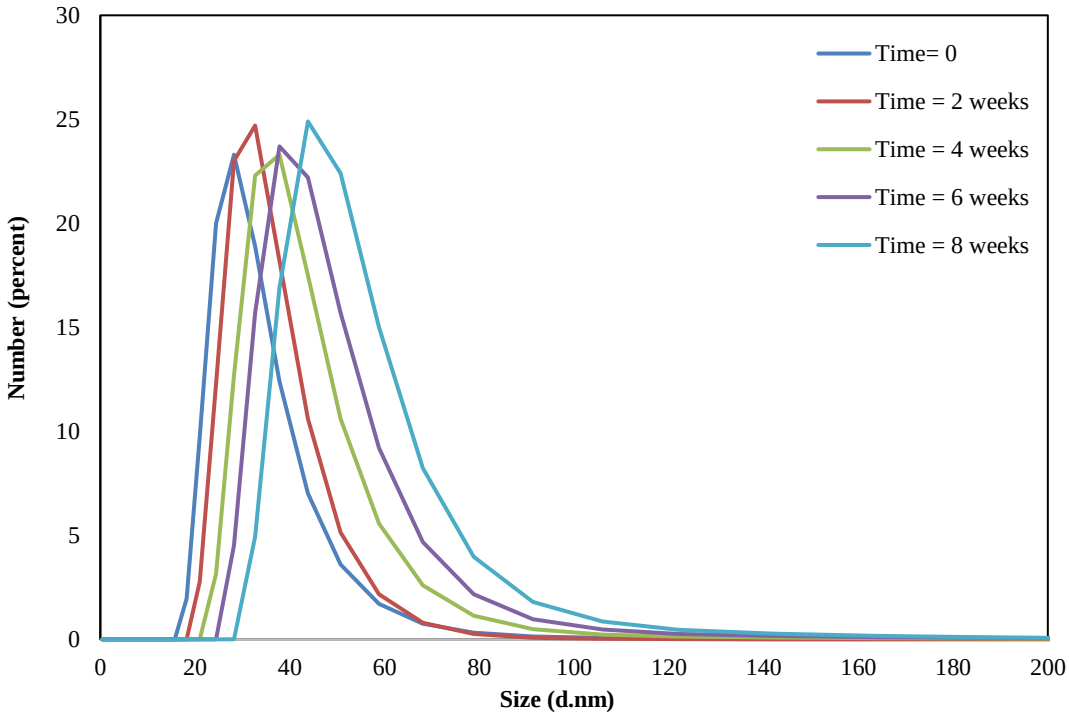

Figure G4.4. The size and standard deviation of each diameter range taken at a different time value for **9A**-AuNPs (reduced by $NaBH_4$), according to DLS measurements. ***Follow Chapter 4.***

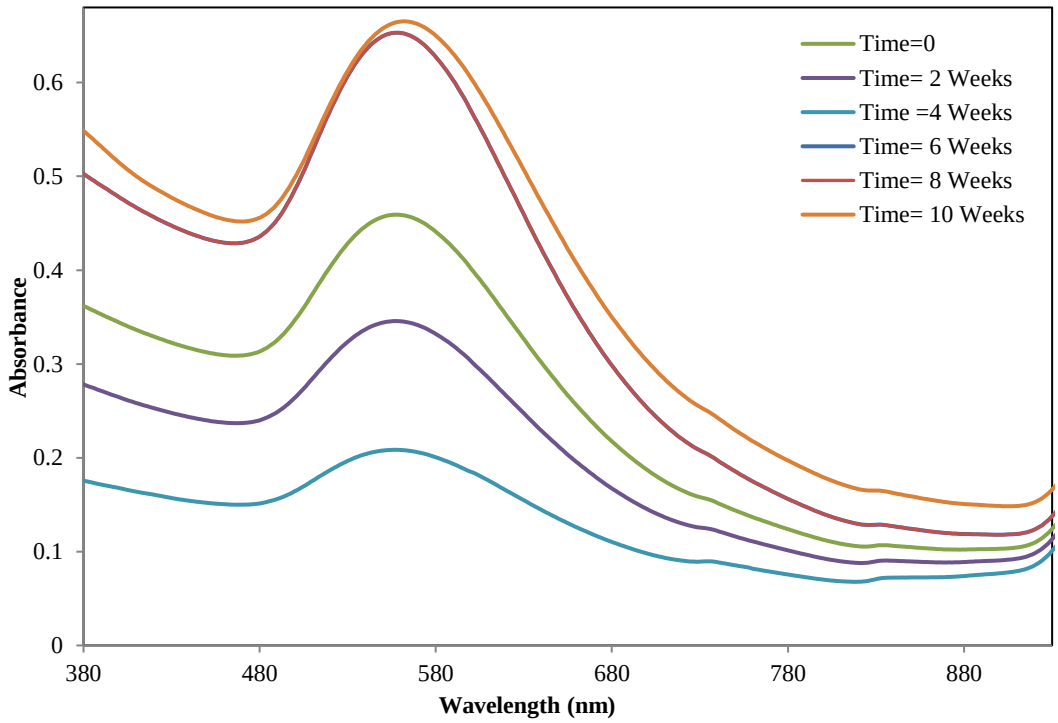

Figure G4.5. UV-Vis for the stability of the **4**-AuNPs using ascorbic acid as reducing agent, dispersed in aqueous solution at time = 0, 2, 4, 6, 8 and 10 weeks respectively. Different wavelength measured. ***Follow Chapter 4.***

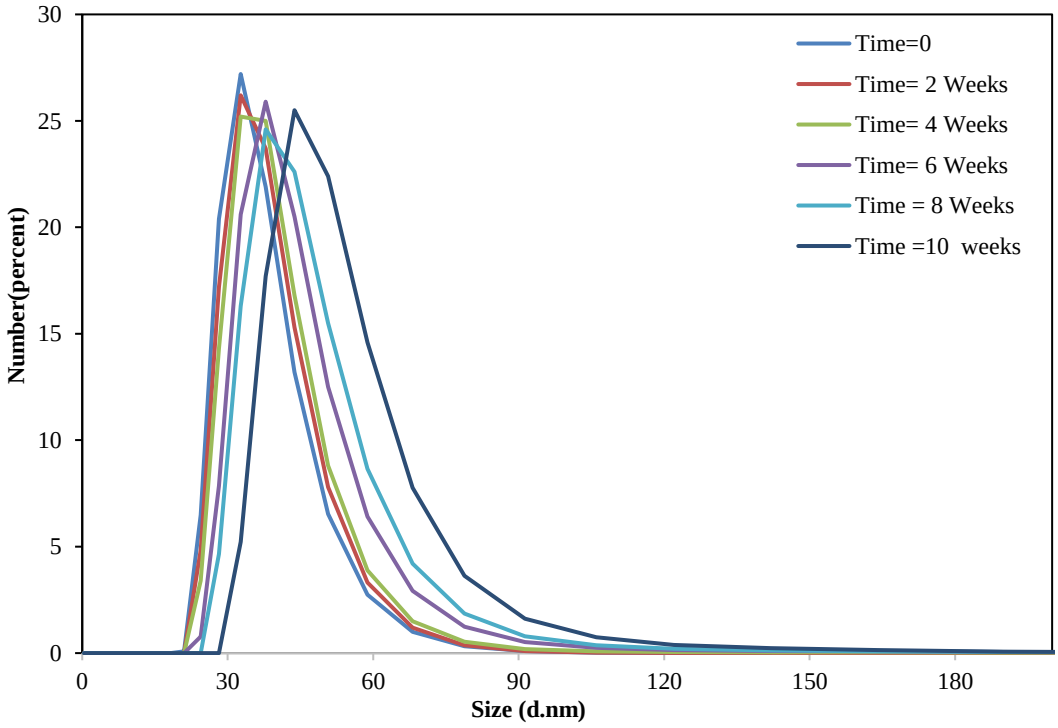

Figure G4.6. The size and standard deviation of each diameter range taken at a different time value for **4**-AuNPs (using ascorbic acid as reducing agent) according to DLS study. ***Follow Chapter 4.***

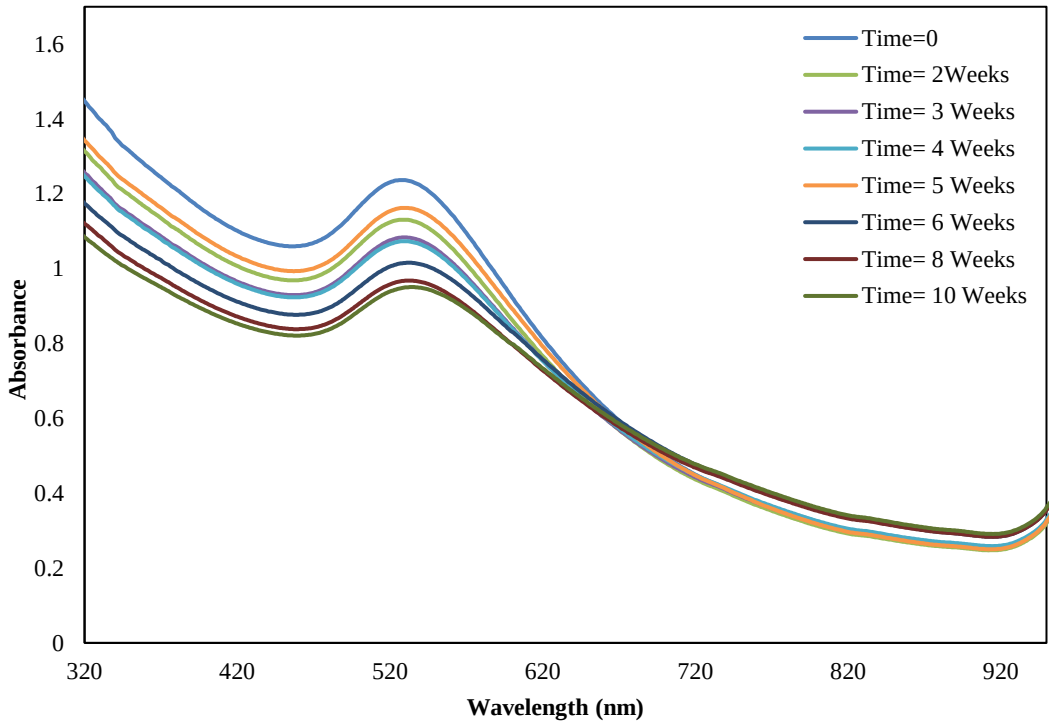

Figure G4.7. UV-Vis for the stability of the **8B**-AuNPs dispersed using ascorbic acid as reducing agent in aqueous solution at different time = 0, 2, 3, 4, 5, 6, 8 and 10 weeks respectively. ***Follow Chapter 4.***

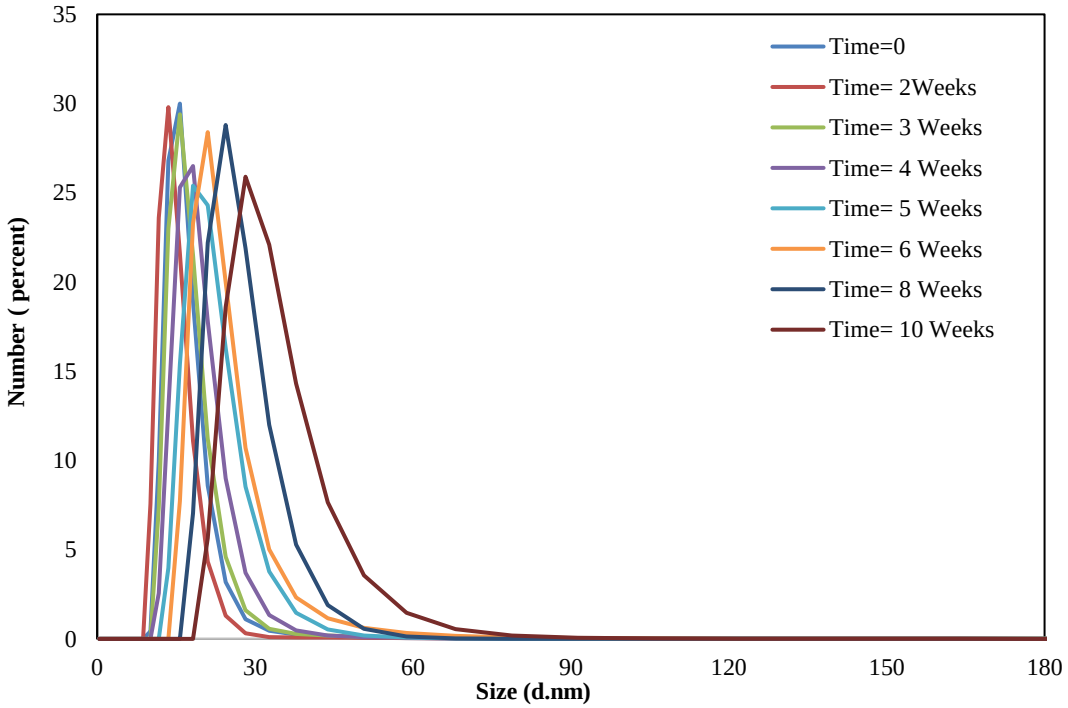

Figure G4.8. The size and standard deviation of each diameter range by DLS measuring taken at a different time value for 8B-AuNPs using ascorbic acid as reducing agent. ***Follow Chapter 4.***

Appendix j

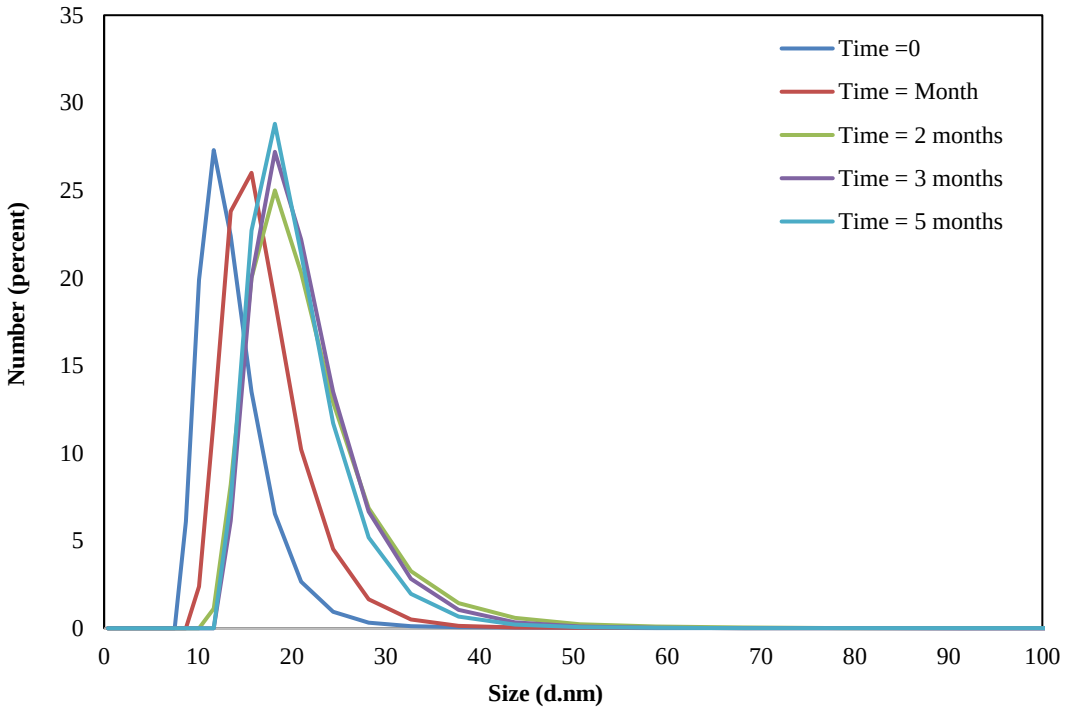

Figure J5.1. The size and standard deviation of each diameter range by DLS measuring taken at a different time value for **12D**-AuNPs using $NaBH_4$ as reducing agent. ***Follow Chapter 5.***

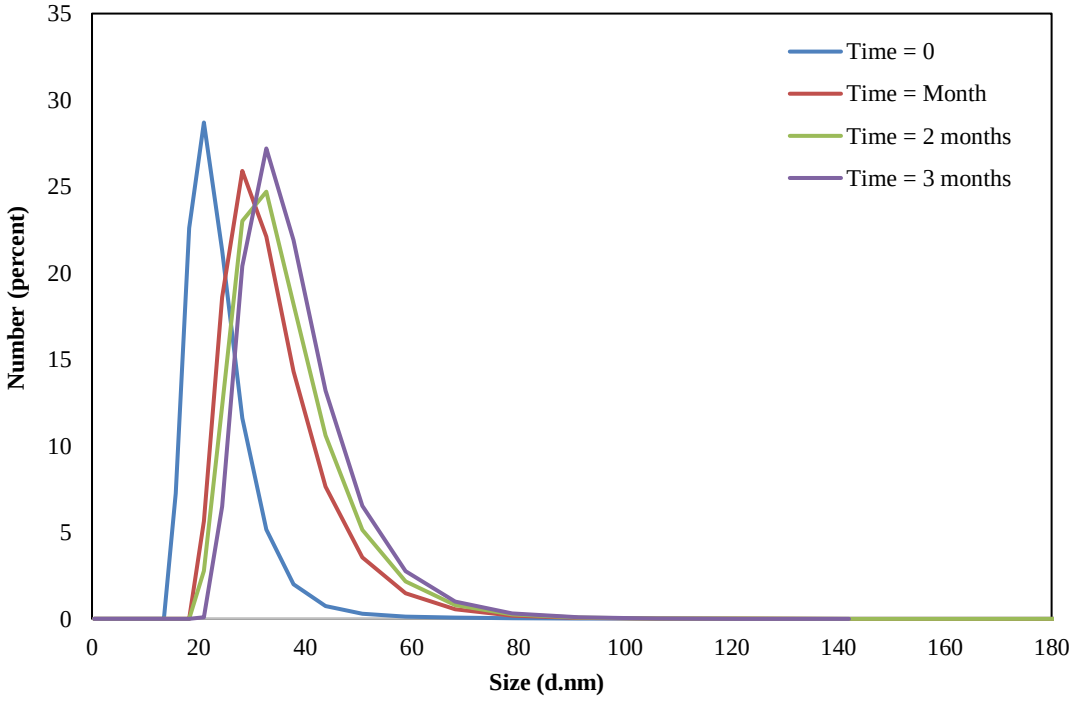

Figure J5.1. The size and standard deviation of each diameter range by DLS measuring taken at a different time value for **12A**-AuNPs using $NaBH_4$ as reducing agent. ***Follow Chapter 5.***

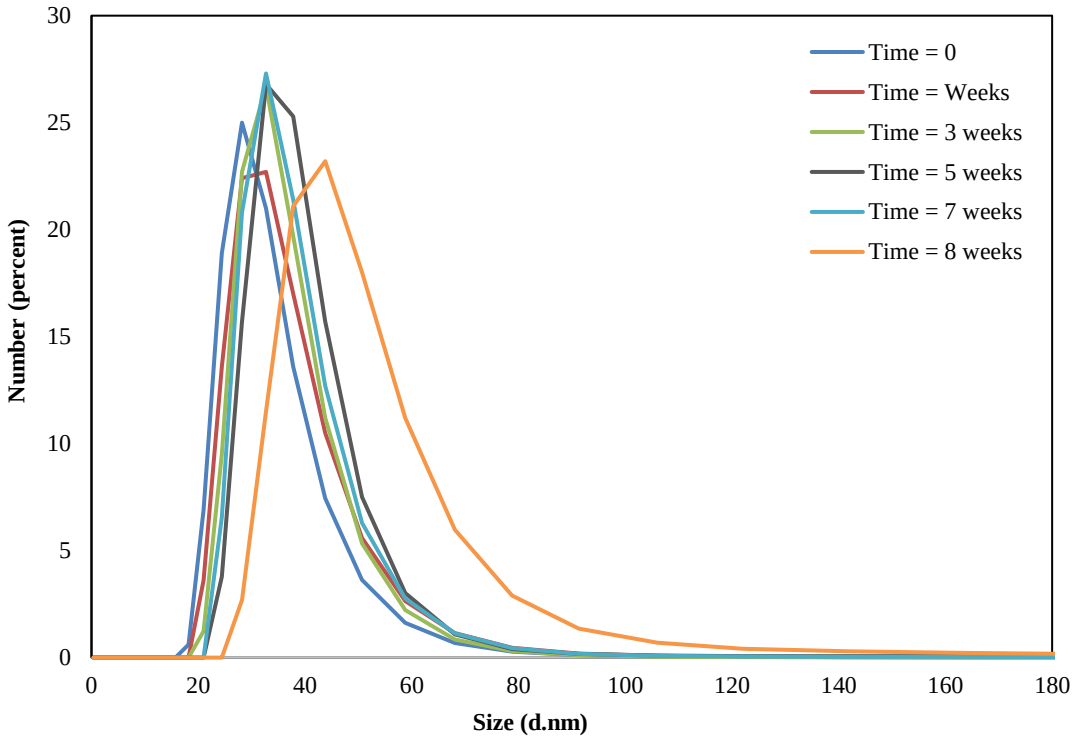

Figure J5.2. The size and standard deviation of each diameter range by DLS measuring taken at a different time value for **12A**-AuNPs using ascorbic acid as reducing agent. ***Follow Chapter 5.***

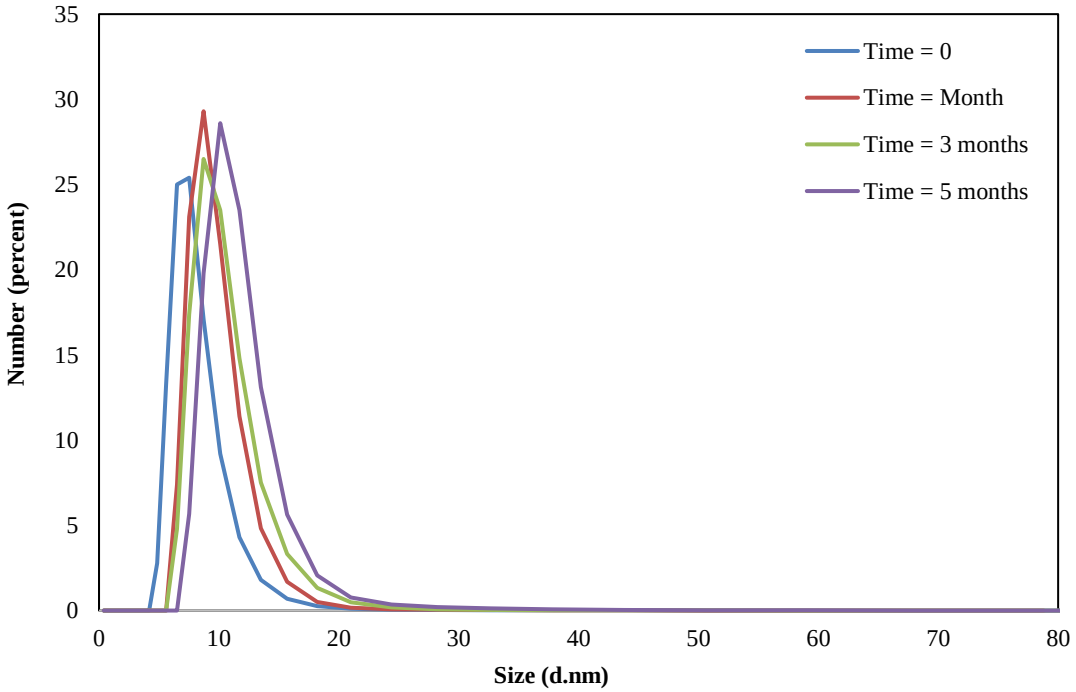

Figure J5.3. The size and standard deviation of each diameter range by DLS measuring taken at a different time value for **15**-AuNPs using $NaBH_4$ as reducing agent. ***Follow Chapter 5.***

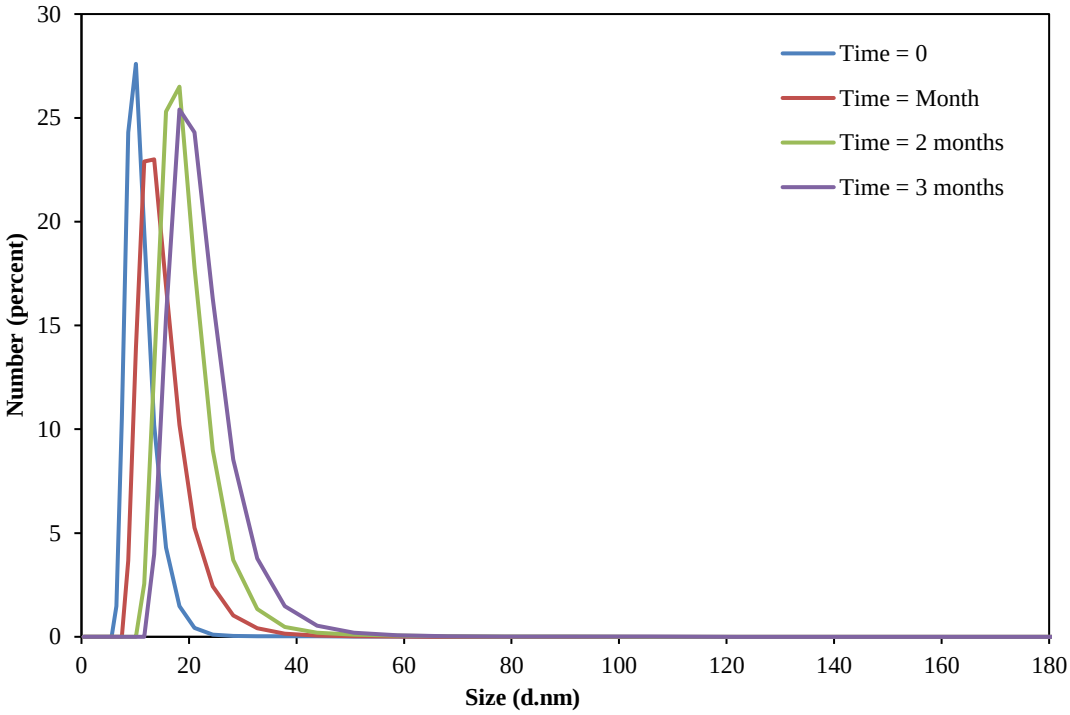

Figure J5.4. The size and standard deviation of each diameter range by DLS measuring taken at a different time value for **18**-AuNPs using $NaBH_4$ as reducing agent. ***Follow Chapter 5.***